UNIVERSITY OF MILANO – BICOCCA

Faculty of Mathematical, Physical and Natural Sciences

Department of Environmental and Territorial Sciences

and

NATIONAL RESEARCH COUNCIL

Institute for the Dynamics of Environmental Processes

School of Doctorate of Sciences

Ph.D. Program in Environmental Sciences

XXII Cycle

Debris flow hazard and risk analysis at medium and local scale

Ph.D. Dissertation of

Jan Blahut

Tutor: Dr. Simone Sterlacchini, CNR-IDPA

Co-tutors: Prof. Thomas Glade, UNIVIE

Prof. Cees J. van Westen, ITC

Dr. Mattia De Amicis, UNIMIB-DISAT

Matr. N. 708778

to Klára and Alžběta

Abstract

Increased population, its wealth and activities lead to increased risk from landslide hazards in the mountain areas. The presented study deal with the analysis of debris flow hazard and risk at medium (regional) and local (site-specific) scale. Study took place in part of Valtellina Valley in Italian Central Alps.

The first part of the study presents information about landslide hazard, risk and debris flow processes. It also shows historical information about natural disasters in the study area of Mountain Consortium of Municipalities of Valtellina di Tirano together with the results from a geo-database built for the study area. The database covers a period from 1600 till 2008 and it represents an important source of information for civil protection purposes.

In the second part of the study, the debris flow susceptibility, hazard and risk analysis is performed at medium scale for the whole studied territory. Firstly, a new debris flow database was prepared and used as an input for susceptibility modelling together with the official sources. Susceptibility modelling was performed, using a bi-variate statistical technique Weights-of-Evidence and then the best performing susceptibility map was selected. Afterwards, spatial comparison of different susceptibility models was made, using advanced statistical techniques (Kappa Statistic, Principal Component Analysis, and Distance Weighted Entropy). Even though the modelling results show similar performance when assessed by standard evaluation techniques, their spatial pattern is very different. This may have serious outcomes in choosing the model which is most correctly delimiting the susceptible areas. Consequently, the results from the susceptibility modelling were coupled with temporal occurrence of debris flows in order to acquire initiation probabilities. These were subsequently used as inputs for runout modelling to obtain hazard maps at medium scale. Finally, medium scale risk maps were prepared by overlaying hazard maps with the elements at risk. Then, three risk maps were obtained. Two of the maps quantify economic risk from debris flows and the third qualitatively delimits total risk areas. Besides limitations and uncertainties within all steps of the analysis, an economic estimation of prospective consequences was done, being very important for the local stakeholders as well for the general public.

Third part of the work presents two case studies related to quantitative risk assessment at local scale. Selvetta debris flow event, which happened in July 2008, was studied in the field obtaining information about the debris flow and building damage. The event was back-calculated and used for estimating synthetic vulnerability functions for buildings. In the second case study, located in Tresenda, hypothetical debris flow hazard was modelled for three return periods. Hazard scenarios were prepared and risk was quantified in economic terms using the vulnerability curves from the first case study of Selvetta. The results and the method applied for the quantification of risk reveal as very promising. As a consequence, it may be very interesting to apply this approach in different socio-economic and environmental settings in order to test its robustness.

Presented thesis proposes a debris flow hazard and risk analyses approach at medium and local scale. Besides its feedbacks arising from available data, models, changing natural and socio-economic conditions and other intrinsic limitations, the study shows a possible approach applicable within integrated debris flow risk management framework.

Table of contents

List of figures

List of tables

Chapter 1

Introduction

Se la montagna viene da te
e tu non sei maometto...
Corri, pirlun,
che e' una frana!

1.2 Introduction to the research problem and framework of the Ph.D. project

Landslides occur worldwide in response to a broad variety of natural predisposing conditions and triggering factors, which include heavy rainfalls, earthquakes, and human activity. Landslides constitute a serious source of danger, causing environmental damage and substantial human and financial losses.

Since the beginning of the 21st century (2000-2008), landslides have affected about 1.5 million people worldwide and have cost approximately more than 875 million US dollars (EM-DAT 2009). These losses are currently increasing as the pressure of population growth causes urban areas to expand into more unstable hillside areas (NRC 2004). The direct and indirect socio-economic costs due to the impact of landslides affect populations and their private and public properties: industries, transport infrastructure, lifelines, communication lines and power supply. Among natural disasters, landslides are reported as the 7th biggest killer, after windstorms, floods, droughts, earthquakes, volcanoes and extreme temperature, claiming 800-1000 lives on average in each of the last 20 years. An average of 940 people annually was killed by landslides in the decade from 1993 to 2002, majority of those victims are from Asia (EM-DAT 2009). It has to be noted however, that in many cases records about landslide consequences are underestimated in the catastrophe databases. Live losses and damages are attributed to primary triggering factor, such as hurricane, earthquake, or flood and not to the landslide that caused the fatalities (Nadim et al. 2006). The reason of this situation is that these events cover larger areas and statistics usually do not distinguish these major events into multi-type incidents.

In mountain regions, such as Italian Alps, hydrogeological disasters are part of everyday people's lives, sometimes causing casualties and considerable economic, social and environmental losses. Considering only landslides, the annual economic damage for the whole Italy is estimated between 1 and 2 billion USD (UNU 2006). This amount is comparable to countries such as USA and India but these countries are wider and more populated than Italy. Moreover, in young mountain areas (Fig. 1.1), and particularly in the Alps, concentration of events is much higher than in other parts of the country (Reichenbach et al. 1998). During the period from 1861 to 2004, landslides in Italy reached second highest mortality rates (0.09 per 100,000) after earthquakes (Guzzetti et al. 2005).

As a consequence, the study of landslide processes, hazards, and risks concern the researchers of many different fields of study. The processes leading to landslides are studied by geologists (mainly engineering geologists and hydro-geologists), physical geographers, geotechnicians, and environmental scientists. Landslides effects are also studied by geographers, civil engineers, urban and spatial planners in order to analyse, to manage and to govern possible risks from landslides.

The research during my Ph.D. studies was conducted and supported by the European Commision and Marie Curie Actions Research Training Network: "Mountain Risks: from

prediction to management and governance" within the 6th Framework Programme (http://mountain-risks.eu/). As an Early Stage Researcher of this project I worked within the Working Block 1 (WB1 – Hazard Analysis) and Working Block 2 (WB2 – Quantitative Risk Assessment), and I also contributed to the WB 4 – Risk Governance (Fig. 1.2). Within the WB1, I focused on preparation of debris flow susceptibility and hazard maps, while within the WB2 my principal aim was to prepare debris flow risk maps and evaluate the risk in terms of prospective economic damage caused by this phenomenon. Within the WB4 I contributed to the knowledge about natural hazards and civil protection legislative framework and insurance possibilities. I also explored the geoinformatic visualisation tools for landslide hazard and risk assessment. Moreover, I worked on the preparation of risk scenarios for civil protection purposes in the study area.

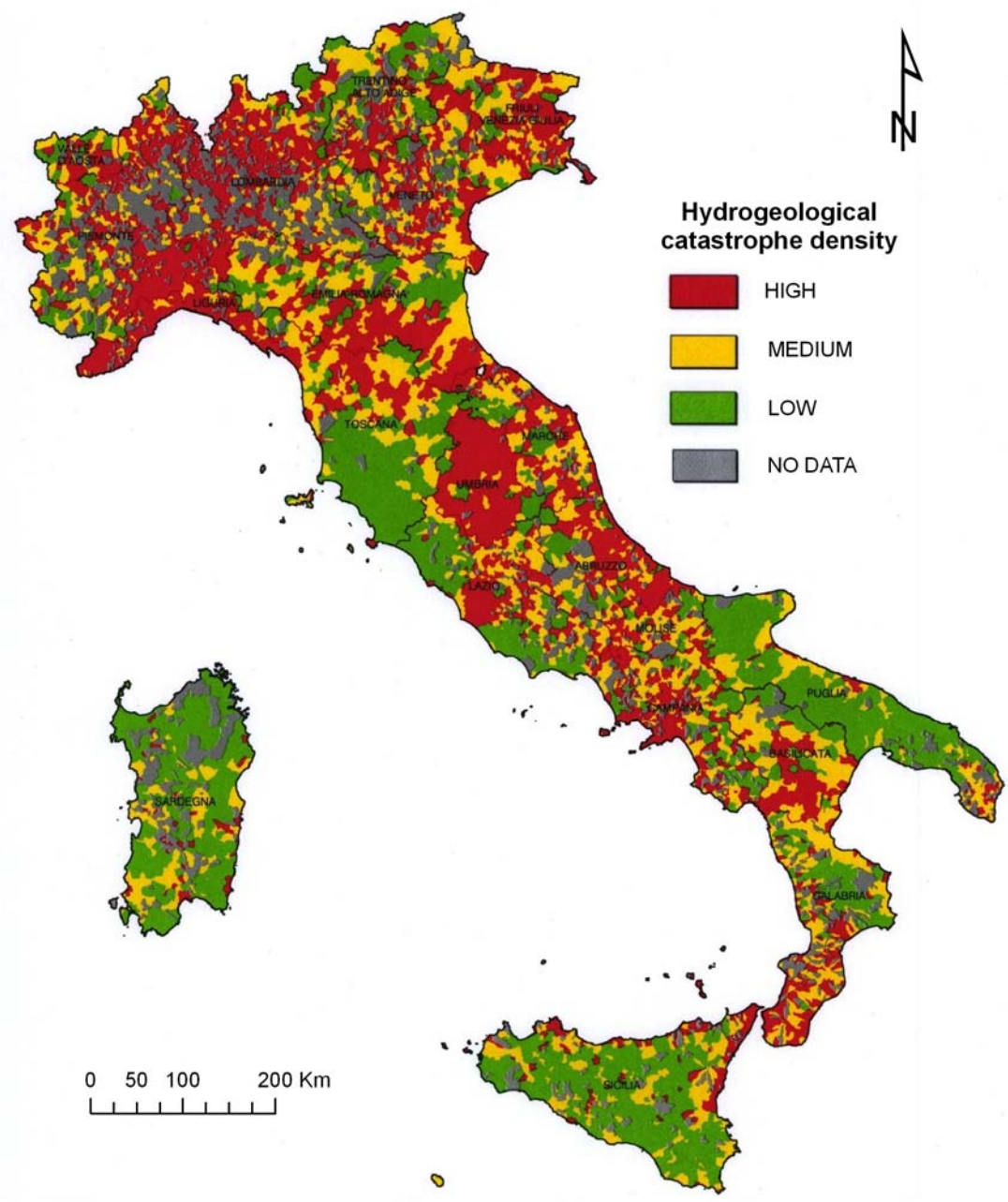

Fig. 1.1 – Density of hydrogeological catastrophes in Italy. Modified after Reichenbach et al. (1998).

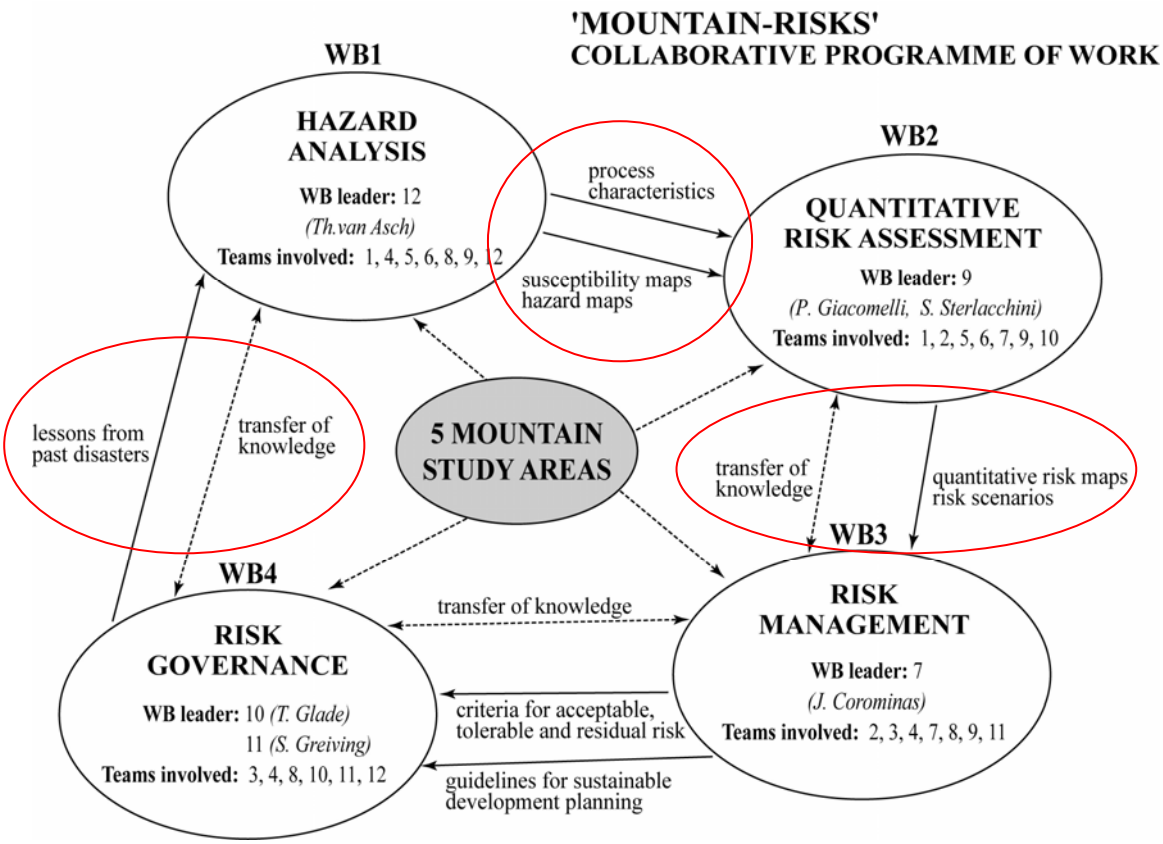

Fig. 1.2 – General framework of the Mountain Risks project. Areas of research interest of the Ph.D. project are signed in red. Source: http://mountain-risks.eu/.

1.2 Principal tasks, workflow and structure of the thesis

The Ph.D. thesis, completed at the University of Milano-Bicocca, Department of Environmental and Territorial Sciences (UNIMIB-DISAT), analyses the susceptibility, hazard and risk from debris flows at the Consortium of Mountain Municipalities – Comunità Montana Valtellina di Tirano (CM Valtellina di Tirano), situated in Italian Central Alps, in the northern part of the Lombardy Region.

The principal tasks to fulfil my Ph.D. research were:

- Exploration of historical data (flood and landslide databases, historical records, newspaper and journal articles) which could be used for hazard and risk analysis and civil protection purposes in the study area;
- Calculation of debris flow susceptibility maps at medium scale (1:25,000 – 1:50,000) and assessment of the spatial variability of the obtained results;
- Debris flow hazard modelling at medium scale using GIS techniques, and incorporation of spatial, as well the temporal probability of debris flows together with the delimitation of possible runout areas in order to obtain debris flow hazard maps;

- Preparation of debris flow risk maps and quantification of possible direct economic losses due to the debris flows on medium scale;
- Debris flow hazard and risk analysis at local scale – preparation of case studies/risk scenarios.

Principal methodological steps performed during the research are presented in Fig. 1.3. At the beginning of the work, an extensive collection of the available data was made. Afterwards, two analyses were carried out at different spatial scales. Analysis at medium scale consisted of identification of sources of potential debris flows using available database and historical information. Results from the study were coupled with temporal probability estimations and runout model to calculate quantitative hazard maps. These maps were afterwards compared with the elements at risk information in order to obtain risk maps. At the detailed scale, quantitative risk analysis was performed using two case studies. Vulnerability information obtained from Selvetta event was applied to a hypothetical scenario at Tresenda village in order to quantify the risk and direct economic consequences.

Analytical chapters of the thesis are based on scientific papers that are published in, or submitted to, or under preparation for national and international peer-reviewed journals. Each chapter has its own conclusions and reference list.

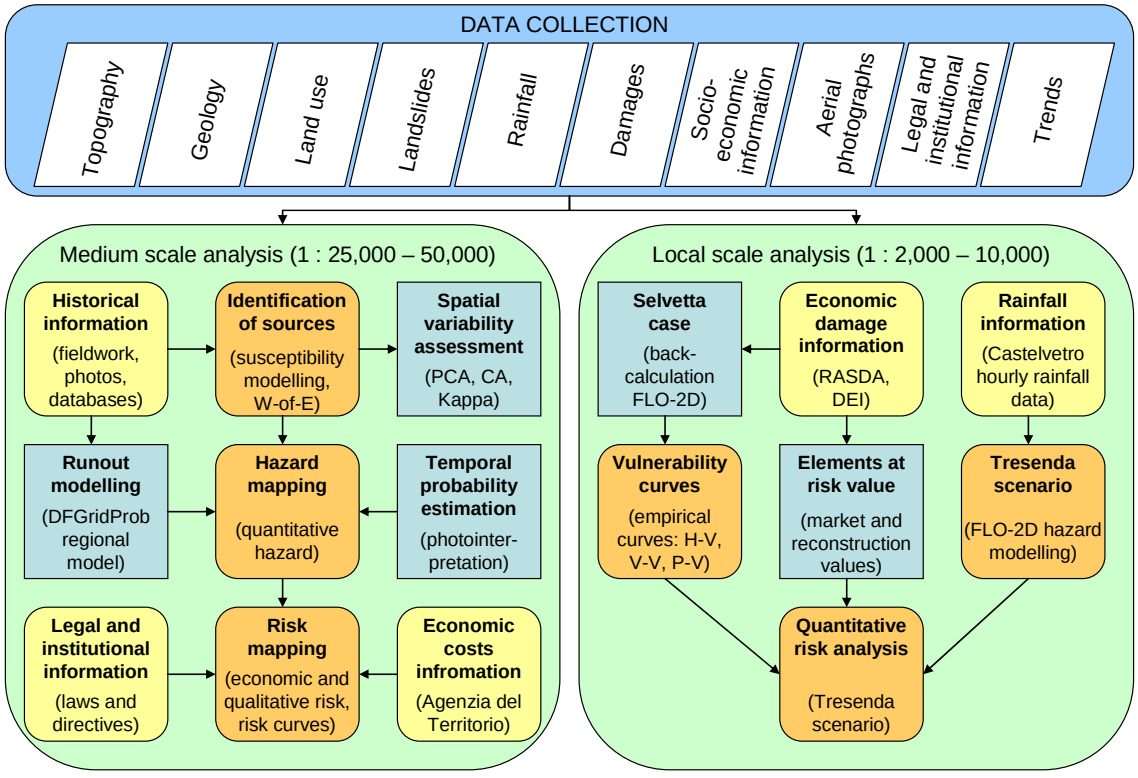

Fig. 1.3 –Principal methodological steps to analyse debris flow hazard and risk. Inputs of the analysis are in yellow and main outputs are in orange rectangles. Blue rectangles show intermediate study steps.

The thesis is divided into three main parts: I) introduction and theoretical framework of the thesis; II) study of debris flow hazard and risk at medium (regional) scale; and III) case study at local (large) scale (Fig. 1.4). In the first part, the basic concepts of hazard and risk are

presented, together with principal information regarding the state-of-art and approaches in landslide hazard and risk studies. The glossary of principal terms is also shown in the Chapter 2. Afterwards, geographical, geological, and social settings of the study area are described, with a focus on features, which affect the debris flow occurrence, hazard and possible consequences (Chapter 3). An analysis of historical information about natural disasters in the study area is presented in Chapter 4. All available information about past hydrogeological disasters was gathered, stored, and analysed. This understanding of historical records is very important for the analysis of future possible damaging events and also crucial for the protection of people. This analysis showed, that landslides, and debris flows in particular, represent an important threat to local population and its assets. Description of the phenomena of debris flows is proposed in Chapter 5.

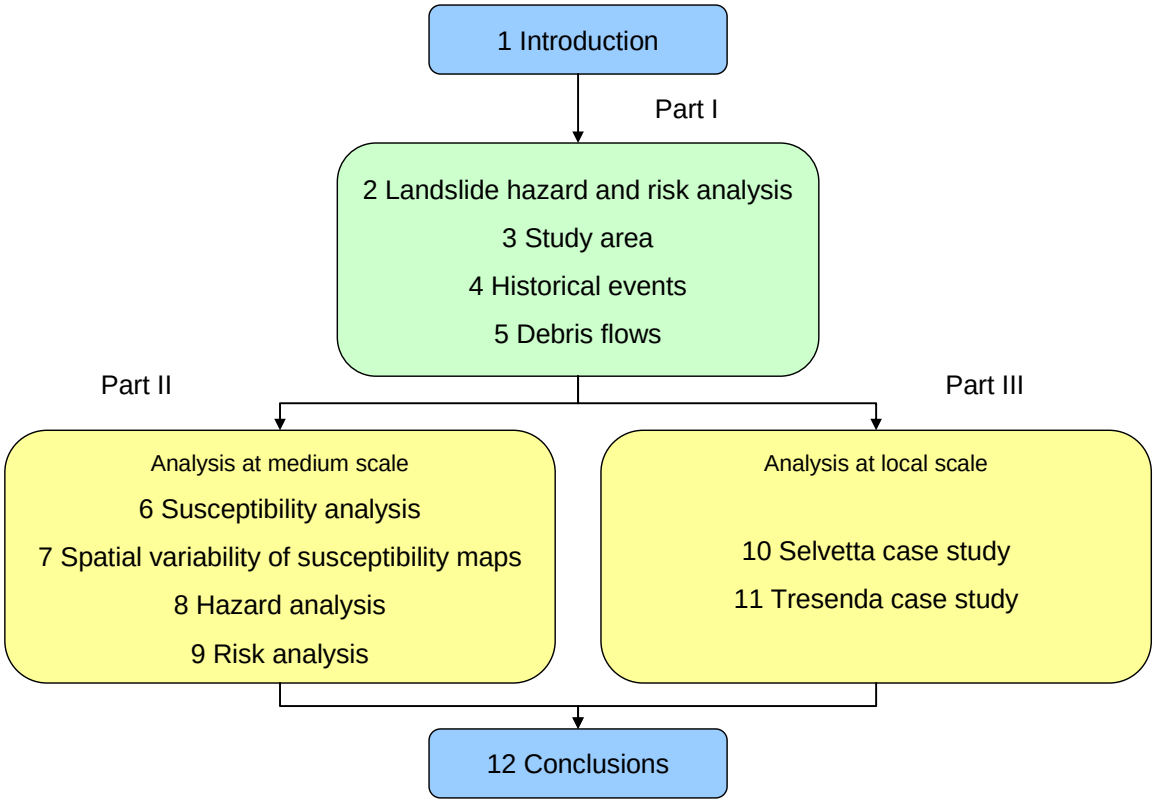

Fig. 1.4 – Structure of the Ph.D. thesis.

The second part of the thesis represents a study at a medium scale (1:25,000 – 1:50,000) using GIS software. This part begins with Chapter 6 focusing on debris flow susceptibility as one of the first steps that is being analysed in the process of hazard and risk assessment. A debris flow inventory was prepared using available information, aerial photographs, and DEM. Bi-variate statistical probabilistic technique Weights-of-Evidence (Bonham-Carter et al. 1988; Agterberg et al. 1989) was used to analyse possible future areas of debris flow sources, taking into account the basic assumption that “past is key to the future” (van Westen et al. 2008). In other words the future occurrence of debris flow sources can be explained by comparison of the past events (debris flow inventories) with thematic/factor maps (slope, aspect, landuse, geology, etc.)

Analysing the outcomes of the susceptibility analysis an interesting problem concerning the spatial variability arose. This interesting problem is investigated in Chapter 7, showing that standard model evaluation and validation techniques used give an important feedback in the sense of loss of spatial information. Possible approaches to overpass this problem are presented, using multi-variate statistical techniques: principal component analysis (PCA), cluster analysis (CA), and Kappa statistic.

Chapter 8 includes creation of debris flow hazard maps by incorporating the information about temporal probability and probable runout with the results from the susceptibility analysis. Empirical model DFGridProb (Horton et al. 2008) was used to model and to map areas of possible runout and deposition of debris flows. As a result of this study, quantitative hazard maps at medium scale were calculated.

Risk maps preparation is illustrated in Chapter 9. In this part, different approaches (quantitative and qualitative) used to create risk maps are described. Afterwards, the possible future direct economic losses were estimated using available official information about land and building values. Finally, risk curves summarizing these possible consequences were calculated.

Methods and models applied in the second part of the study are connected with medium (regional) scale. For that purpose, statistical and probabilistic techniques, together with empirical models, were used to analyse the susceptibility, spatial variability, and hazard and risk from debris flows. In case of the debris flow risk mapping, a qualitative "risk matrix" approach was also tested.

Third part of the thesis focuses at large scale (1:2,000 – 1:10,000) site-specific quantitative risk analysis. In this part, two case studies were investigated. Firstly, a debris flow event from July 2008 in Selvetta was examined in order to calculate vulnerability functions of buildings in relation to the intensity of the process (Chapter 10). Secondly, the obtained vulnerability functions were applied in a hypothetical debris flow scenario at Tresenda (Chapter 11). There, the quantitative risk scenarios were prepared and prospective direct losses were estimated. These scenarios also provide useful information for the civil protection purposes.

Models and maps were mostly produced using ESRI© software ArcGIS 9.2 with its specific extensions: Spatial Analyst, 3D Analyst and Spatial Data Modeler (Sawatzky et al. 2008). For the preparation of debris flow inventories, orthorectification and processing of the aerial photographs the ILWIS software (ITC 2009) was used. The runout calculation of the debris flows was made within a standalone version of DFGridProb software (Horton et al. 2008) programmed in MATLAB© programming language. At the local scale (Chapter 10 and 11) a two-dimensional hydraulic/hydrological model FLO-2D (2009) was used to prepare the debris flow hazard and risk scenarios.

1.3 References

Agterberg, F.P., Bonham-Carter, G.F., Wright, D.F. (1989): Weights of Evidence modelling: a new approach to mapping mineral potential. In: Agterberg, F.P., Bonham-Carter, G.F. (Eds.), Statistical Applications in the Earth Sciences. Geological Survey of Canada, Paper 89-9: 171-183.

Bonham-Carter, G.F., Agterberg, F.P., Wright, D.F. (1988): Integration of geological datasets for gold exploration in Nova Scotia. Photogrammetric Engineering 54: 1585-1592.

EM-DAT (2009): The OFDA/CRED International Disaster Database. Available at: http://www.emdat.be

FLO-2D (2009): Reference manual 2009. FLO-2D Software Inc., 73 p. Available at: http://www.flo-2d.com/wp-content/uploads/FLO-2D-Reference-Manual-2009.pdf

Guzzetti, F., Salvati, P., Stark, C.P. (2005): Evaluation of risk to population posed by natural hazards in Italy. In: Hungr, O., Fell, R., Couture, R., Eberhardt (Eds.): Landslide Risk Management. Taylor and Francis, London, pp. 381-389.

Horton, P., Jaboyedoff, M., Bardou E. (2008): Debris flow susceptibility mapping at a regional scale, Géorisques IV Geohazards: 4e Conférence canadienne sur les géorisques - 4th Canadian Conference on Geohazards, 20-24 mai 2008 Québec, Canada, 20-24 May 2008.

ITC (2009): ILWIS - Remote Sensing and GIS software: Integrated Land and Water Information System. Available at: http://www.itc.nl/Pub/Home/Research/Research_output/ILWIS_-_Remote_Sensing_and_GIS_software.html

Nadim, F., Kjekstad, O., Peduzzi, P., Herold, C., Jaedicke, C. (2006): Global landslide and avalanche hotspots. Landslides, 3: 159-173.

NRC (2004): Partnerships for Reducing Landslide Risk: Assessment of the National Landslide Hazards Mitigation Strategy. Committee on the Review of the National Landslide Hazards Mitigation Strategy, National Research Council. 144 p. Available at: http://www.nap.edu/catalog/10946.html

Reichenbach, P., Guzzetti, F., Cardinali, M. (1998): Carta delle aree colpite da movimenti franosi e da inondazioni – Progetto AVI, 2a edizione. CNR-IRPI, Perugia.

Sawatzky, D.L., Raines, G.L., Bonham-Carter, G.F., Looney, C.G. (2008): Spatial Data Modeller (SDM): ArcMAP 9.2 geoprocessing tools for spatial data modelling using weights of evidence, logistic regression, fuzzy logic and neural networks. Available at: http://arcscripts.esri.com/details.asp?dbid=15341

UNU (2006): Landslides. News release, United Nations University, Tokio, Japan, 6 p. Available at: http://www.ehs.unu.edu/file.php?id=81

Van Westen, C.J., Castellanos, E., Kuriakose, S.L. (2008): Spatial data for landslide susceptibility, hazard, and vulnerability assessment: An overview. Engineering Geology, 102: 112-131.

Chapter 2

Landslide hazard and risk

Is this the real life?
Is this just fantasy?
Caught in a landslide,
No escape from reality.

(Queen, Bohemian Rhapsody)

Based on:

Blahut, J., Klimeš, J. (2010): Contribution to the Czech terminology in landslide risk studies. Geografie – Sborník ČGS, 17 p. [in Czech]. (submitted, under review)

2.1 Introduction

In this chapter basic concepts of risk are presented together with its components. Difference between hazard and risk is outlined and other basic terms are presented in the glossary. State-of-art information of landslide hazard and risk analysis is presented as well.

2.2 Basic concepts of landslide risk

Term “hazard” has its origin in Arabic “al zahr”, which mean “dices”. From this word Spanish “azar” (play of chance) developed. This word consequently spread into English as “hazard” (Valášek 2005). The basic paradigm of hazard was postulated by Gilbert White in the 60´s (Gares et al. 1994). According to him, hazard is defined by seven parameters: magnitude, frequency, duration, dimension, speed of onset, spatial extent, and temporal distribution. As a consequence, hazard encompasses spatial and temporal probability of a potentially harmful phenomenon of certain magnitude and of certain intensity. Glade et al. (2005) define hazard as: “a potentially damaging process or situation (the landslide), or the probability of a potentially damaging event (a landslide) which is occurring in a unit of time, or the probability of occurrence of a given magnitude of event”. Defined in this way, hazard represents a state or condition and is assessed and applied to a particular place, for example site, unit area of land surface, region or object, lifelines, and so on.

Roots of the “risk” term come from the Ancient Greek “rhiza” (pitfall) and Arabic “al-rizq” (sudden prize, luck, or fatal turn-over). It also appeared in Moor Spanish as “arisco” and Ancient German as “arreschq”. In the 16th Century it changed into “risigio” as a precursor of the word “risiko”. After that, it appears in English as “risk” (Valášek 2005). Risk represents a hypothetical concept, which in case of realization becomes a disaster or catastrophe. Risk is thus defined as: “a measure of the probability and severity of loss to the elements at risk, usually expressed for a unit area, object, or activity, over a specified period of time” (Glade et al. 2005).

International terminology in landslide hazard and risk studies has undergo important development during last years. Many scientists tried to unify the terminology (AGS 2000; Glade et al. 2005; Tsotsos 2006), yet there still remain problems of different nomenclature. However, most of the approaches come out from the basic concept presented in 1979 in the United Nations Disaster Relief Organization (UNDRO 1979) in Geneva, Switzerland. The concept is represented by the “most difficult” simple equation:

$$R = H \times V \times E \tag{2.1}$$

or

$$R = H \times \Sigma (V \times E) \tag{2.2}$$

Where: R = risk; H = hazard; V = vulnerability, E = elements at risk. After UNDRO (1979), Varnes (1984), Alexander (1993).

Other approach – geotechnical or engineering geological presents for example Rozsypal (2009):

$$R = P \times D \tag{2.3}$$

Where: R = risk; P = probability; D = damage. Possible damage (outcomes) from the hazard is usually expressed in monetary value.

Fuchs et al. (2008) present a more complex equation developed from the technical concept of landslide risk analysis in Austria:

$$R_{i,j} = f(pS_i, AO_j, vO_j, S_i, pO_j, S_i) \tag{2.4}$$

Where: $R_{i,j}$ = risk; pS_i = probability of defined scenario; AO_j = value of elements at risk in defined scenario; vO_j,S_i = vulnerability of element at risk in a defined scenario; pO_j,S_i = probability of damage of element at risk j in a scenario i.

All of the definitions imply that risk is a result of the probability and intensity of hazard, value, and vulnerability of the elements at risk (Fig. 2.1). As a consequence, hazard analysis coupled with the consequence analysis, which is a part of the risk management framework (Fig. 2.2), results in risk analysis (for further readings see: Glade et al. 2005). In this thesis, the first equation (2.1) introduced by UNDRO (1979) is used, as it represents probably the most common characterization of risk in landslide risk studies.

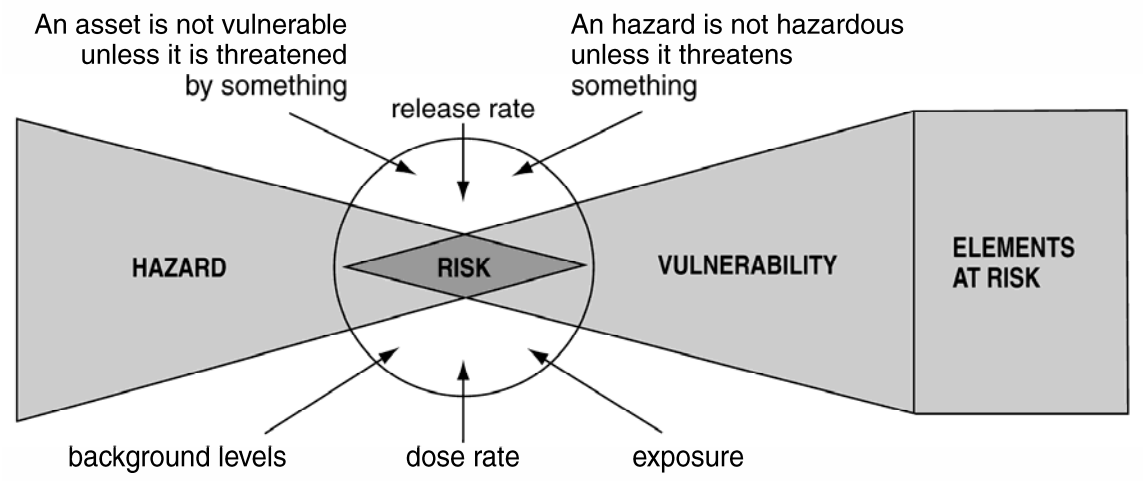

Fig. 2.1 – Conceptual relationship between hazard, elements at risk, vulnerability and risk.
Source: Glade et al. (2005) after Alexander (2002).

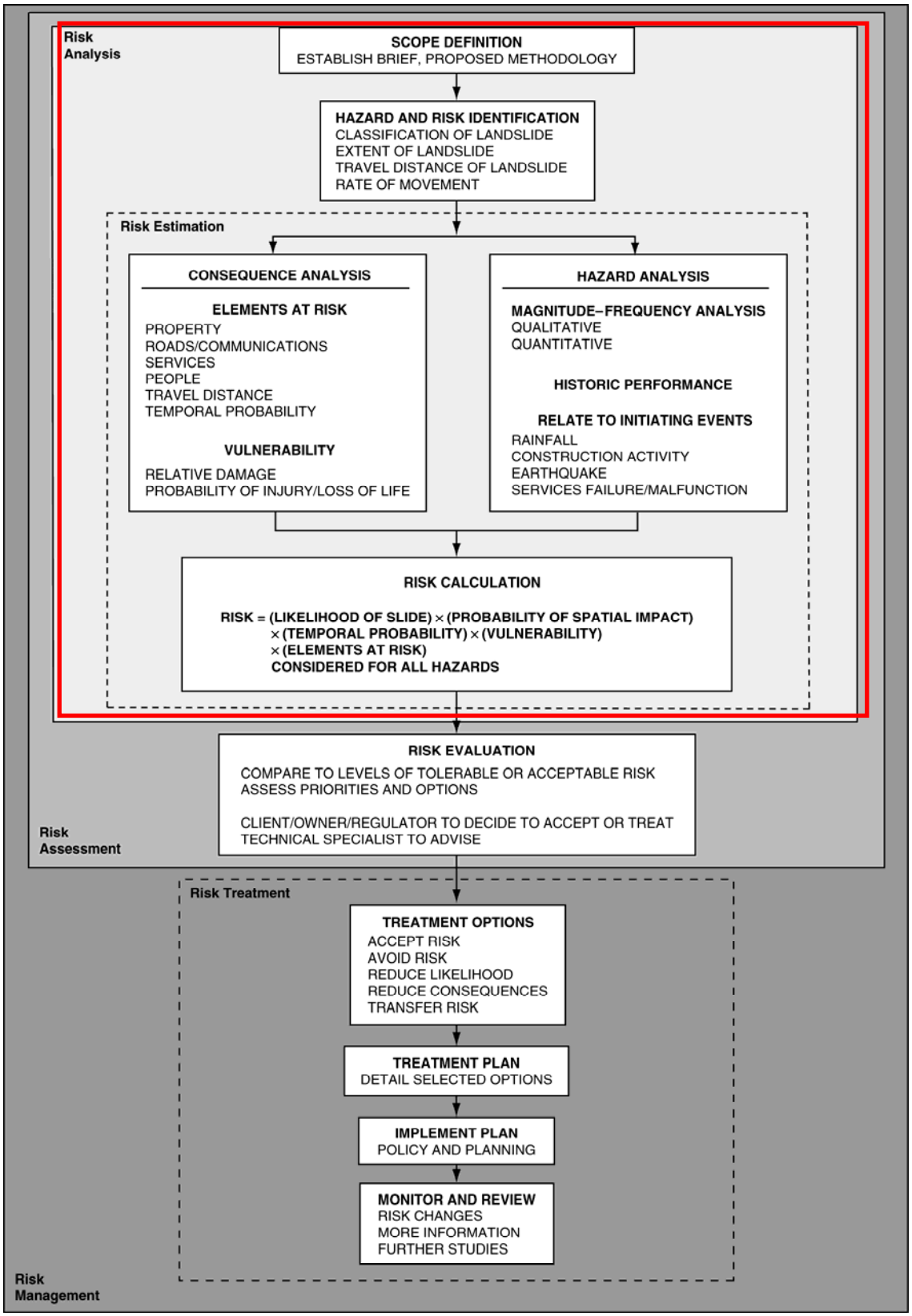

Fig. 2.2 – Flowchart showing all the stages involved in landslide risk management. Area of Ph.D. project interest is delimited by red rectangle. Source: Glade et al. (2005) after AGS (2000).

2.3 Landslide hazard analysis

Landslide hazard analysis is considered as one of the first steps of landslide risk management framework. Since exhaustive description of the landslide hazard analysis issues was already done by Glade et al. (2005), van Westen et al. (2007, 2008), and Castellanos Abella (2008), only brief explanation of this topic is presented here.

The main goal of hazard analysis is to help protect people and their assets by delimiting areas, where landslides can eventually occur. Ideally, hazard can be characterized by statements of "what", "where", "when", "how strong", and "how often" an event can happen (Crozier and Glade 2005). To achieve this aim, hazard analysis usually starts with identification of landslide types, which could pose a potential threat. Afterwards, depending on type and scale of the analysis, an appropriate approach must be chosen, taking into account available data and extent of the area of interest. The data inputs, model types and analyses scales are summarized in Fig. 2.3.

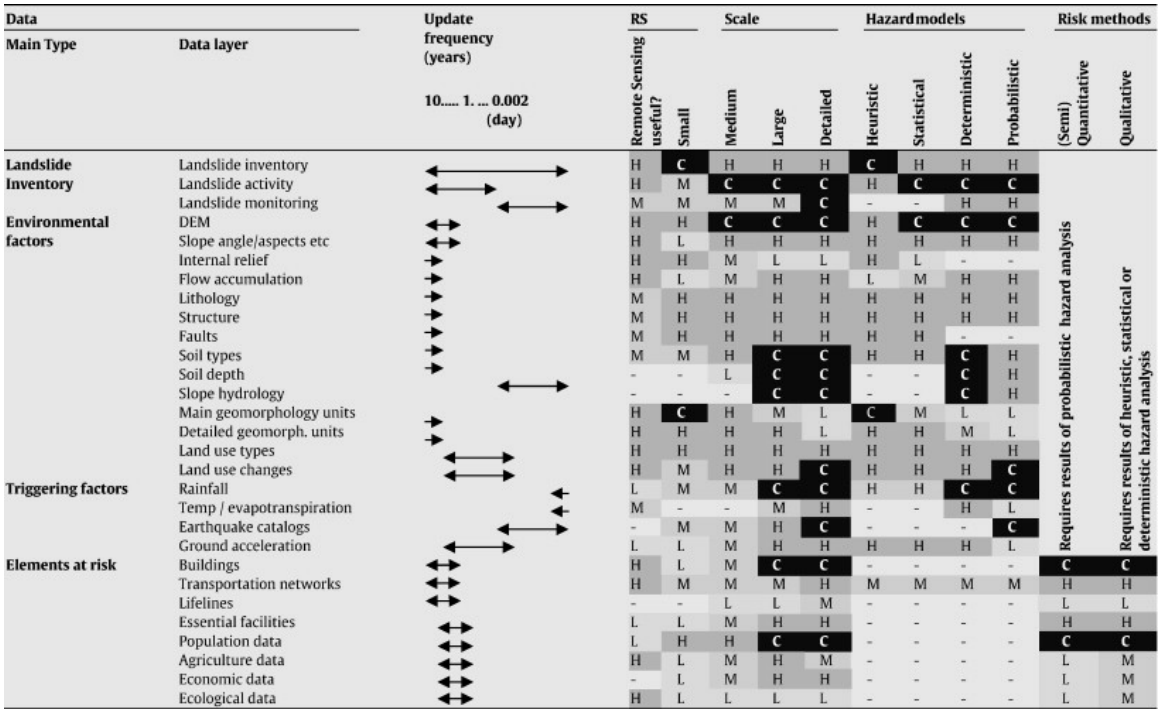

Fig. 2.3 – Relationships between data layers, working scales, and types of hazard modelling. Source: van Westen et al. (2008).

At small (national) scales (1:100,000 – 1:1,000,000), where large territory is analysed and not detailed data are available, usually a qualitative heuristic analysis is performed. The approach is usually based on determining the main well-known factors contributing to landslide hazard (landslide inventories, presence of landslide-prone geological units, presence of high slopes, etc...).

At medium (regional) scales (1:25,000 – 1:50,000), where more data are available (DEM, geological and soil maps, structural map, etc…), statistical analysis is usually performed. At this working scale known presence of landslides is compared to explanatory

variables (slope, aspect, internal relief, landuse) and found relationships are analysed by bi-variate or multi-variate statistical techniques. The results could be interpreted in a qualitative, semi-quantitative or quantitative way. However, quantitative approaches are preferred, even though they may contain errors due to the limited information.

At local (detailed) scales (1:2,000 – 1:10,000), usually deterministic and probabilistic analyses are carried out. Detailed scale and small area extent allows to collect enough data to create deterministic physical models and verify the stability of slopes and potential hazards in a quantitative way.

Nowadays, most of the hazard analyses are carried out at local site-specific scales, driven by engineering and geotechnical projects (Crozier and Glade 2005), while probably one of the main goals in landslide hazard analysis is to perform quantitative study at a medium, or even small scale.

The hazard analysis usually starts with the determination of landslide susceptibility, when areas where landslides may occur, are delimited. Afterwards, magnitude and frequency relationships are analysed in order to determine potential size and temporal probability of landslides. Sometimes, triggering threshold analysis is carried out in order to determine probability of triggering factors, such as rainfalls and earthquakes, which may lead to landslide initiation. The methods applied in this thesis are more thoroughly discussed in the following chapters, dealing with susceptibility and hazard analysis.

2.4 Landslide risk analysis

As already stated, landslide risk analysis couples the hazard and consequence analyses. Landslide risk could be calculated in qualitative, semi-quantitative, and quantitative way.

Qualitative approaches are based on experience of experts and the risk areas are categorized with terms as “very high”, “high”, “moderate”, “low”, and “very low” risk (Castellanos Abella 2008). To classify risk areas, risk matrices are usually used (Fig. 2.4). In those matrices the hazard probability (likelihood) is plotted against the possible consequences (impact) to obtain risk classes.

A semi-quantitative risk analysis approach basically assigns weights to expert-based estimates to obtain numerical values of risk. As a result, rankings are obtained and they represent the risk in a numerical way.

Quantitative risk analysis or assessment (QRA) is based on quantitative estimation of outcomes from landslide hazard and vulnerability studies. Several different approaches for quantitative risk analysis and estimation exist (Castellanos Abella 2008). However, they are usually based on the probability of a hazard multiplied by the vulnerability of the elements at risk multiplied by the value of the elements at risk. Total risk is expressed as a sum of all specific risks in a particular place/area and it could be plotted against the probabilities of occurrence in order to obtain a risk curve. Specific risk is the probability of losses for a particular asset (building, road) and/or for particular hazard type. Quantifications of total and specific risk can be used for cost-benefit analyses in the integrated risk management framework.

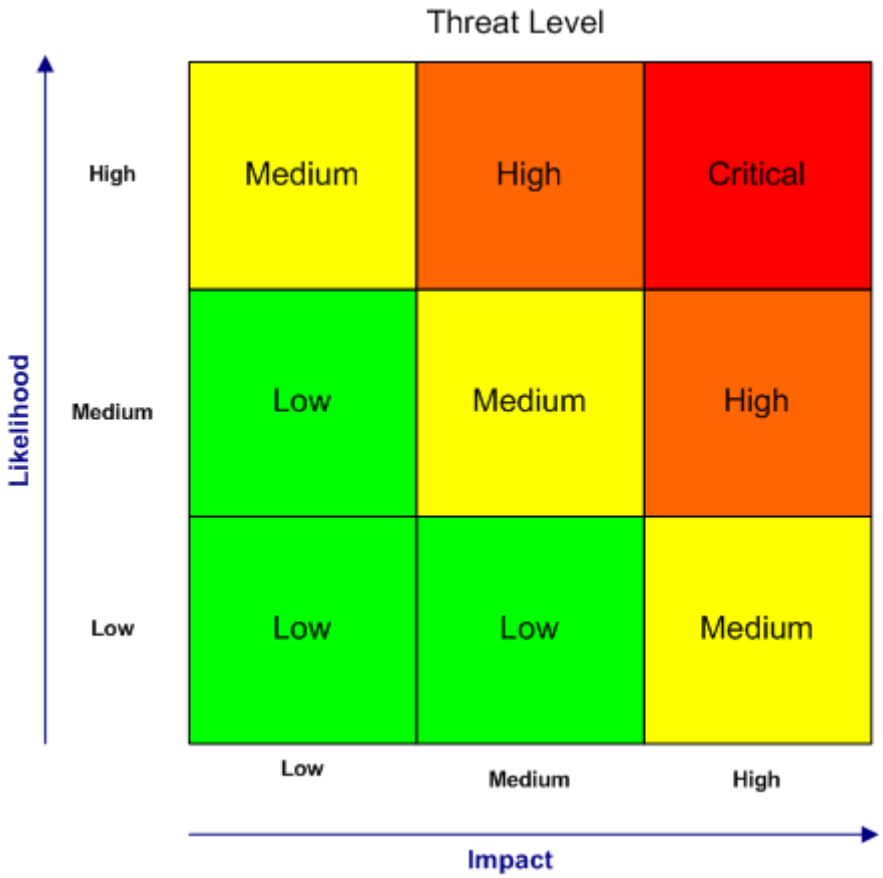

Fig. 2.4 – Example of a matrix used for qualitative risk estimation.
Source: http://www.charityvillage.com/cv/research/rom18.html

2.4.1 Consequence analysis

The consequence analysis deals with evaluation of hazard outcomes on the elements at risk. Elements at risk are represented by people, buildings, lifelines, infrastructure, as well as the environment and economic activities which could be affected by a damaging event. Consequences from landslide hazard could be expressed as potential costs. These costs can be distinguished as direct and indirect losses, and tangible and intangible losses. Direct costs are the repair, replacement, or maintenance resulting from damage to property or installations. All other costs of landslides are indirect (Schuster 1996). Indirect costs are the following (after Schuster 1996):

- Loss of industrial, agricultural, and forest productivity as a result of interruption of transportation systems.
- Reduction of real estate values.
- Loss of tax revenues.
- Preventive and mitigation measures.
- Adverse effects on water and landscape quality.
- Loss of human and animal productivity.

Losses induced by a landslide hazard are usually only estimated as direct costs. However, large amount of old and recent studies focused on landslide consequences (Rybář and Stemberk 1994; Giacomelli 2005; Sterlacchini et al. 2007) show that indirect costs can be comparable or even higher than direct costs. For example, a blockage of road or interruption of a power line could have low direct costs. However, indirect costs like interruption of people transport and goods flows can reach much higher values than the direct damage.

Physical losses from landslides in Italy can be distinguished among structural, functional, and aesthetic (Cardinali et al. 2002). The structural losses represent physical damage of the building or infrastructure, needed to be reconstructed or replaced. The functional losses represent only temporal limitation of usage and aesthetic losses that change the visual state of an asset.

In many cases, the expression of consequences in monetary values is quite problematic as it encompasses also hardly calculable or incalculable damage (intangible losses), such as landscape or environmental damage, psychological and social losses.

2.4.2 Vulnerability analysis

Vulnerability analysis represents probably the biggest gap in landslide risk studies. This situation is caused mainly by the need of interdisciplinary approach in the study. Vulnerability is described as hypothetical loss depending on consequences of landslide (Lewis 1999). But it also depends on the current state and development level of society facing the landslide hazard. It could be also defined as a condition and evolution of physical, social, economic and environmental factors which increase the susceptibility of society to landslide hazard.

Nathan (2005) differentiates physical, legal, institutional, technical, political, socioeconomic, psychological, and cultural vulnerability. In landslide risk quantification, the physical vulnerability is usually calculated. It corresponds to a potential loss of elements at risk depending on intensity of hazard and state of the assets. Physical vulnerability is expressed on a scale from 0 (no loss) to 1 (total destruction), which correspond to the percentage of future loss on a building or infrastructure. Physical vulnerability is a function of construction materials and techniques, maintenance, presence of early warning systems and mitigation measures and, obviously, the intensity of the damaging event (Fell 1994; Fell and Hartford 1997). Physical vulnerability is usually expressed by a vulnerability function, which plots process intensity (velocity, height of accumulation, etc.) against the possible degree of loss (from 0 to 1).

2.5 Assumptions and uncertainties

During landslide risk analysis, several assumptions have to be made regarding the scale and extent of the work. One of the basic assumptions in landslide hazard analysis is that conditions that lead to landslides in the past will cause landslides in the future. This “present is key to the future” assumption is widely assumed, however in the times of global and regional environmental changes, this assumption starts to be questionable.

Other uncertainties are connected with the resolution and precision of input data. Generally, at a more site-specific scale, precision and resolution of information increase. Nevertheless, the costs to obtain more precise information increase as well. For that reason, an appropriate selection of analysis approaches is crucial.

Uncertainties connected with the estimation of values of elements at risk are probably much lower that those connected with extrapolation of information from one study site to other areas. However, correct use of values (construction × market values) is important in the final risk estimation.

One of the possibilities to deal with uncertainties is to express the final risk probabilities in a qualitative way. This is probably more interpretable by the end-user, although it may lead to some loss of information.

It has to be noted that uncertainty increases with each step of the risk analysis. As a consequence, final results have high value of uncertainty and have to be handled carefully in order to avoid important mistakes.

2.6 Glossary

Presented glossary is based on studies of UNDP (1994, 2004), Cruden and Varnes (1996), Dikau et al. (1996), AGS (2000), Alexander (2002), UN/ISDR (2004), Glade et al. (2005), and Fell et al. (2005). This glossary is also available in extended form at: http://mountain-risks.eu/. Principal terms of landslide hazard and risk are presented together with other basic terms related to risk studies.

Acceptable risk:

A risk which everyone impacted is prepared to accept. Action to further reduce such risk is usually not required unless reasonably practicable measures are available at low cost in terms of money, time and effort.

Alarm:

A visible or audible signal giving warning of danger.

ALARP (As Low As Reasonably Practicable) principle:

That principle which states that risks, lower than the limit of tolerability, are tolerable only if risk reduction is impracticable or if its cost is grossly in disproportion (depending on the level of risk) to the improvement gained.

Alert:

Advisory that hazard is approaching and that places emergency forces on standby, pending mobilization, but is less imminent than implied by warning message (see warning).

Assessment:

The process of determining the impact of a disaster or events on a society, the needs for immediate, emergency measures to save and sustain the lives of survivors, and the possibilities for expediting recovery and development. Assessment is an interdisciplinary process undertaken in phases and involving on-the-spot surveys and the collation, evaluation and interpretation of

information from various sources concerning both direct and indirect losses, short- and long-term effects. It involves determining not only what has happened and what assistance might be needed, but also defining objectives and how relevant assistance can actually be provided to the victims. It requires attention to both short-term needs and long-term implications.

Background levels (of risk):

In risk analysis, inherent natural or normal levels of risk in addition to risk from any specific factor.

Bayes theorem:

A theorem, which provides the logical basis for updating a probability on the basis of new information.

Casualty:

Death or injury (mortality or morbidity) in disaster. Injury can be divided into physical trauma (e.g. fracture bones) and psychological trauma (e.g. post-traumatic stress disorder).

Catastrophe:

A catastrophe is more cataclysmic than a disaster and affects a larger area. Jurisdictions affected by catastrophe are more thoroughly overwhelmed by it that they would be in the case of a mere disaster.

Civil defence:

The progenitor of civil protection. The system of measures, usually run by a government agency, to protect the civilian population in war time, to respond to disasters, and to prevent and mitigate the consequences of major emergencies in peacetime. The term 'civil defence' is now often referred to as emergency management

Civil protection:

The process of protecting the general public, organizations, institutions, commerce and industry against disaster, by creating an operational structure for mitigation, preparedness, response and recovery. Military forces do not play a central role in civil protection, which is in the hands of administrative authorities, such as municipal, provincial, state or national governments.

Conditional probability:

The probability of an outcome, given the occurrence of some event. For example, given that a flood has reached the crest of an embankment dam, the probability of the dam failing is a conditional probability.

Consequence:

In relation to risk analysis, the outcome or result of an event expressed qualitatively or quantitatively, being a loss, injury, disadvantage or gain. There may be a range of possible outcomes associated with an event.

Consequence analysis:

Sometimes referred to as risk identification, the identification of elements at risk, their vulnerability and the type of impact or loss expected from a given hazard or hazards and dependent initially on hazard identification.

Cost (of event, situation or activities):

The negative impacts: these may be extend beyond damage and losses and may or not be quantifiable, both direct and indirect, including damage , time, labour, disruption, goodwill, political and intangible losses etc. Whereas losses refer to negative effects to existing resources, costs refer to adverse effects that go beyond existing use.

Cost-benefit-analysis:

Assessment and comparison of the costs and benefits associated with an activity or proposed activity. For example, a comparison of the costs of establishing slope stability measures compared to the accrued economic benefits of being able to occupy that place as a result of the achieved reduction of landslide risk.

Cost-effectiveness:

A measure of efficacy obtained by quantifying the costs and benefits of an activity and comparing them in cost-benfit-ratio. Cost-effectiveness does not necessarily require a predominance of benefits over costs, nor can all benefits always be quantified as readily as costs can.

Countermeasures:

All measures taken to counter and reduce a hazard or consequences of a hazard. They most commonly refer to engineering (structural) measures but can also include other non-structural measures and tools designed and employed to avoid or limit the adverse impact of natural hazards and related environmental and technological disasters.

Crisis:

In disaster, a point at which normal mechanisms for coping (personal, organization or institutional) suddenly cease to function as a result of the seriousness of the impact.

Damage assessment:

Investigation of damaged property and quantification of the value of losses. Monetary estimates usually depend on the cost of repairing the damage, which in turn depends on the adoption of particular techniques and components whose values are known.

Damage classification:

Evaluation and recording of damage structures, facilities, or objects according to different categories.

Damage ratio:

The cost of damage expressed as a ratio of the total value of the object damaged during an event. When referred to a given magnitude of event, this ratio represents vulnerability.

Danger (Threat):

The natural phenomenon that could lead to damage, described in terms of its geometry, mechanical and other characteristics. The danger can be an existing one (such as a creeping slope) or a potential one (such as a rockfall). The characterisation of a danger or threat does not include any forecasting.

Debris flow:

A sediment transport of a mixture of fine material (sand, silt and clay), coarse material (gravel and boulders), with a variable quantity of water, that forms a muddy or a coarse slurry which move downvalley in a series of surge with steep fronts mostly made of large boulders.

Three distinctive elements are distinguishable in a debris flow: the source area (triggering), the main track (runout), and the depositional toe (deposition). Triggering mechanisms of debris flows are frequently related to an increase in pore pressures due to high-intensity rainfall events or rapid snowmelt.

Decision-maker:

The person or organizational unit who decides on a course of action in relation safety.

Declaration of disaster:

Official issuance of a state of emergency upon the occurrence of a large-scale calamity, in order to activate measures aimed at the reduction of the disaster's impact.

Disaster:

A serious disruption of the functioning of a community or a society causing widespread human, material, economic or environmental losses which exceed the ability of the affected community or society to cope using its own resources. A disaster results from the combination of hazards, vulnerability, and insufficient capacity or measures to reduce the negative consequences of risk. Disaster is sometimes also used to describe a catastrophic situation in which the normal patterns of life (or eco-systems) have been disrupted and extraordinary, emergency interventions are required to save and preserve human lives and/or the environment. Disasters are frequently categorized according to their perceived causes and speed of impact.

Disaster insurance:

Government-sponsored or private insurance policies for protection against economic losses resulting from disaster.

Disaster legislation:

The body of laws and regulations that governs and designates responsibility for disaster management concerning the various phases of disaster.

Disaster management:

A collective term encompassing all aspects of planning for and responding to disasters, including both pre- and post-disaster activities. It refers to the management of both the risks and the consequences of disasters.

Disaster mitigation:

A collective term used to encompass all activities undertaken in anticipation of the occurrence of a potentially disastrous event, including preparedness and long-term risk reduction measures. The process of planning and implementing measures to reduce the risks associated with known natural and man-made hazards and to deal with disasters which do occur. Strategies and specific measures are designed on the basis of risk assessments and political decisions concerning the levels of risk which are considered to be acceptable and the resources to be allocated (by the national and sub-national authorities and external donors). Mitigation has been used by some institutions/ authors in a narrower sense, excluding preparedness.

Disaster preparedness:

Measures that ensure the readiness and ability of a society to (a) forecast and take precautionary measures in advance of an imminent threat (in cases where advance warnings are possible), and (b) respond to and cope with the effects of a disaster by organizing and delivering timely and effective rescue, relief and other appropriate post-disaster assistance.

Disaster response:

A sum of decisions and actions taken during and after disaster, including immediate relief, rehabilitation and reconstruction.

Drainage basin:

(syn. catchments, river basin, watershed) Area having a common outlet for its runoff.

Earthflow:

A mass movement characterized by downslope translation by flowage of fine surficial materials, such as regolith or soil.

Elements at risk:

Population, buildings and engineering works, infrastructure, environmental features and economic activities in the area affected by a hazard.

Emergency:

An imminent or actual event that threatens people, property or the environment and which requires a coordinated and rapid response to minimize its adverse consequences. Emergencies are usually unforeseen and unanticipated, even though they can, and should be planned for. It is implicit that the consequences of ignoring an emergency or not dealing with it properly are avoidable casualties or damage.

Emergency management:

(see also civil defence) Short-term measures taken to respond to particular hazards, risks, incidents, or disasters. Resources and manpower pertaining to government, voluntary and private agencies are organized and directed on the basis of a plan that anticipates needs and coordinates efforts by assigning to particular responders, organizations of field units.

Emergency mapping:

The cartographic depiction of selected aspects of disaster impact or the subsequent emergency relief effort. As the situation can change rapidly because of increases in the knowledge of damage and casualties, or to developments in the relief effort, there is a certain imperative to emergency mapping. It is therefore best carried out using computers with programs, such as geographical information systems, that produce refresher graphics.

Emergency planning:

Planning of actions for the case of a disaster, training of special teams and of population, contingency planning, testing of disaster scenario.

Emergency preparedness plan:

Document which contains procedures for dealing with various emergencies which could result from a disaster.

Erosion:

Localized removal of rock or soil as a result of the action of water, ice, wind; coastal processes or mass movement.

Evacuation:

Precautionary, temporary, planned removal of people or moveable items that, if left in place, would result in avoidable casualties or damage.

Evaluation:

(post-disaster) Appraisal of all aspects of the disaster and its effects.

Event:

An incident or situation, which occurs in a particular place during a particular interval of time.

Expected losses/effects:

The expected number of lives lost, persons injured, damage to property and disruption of essential services and economic activity due to the impact of a particular natural or man-made hazard. It includes physical, social/functional and economic effects.

Exposure:

The length or proportion of time that a person, building or other entity runs a risk. Fixed capital (e.g. houses, bridge, factories) permanently varies the proportion and intensity of exposure. Routine behaviour problems also cause exposure to vary. For example, if the principal risk arises from the collapse of bridges during a landslide, people will be most exposed to it during daily commuting to or from on other forms of regular journey.

Extreme event:

Event, which has a very low annual excedance probability (AEP). Sometimes defined as an event beyond the credible limit of extrapolation and therefore dependent on the length of record and the quality of the data available.

F, N pairs:

Refers to f, the probability of life loss due to failure for each scenario studied, and N, the number of lives expected to be lost in the event of such a failure scenario. The term N can be replaced by any other quantitative measure of failure consequences, such as monetary measures.

F-N curves:

Curves relating the probability per year of causing N or more fatalities (F) to N. This is the complementary cumulative distribution function. Such curves may be used to express societal risk criteria and to describe the safety levels of particular facilities.

Failure:

The inability of a system, or part thereof, to function as intended. In the context of structural safety (including geotechnical structures), failure is generally confined to issues of structural integrity, and in some contexts to the special case of collapse of the structure or some part of it.

Fault:

A planar or gently curved fracture in the earth's upper layers across which displacement occurs. When this displacement is abrupt it gives rise to an earthquake.

Floods:

The most frequent and costly natural disasters in terms of human hardship and economic loss. As much as 90 percent of the damage related to all natural disasters (excluding droughts) is caused by floods. Flooding occurs in known floodplains when prolonged rainfall over several days, intense rainfall over a short period of time, or an ice or debris jam causes a river or stream to overflow and flood the surrounding area. Melting snow can combine with rain in the winter and early spring; severe thunderstorms can bring heavy rain in the spring and summer; or tropical cyclones can bring intense rainfall to the coastal and inland states in the

summer and fall. Several factors contribute to flooding. Two key elements are rainfall intensity and duration.

Forecast:

Statement or statistical estimate of the occurrence of a future event. This term is used with different meanings in different disciplines (see prediction). A forecast is often considered to represent the most rigorous form of prediction by stating, for the occurrence, what will occur, as well as the time and place of occurrence. Lesser forms of prediction may simply provide a probability of occurrence.

Fragility curve:

Defines the probability of failure as a function of an applied load level; a particular form of the more general system response.

Frequency:

A measure of likelihood expressed as the number of occurrences of an event in a given time or in a given number of trials (see also likelihood and probability).

Groundwater level:

The level at which soil and porous rock begins to be saturated with water. Usually measured as a depth below the ground surface or as a depth above a defined level, such as a shear surface.

Hazard:

Probability that a particular danger (threat) occurs within a given period of time. A rare or extreme event in the natural or man-made environment, that adversely affects human life, property or activity to the extent of causing disaster. A hazard is a natural or man-made phenomenon which may cause physical damage, economic losses, or threaten human life and well-being if it occurs in an area of human settlement, agricultural, or industrial activity. Note, however, that in engineering, the term is used in a more specific, mathematical sense to mean the probability of the occurrence, within a specified period of time and a given area, of a particular, potentially damaging phenomenon of a given severity/intensity.

Hazard Analysis:

Hazard analysis takes the outcomes of susceptibility analysis, and assigns an estimated frequency (annual probability) to the potential hazardous events. This may be expressed as the frequency of a particular type of event of a certain volume, or events of a particular type, volume and velocity (which may vary with distance from the source), or in some cases as the frequency of events with a particular intensity, where intensity may be measures in kinetic energy terms. The latter is most useful for rock falls.

Hazard assessment:

(Sometimes Hazard Analysis/Evaluation) The process of estimating, for defined areas, the probabilities of the occurrence of potentially damaging phenomenon of given magnitudes within a specified period of time. Hazard assessment involves analysis of formal and informal historical records, and skilled interpretation of existing topographical, geological, geomorphological, hydrological, and land-use maps.

Hazard estimation:

The process of identifying the probability of occurrence of a damaging event.

Hazard identification:

The process of recognizing and accounting for all possible hazards that might occur within the place and time period of interest. For landslides this involves identifying landslide type, landslide impact characteristics and consequential landslide hazards. The process needs to consider the types of element at risk as well the relationship in time and space between landslides and elements at risk. In the overall process of risk assessment, hazard identification and consequence analysis are interdependent should be carried out simultaneously.

Hazard mapping:

The process of establishing geographically where and to what extent particular phenomena are likely to pose a threat to people, property, infrastructure, and economic activities. Hazard mapping represents the result of hazard assessment on a map, showing the frequency/probability of occurrences of various magnitudes or durations.

Incidence:

The number of specified occurrences in a given place in a period of time.

Individual risk to life:

The increment of risk imposed on a particular individual by the existence of a hazard. This increment of risk is an addition to the background risk to life, which the person would live with on a daily basis if the facility did not exist.

Intensity of disaster impact:

In broad terms, number of deaths, physical and psychological injuries, and people rendered homeless by the disaster; scope of destruction and damage; effect on industrial and commercial productivity, and on employment; effect on human activities, and scale of donations, extra taxation and other financial reparations.

Involuntary risk:

A risk imposed on people by a controlling body and not assumed by free choice of the people at risk. It has occasionally been defined to include post disaster response, then being equivalent to disaster management, as defined in this glossary.

Joint probability:

The probability that two or more variables will assume certain values simultaneously or within particular time intervals.

Judgement:

Contribution to decision-making which depends on a person s experience, technical know-how, and ethical or moral values. Landslide hazard represents the expectation of future landslide occurrence based on the existing conditions of an area. Land use change (i.e. forest fires, forest logging, and development activities) and changes in the rate of occurrence of the triggering factors (i.e. climate change) may require new hazard assessment of the particular area.

Land-use (urban) planning:

Branch of physical planning that determines the means and assesses the values or limitations of various options in which land (urban area) is to be utilised, with the corresponding effects on different segments of the population or interests of a community taken into account in resulting decisions.

Landslide:

Downward or outward movement of slope (mass of rock, earth (soil) or debris) under the influence of gravity. Some authors prefer the term of 'mass movement'. There are numerous classifications within the landslide literature considering various factors as mechanism, morphology, type of material or rate of movement: fall, topple, slide (rotational), slide (translational), lateral spreading, flow … Land-use planning can help to mitigate disasters and reduce risks by discouraging settlements and construction of key installations in hazard prone areas, control of population density and expansion, and in the setting of life lines such as service routes for transport, power, water, sewage and other critical facilities. Land-use planning involves mapping, analysis of data acquired, formulation of alternative land-use decisions and design of a long-range plan for different geographical and administrative scales.

Landslide hazard:

The probability of occurrence within a specific period of time and within a given area of a potentially damaging phenomenon. More specifically, landslide hazard expresses the annual probability of occurrence of a class of landslide (e.g. rock fall) of a given size which may occur in or travel or retrogress into the hazard class area. Quantifying hazard may also require the estimation of the velocity or intensity of the potential landsliding. Landslide hazard may be expressed in several ways: the number of landslides per annum per unit area of the hazard class area or per unit length of the source area (e.g. for a cliff or for road cuttings or fills), or the annual probability that landsliding will occur to affect a point within the hazard class area.

Landslide risk:

(a) For life loss, the annual probability that the person most at risk in the risk zone will lose his on her life taking account of the landslide hazard, and the temporal spatial probability and vulnerability of the person. (b) For property loss, the annual probability of the consequence (e.g. a 0.001 probability/annum of damage) or the annualised loss (e.g. /annum) taking account of the elements at risk, their temporal spatial probability and vulnerability.

Landslide susceptibility:

The propensity of the terrain to produce a slope failure or that a landslide may travel onto or retrogress into it. For an existing landslide, susceptibility expresses its capability to reactive. Susceptibility may also include a description of the magnitude (volume) of the potential or existing landslide and the state of activity.

Lifelines:

Vital communications and essential services that are liable to be compromised in disaster. They include the transportation networks along which emergency vehicles and evacuees will travel; main utility corridors for the distribution of electricity and water, and the medical assistance infrastructure.

Likelihood:

Conditional probability of an outcome given a set of data, assumptions and information. Also used as a qualitative description of probability and frequency (Fell et al., 2005).

Loss:

Any negative consequence, financial or otherwise; a reduction in the value of pre-existing resources (part of the costs experienced as the result of a hazard occurrence).

Mass movement:

A general term for the outward and downward movement of slope-forming material under the influence of gravity, without the assistance of water as a transport agent. Mass movement includes abrupt movements such as landslides, as well as slower, more widespread movements such as creep and subsidence.

Mass wasting:

A general term for the reduction of the mass of landforms by downslope transport of soil and rock material brought about by slope processes including mass movement, fluvial, pluvial and wind action.

Mean return period:

The average time between occurrences of a particular hazardous event.

Mitigation:

Measures undertaken to limit the adverse impact of, for instance, natural hazards, environmental degradation and technological hazards.

Monitor:

To check, supervise, observe critically, or record the progress of an activity, action or system on a regular basis in order to identify change.

Mudflow:

The rapid and localized downslope transfer of fine earth material mixed with water.

Natural hazard:

Natural phenomena which occur in proximity and pose a threat to people, structures or economic assets and may cause disaster. They are caused by biological, geological, seismic, hydrological, or meteorological conditions or processes in the natural environment.

Non-structural elements:

Those part of a building (e.g. partitions, ceilings, etc.) that do not belong to the load-bearing system.

Non-structural measures:

Actions taken to reduce risk that do not directly involve physical, engineering, or technical measures. For example, land use and building regulations, disaster legislation, public education and information, disaster insurance.

Non-structural mitigation:

Measures used to reduce the impact of future disasters without the use of engineering or architectural techniques. Non-structural mitigation includes insurance coverage, land use and planning measures, and emergency management.

Nowcast:

A description of a current situation, e.g. weather over a short-period (0-2 hours) forecast.

Owner:

Legal entity which either holds a government license to operate a facility or retains the legal property title on the facility, and which is responsible for the safety of the facility.

Population at risk:

All those persons who would be directly exposed to the consequences of failure of a structure or facility if they did not evacuate.

Precondition factors (stability):

Inherent factors (usually static) that are necessary but not sufficient for causing a slope to fail.

Prediction:

A statement to the effect that a particular impact will occur in a particular area, with a particular magnitude and set of effects, during a particular time interval. Predictions are the responsibility of bona fide scientists and are usually given in a probabilistic terms. The word is virtually synonymous but not as definitive as forecast.

Predictor:

A variable or index compiled from several elements, which is known (often empirically) to be highly correlated with a quantity which is to be forecast and is used to forecast it.

Preparatory factors (stability):

Factors (usually dynamic) that reduce the margin of stability of a slope without actually causing failure. Preparedness involves the development and regular testing of warning systems (linked to forecasting systems) and plans for evacuation or other measures to be taken during a disaster alert period to minimize potential loss of life and physical damage; the education and training of officials and the population at risk; the establishment of policies, standards, organizational arrangements and operational plans to be applied following a disaster impact; the securing of resources (possibly including the stockpiling of supplies and the earmarking of funds); and the training of intervention teams. It must be supported by enabling legislation.

Preparedness:

Activities and measures taken in advance to ensure effective response to hazards and their consequences.

Prevention:

Activities to provide outright avoidance of the hazards and their consequences.

Probabilistic:

A description of procedures, which are based on the application of the laws of probability. Contrasts with deterministic.

Probability:

A measure of the degree of certainty. This measure has a value between zero (impossibility) and 1.0 (certainty). It is an estimate of the likelihood of the magnitude of the uncertain quantity, or the likelihood of the occurrence of the uncertain future event. There are two main interpretations: i) Statistical - frequency or fraction – The outcome of a repetitive experiment of some kind like flipping coins. It includes also the idea of population variability. Such a number is called an objective or relative frequent probability because it exists in the real world and is in principle measurable by doing the experiment; ii) Subjective probability (degree of belief) – Quantified measure of belief, judgement, or confidence in the likelihood of an outcome, obtained by considering all available information honestly, fairly, and with a

minimum of bias. Subjective probability is affected by the state of understanding of a process, judgement regarding an evaluation, or the quality and quantity of information. It may change over time as the state of knowledge changes.

Qualitative approach:

A method by which information is analysed and evaluated verbally, with argument based on judgement and logic.

Quantitative approach:

A method by which information is recorded, analysed and evaluated using numerical scales and techniques.

Random variable:

A quantity, the magnitude of which is not exactly fixed, but rather the quantity may assume any of a number of values described by a probability distribution.

Regulatory agency (synonymous with Regulator):

Usually a government ministry, department, office, directorate or other unit of government entrusted by law or administrative act with the responsibility for the general supervision of the safe design, construction and operations of structures or facilities, as well as any entity to which all or part of the executive or operational tasks and functions have been delegated by legal power.

Reliability:

Likelihood of successful performance of a given project element. Mathematically, Reliability = 1 - Probability of failure. See definitions of probability and failure.

Remote sensing:

The observation and/or study of an area, object or phenomenon from an aerial distance, frequently using data collected by satellite.

Residual risk:

The remaining level of risk at anytime before, during and after a program of risk mitigation measures has been taken.

Risk:

Measure of the probability and severity of an adverse effect to life, health, property, or the environment. Quantitatively, Risk = Hazard Potential Worth of Loss. This can be also expressed as Probability of an adverse event times the consequences if the event occurs.

Risk acceptance:

An informed decision to accept the consequences and the likelihood of a particular risk.

Risk analysis:

The use of available information to estimate the risk to individuals or populations, property or the environment, from hazards. Risk analyses generally contain the following steps: definition of scope, danger (threat) identification, estimation of probability of occurrence to estimate hazard, evaluation of the vulnerability of the element(s) at risk, consequence identification, and risk estimation. Consistent with the common dictionary definition of analysis. A detailed examination of anything complex made in order to understand its nature or to determine its essential features, risk analysis involves the desegregation or decomposition of the system and sources of risk into their fundamental parts. Qualitative risk analysis is the

analysis which uses word form, descriptive or numeric rating scales to describe the magnitude of potential consequences and the likelihood that those consequences will occur. Quantitative risk analysis is the analysis based on numerical values of the probability, vulnerability and consequences, and resulting in a numerical value of the risk.

Risk assessment:

The process of making a decision recommendation on whether existing risks are tolerable and present risk control measures are adequate, and if not, whether alternative risk control measures are justified or will be implemented. Risk assessment incorporates the risk analysis and risk evaluation phases.

Risk avoidance:

An informed decision not to become involved in a risk situation.

Risk communication:

The communications of information about particular risks to the public (individuals, groups, organizations, institutions) and monitoring of the public s response.

Risk control:

The implementation and enforcement of actions to control risk, and the periodic re-evaluation of the effectiveness of these actions.

Risk estimation:

The process used to produce a measure of the level of risks being analysed. Risk estimation consists of the following steps: frequency analysis, consequence analysis and their integration.

Risk evaluation:

The stage at which values and judgement enter the decision process, explicitly or implicitly, by including consideration of the importance of the estimated risks and the associated social, environmental, and economic consequences, in order to identify a range of alternatives for managing the risks.

Risk financing:

The methods applied to fund risk treatment and the financial consequences of risk.

Risk governance:

The process by which the risk information is collected, analysed and communicated to the stakeholders in order for them to take a decision. Once all the different alternatives have been considered and the existing risk is confronted according to the risk acceptance criteria (either quantitative or qualitative), the management decisions will be taken.

Risk identification:

The process of determining what can happen, why and how.

Risk level:

The level of risk calculated as a function of likelihood and consequences.

Risk management:

The systematic application of management policies, procedures and practices to the tasks of identifying, analysing, assessing, mitigating and monitoring risk.

Risk mitigation:

A selective application of appropriate techniques and management principles to reduce either likelihood of an occurrence or its adverse consequences, or both.

Risk perception:

Intuitive understanding of risk based on an individual's own experience and judgement.

Risk reduction (long-term):

Long-term measures to reduce the scale and/or the duration eventual adverse effects of unavoidable or unpreventable disaster hazards on a society which is at risk, by reducing the vulnerability of its people, structures, services, and economic activities to the impact of known disaster hazards. Typical risk reduction measures include improved building standards, flood plain zoning and landuse planning, crop diversification, and planting windbreaks. The measures are frequently subdivided into structural and non-structural, active and passive measures.

Risk retention:

Intentionally or unintentionally retaining the responsibility for loss or financial burden of loss within the organization.

Risk tolerance:

A decision on the level of the tolerable residual risk after protection measures have been implemented.

Risk transfer:

Shifting the responsibility or burden for loss to another party through legislation, contract, insurance or other means. Risk transfer can also refer to shifting a physical risk or part thereof elsewhere.

Risk treatment:

Selection and implementation of appropriate options for dealing with risk.

Risk-based decision-making:

Decision-making, which has as a main input the results of risk assessment. It involves a balancing of social and other benefits and the residual risks.

Risk-benefit analysis:

In terms of disasters, the benefits of inhabiting areas at risk, of carrying out various activities in them and of putting oneself at risk, set off against the cost of damage and losses in disaster (including estimated future costs of the event) and of mitigation works.

Rock fall:

A free movement of rocky material away from steep slopes such as cliffs. The materials are usually described as moving en masse. The detachment of a part of the bedrock and subsequent fall form the slope is followed by impact with the slope below when secondary processes take place. The detachment process may take time and it arises from internal or external factors that are often combined.

Rock slide:

A downward, usually sudden and rapid movement of newly detached segments of bedrock over an inclined surface or over pre-existing features.

Rupture zone:

Area representing the parting of displaced mass from the in situ slope.

Scenario:

A unique combination of states. A scenario defines a suite of circumstances of interest in a risk assessment, for example loading scenarios or failure scenarios.

Sensitivity analysis:

An analysis to determine the range over which the result varies, given unit change in one or more input parameters.

Snow avalanche:

A gravity-driven mass of snow moving down mountain slope. A moving avalanche may also contain soil, rock, vegetation or water, but by definition the initial failure that triggers an avalanche occurs within the snowpack or at the interface between snow and subjacent terrain. Avalanches range from a harmless trickle of loose snow descending to a new angle of repose to a huge and devastating mass of snow moving at high speed down a long steep slope, with enough energy to destroy everything in its path. Snow avalanches automatically reload with each snowfall and can fire several times in a given year.

Societal risk:

The risk of widespread or large scale detriment from the realisation of a defined risk, the implication being that the consequence would be on such a scale as to provoke a socio/political response.

Specific risk:

Hazard probability multiplied by vulnerability for a given element at risk and/or for a given type of process.

Stakeholder:

A person or an organization that has a legitimate interest in a project or an entity.

System:

Assembly that consists of interacting elements.

Temporal probability:

The probability that the element at risk is in the area affected by the danger (threat) at the time of its occurrence.

Tolerable risk:

A risk within a range that society can live with so as to secure certain net benefits. It is a range of risk regarded as non-negligible and needing to be kept under review and reduced further if possible.

Total risk:

The expected consequences (loss) resulting from the level of hazard in a place, over a specified time period. It depends not only on the different hazardous process involved but also on elements at risk and their vulnerability.

Topple:

A forward rotation of a mass of rock, debris or soil about a pivot or hinge on a hillslope. The toppling may culminate in an abrupt falling or sliding, but the form of movement is tilting without collapse. Toppling involves overturning of interacting columns. Such blocks are formed by irregular bedding planes, cleavages, joints or tension cracks which strike approximately parallel to the slope crest or dip out of the rock mass.

Uncertainty:

Describes any situation without certainty, whether or not described by a probability distribution. Uncertainty is caused by natural variation and/or incomplete knowledge (lack of understanding or insufficient data). In the context of structural safety, uncertainty can be attributed to (i) aleatory uncertainty: inherent variability in natural properties and events, and (ii) epistemic uncertainty: incomplete knowledge of parameters and the relationships between input and output values.

Voluntary risk:

A risk that a person faces voluntarily in order to gain some benefit.

Vulnerability:

The degree of loss to a given element or set of elements within the area affected by a hazard. It is expressed on a scale of 0 (no loss) to 1 (total loss). Also, a set of conditions and processes resulting from physical, social, economic, and environmental factors, which increase the susceptibility of a community to the impact of hazards.

Vulnerability analysis:

The process of estimating the vulnerability to potential disaster hazards of specified elements at risk. For engineering purposes, vulnerability analysis involves the analysis of theoretical and empirical data concerning the effects of particular phenomena on particular types of structures. For more general socio-economic purposes, it involves consideration of all significant elements in society, including physical, social and economic considerations (both short- and long-term), and the extent to which essential services (and traditional and local coping mechanisms) are able to continue functioning.

2.7 Concluding remarks

Presented concepts of landslide risk and its components, together with the basic definitions, show some terminological problems and inaccuracies. These problems are mainly caused by different goals and aims of different specialists dealing with landslide hazards and risks. These problems need to be solved in the near future in order to be able to cooperate between different fields of science and practice. The presented concept also illustrates the need of interdisciplinary approach of natural, social, technical and security sciences. Only this approach will lead to better protection of people and their environment in the future.

2.8 References

AGS (2000): Landslide risk management concepts and guidelines. Australian Geomechanics, 35 (1): 49-92.

Alexander, D.E. (1993): Natural Disasters, UCL Press Limited, 632 p.

Alexander, D.E. (2002): Principles of Emergency Planning and Management (New York: Oxford University Press), 374 p.

Cardinalli, M., Reichenbach, P., Guzzetti, F., Ardizzone, F., Antonini, G., Galli, M., Cacciano, M., Castellani, M., Salvati, P. (2002): A geomorphological approach to the estimation of landslide hazards and risks in Umbria, Central Italy. Natural Hazards and Earth System Sciences, 2: 57-72.

Castellanos Abella, E.A. (2008): Multi-scale landslide risk assessment in Cuba, Utrecht, Utrecht University, ITC Dissertation 154, 293 p.

Crozier, M.J., Glade, T. (2005): Landslide Hazard and Risk: Issues, Concepts and Approach. In: Glade, T., Anderson, M., Crozier, M.J. (Eds.) Landslide Hazard and Risk. John Wiley & Sons Ltd, Chichester, pp. 1-40.

Cruden, D.M., Varnes, D.J. (1996): Landslide types and processes, In: Turner, A.K., Schuster, R.L. (Eds.): Landslides: Investigation and Mitigation, Special Report 147 Washington, D.C.: National Academy Press, pp. 36-75.

Dikau, R., Brundsen, D., Schrott, L. and Ibsen, M. (1996): Landslide Recognition Identification, Movement and Causes. John Wiley & Sons Ltd, Chichester, 210 p.

Fell, R. (1994): Landslide risk assessment and acceptable risk. Canadian Geotechnical Journal, 31: 261-272.

Fell, R., Hartford, D. (1997): Landslide risk management. In: Cruden, D., Fell, R. (Eds.): Landslide risk assessment. Balkema, Rotterdam, pp. 51-109.

Fell, R., Ho, K.K.S., Lacasse, S., and Leroi, E. (2005): A framework for landslide risk assessment and management. In: Hungr, O., Fell, R., Couture, R., Eberhardt, E. (Eds.): Landslide Risk Management. Taylor & Francis Group, London, pp. 3-25.

Fuchs, S., Kaitna, R., Scheidl, C., Hübl, J. (2008): The application of the risk concept to debris flow hazards. Geomechanics and Tunnelling, 2: 120-129.

Gares, P. A., Sherman, D. J., Nordstrom, K. F. (1994): Geomorphology and natural hazards. Geomorphology, 10: 1-18.

Giacomelli, P. (2005): Economic evaluation of risk. The case of a mountain area. Aracne, Roma, 145 p.

Glade, T., Anderson, M., Crozier, M. J. (2005): Landslide Hazard and Risk. John Wiley & Sons Ltd, Chichester, 802 p.

Lewis, J. (1999): Development in Disaster-Prone Places: Studies of Vulnerability, Intermediate Technology Publications, London, 174 p.

Nathan, F. (2005): Vulnerabilities to Natural Hazard: Case Study on Landslide Risks in La Paz. In: Proceedings of the World International Studies Conference (WISC) at Bilgi University, Turkey, 13 p.

Rozsypal, A. (2009): Problematika řízení rizik v inženýrské geologii, význam základní geotechnické zprávy pro řízení rizik podzemních staveb. In: Pašek, J., Marschalko, M., Pospíšil, P. (Eds.): Sborník 1. národního inženýrskogeologického kongresu s mezinárodní účastí– Rizika v inženýrské geologii, VŠB – TU, Ostrava, pp. 29-37.

Rybář, J., Stemberk, J. (1994): Nepříznivé společenské dopady svahových pohybů. In: Zb. ref. z konf. „Výsledky, problémy a perspektivy inžinierskej geológie v Slovenskej republike“, SAIG, Bratislava, pp. 57-60.

Schuster, R.L. (1996): Socioeconomic significance of landslides. In: Turner, A.K., Schuster, R.L. (Eds.): Landslides: Investigation and Mitigation, Special Report 147 Washington, D.C.: National Academy Press, pp. 12-35.

Sterlacchini, S., Frigerio, S., Giacomelli, P., Brambilla, M. (2007): Landslide risk analysis: a multi-disciplinary methodological approach. Natural Hazards and Earth System Sciences, 7: 657-675.

Tsotsos, S. (ed.) (2006): Glossary of LANDSLIDE terms. EU-MEDIN, Athens, 22 p.

UN/ISDR (2004): Living with Risk: A global review of disaster reduction initiatives. UN/ISDR, Geneva, 430 p.

UNDP (1994): Vulnerability and Risk Assessment. Disaster Management Training Programme (DMTP), Cambridge Architectural Research Ltd, Cambridge, 63 p.

UNDP (2004): Reducing Disaster Risk: A Challenge for Development. John S. Swift, New York, 161 p.

UNDRO (1979): Natural Disasters and Vulnerability Analysis. Report of Expert Group Meeting. (9-12 July 1979), Office of the United Nations Disaster Relief Coordinator, Geneva.

Valášek, J. (2005): Metody analýzy rizik spojených se živelními pohromami a haváriemi. Dissertation, Univerzita Obrany, Fakulta vojenských technologií, 136 p.

Varnes, D.J. (1984): Landslide hazard zonation: A review of principles and practice. UNESCO, Paris, 63 p.

van Westen, C. J., van Asch, T. W. J., Soeters, R. (2007): Landslide hazard and risk zonation – why is it still so difficult? Bulletin of Engineering Geology and the Environment, 65: 167-184.

van Westen, C.J., Castellanos, E., Kuriakose, S.L. (2008): Spatial data for landslide susceptibility, hazard, and vulnerability assessment: An overview. Engineering Geology, 102: 112-131.

Chapter 3

Study area

Ground truth is important,
it shows that your model is wrong.

3.1 Geographical settings

The regional study was conducted in the Mountain Consortium of Municipalities of Valtellina di Tirano (Communitá Montana Valtellina di Tirano – CM Valtellina di Tirano). CM Valtellina di Tirano is located in the Central Italian Alps, and is composed of twelve municipalities, which cover an area of about 450 km^2. Administratively it belongs to Sondrio Province in Lombardy Region (Fig. 3.1). Study area lies in the Valtellina Valley, which is one of the main alpine valleys in Italian Alps. The valley starts near Bormio (1,225 m a.s.l.) and it runs for about 100 km to Colico (218 m a.s.l.) near Como Lake where it ends. The axis of the valley is formed by the Adda River, originating from small lakes in the Rhaetian Alps at 2,335 m a.s.l. Adda River flows through the entire valley and it joins the Po River in the Lombardy Plain.

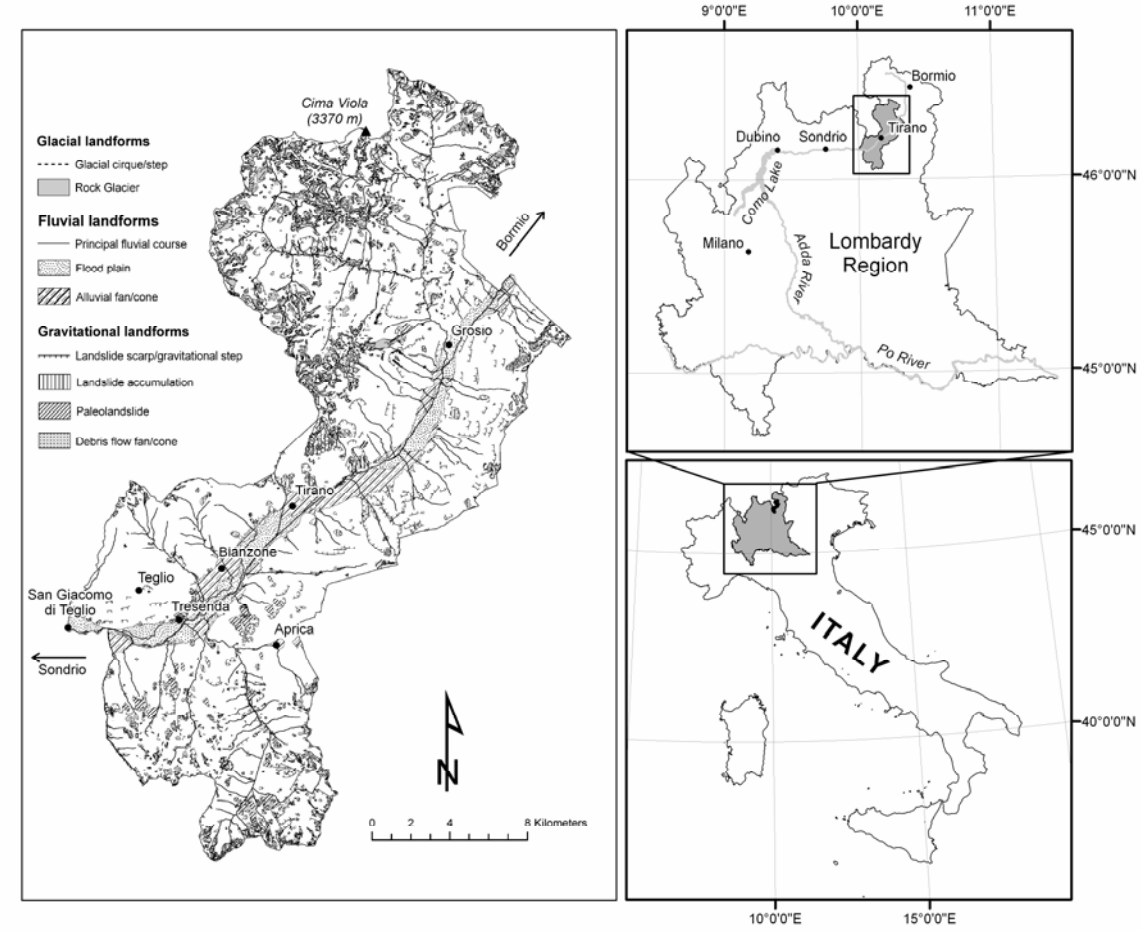

Fig. 3.1 – Geomorphological sketch and location of the study area.

Valtellina is an area of particular interest from the natural science point of view. Mainly geologists and geomorphologists are studying the zone because of its interesting features, hydrological and geological hazards and disasters. However, also human scientists find the area very interesting from the archaeological and cultural point of view. The region is also important as the well known tourist area for Lombardy Region and adjacent Swiss and Austrian regions.

3.2 Geology and geomorphology

The Alps are part of a collision belt that was formed since the Early Cretaceous as a response to the closure of oceanic troughs (Liguride-Piedmont Ocean or Alpine Tethys; Valais Trough). These oceans started to open between southern Europe and the north-western margin of Gondwana since the Early Jurassic as a side-effect of incipient sea-floor spreading in the Central Atlantic. The Alpine collision resulted in the juxtaposition of distinct tectonic domains, each of them belonging to a distinct part of the pre-collision palaeographic scenario (Amanti and Cesi 2004). Orogeny in the Alps has involved collisional tectonogenesis among continental rocks from several crustal plates and microplates situated above a crystalline basement. Folding mainly occurred in the first half of the Tertiary (65-25 MA B.P.), with phases of quiescence during which erosion succeeded in keeping pace with the bursts of uplift (Embleton 1984). More recently, the Alpine Orogeny ended in the Pliocene and early Quaternary, after which neotectonics continued the process of active crustal adjustment to pre-existing stresses.

Among five or six Quaternary glaciations, the penultimate or Riss (200,000 B.P.) and the last or Wurm (80-60,000 B.P.) appear to have extended the furthest and removed many traces of earlier cold periods (Embleton 1984). Hence, the valley is undergoing morphological adjustment to both neotectonics and the post-glacial conditions of the last 11-14,000 years. The Adda River has not yet removed all fluvioglacial deposits from its valley, and the most unstable slopes include those cut in moraines, tills and debris cones at the foot of hanging valleys (Alexander 1988).

The Penninic Units consist of metamorphosed ophiolitic sequences, representing the ocean floor of the Alpine Tethys and Valais Trough, as well as of metamorphosed continental lithosphere of the interposed Brianconnes Terrane. The crustal elements from the southern passive continental margin of Europe are conventionally termed Helvetic Units, whereas the Austroalpine Units are crustal elements from the northern passive continental margin of Adria. All these units underwent Alpine metamorphism up to eclogite facies (Amanti and Cesi 2004).

The Southern Alps represent a more internal part of the northern margin of Adria, which during the Alpine Orogeny experienced only deep diagenesis to anchimetamorphism and extensive south-verging, thin-skinned backthrusting. The Southern Alps are bounded to the north by a prominent tectonic line, the Periadriatic Fault, commonly known in Lombardy also as Insubric Line or Tonale Fault. Periadriatic Fault has mostly W-E trend in Valtellina, running on northern slopes about 500 m above Adda River floodplain and crossing the valley south from Tirano. It sharply separates the properly called Alps (Austroalpine, Penninic and Helvetic nappes) to the north from Variscan basement of the Southern Alps to the south.

The bedrock of the northern part of CM Valtellina di Tirano is composed mainly of metamorphic rocks of Campo, Tonale and Grosina units (gneiss, micaschists, phyllites), withal intrusive rocks are present. The rocks in the northern part of the study area belong to Palaeozoic Austroalpine nappe. In the southern part of the study area metamorphic rocks are represented by Edolo micaschists and quarzites belonging to South-alpine basement, with subordinate sedimentary rocks (sandstones and conglomerates of Colio formation) belonging to sedimentary

cover of Southern Alps. Due to the proximity of the tectonic lineament, cataclastic and mylonitic zones are present in the bedrock.

Geomorphologically, Valtellina lies on the border of Southern Alps (Orobic Range) and Central Alps (Rhaetic Range). The valley has prevalently U-shaped profile derived from Quaternary glacial activity. Valtellina represents the upper drainage basin of the Adda River, which flows in a flat alluvial plain up to 3 km wide. The lowest altitude in the study area is about 350 m a.s.l. near San Giacomo di Teglio where Adda River flows out from the study area. The highest elevation is reached in the northern part of Val Grosina Valley on Cima Viola (3,370 m a.s.l.).

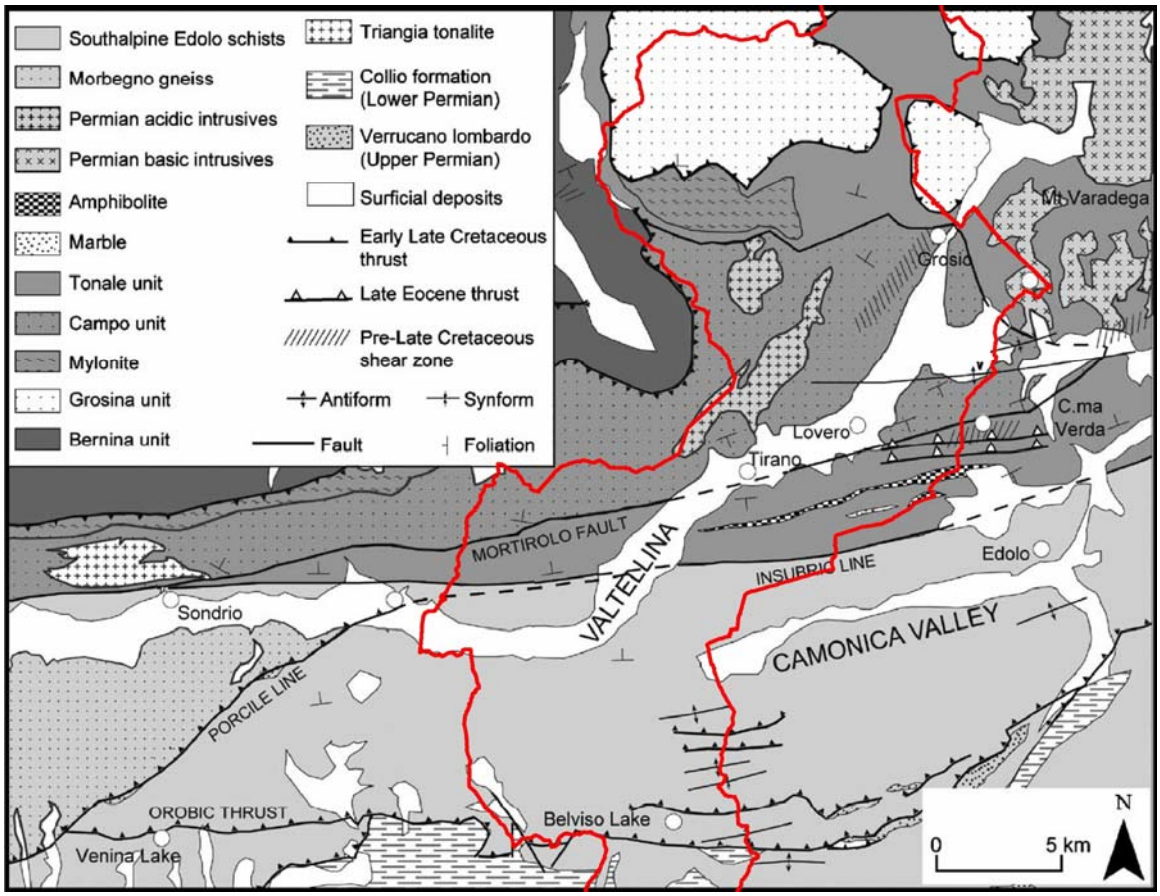

Fig. 3.2 – Geological map of Valtellina showing main geological units in the study area (red outline). Modified after Ambrosi and Crosta (2006).

In the highest altitudes glacial and fluvio-glacial landforms (cirques, moraines, etc…) are prevalently present. Nevertheless, torrential and erosional processes had changed some of these glacial morphostructures. The lower part of the valley flanks are covered with glacial, fluvio-glacial, and colluvial deposits of variable thickness. The bottom of the main valley is filled with alluvial deposits and alluvial plain is well developed. Alluvial fans at the outlet of tributary valleys can reach a considerable size, with a longitudinal length up to 3 km.

3.3 Climate

Climate of the study area is not very uniform as a cause of high difference in altitude and exposition. Most of Valtellina has a continental type of climate with precipitation increasing towards the Como Lake. Differences in precipitation are also present between the diverse slopes of the valley (Fig. 3.3). Climate of the northern Rhaetic slopes (south facing) is milder and dryer than the climate of north facing Orobic slopes in the southern part of the valley. Precipitation is strongly controlled by the altitude. Rain gauge records (Agostoni et al. 1997) show that mean annual precipitation in Tirano (430 m a.s.l.) is 726.6 mm (years 1881-1979) with minimum of 296.0 mm per year and maximum of 1286.6 mm per year. While in Aprica (1,181 m a.s.l.) the mean annual precipitation in years 1891-1985 was 1,188.6 mm, with minimum of 241.0 mm per year and maximum of 2216.0 mm per year. Northern part of the study area (Val Grosina) is much dryer compared to the same altitudes in the south of CM Valtellina di Tirano (Aprica). Rain gauge at Malghera (1,960 m a.s.l.) had mean annual precipitation of 1,559.0 mm in years 1972-1982, with annual minimum of 1,160.0 mm and annual maximum of 1,913.0 mm. The temperatures in the area are also strongly controlled by the altitude and by the exposition to the sun.

3.4 Land use

Land use on the territory of Valtellina is strongly controlled by climate and relief. Agriculture and light industry is concentrated on the bottom of the valley and on alluvial fans, while lower parts of south facing slopes are covered by vineyards and apple orchards. Rest of the slopes is dominated by leafy forests till the altitude of 600-700 m a.s.l. From this altitude till 1,000 m a.s.l. chestnut trees prevail in the forests. From 1,400 m a.s.l. coniferous trees start to dominate in the forests and reach (as single trees) altitude of 2,300 m a.s.l. (Agostoni et al. 1997). At higher altitudes only alpine meadows, scarce vegetation and rocks are present.

3.5 Population and economy

Twelve municipalities of CM Valtellina di Tirano have 29,063 inhabitants (ISTAT 2001). Most of them are settled on the bottom of the valley, about one third in Tirano (Fig. 3.4). Valtellina, as the rest of Italy suffers from negative natural population balance (-74 people in 2005) which is balance by immigration (+42 people in 2005) and results in total population balance of -32 people (Camera di Commercio 2007).

Most of the people work in services 61.9%; 32.4% in industry and the remaining 5.7% in agriculture. However, agriculture represents 35.2% of the enterprises in the area resulting in high number of small traditional business companies. Average unemployment rate in 2001 was 4.2% varying from 1.6% in Tovo di Sant'Agata to 7.5% in Vervio.

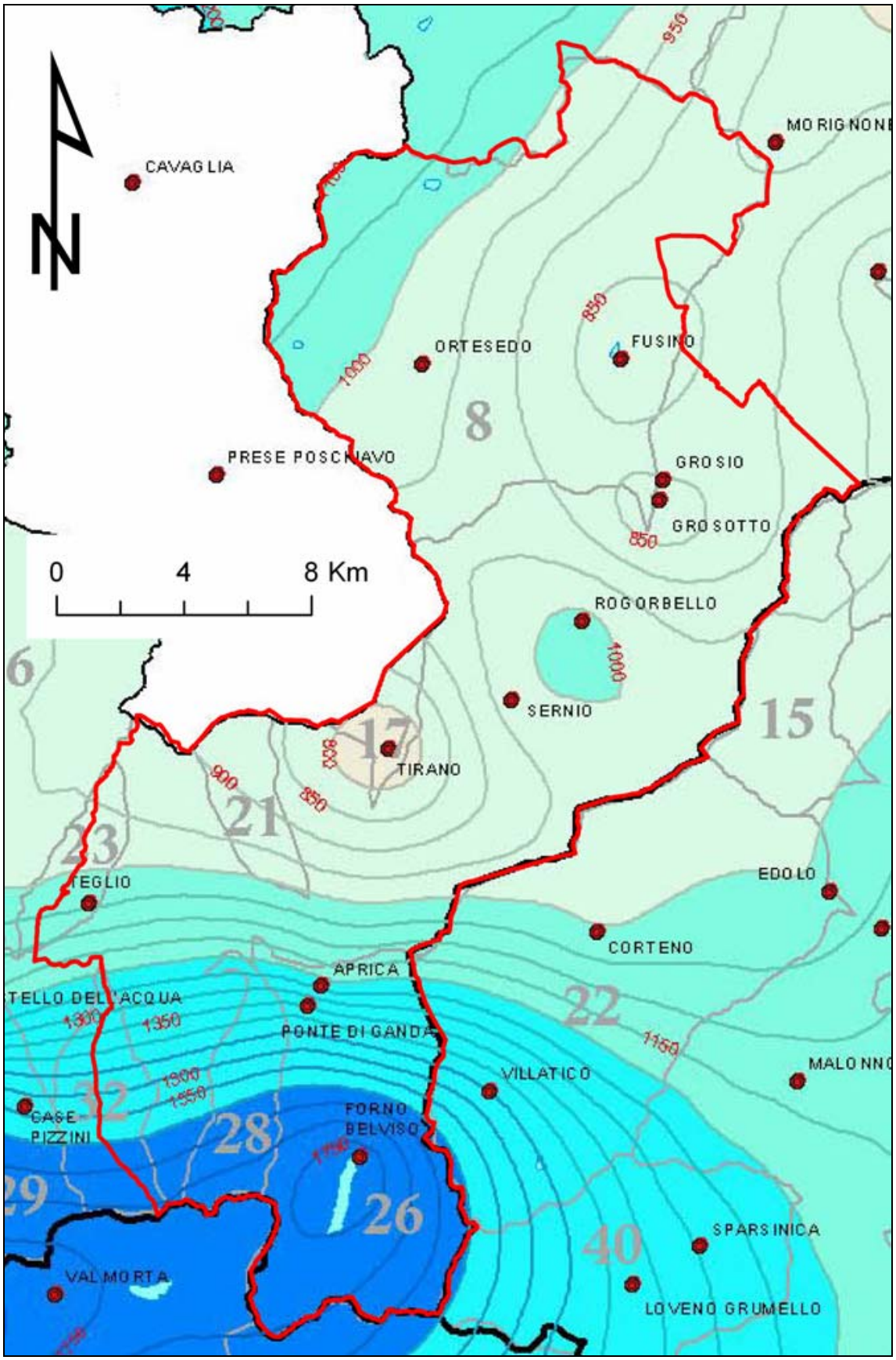

Fig. 3.3 – Mean annual rainfall in the study area (outlined by the red line) in the period 1891-1990. Modified after Ceriani and Carelli (1991).

Index	Value
Masculinity index	0.94
Oldness index	142.2
Dependency index	51

Municipality	Inhabitants	Pop.density
Aprica	1588	78
Bianzone	1220	71
Grosio	4827	38
Grosotto	1686	32
Lovero	635	47
Mazzo di Valtellina	1045	68
Sernio	445	46
Teglio	4797	42
Tirano	9044	279
Tovo di Sant'Agata	569	52
Vervio	239	19
Villa di Tirano	2968	121
Total	**29063**	**74**

Fig. 3.4 – Map of municipalities and main information about the population of CM Valtellina di Tirano. Source: ISTAT (2001).

According to the data of the Chamber of Commerce of Sondrio Province from 2007 (Camera di Commercio 2008) the added value produced in the whole province remains under the regional average, but remains over the national average, and is stable during last 5 years.

Valtellina valley is mainly a tourist area with important agricultural vocation. Tourism represents more than one third of the overall added value produced in Valtellina, (an estimated value of 3.84 million EUR in 2004) and the tourism-oriented service sector generates about 70% of the overall income. On the other side, agriculture plays a very important role; the valley is famous for the cultivation of apples and also for Nebbiolo grapes that produce high quality red wines Valtellina Superiore (Valgella, Sassella, Grumello, Inferno) and Sfursat. Many of the produced wines have quality assurance label DOC – Controlled Origin Denomination or DOCG – Controlled and Guaranteed Origin of Denomination. These agricultural activities have been intensively practised for many years and they have always represented one of the most important sources of sustenance for the local economy.

3.6 Environmental management

A significant situation which contributed to slope instabilities and possible hydro-geomorphologic disasters was poor environmental management, mainly involving deforestation, mismanagement of water resources and overdevelopment of settlements and routeways (Alexander 1988). In 1987, about 8.7 million hectares (28.8%) of Italy was forested, an area that

compares well with European Community averages. Most trees occur on 20-25% slopes and about 0.9% of the woody biomass of 1000 million m3 is cut each year. But 40% of forests suffered damage to a greater or lesser extent as a result of soil erosion, fires or acid deposition (Cultrera 1987). Additionally, since 1918 Valtellina has suffered from progressive deforestation. Demand for wood as a building material and fuel has recently been replaced by demand for steeper land.

Although much of the area is theoretically protected under conservation laws of years 1923 (for drainage basin management) and 1939 (regarding preservation of scenic beauty), as well as a Ministerial Decree of year 1963, the laws are seldom respected at any level of authority (Alexander 1988). Cederna (1975) regarded the nearby Stelvio National Park as merely a "geographical expression", utterly unprotected against incursion by developers. In 1984-85, 3,200 trees were cut down to open up new runs for the World Ski Championships and this signalled a renewal of demands for planning permission to develop chair lifts, hotels, restaurants and access roads in many parts of the valley. No environmental impact statement was prepared. In short, development to some extent followed the model identified by Kariel and Kariel (1982) for an Austrian valley that had changed from a traditional agricultural economy to a one based largely on commercial tourism. Environmental and natural hazard safeguards were minimal till the disaster in 1987 (Alexander 1988). In recent years, thanks to the new legislation and to activities of Mountain Consortiums of Municipalities as well as Provincial and Regional authorities this situation is no more present. Much more attention is paid to the management of the territory with respect to sustainable development and natural hazards. Most of the activities connected with natural hazards concern hazard mapping, mitigation measures and especially civil protection management. As a consequence, the situation is getting better.

3.7 Landslides

According to Agostoni et al. (1997) and GeoIFFI (2006), plenty of landslide types and processes are present in the study area. Largest slope processes consist of deep-seated slope gravitational deformations (DSGD) which are mostly connected with the presence of the main active fault system. Conserved paleo-landslides are also present in the area. Their age is related to the last glacial extent as they do not have morainic sediments or signs of reworking on its bodies. Other landslides acting in the area consist of a variety of types. Translational and rotational landslides as well as earth, debris and mud flows are present. Together with rock falls they represent range of velocities, volumes and rocks involved. Most of the landslides are caused by intense precipitations. Other landslide (debris flow) characteristics are discussed in Chapters 4 and 5.

3.8 References

Agostoni, S., Laffi, R., Sciesa, E. (1997): Centri abitati instabili della provincia di Sondrio. CNR-GNDCI, Milano. 59 pp. + Annexes.

Alexander, D. (1988): Valtellina Landslide and Flood Emergency. Northern Italy, 1987. Disasters, 12(3): 212-222.

Amanti, M., Cesi, C. (2004): Italian Alpine Landslides. Field Trip Guide Book, 32nd International Geological Congress, Florence, 3, 368 pp.

Ambrosi, C., Crosta, G.B. (2006): Large sackung along major tectonic features in the Central Italian Alps. Engineering Geology, 83: 183–200.

Camera di Commercio (2007): Relazione sull´andamento economico della provincia di Sondrio – 2006. Camera di Commercio, Industria, Artigianato e Agricoltura, Sondrio, 141 p.

Camera di Commercio (2008): Relazione sull´andamento economico della provincia di Sondrio – 2007. Camera di Commercio, Industria, Artigianato e Agricoltura, Sondrio, 118 p.

Cederna, A. (1975): La distruzione della natura in Italia. Piccola Biblioteca Einaudi, Torino, 243 p.

Ceriani, M., Carelli, M. (1991): Carta delle precipitazioni medie annuedel territorio alpino lombardo (registrate nel periodo 1891-1990). Servizio Geologico – Ufficio Rischi Geologici, Regione Lombardia, Milano, Italy.

Cultrera, A. (1987): European Environmental Yearbook. DocTer Institute for Environmental Studies, Milano, 897 p.

Embleton, C. (Ed.) (1984): Geomorphology of Europe. Macmillan, London, 465 p.

GeoIFFI (2006): The Regional Inventory (1:10 000) of Landslides and Hydrogeological Events, Lombardy Region, Milano, Italy.
Available at: http://www.cartografia.regione.lombardia.it/GeoIFFI.

ISTAT (2001): 14th General Population and Housing Census. The National Institute of Statistics – ISTAT, Rome, Italy. Available at: http://dawinci.istat.it/pl/index_eng.html.

Kariel, H.G. and Kariel, P.E. (1982): Socio-cultural impacts of tourism; an example from Austrian Alps. Geografiska Annaler, 64(B): 1-16.

Chapter 4

Historical events

It will never happen to me.

Based on:

Blahut, J., Poretti, I., Sterlacchini, S., De Amicis, M. (2010): Database of Historical Disasters for Civil Protection Purposes. Natural Hazards. (submitted, under review)

4.1 Introduction

Situation of widespread hazard in mountain regions in Italy has led to a policy of risk management centred on prevision, prevention, and mitigation of the impacts. This approach requires a preliminary intensive study of the damaging natural phenomena that could affect the territory, i.e. identification and characterization of the hazard, and subsequent profiling of expected events and possible effects on the elements at risk.

Databases of past events are a very useful tool for both of the purposes, because they give an idea of possible affected areas, expected magnitude and intensity of events, their temporal frequency and possible impacts on the territory (Tropeano and Turconi 2002). These databases generally contain geographical, numerical and alphanumerical information in various digital formats, including vector and raster maps, terrestrial, aerial and satellite imagery, time series, tabular data, texts, documents and images (Couture and Guzzetti 2004).

The principal aim of this chapter is to construct a geo-database of past harmful natural events that affected the study area and its neighbourhood, and to explore how the information gathered can be used to contribute to future hazard delimitation and public safety. The structure and contents of the database are briefly presented, together with preliminary statistics and trends. Availability of data is discussed together with their reliability.

4.2 Historical overview of past events

A brief historical overview is presented based on available sources, i.e. books, chronicles, journals, newspapers, and reports with a special focus on the study area. It is worth emphasizing that in most cases the identification of processes (landslides, floods, torrential/erosional processes) in old chronicles and news is quite confused. Damaging events were often defined as “acts of God” or unnatural phenomena, without a clear description of acting processes or triggering factors.

The history of natural disasters in Valtellina began when the first population was established in the region. During antique times people were settled mainly on the slopes over the main valley floor, probably as a result of historical knowledge about flooding. On the other hand, these settlements had to suffer from landslides. However, no information was found about floods or landslides in old chronicles till 1338. The first historical information comes from the area of Montagna in Valtellina, just few kilometers east from Sondrio, the capital of the province: “one Thursday afternoon in August 1338 after a tremendous hailstorm followed by intensive rainfall, several large landslides occurred, causing seven victims” (de Bernardi 1987).

F. A. Chiesa (1752 in Franceschi 1912) reports about a huge flood of the Adda River in 1404. This flood formed a large lake and made it difficult to reach the upper part of the valley. Other information about landslides comes from the 16th to 18th centuries: they happened in 1520 in Castione (Parravicini 1612 in Franceschi 1912), in 1535 or 1538 in Ardenno (Damiani 1898

in Franceschi 1912), in 1600 in Boalzo (Damiani 1898 in Franceschi 1912), and in 1755 in Mazzo (de Bernardi 1987). Floods occurred in 1550, 1678, and 1750 in the lower part of the valley (Chiesa 1752 and Morselli 1859 in Franceschi 1912). In 1792 an event very similar to the one happened in 1987 was reported (de Bernardi 1987).

In the 19th century information about disasters becomes more exhaustive, starting with the detailed description of the Sernio landslide in 1807 by F. Ferranti (1814). Processes are better distinguished, e.g. snow avalanches, torrential processes, landslides, and floods are described (de Castro 1885 in Franceschi 1912). More information about damages and morphological consequences is also available, e.g. on 14th August 1851 in Valmaggiore a landslide caused 6 victims, destroyed houses, and raised the river bed for about 9 meters, and in July 1852 in Berbenno and Polaggia 1 million of Lire of damages were caused by torrential processes (Franceschi 1912). Remarkable damages happened also in 1829, 1834, 1844, 1855, 1885, and 1888 when after intense rainfalls the Adda valley was flooded by the tributary torrents of Tartano, Mallero, and Madrasco (de Bernardi 1987). Many torrential processes were recorded: in Boalzo torrent (1820, 1821, 1871, and 1882), Rezzalasco torrent (1864), Ron torrent (1880, 1882) and Bitto torrent (1890). Landslides were reported in Bianzone (1891) and Grosotto in 1894 (de Bernardi 1987).

Obviously, the data in the last century is much more consistent than in the past. From the information gathered it can be observed that landslides and floods very often acted in synergy. Floods were generally accompanied by abundant transport of debris coming from tributary valleys; this load of material often caused the obstruction or rising of riverbeds both on alluvial fans and the plain, inducing consequent overflows. Many landslides were also triggered by river banks erosion.

The largest documented disasters affecting the study area happened in 1983 and 1987. The 1983 event is described in the case study section of this thesis (Chapter 11). In summer 1987, after a long rainfall period, the entire valley was affected by floods and many landslides were triggered all over the region. A total of 25,000 people were evacuated and 53 casualties were recorded (Magistretti 2002). On 28th July 1987 the well known Val Pola complex rock avalanche caused 27 victims.

Other major events occurred at the beginning of 21st century. From 14th to 17th November 2000, prolonged and intense rainfalls triggered about 260 shallow landslides in Valtellina, most of them concentrated on vine-terraced slopes. The highest landslide density in the study area was observed around Bianzone, with 49 landslides per km^2, and near Tirano, with 26.8 landslides per km^2 (Crosta et al. 2003).

The last larger event that affected the study area occurred in November 2002, when several shallow landslides and soil-slips were released mainly on terraced areas. The event caused two casualties and the damage was estimated to 500 millions of EUR (Aleotti et al. 2004).

4.3 Database

4.3.1 Available resources

Official databases

Official sources of information about landslides and floods in the study area are provided by national, regional, local authorities or research institutes, and they are listed below:

- National AVI Database: A Bibliographical and Archive Inventory of Landslides and Floods in Italy (Guzzetti et al. 1994), developed by CNR-GNDCI;
- Regional Database of Landslides of the Lombardy Region (Lombardy Region 2002);
- GeoIFFI Database: National Landslide Geographic Inventory Database for Lombardy Region (GeoIFFI 2006), set up within the National IFFI Project (IFFI 1997);
- SCAI Project: Study on the Unstable Inhabited Areas of the Sondrio Province (Agostoni et al. 1997), lead by CNR-GNDCI;
- PAI Project: Hydrogeological Plan of the Po River Basin, issued by the Po Basin Authority (PAI 2001);
- Geological Reports for the Municipalities of the study area, required by legislation to support Territorial Governance Plans.

The AVI Database has 80 records within the study area; among them, 26 have a complete date (day, month, and year), while 39 only have the year of occurrence. At the date of this study, the database is covering the period from year 1918 to 2000, but an updating is expected.

The Regional Database contains 501 records for the study area; among them 61 have the complete date, while 450 report only the year of occurrence. This database covers the period from year 1600 to 2000.

Some problems arise when analysing these two sources. The first problem is related to the spatial location of events. Both databases have coordinates associated to events but they are identified as points. In some cases these points are located in scarp areas, sometimes in transport or deposition areas, while in other cases they only refer to the locality where the event occurred. Spatial extent is never bounded, even if in some cases it can be approximately deduced by considering information about the magnitude (area, average length, and width). The second problem is related to the way how these harmful events are classified. As most of the primary sources for the databases are local chronicles and news written by non-experts, the correct type of phenomena is often misunderstood (e.g. an apparent debris flow is described as flood).

The GeoIFFI Database is a vector database of landslides. In the study area there is a total of 5,547 starting points of landslides and 1,200 landslide polygons (including deep seated slope deformations). Also rock falls prone areas are mapped as well as alluvial fans. It is

generally possible to identify source, spreading and depositional areas. Unfortunately, no temporal information is available, i.e. the date of occurrence, except for few events, even if it is known that the database should cover the period from 1850 to 2006. For this database only well know events that could be associated to the date of occurrence were considered.

The SCAI database is very detailed both for the cartographic and descriptive part. It also provides information on geologic and geomorphologic causes of failure. Unfortunately, it is limited to events occurred until 1996 and only 14 records are available for the study area.

The PAI database is quite scarce, but has the advantage of highlighting the most hydro-geological critical sites.

In the available Geological Reports for the Municipalities, some basic information is provided about the main historical events that affected the territory.

Other sources

Available books and papers useful for the construction of the database were also examined. They are mostly produced during the last 20 years by the Hydrogeological Protection Research Institute (CNR-IRPI) and the National Group for Defence against Hydrogeological Catastrophes (CNR-GNDCI) of the National Research Council (Guida et al. 1979; CNR-GNDCI 1983; Govi et al. 1996; Cardinali et al. 1998; Tropeano et al. 1999, 2006). A book describing the 1987 flood event was also produced by the Bank of Sondrio (Giacomelli 1987). The information gathered covers mostly the second half of the 20th century, but only text information is usually available. A very valuable source is the Bibliographical Research for a Catalogue on Landslides and Floods in Valtellina compiled by Govi and Turitto (1994). Some photographs and videos have been also collected and analyzed.

4.3.2 Structure of the database and current results

The initial phase of the process consisted in joining the official databases. As a result, 489 records of damaging events reported from the year 1600 up to 2001 were compiled and checked in order to avoid redundancies. A main problem was that these sources were compiled with different purposes and at different scales. This affected the spatial resolution consistency of the database, i.e. in some cases the exact point location or the extent polygon is provided, while in others only the locality, the stream/mountain name, or the municipality is indicated. In order to adopt a normalized way to locate events, georeferenced points were used as basic spatial information. However, these points do not always refer to the same part of the process: it could be the initiation area, the transport area, or the impact/deposition area, and not always it is easy to distinguish among them. Additional text information about location was also stored.

Afterwards, other sources such as books, chronicles, local newspapers, historical surveys and information from the municipalities were examined. As a result, 126 records were added to the database, covering the period from the year 1600 till 2008. Two drawbacks arose regarding the information provided by the oldest sources: uncertainties in the identification of processes typology and vague location of events. The first is probably caused by low knowledge

about natural hazards during past times, and probable tendency to overestimate the phenomena, while the second is mainly due to lack of coordinates, imprecise definition of affected areas or use of old place names.

The final database contains 615 records covering the period from 1600 till 2008 (Fig.4.1), but only 58% of the events are dated with at least year of occurrence. Obviously the number of dated events is increasing during the last centuries when more information sources are available; however, there are still some information gaps even during the 20th century (Fig. 4.2), mainly during World War II and the post-war period. As a result, the apparent increase of frequency of the harmful events seems to be caused mainly by better recording techniques than by other causes.

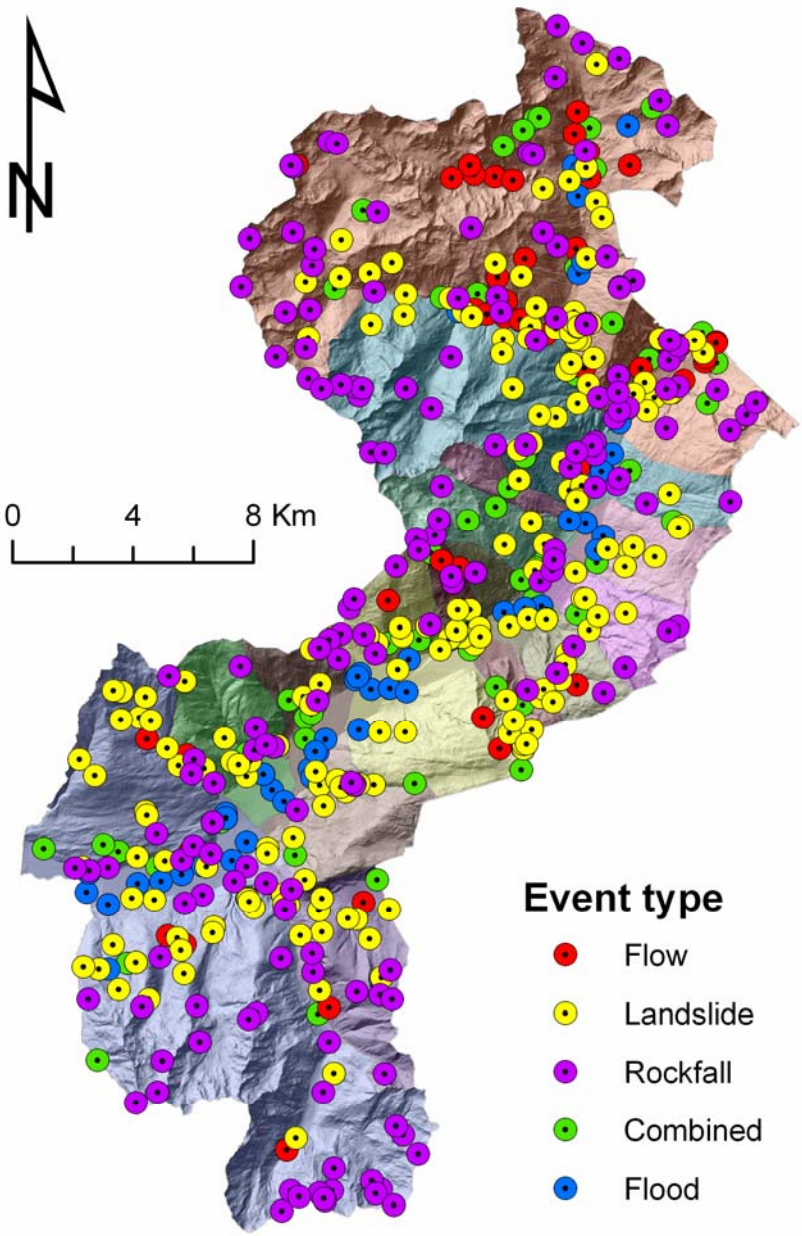

Fig. 4.1 – Distribution of database records within the study area. Records are generalized into five groups.

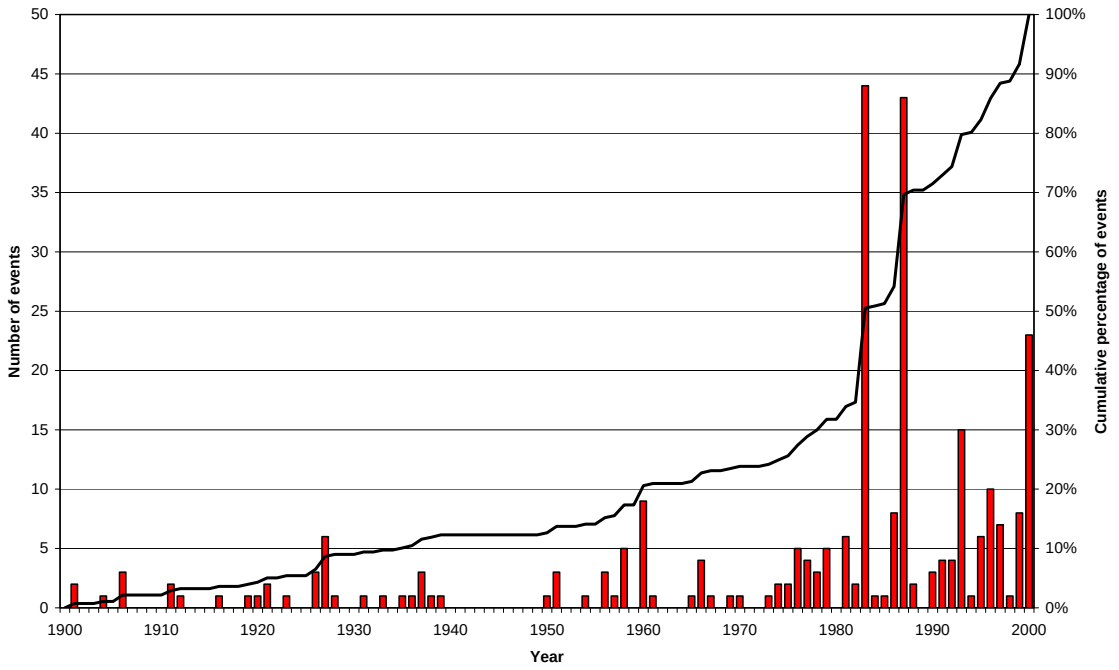

Fig. 4.2 – Distribution of dated events in the database during the 20th century.

The database was organized as a relational database (Fig. 4.3) with an associated geographical representation. Each event has an ID code, so it can be linked with joined tables to get extensive data. A summarizing table has been produced to allow performing some simple statistical analyses.

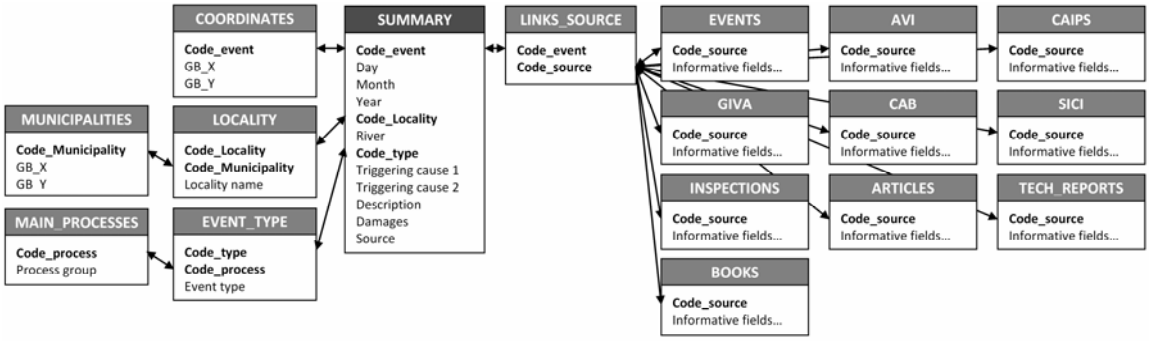

Fig. 4.3 – Scheme of the constructed relational database.

Event types have been generalised and five main groups of processes have been distinguished: floods (14%), debris and earth flows (9%), rock falls (30%), other landslides (37%) and combined events (11%). Regarding the temporal information, 20% of events have complete date (day, month, and year); almost half of the events (48%) have at least the year of occurrence, while for the others temporal information is not available. It is interesting to notice that all flood events have temporal information, with at least the year, while most of the rock falls are not dated; for the other processes the distribution among dated/undated events is more balanced.

At least one triggering cause is provided for 70% of the events. Fig. 4.4 shows causes associated to the various processes: precipitations, which are the most frequent, triggered events

mainly in May, July, October and November (Fig. 4.5); erosion is the second main cause, proving how important is the contribution of sediment transport in causing damaging events in the territory. For landslides, data about magnitude (length, area) is often available. Unfortunately, data referring to damage potential (velocity, depth of mass) is almost absent.

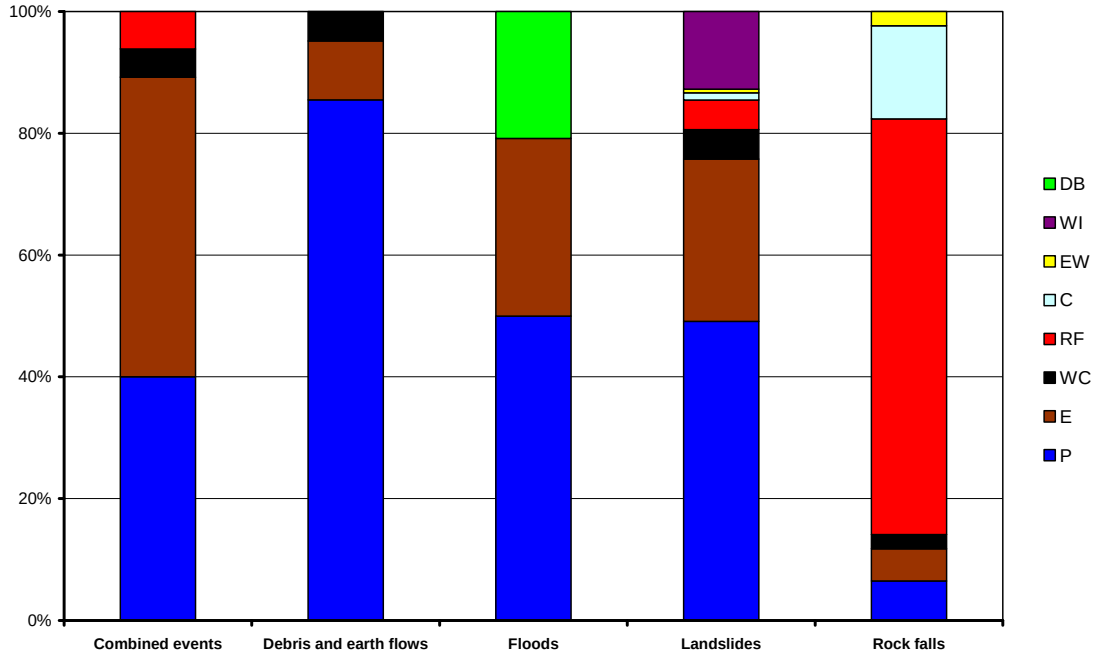

Fig. 4.4 – Triggering causes associated to the main five hazardous processes: DB= Dike Breaks; WI= Water Infiltrations; EW= Excavation Works; C= Cryoclastism; RF= Rock Fractures; WC= (dry stone) Walls Collapse; E= Erosion; P= Precipitation.

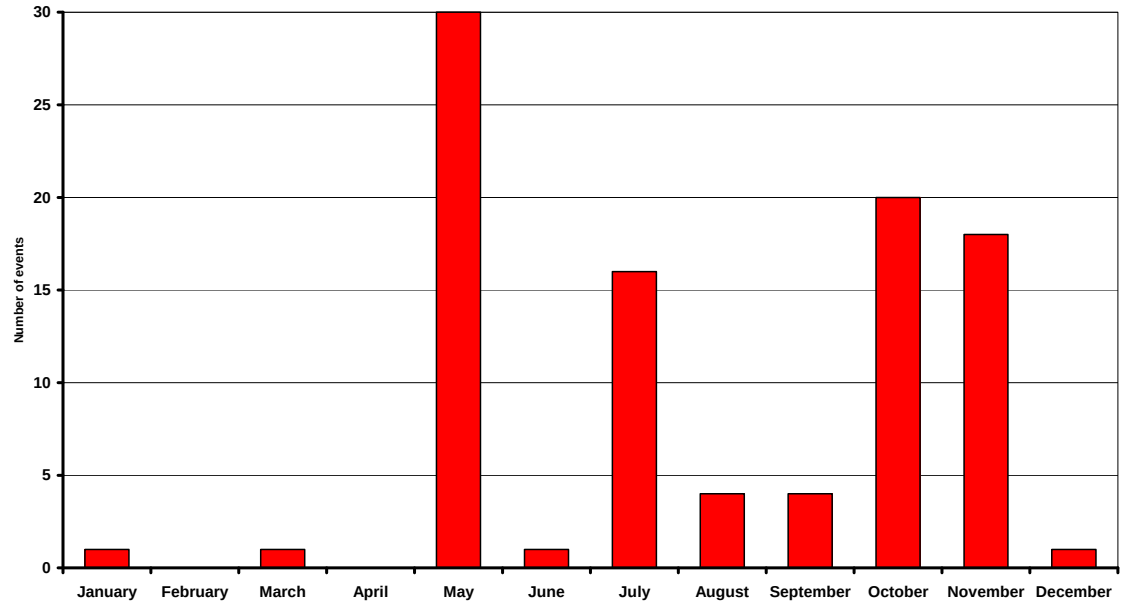

Fig. 4.5 – Monthly distribution of events triggered by high precipitations.

Floods

In the database there are 74 flood records distributed all over the territory, but especially in Teglio and Tirano. The records cover the period from year 1616 to 1987 and even if the characterization is not always clear, they can be separated in inundations (about 60%) and events in which only a rapid increase of discharge was registered (about 40%). The events for which information about the month is available occurred mainly in the period between July and November. Quantitative data is available only for the records related to high discharges and only for the Adda River, while for inundations a general description of affected areas and damages is usually provided. Georeferencing of inundations made several problems since most of them are defined as points without any further specification of extent. Aerial photos could help in defining flooded areas, but unfortunately they are not available for the entire study area, and not even many ground photos have been found. Adda River is responsible for almost half of the events, and in 9 cases it acted in synergy with two of its main tributaries, Poschiavino and Roasco. The other events are caused by minor rivers/torrents. Regarding the location, 30% of floods occurred on fan areas. In 5 cases, inundations were caused by dike breaks; they happened in Bianzone, Teglio and Tirano in the second half of the 19th century.

Landslides, rock falls and debris flows

Totally 458 landslide events, from the year 1600 to 2008, have been stored with geographical coordinates. Half of them are dated, 64% occurring during the 20th century, mostly during its last quarter. More than one third of events are rock falls and 30% are rotational and translational slides. About 14% of the records are not precisely classified. Event magnitude, expressed as length, width and area, is reported in 27% of the records.

Most of the events (37%) occurred in Grosio municipality, which has an area of 127 km^2, being the largest municipality within the Consortium. It could be surprising that the smallest municipality, Sernio (9.6 km^2), has the highest number of events compared to its area (44 recorded events – 4.9 events/km^2). This is due to the presence of an alluvial fan with frequent torrential activity and a deep gravitational slope deformation with large number of superficial sliding (Masuccio Mountain). The rest of the territory has an average density of 1.3 events/km^2.

Combined events

About 11% of the recorded events are related to combined events. They are usually a combination of intensive erosion processes, flooding and/or consequent landsliding. The erosion was generally linear along drainage channels. In some cases, also slope toe erosion or processes on alluvial fans were observed. In three cases several houses were filled by eroded material and water. Events are geographically distributed over the entire study area, even if most of them occurred close to existing streams and torrents. Temporal information is available for half of the events.

4.3.3 Damage records

For a rough estimation of losses from hydro-geomorphologic disasters, a classification of the database records was made distinguishing four levels of damage. High damage class is related to situations where human casualties were registered or buildings were affected. Medium damage class corresponds to destruction or damage of infrastructure (roads, power lines), while low damage class is restricted only to losses of agricultural land or forests. The last class (N.A.) was assigned where no direct losses were reported or no information is available.

As it can be seen from Fig. 4.6, the last class is the more frequent. Most of the information about damage is connected with debris and earth flows, and less with floods. This situation can be caused by the different spatial extent of these two types of events. While for earth and debris flows the localisation is well defined and losses can be well estimated, in case of floods, which usually cover a larger area, damage estimation is much more complicated. The percentage of hard, medium and light damage levels is almost proportional in all types of phenomena. The majority of recorded losses are in the medium damage class (infrastructure).

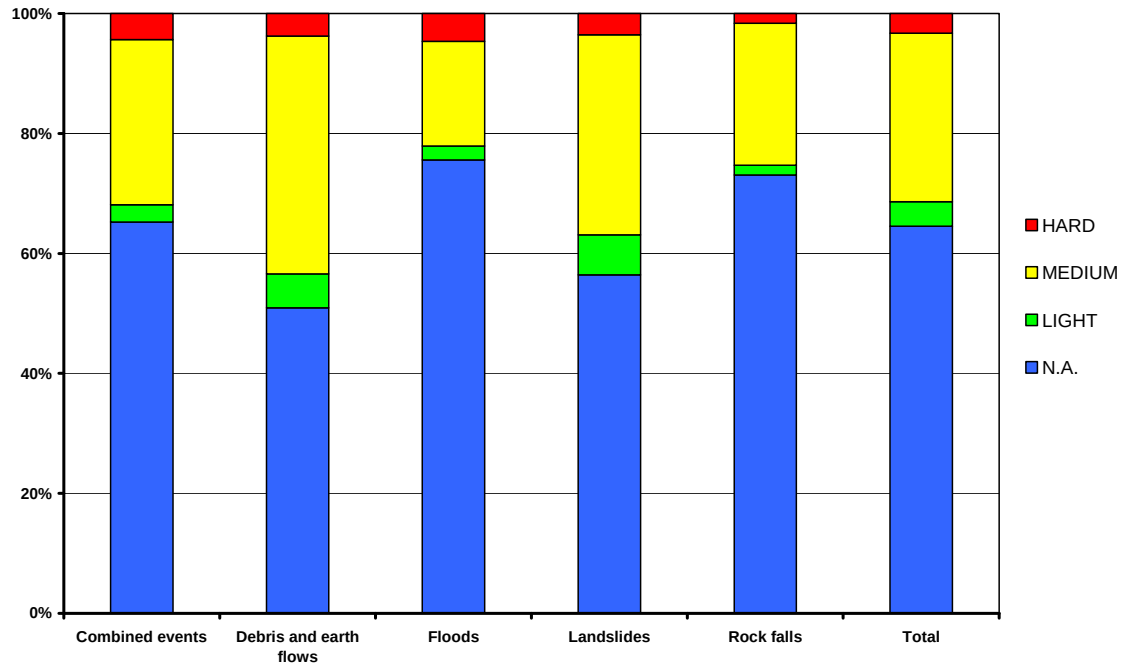

Fig. 4.6 – Damage records for the five main hazardous processes.

4.4 Concluding remarks

A georeferenced database of past events related to landslides and floods was designed for the area of Valtellina di Tirano, in the Italian Central Alps. It uses of all the available information and covers a period from 1600 till 2008. Five main types of natural processes acting on slopes and at the valley bottom were distinguished and their causes were analyzed. Losses from the damaging events were classified into four categories of damage intensity.

Despite its limitations, mainly due to availability and reliability of data, the database represents a valuable source of information which can support local studies on natural hazards, decision making, urban planning, or scenario preparation for civil protection purposes.

Results also showed that debris flows, despite their spatial limitation, can cause considerable damage to people and their assets. They are not spatially limited to certain parts of the study area. As a consequence they pose an important threat to local population and their hazard and risk need to be studied.

Obviously, results will improve when more information about intensity of past events becomes available. For this reason it is important to keep this database as rich as possible of information and continuously updated. Future work shall focus on that, and particularly on trying to define with more accuracy the type of processes that caused disruptions and to describe their evolution (spatial and temporal) and effects with more details. This will allow to better distinguish among processes and their causes and to avoid misunderstandings which could have serious consequences in emergency planning.

4.5 References

Agostoni, S., Laffi, R., Sciesa, E. (1997): Centri abitati instabili della provincia di Sondrio. CNR-GNDCI, Milano. 59 pp. + Annexes.

Aleotti, P., Ceriani, M., Fossati, D., Polloni, G., Pozza, F. (2004): I fenomeni franosi connesi alle precipitazioni del Novembre 2002 in Valtellina. International Symposium Interpraevent 2004, Riva/Trient, Italy, pp. 11-20.

Cardinali, M., Cipolla, F., Guzzetti, F., Lolli, O., Pagliacci, S., Reichenbach, P., Sebastiani, C., Tonelli, G. (1998): Catalogo delle informazioni sulle località italiane colpite da frane e da inondazion, Volume I – frane. CNR-GNDCI, Pubblicazione n. 1799, Perugia, 404 p..

CNR-GNDCI (1983): Eventi alluvionali e frane nell´Italia Settentrionale: Periodo 1972-74. CNR-GNDCI, Pubblicazione n. 1897, Torino, 485 p.

Couture, R., Guzzetti, F. (2004): Geo-databases for Natural Hazards and Risk Assessment. Natural Hazards and Earth System Sciences, 4: 183-185.

Crosta, G.B., Dal Negro, P., Frattini, P. (2003): Soil slips and debris flows on terraced slopes. Natural Hazard and Earth System Sciences, 3: 31-42.

de Bernardi, L. (1987): Un male antico. In: Giacomelli, L. (Ed.): Speciale Valtellina 1987: Cronaca, storia, commenti, Notiziario della Banca Popolare di Sondrio, No. 45, Bergamo, pp. 92-119.

Ferranti, F. (1814): Su la frana di Sernio che generò nel 1807 un nuovo lago e sui mezzi praticati per scemare le dannose conseguenze. Como, 54 p.

Franceschi, O. (1912): Intemperie, frane ed alluvioni in Valtellina. Pro Valtellina, VII (19-24): 2 p.

GeoIFFI (2006.): The Regional Inventory (1:10 000) of Landslides and Hydrogeological Events, Lombardy Region, Italy. Within IFFI Project (1997) – Italian Landslides Inventory, National Geological Survey, Rome, Italy. Available at: http://www.cartografia.regione.lombardia.it/GeoIFFI

Giacomelli, L. (1987): Speciale Valtellina 1987: Cronaca, storia, commenti. Notiziario della Banca Popolare di Sondrio, No. 45, Bergamo, 227 p.

Govi, M., Luino, F., Turitto, O. (1996): Tipologie dei processi e sequenze di sviluppo: due esempi recenti. In: Luino, F. (Ed.): La prevenzione delle catastrofi idrogeologiche: il contributo della ricerca scientifica, Convegno internazionale, Atti Vol. 2, CNR-GNDCI, Alba, Pubblicazione n. 1600, pp. 261-278.

Govi, M., Turitto, O. (1994): Ricerche bibliografiche per un catalogo sulle inondazioni, piene torrentizie e frane in Valtellina e Valchiavenna. Associazione Mineraria Subalpina, Quaderni di Studi e di Documentazione n. 16, 249 p.

Guida, M., Iaccarino, G., Metcalf, G., Vallario, A. (1979): Bibliografia delle frane dal 1900 al 1978. Vol. XL, CNR, Roma, 362 p.

Guzzetti, F., Cardinali, M., Reichenbach, P. (1994): The AVI Project: A bibliographical and archive inventory of landslides and floods in Italy. Environmental Management, 18: 623-633.

IFFI (1997): IFFI Project – Italian Landslides Inventory Database. National Geological Survey, Rome.

Lombardy Region (2002): Inventario delle frane e dei dissesti idrogeologici della Regione Lombardia. Direzione generale territorio e urbanistica, Struttura rischi idrogeologici, Milano, 2 CD-ROM.

Magistretti, S. (2002): Rituals and Rhetorics of Disaster: Patterns of Catastrophe in the Italian Media: Sarno, 1998. In: Dickie, F., Foot, J., Snowden, F.M. (Eds.): Disastro!: Disasters in Italy Since 1860: Culture, Politics, Society, Palgrave, New York, pp. 301-322.

PAI (2001): Piano stralcio per l'Assetto Idrogeologico (PAI): Interventi sulla rete idrografica e sui versanti. Linee generali di assetto idraulico e idrogeologico, Adda sopralacuale (Valtellina e Valchiavenna). Autorità di bacino del fiume Po, Parma, 100 p.

Tropeano, D., Govi, M., Mortara, G., Turitto, O., Sorzana, P., Negrini, G., Arattano, M. (1999): Eventi alluvionali e frane nell´Italia Settentrionale: Periodo 1975-1981. CNR-GNDCI, Pubblicazione n. 1927, Torino, 279 p.

Tropeano, D., Luino, F., Turconi, L. (2006): Eventi di piena e frana in Italia settentrionale nel periodo 2002-2004. CNR-IRPI and CNR-GNDCI, Pubblicazione n. 2911, Torino, 159 p.

Tropeano, D., Turconi, L. (2002): Using Historical Documents for Landslide, Debris Flow and Stream Flood Prevention. Applications in Northern Italy. Natural Hazards, 31: 663-679.

Chapter 5

Debris flows

How does it feel
How does it feel
To be without a home
Like a complete unknown
Like a rolling stone?

(Bob Dylan, Like a Rolling Stone)

5.1 Introduction and description of phenomena

In the mountainous areas on steep slopes various types of flow or mass movements involving water and sediments occur: flood, solid transport, hyperconcentrated flows, mudflows, debris flows, landslides, debris avalanches, etc. Among them, debris flows are processes that have several sub-categories and different characteristics. In English studies, debris flows are usually considered as a type of landslide (Fig. 5.1). For the purpose of this study, a brief overview of debris flow phenomena is presented in order to understand this process better.

Debris flows are gravity-induced mass movements intermediate between land sliding and water flooding, with mechanical characteristics different from either of these processes (Johnson 1970). According to Němčok et al. (1972) and Varnes (1978), debris flow is a form of rapid mass movement of rocks and soils in a body of granular solid, water, and air analogous to the movement of liquids. In the landslide classification of Cruden and Varnes (1996), debris flows are flow-like landslides with less than 80% of sand and finer particles. Velocities vary between very rapid and extremely rapid with typical velocities of 3 m/min and 5 m/sec respectively. Debris flows and their temporal and spatial properties are compared to other types of mass movements in Figure 5.2.

Debris flows consist of a mixture of fine material (sand, silt, and clay), coarse material (gravel and boulders), with variable quantity of water, that forms a muddy slurry which moves down slope, usually in surges induced by gravity and the sudden collapse of bank material. Large displacements occur within the moving mass.

According to Coussot and Meunier (1996), debris flows are an intermediate phenomena between hyperconcentrated flows (intense bed load transport) and landslides separated from them by sharp transitions of some characteristics: speed, deposit nature and flow type (Fig. 5.3). Debris flows usually take place on slopes covered by thin unconsolidated rock and soil debris, especially where the vegetative cover has been removed by logging or fires. Three distinctive elements are distinguishable in a debris flow: the source area, the main track, and the depositional toe (Fig.5.4). The flows commonly follow pre-existing drainage paths, and tracks have a V-shaped or rectangular cross-section. Some of the coarse debris will be heaped at the side of the track to form lateral ridges (levées). Debris flow deposits are left where the channel gradient decreases or at the toe of the mountain fronts. Successive surges will build up into a debris fan (Corominas et al. 1996).

Debris flows occur in most climatic regions. They are potentially a very destructive form of slope movement in mountainous areas, where sudden access of water (usually from heavy rain or melting snow) can mobilise debris mantling the slopes and it can incorporate it into debris flow (Hutchinson 1988). In alpine environments debris flows are composed usually of coarser material which has fallen into the source area by mechanical weathering. These debris flows subsequently form significant elongated tracks with lateral ridges (Corominas et al. 1996).

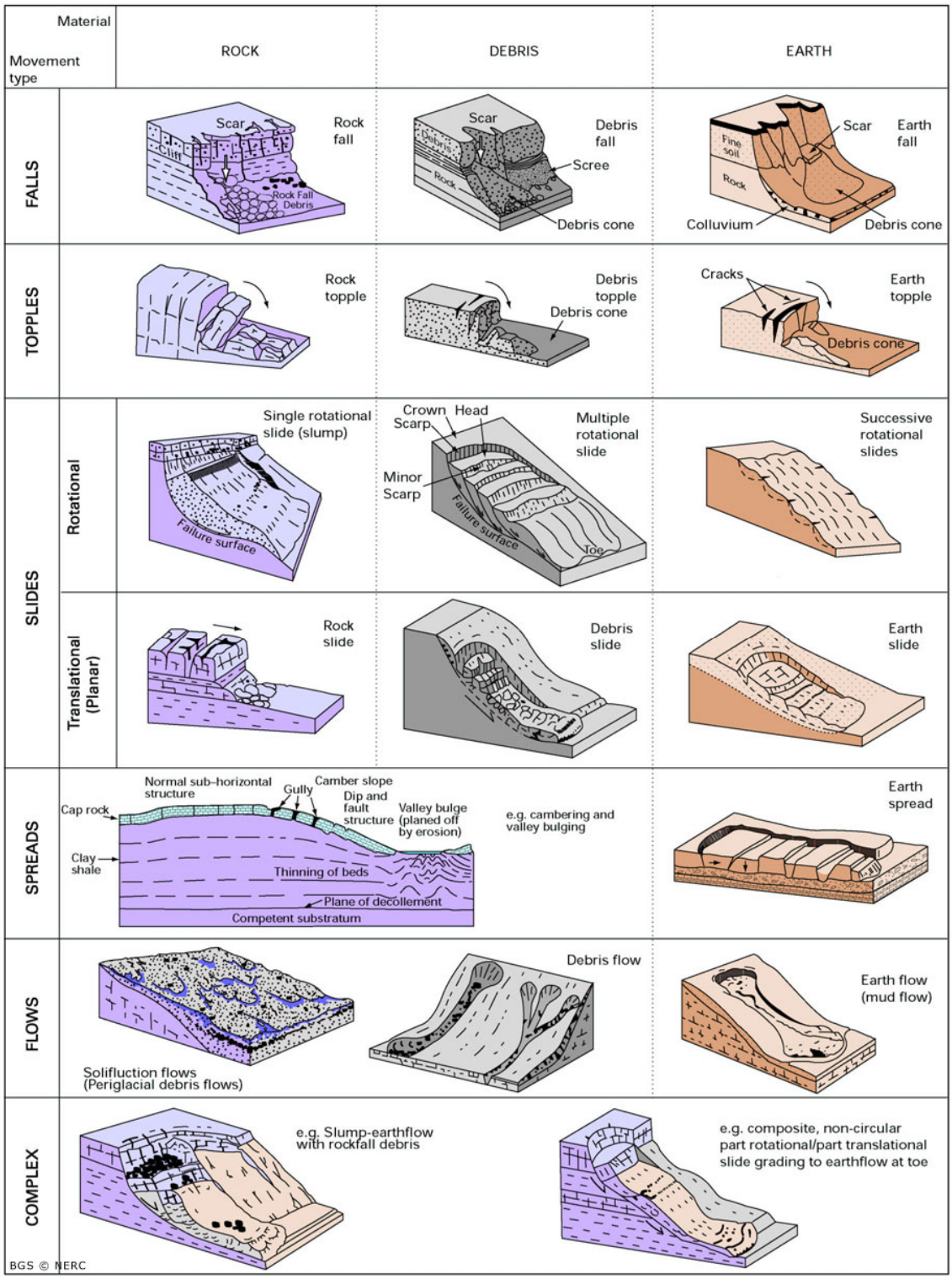

Fig. 5.1 – Landslides types according to classification of Cruden and Varnes (1996). After British Geological Society.

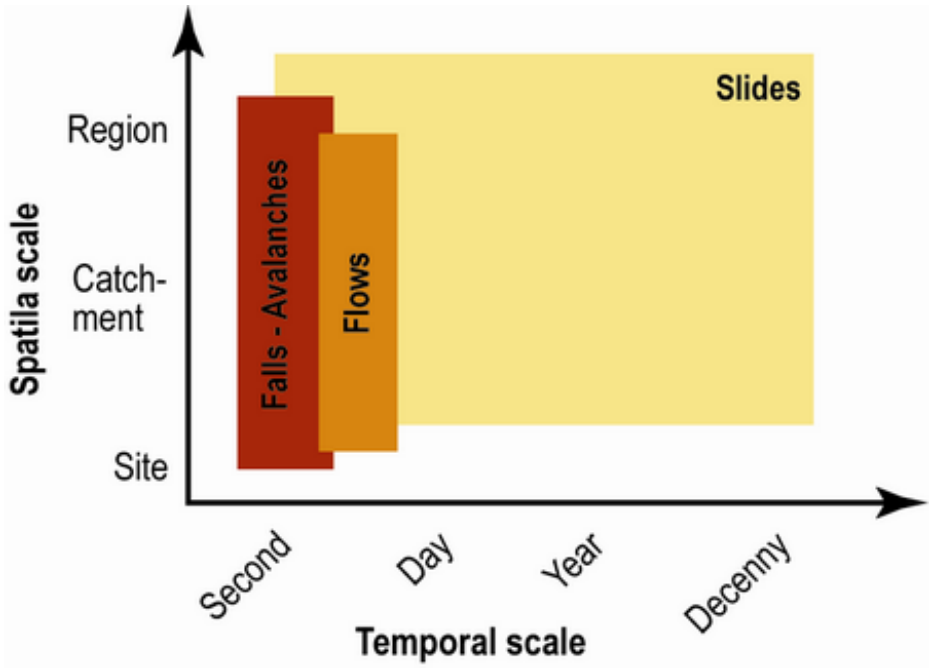

Fig. 5.2 – Spatial and temporal scales of debris flows compared to other types of mass movements. Source: Glade and Crozier (2005).

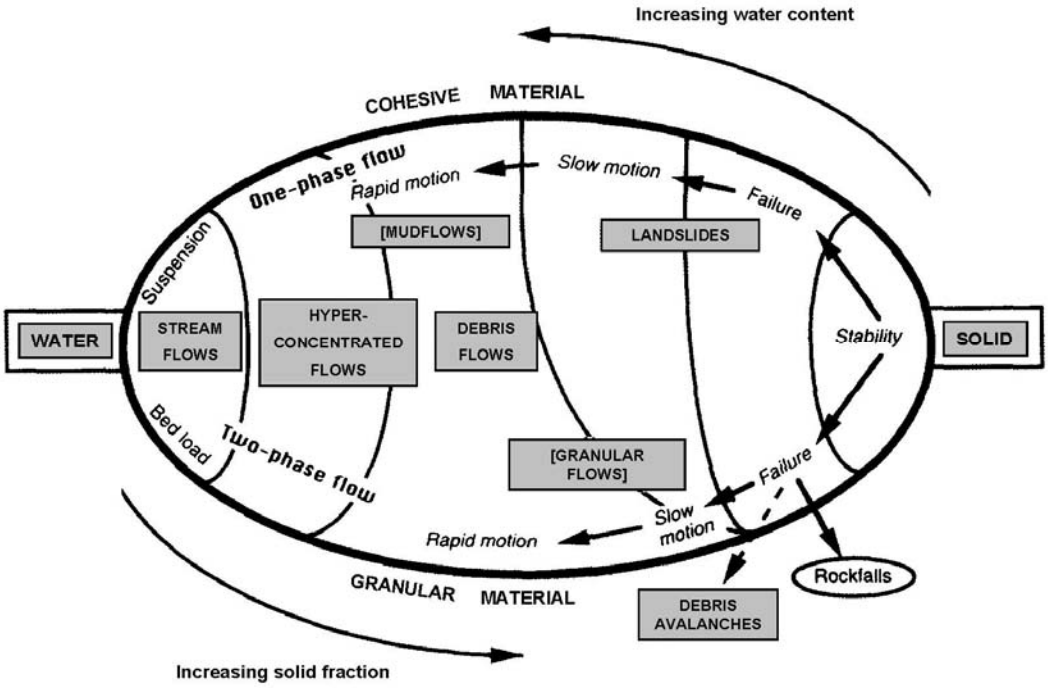

Fig. 5.3 – Classification of mass movements on slopes as a ratio of solid fraction and material type. Modified after Coussot and Meunier (1996).

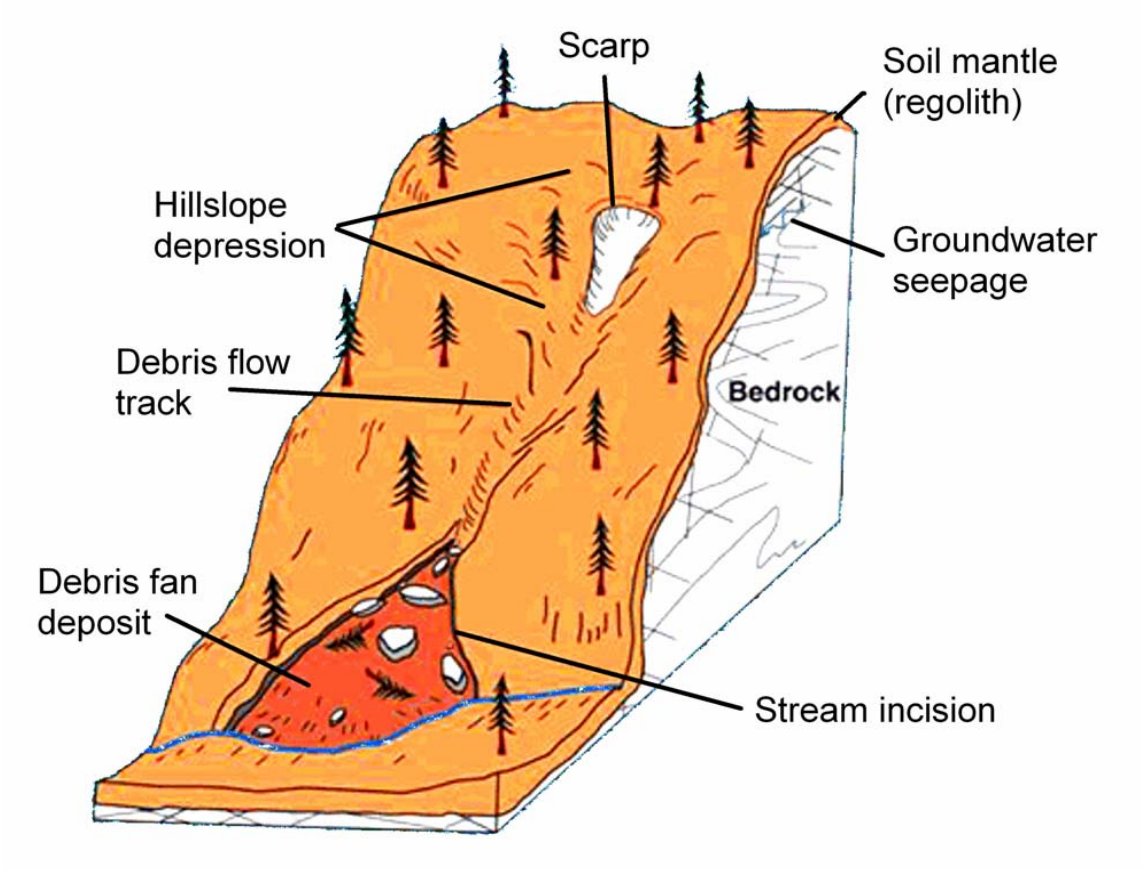

Fig. 5.4 – Main morphological properties of debris flows. Modified after North Carolina Geological Survey.

Alternative terms and translations exist for the term debris flow:

- mudflow (old usage), lahar (volcanic mudflow) (*English*)
- colata di detrito (*Italian*)
- corriente de derrubios, huaycos, flujos de derrubios (*Spanish*)
- Mure, Murgang (*German*)
- lave torrentielle, coulées de debris (*French*)
- přívalový proud, zemní lavina, suťový proud, horninový proud, mura (*Czech*)
- сель (muddy debris flow) (*Russian*)

5.2 Causes and failure mechanisms

Debris flows are commonly triggered by an unusual presence of water. There are three potential sources of excess water (Innes 1983; Costa 1984; Selby 1993): intense rainfall, rapid snowmelt, and more rarely, glacier or lake overflows which mobilize unconsolidated material in their path.

The frequency of debris flow events from individual source areas is controlled by the rate of accumulation of available debris, and by the recurrence of climatic triggering events. Because the rate of accumulated debris is limited, there must be an upper limit to the

magnitude-frequency of debris flows (Innes 1985). A small rainstorm may produce a debris flow in a basin at one time, but a rarer (larger) storm may produce only flash flooding other time. Sediment availability must be considered (Costa 1984).

Rainfall intensity and duration, along with the antecedent rainfall and soil moisture conditions, represent strong controls for debris flow triggering. Rainfall thresholds are commonly defined as the line fitting the minimum intensity of rainfall associated with the occurrence of landslides in different areas (Crosta 1998). The rainfall thresholds were introduced by Caine (1980). A global threshold for shallow landslides and debris flows was calculated by Guzzetti et al. (2008). For the territory of Italian Central Alps or Valtellina, several rainfall thresholds were made (Govi et al. 1984; Cancelli and Nova 1985; Ceriani et al. 1992; Agostoni et al. 1997; Luino et al. 2008). The thresholds are summarized in Table 5.1.

Debris flows are frequent in topographic concavities or hollows. This geometry favours the accumulation of colluvium and the convergence of groundwater flow necessary to cause the failure. Often the material from the source consists of slightly consolidated or unconsolidated moraines, colluvium and weathered rocks. Other source areas include the lower limit of alpine discontinuities, i.e. permafrost above the treeline in the European Alps, in the neighbourhood of debris-filled steep couloirs, mountain torrents, snow patches and contact zones of steep rock walls of rock drifts with talus slope deposits (Corominas et al. 1996). Most debris flows begin as slope failures on steep (greater than 15°-20°) side slopes from a relatively quick influx of large amounts of water. The mass movement usually originates at the head of swales (small first-order drainages), but about one third originates on flat and convex (ridge spurs) side slopes (Smith and Hart 1982). The initial failure can be a slide, slump, or topple (Costa 1984).

Author	Threshold type	Zone	Equation	Note
Govi et al. (1984)	I-D	Central Alps, Lombardy Region	$I = 16.24 \times D^{-0.46}$	
Cancelli and Nova (1985)	I-D	Valtellina, Lombardy Region	$I = 44.668 \times D^{-0.78}$	
Ceriani et al. (1992)	I-D	Lombardy Region	$I = 20.0 \times D^{-0.55}$	
Agostoni et al. (1997)	IMAP-D	Central Alps, Lombardy Region	$I_{MAP} = 2.01 \times D^{-0.55}$	
Luino et al. (2008)	IMAP-D	Sondrio Province, Lombardy Region	$I_{MAP} = 0.68 \times D^{-0.50}$	for $D \leq 10$ h
Luino et al. (2008)	IMAP-D	Sondrio Province, Lombardy Region	$I_{MAP} = 0.32 \times D^{-0.17}$	for $D > 10$ h

Table 5.1 – Rainfall thresholds calculated for the study area. I = Intensity, I_{MAP} = Intensity normalized by mean annual precipitation, D = Duration, h = hour.

When a relatively competent, rigid slab or block of soil becomes saturated above a failure surface, pore pressure increases and shear strength decreases. Overlying soils may or may not be saturated. Pore pressure in soils increases when the rate of deep percolation is slower than the rate of infiltration from melting snow or rainfall. The failure of mass of debris under high pore pressures and diminished shear strength can cause soil particles to lose coherency and to rework the soil mass thoroughly enough to cause remoulding. This causes the debris to change by spontaneous liquefaction from a rigid slab into a viscous fluid, and flow (Terzaghi and Peck 1967).

The transformation from a solid, rigid mass to a viscous fluid can also occur through dilatancy. Dilatancy is described as an increase in the bulk volume of a soil mass which occurs during deformation accompanying slope failures. It is caused by a change from close-packed

structure to open-packed structure, accompanied by an increase in the pore volume. With the additional moisture and remoulding, the solid mass can become a flowing, viscous fluid (Costa 1984). Channel deposits can be also mobilized by runoff and act as sources for debris flows.

5.3 Movement

Debris flows usually follow pre-existing drainage paths, but can move down hill slopes and across unobstructed fan surfaces in almost any direction because flows tend to build their own channels as levées form at the lateral boundaries of the flow. Observed debris flows resemble wet concrete that generally moves down valley in a series of waves or surges, with periods ranging from a few seconds to several hours. Surges originate from the temporary damming and breaching of channels by debris, and damming at constrictions in the channel. The front of debris flow surges are usually higher than trailing portions, and contain the largest boulders being moved. The surges are followed by more fluid, watery, turbulent slurries with unusually high suspended sediment concentrations, but fewer boulders. This more fluid phase continues until next surge arrives or until debris flow activity ceases (Johnson 1970; Pierson 1980; Costa 1984).

The velocity of debris flows varies due to the characteristics of the debris (the size concentration, and sorting of material) and due to channel geometry including shape, slope, width, and sinuosity. Observed velocities range from 0.5 to about 20 m/s (Costa 1984).

Measured bulk densities range from 1.40 g/cm^3 or less for very fluid sediment flows in Japan (Okuda et al. 1980) and Costa Rica (Waldron 1967) to 2.53 g/cm^3 for relatively dry debris flows in the Southern Rocky Mountains (Curry 1966). Costa (1984) classifies flows with bulk densities less than 1.80 g/cm^3 as hyperconcentrated flows. Debris flows have a range in volume concentration of solids of 25 to 86%, with the weight proportion of about 35 to 90%. The water content of debris flows generally ranges from about 10 to 30% or greater by weight. These measured values strongly support the statement that “all that flows is not water” (Costa 1984). There is clearly a continuum from rivers to debris flows. Fluids with a large sediment concentration do not deform until threshold strength is exceeded and behave like a non-Newtonian fluid (Corominas et al. 1996).

Debris flows can be very erosive during passage through steep channels (Pierson 1980). During passage the density can be twice as great as during water floods, and the flow depth during debris surges is greater than that of muddy streamflow between surges (Costa 1984). Some debris flows may be less viscous and move very fast without causing much erosion, while others are more viscous, and leave lateral ridges and scour channels (Selby 1993). The erosion caused on both the channel floor and banks leads some debris flows to significantly increase their volume (Jibson 1989).

5.4 Deposition

Although exceptionally large, fluid debris flows can move many kilometres far from the source areas, viscous flows tend to stop upon reaching a relatively low gradient or in areas of decreased confinement, such as on alluvial fans at the mouth of small basins and canyons. These flows can spread out, thin, and stop in place where internal shear stress is exceeded by the shear strength of the flow (Costa 1984). Some authors (Corominas et al. 1996) distinguish debris fans from alluvial fans. The former have a small basin (first or second order streams) and steep fans. Most of the alluvial fans have slopes smaller than 2°-5°, whereas debris flow fans have slopes greater than 4° (Jackson et al. 1987).

The exact mechanism by which debris flows stop flowing is uncertain. Lateral spreading may permit thickness of flows to decrease below that is needed to flow. Some debris flows spread out onto fan surface as sheets, closely paralleling older fan topography. The aerial extent of debris flow deposits is controlled by volume and strength of flows, and by the slope of fan surface. Debris flows also stop flowing when escaping pore fluids (water, clay, and fine silt) cause an increase in internal friction (Costa 1984).

Takahashi (1981) experimentally determined that the stable slope angle for debris flow deposition is a function of grain concentration by volume in the static debris deposits, density of fluid and solids, particle size, depth of flow, and angle of internal friction. Debris flows cease flowing in drainage channels when internal friction increases and volume, thickness, strength, and channel slope decrease, causing deposition. Debris flows that stop flowing in channels can form temporary debris dams that can be remobilized by another surge. Alternatively, such deposits can remain in the channel for some time before being eroded by either another debris flow or by normal stream flows.

At the distal and marginal edges of flows, lobes with steep fronts and concentration of boulders frequently occur (Fig. 5.5). Thicknesses of deposits decrease downfan. Just prior to deposition, debris flows must be moving quite slowly since small vegetation on fans and in channels is capable of diverting debris flows transporting very coarse boulders, without being knocked over or scarred (Costa and Jarrett 1981).

When debris flow stops, the resulting deposits consist of a uniform distribution of sizes up through boulders in matrix of fine grained sediments, forming a pebbly-mud-stone deposit (diamicton). Boulders are supported in a matrix containing substantial amounts of fine grained sediment. Some debris flows can be clast-supported when the matrix drains or is washed away. However, some matrix material may occasionally be found beneath the washed surface boulders (Costa and Jarrett 1981). Debris flow matrix may also contain light weight material such as wood and bark fragments, pine needles and cone chips, and animal droppings which should have floated away if water and mud floods were responsible for the deposits (Sharp and Nobles 1953). Debris flow deposits are much more poorly sorted than water-laid deposits, and bedding is virtually non-existent. Contacts tend to be sharp (Costa 1984). Because of the small difference in density between boulders and fluid material in debris flows, buoyant forces and dispersive pressures may concentrate boulders at the top of the deposit, forming reverse grading (Fisher 1971).

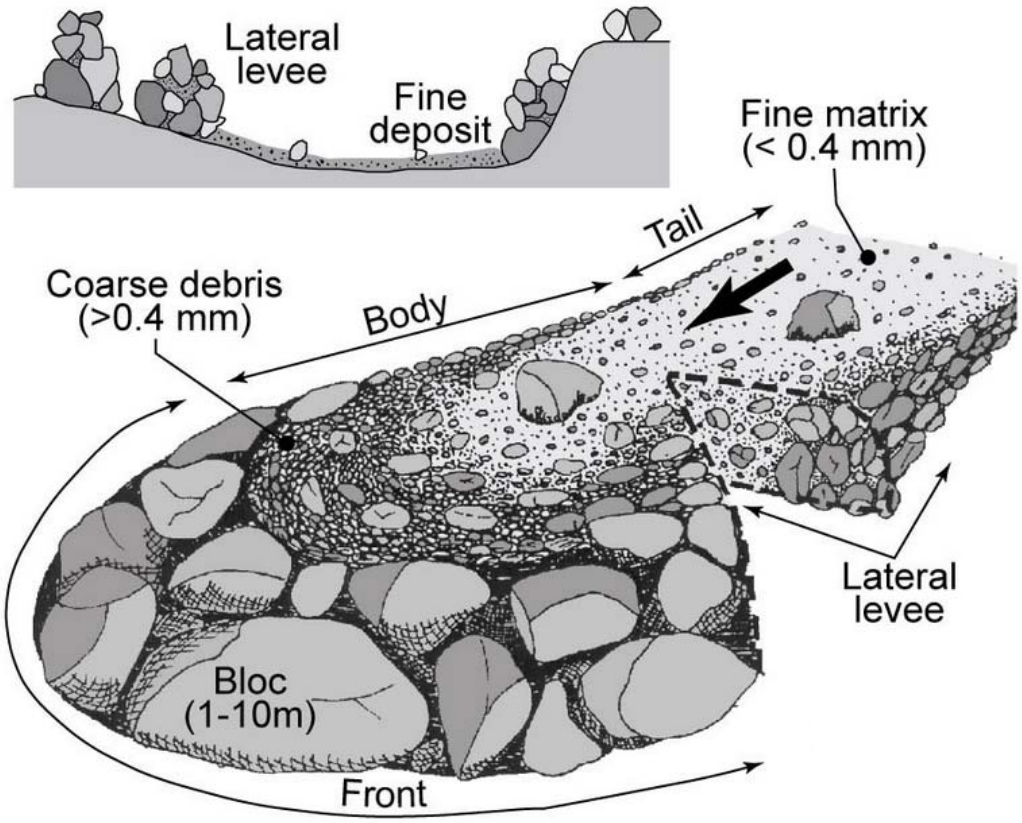

Fig. 5.5 – Morphology of the deposition area of debris flows. Source: Bardou (2002).

Debris flow deposits are commonly reworked, sorted, and stratified by the watery tails of debris flows or by subsequent water flows (Costa 1984). Debris flows have well graded deposits with small clay content, generally less than 5% (Corominas et al 1996).

5.5 Types of debris flows

Debris flow types and properties have been recognized and studied by a number of authors (Takahashi 1981; Costa 1984; Davies 1986; Pierson 1986; van Steijn 1988; Corominas et al. 1996; Hungr et al. 2001; Jakob 2005) and they were studied from different points of view: field observations, flow characteristics, material behaviour, material components, etc. However, there is no general agreement on classification and flow modelling in present literature.

Coussot and Meunier (1996) present two basic types of debris flows: muddy debris flows and granular debris flows. Both of them are present in the study area of Valtellina di Tirano (Fig. 5.6).

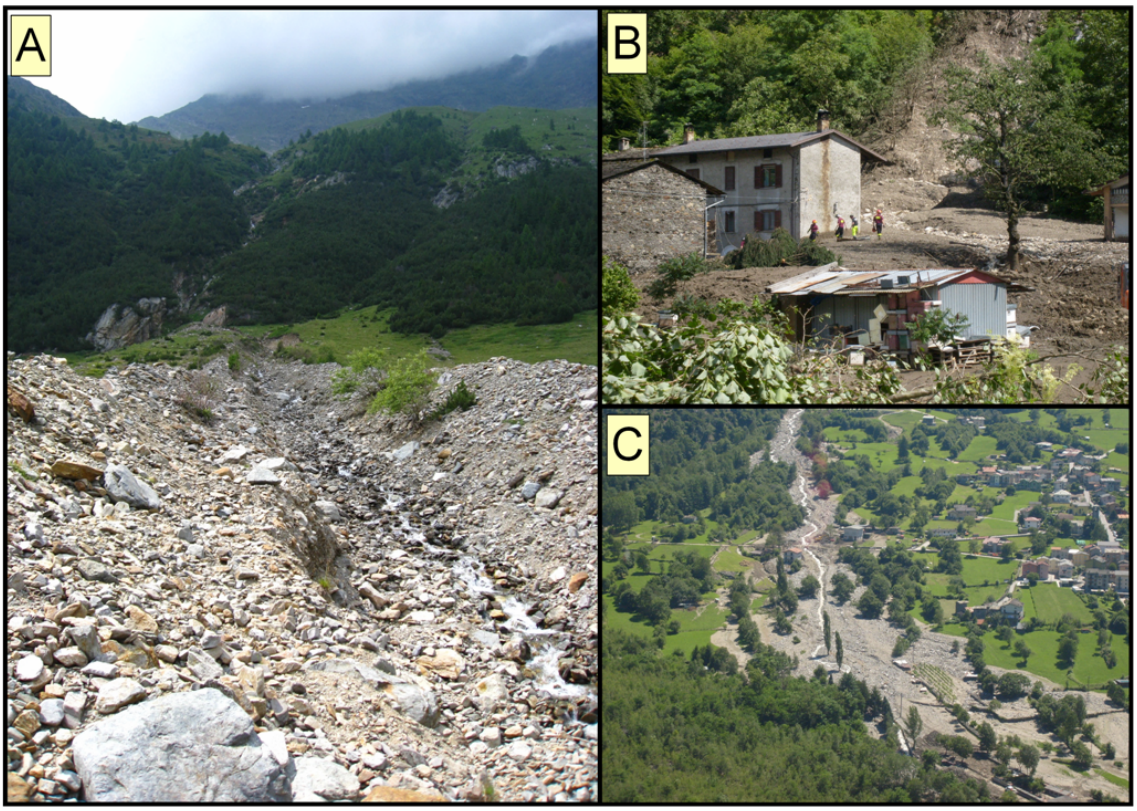

Fig. 5.6 – Photographs of two main types of debris flows present in the study area. A = lateral levees of a granular debris flow in Val Grosina, B = Deposits of muddy-debris flow in Selvetta, C = deposits of granular debris flow in Talamona. Photo A: J. Blahut, photos B and C: F. Luino.

Crosta et al. (1990) made a classification of debris flows for Valtellina area. According to their investigations in 1987, four categories of debris flows were distinguished in the study area:

1) Debris flows in unchannelled basins
2) Debris flows in channelled basins
3) Debris avalanches
4) Debris torrents

Ad 1): Debris flows in unchannelled basins, or zero order basins originated as soil-slips or shallow slides in the grass covered colluvium that accumulates in the concave axial regions, or hollows, commonly present upslope of the channel network. The hydrogeological conditions that led to the failure of these debris flows were related to the lithological and morphological settings. The catchment areas were small and limited to hollows.

Ad 2): Debris flow in channelled basins occurred on slopes of intermediate steepness (15°-40°), drained by the exterior links of the drainage network. They originated as rotational or translational soil slides in colluvial deposits. The hydrogeological conditions that promoted the initiation of channelled debris flows were similar to those of unchanneled debris flows. The former differ from the latter mostly because scouring and erosion were not limited to the source area. Channelled debris flows had enough erosional power to scour downslope from the source area, picking-up material along the trail, thus increasing the volume of debris delivered to the deposition area. This resulted in abundant elongated scars along the drainage channels. The

catchment areas were, on average, slightly larger than in the case of unchannelled debris flows and the material was slightly coarser (Crosta 1990).

Ad 3): Debris flows in the interbasins were mostly debris avalanches and, occasionally rock-slides or soil-slips. They originated from the thin cover of colluvial deposits present on very steep (>45°), forested slopes. The catchment areas were generally limited to few tens or few hundreds of square meters. This suggests that the hydrogeological conditions prone to the failure of debris avalanches were extremely localized, and therefore quite difficult to detect with certainty.

Ad 4): Debris torrents initiated in gorges or narrow valleys, and caused by the failure or breaching of landslide dams, debris flow or snow avalanche blockages, and alternatively by the failure of embankments, check dams, or bridges, that released in sudden bursts, the accumulated debris. The flowing mass carried large boulders and blocks up to 3 m in diameter and delivered large volumes of debris, and organic material to the alluvial fans at the outlet of the main drainage channels.

5.6 Mitigation of hazards

Costa (1984) distinguishes four main categories of debris flow mitigation measures:

1) Avoidance of hazardous areas;
2) Control of grading, clearing, and drainage;
3) Protective structures;
4) Warning and evacuation.

Ad 1): Because of the favourable conditions above floodplains, alluvial fans have been favoured for development for long time. Unfortunately, compared to water floods, mitigation procedures and identification of risk areas for debris flows are still poorly developed. Moreover, number of scientific studies focus on one-site investigations of hazard and risk assessment from debris flows and less attention is paid to medium/regional scale analysis which could be used for spatial planning purposes. Sometimes, this situation consequently leads to an underestimation of debris flow hazard and risk on medium/regional scale.

Ad 2): Several techniques can be applied to reduce erosion and thus control the availability of material which can be mobilised. For that purpose, check dams are often used as "sediment traps" to capture available debris on torrent streams. Sometimes, this approach can lead to a growth of problems in the case of low maintenance and no cleaning of the dams. After a hypothetical rupture of the dam, a debris flow has much more material that could be mobilised, in comparison with natural torrents where debris flows happen more frequently and clean the stream. Other techniques of gully and slope erosion control are: channel linings, revegetation of gully sides, regrading of steep gully walls, diversion dykes and ditches, etc.

Ad 3): Protective structures are constructed in cases where the avoidance of hazardous areas is not possible. The main purpose of these structures is to stop, to slow, or to divert debris

flows. According to Costa (1984), protective measures to reduce property damage from debris flows are different from mitigation measures for water floods. For example, canalisation for debris flows is usually ineffective because channels can quickly become blocked, causing subsequent surges to flow in new directions. Reservoirs can be filled quickly and require extensive dredging to maintain designed capacity. Structural fences of steel or reinforced concrete and open-work dams can be quite effective in separating coarse debris (large boulders) from finer fraction and water. Retaining and deflecting walls are probably most used protection against debris flows in the Alps.

Ad 4): Direct warning and evacuation for specific flows are quite difficult to provide since debris flows frequently result from sudden ground failures and travel at high velocities. In the case of rainfall triggered debris flows, a warning system based on rainfall thresholds can be adopted to warn people and to evacuate large areas (as in Lombardy Region).

5.7 Final remarks

Debris flows are frequent and recurrent phenomena in mountainous areas throughout the world and till nowadays they pose serious threat to lives of people and their properties. The socioeconomic impact and the loss of life, property and agriculture can be catastrophic in the case of large debris flows through populated areas. However, smaller debris flows may also cause serious damage in mountainous regions (e.g. Valtellina Valley) destroying houses, roads, railways and bridges (Corominas et al. 1996). One example of small but destructive debris flow is the case of Selvetta debris flow from July 2008 (Chapter 10). It is essential that potential source areas and runout zones are correctly assessed and mitigation measures adopted using modern mapping and monitoring techniques.

5.8 References

Agostoni, S., Laffi, R., Sciesa, E. (1997): Centri abitati instabili della provincia di Sondrio. CNR-GNDCI, Milano, 59 pp. + Annexes.

Bardou, E. (2002): Méthodologie de diagnostic des laves torrentielles sur un bassin versant alpin. Thesis, no. 2479, EPFL, Lausanne. 171 p.

Cancelli, A., Nova, R. (1985): Landslides in soil debris cover triggered by rainstorms in Valtellina (Central Alps – Italy). In: Proceedings of 4th International Conference and Field Workshop on Landslides. The Japan Geological Society, Tokyo, pp. 267–272.

Caine, N. (1980): The rainfall intensity duration control of shallow landslides and debris flow. Geografiska Annaler Series A Physical Geography, 62: 23-27.

Ceriani, M., Lauzi, S., Padovan, N. (1992): Rainfall and landslides in the Alpine area of Lombardia Region, Central Alps, Italy. In: Proceedings of the Internationales Symposium Interpraevent. Bern, 2: 9-20.

Corominas, J., Remondo, J., Farias, P., Estevao, M., Zézere, J., de Terán, J.D., Dikau, R., Schrott, L., Moya, J., Gonzáles, A. (1996): Debris flow. In: Dikau, R., Brundsen, D., Schrott, L., Ibsen, M.-L. (Eds.): Landslide Recognition: Identification, Movement and Causes. John Wiley & Sons, pp. 161-180.

Costa, J.E. (1984): Physical geomorphology of debris flows. In: Costa, J.E., Fleisher, P.J. (Eds.): Developments and Applications of Geomorphology, Springer-Verlag, pp. 268-317.

Costa, J.E., Jarrett, R.D. (1981): Debris Flows in Small Mountain Stream Channels of Colorado and Their Hydrologic Implications. Bulletin of the Association of Engineering Geologists, 18: 309-322.

Coussot, P., Meunier, M. (1996): Recognition, classification and mechanical description of debris flows. Earth-Science Reviews, 40: 209-227.

Crosta, G. (1990): A study of slope movements caused by heavy rainfall in Valtellina (Italy – July 1987). In: Cancelli, A. (Ed.): Proceedings of ALPS90, Alpine Landslide Practical Seminar – 6th ICFL International Conference and Field Workshop on Landslides, University of Milano, Milano, pp. 247–258.

Crosta, G. (1998): Regionalization of rainfall thresholds: an aid to landslide hazard evaluation. Environmental Geology, 35: 131-145.

Crosta, G., Marchetti, M., Guzzetti, F., Reichenbach, P. (1990): Morphological classification of debris-flow processes in South-Central Alps (Italy). Proceedings of the 6th International IAEG Congress, Amsterdam, pp. 1565-1572.

Cruden D.M., Varnes, D.J. (1996): Landslide types and processes. In: Turner A.K.; Shuster R.L. (Eds.): Landslides: Investigation and Mitigation. Transportation Research Board, Special Report No. 247, pp. 36-75.

Curry, R.R. (1966): Observation of alpine mudflows in the Tenmile Range, Central Colorado. Geological Society of America Bulletin, 77: 771-776.

Davies, T.R.H. (1986): Large debris flows: A macro-viscous phenomenon. Acta Mechanica, 63: 161-178.

Fisher, R.V. (1971): Features of coarse-grained, high-concentration fluids and their deposits. Journal of Sedimentary Petrology, 41: 916-927.

Glade, T., Crozier, M.J. (2005): A Review of Scale Dependency in Landslide Hazard and Risk Analysis. In: Glade, T., Anderson, M., Crozier, M.J. (Eds.): Landslide Hazard and Risk. John Wiley & Sons Ltd, Chichester, pp. 75-138.

Govi, M., Mortara, G., Sorzana, P. (1984): Eventi idrologici e frane. Geologia Applicata e Idrogeologia, XCVIII, 3 p.

Guzzetti, F., Peruccacci, S., Rossi, M., Stark, C.P. (2008): The rainfall intensity–duration control of shallow landslides and debris flows: an update. Landslides, 5: 3-17.

Hungr, O., Evans, S.G., Bovis, M., Hutchinson, J.N. (2001): Review of the classification of landslides of the flow type. Environmental and Engineering Geoscience, VII: 221-238.

Hutchinson, J.N. (1988): Morphological and geotechnical parameters of landslides in relation to geology and hydrogeology. In: Bonnard, C. (Ed.): Landslides. Proceedings of 5th International Symposium on Landslides, 1, pp. 3-35.

Innes, J. (1983): Debris flows. Progress in Physical Geography, 7: 469-501.

Innes, J. (1985): Lichenometric dating of debris flow deposits on alpine colluvial fans in southwest Norway. Earth Surface Processes and Landforms, 10: 519-524.

Jackson, L.E., Kostaschuk, R.A., MacDonald, G.M. (1987): Identification of debris flow hazard on alluvial fans in the Canadian Rocky Mountains. Geological Society of America Review Engineering Geology, VII: 115-124.

Jakob, M. (2005): A size classification for debris flows. Engineering Geology, 79: 151-161.

Jibson, R.W. (1989): Debris flows in southern Puerto Rico. Geological Society of America Special Paper, 236: 29-56.

Johnson, A.M. (1970): Physical Processes in Geology. W.H. Freeman, 557 p.

Luino, F., Nigrelli, G., Biddoccu, M., Cirio, C.G., Di Palma, M., Missaglia, M., Fassi, P. (2008): Definizione delle soglie pluviometriche d´innesco di frane superficiali e colate torrentizie: accorpamento per aree omogenee. IRER, Milano, 125 p.

Němčok, A., Pašek, J., Rybář, J. (1972): Classification of landslides and other mass movements. Rock Mechanics and Rock Engineering, 4: 71-78.

Okuda, S., Suwa, H., Okunishi, K. Yokoyama, K., Nakano, M. (1980): Observation on the motion of a debris flow and its geomorphological effects. Zeitschrift für Geomorphologie, Suppl., 35: 142-163.

Pierson, T.C. (1980): Erosion and deposition by debris flows at Mt Thomas, North Canterbury, New Zealand. Earth Surface Processes, 5: 227-247.

Pierson, T.C. (1986): Flow behavior of channelized debris flows, Mount St. Helens, Washington. In: Abrahams, A.D. (Ed.): Hillslope Processes. Allen and Unwin, Boston, pp. 269-296.

Sharp, R.P., Nobles, L.H. (1953): Mudflow of 1941 at Wrightwood, southern California. Geological Society of America Bulletin, 64: 547-560.

Selby, M.J. (1993): Hillslope Materials and Processes. Oxford University Press, 451 p.

Smith, T.C., Hart, E.W. (1982): Landslides and related storm damage, January 1982, San Francisco Bay region. California Geology, 35: 139-152.

Takahashi, T. (1981): Debris flow. Annual Review of Fluid Mechanics, 13: 57-77.

Terzaghi, K., Peck, R.B. (1967): Soil Mechanics in Engineering Practice. Wiley, New York, 549 p.

Varnes, D.J. (1978): Slope movement types and processes. In: Schuster R.L., Krizek R. J. (Eds.): Landslides, analysis and control. Transportation Research Board, Special Report No. 176, National Academy of Sciences, pp. 11-33.

van Steijn, H. (1988): Debris flows involved in the development of Pleistocene stratified slope deposits. Zeitschrift für Geomorphologie, 71: 45-58.

Waldron, H.H. (1967): Debris flow and erosion control problems caused by the ash eruptions of Irazu Volcano, Costa Rica. U.S. Geological Survey Bulletin. 1241-I: 1–37.

Chapter 6

Susceptibility analysis

Not everything that can be counted counts,
and not everything that counts can be counted.

(A. Einstein)

Based on:

Blahut, J., van Westen, C.J., Sterlacchini, S. (2010): Analysis of landslide inventories for accurate prediction of debris-flow source areas. Geomorphology, 16 p. (in press)

6.1 Introduction

Landslides are among the most significant natural damaging events in mountain environments. They are one of the primary causes of property damage, loss of life and injuries of persons. To better predict future occurrences of landslides and improve prevention and mitigation measures, hazard or susceptibility analyses are performed. Landslide susceptibility analysis (or so called spatial probability of landslide occurrence) using statistical techniques is based on the assessment of terrain conditions in an area subjected to previous landslides (Carrara et al. 1995). The conditions that caused the landslides are assumed to be the same for future landslides. Such a landslide susceptibility analysis at a medium scale (1:25,000 to 1:50,000) has been used as one of the first steps in landslide hazard assessment (Remondo et al. 2005; Fell et al. 2008). The performance of the models can be effectively evaluated and the prediction power of the models could be validated using techniques such as ROC curves or success and prediction rate curves to compute areas under curves (Chung and Fabbri 1999, 2003; Beguería 2006).

A main problem in landslide hazard assessment is the definition of magnitude and frequency of prospective events. Although there are many methods for landslide susceptibility assessment, only few techniques convert the result into landslide hazard maps based on temporal probability assessment. One of them is the use of event based inventory maps. The return periods of landslide triggering events are used for assessing temporal probability which is then combined with size and spatial probabilities generated from event-based inventories (Guzzetti et al. 2006a). However, only a few complete landslide inventories are available. Italy is one of the countries where such inventory databases have been made in a consistent manner.

This study focuses on the mapping of source areas of landslide-induced debris flows in the Valtellina Valley. According to Crosta et al. (1990), the majority of debris flows in the study area originates from soil-slips or shallow slides. They usually leave broad sheet-like scars which are easily recognizable on aerial photographs.

For the generation of susceptibility maps on medium scales (1:25,000 to 1:50,000) using statistical techniques, a reliable landslide inventory is needed, together with factor maps used as inputs of the analysis. This chapter presents a comparison of landslide susceptibility maps obtained with the same methodology but using different landslide inventories. Analysis results using the official Italian landslide inventory GeoIFFI (2006) for the Lombardy Region were compared with the results from a recently mapped inventory (DF2001). The analysis included four main steps: (i) preparation of the debris flow inventories (random and spatial partition) and factor maps (explanatory variables), (ii) calculation of accountability and reliability indices for a preliminary susceptibility analysis and selection of an appropriate combination of the factor maps used in the detailed analysis, (iii) evaluation and validation of the susceptibility maps, and (iv) comparison of the results and selection of the final map.

Statistically-based susceptibility assessment for the source areas of landslide-induced debris flow was performed using different landslide inventories in order to evaluate the effect of the accuracy of the input data on the prediction capabilities of the resulting susceptibility maps.

The same input data and analytical methods were used for all inventories. This study also evaluates the improvement of the predictions when the area is divided into geomorphologically homogeneous zones.

6.2 Materials and methods

In order to compare susceptibility maps created from different inventories, the methodology was applied as presented in Fig. 6.1. Firstly, the existing inventory was compared with a newly generated landslide inventory. Based on an initial set of factor maps, accountability and reliability indices were estimated to choose different combinations of factor maps as inputs for Weights-of-Evidence (WofE) modelling. The two landslide inventories were randomly and spatially subdivided and WofE modelling was applied to calculate susceptibility models. The assessment of the model performance and prediction power of the susceptibility maps was made by the analysis of success and prediction rate curves with corresponding areas under curves (Chung and Fabbri 1999, 2003). Afterwards, highly performing models were compared and their spatial variability was assessed. Finally, the best model was chosen to create the final debris flow susceptibility map.

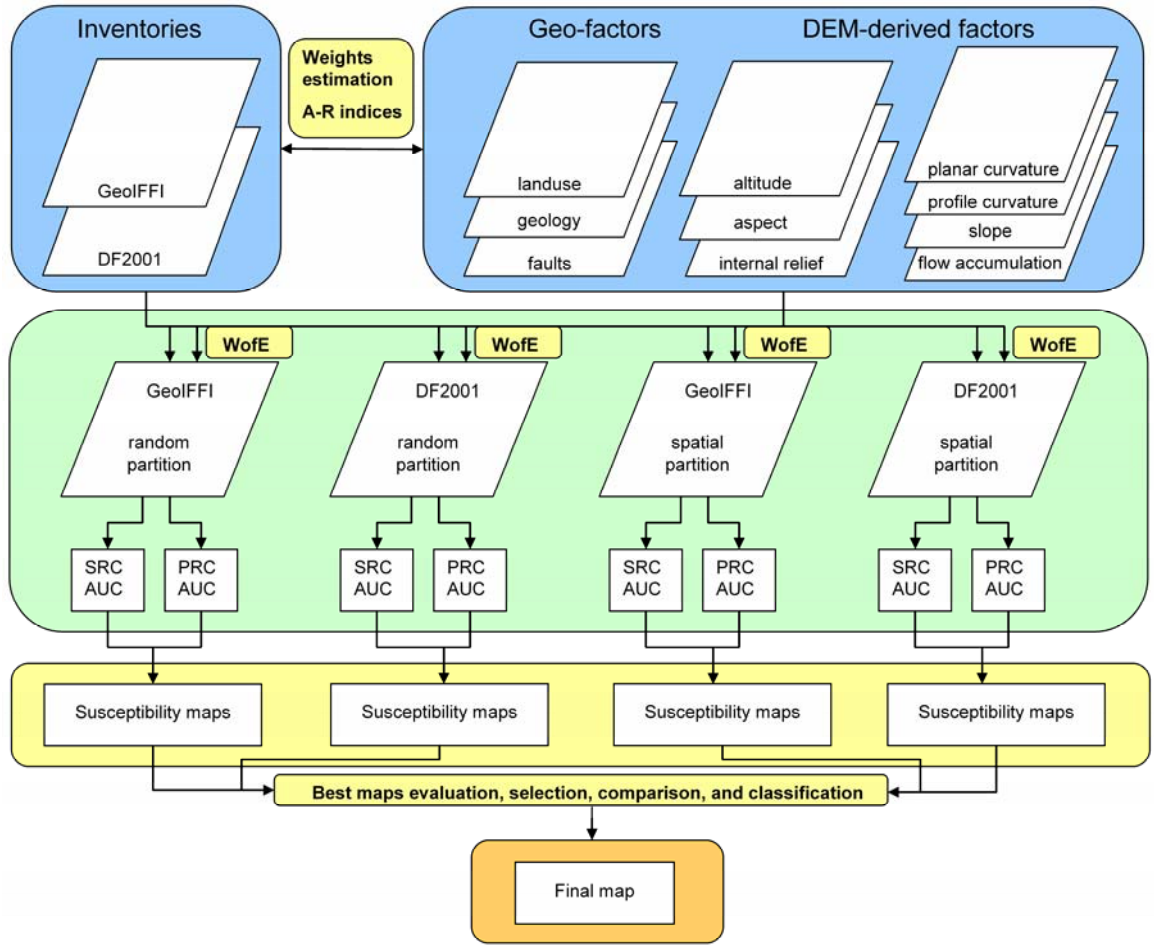

Fig. 6.1 – Flowchart of the applied susceptibility analysis methodology.

6.2.1 Landslide inventories

There are three official landslide inventory databases available for the study area:

- The AVI database: a bibliographical and archive inventory of landslides and floods in Italy (Guzzetti et al. 1994), which is updated regularly. The AVI Database was originally designed to inventorize all places in Italy which were harmed by landslides or floods. No spatial scale was defined for this database, and the information was visualized as georeferenced points.
- The regional database of landslides of the Lombardy Region (Lombardy Region 2002), mapped at 1:10,000 scale.
- The GeoIFFI landslide inventory database for the Lombardy Region (GeoIFFI 2006), which is part of the IFFI National Database.

Unfortunately, there is only limited information about debris flow source areas in the AVI and Regional databases. In the AVI database there are a total of 80 events within the study area, but only 12 of them are classified as debris flows and only 3 events have a precise date (day, month and year). In the regional database there are a total of 501 events within the study area, of which 46 are classified as debris flows. Unfortunately, only 7 of them have information about the exact date of occurrence. Another problem with using these databases is related to the spatial location of the events. Both databases have coordinates with location of the events but only in some cases the points are located in the scarp areas, and mostly they are in the transport or deposition areas.

The GeoIFFI database was made by incorporating the two previously mentioned inventories. The database consists of different types of landslides such as debris flows, earth flows, shallow landslides, and deep seated gravitational slope deformations mapped by points, lines, and polygons. Unfortunately, there is no information on the time of occurrence of the debris flows; as a consequence, there is no possibility to divide the inventory into temporal subsets related to past triggering events. For this study, only debris flow scarp areas mapped as points were considered because there are only few debris flows mapped as polygons or lines in the database. Moreover, in the case of polygons and lines the scarp areas are not clearly distinguishable from the rest of the flow.

The GEoIFFI inventory contained 1,478 debris flow scarps. Because the inventory included mistakes with the positions of the scarps, we decided to make a new inventory (abbreviated as DF2001). We prepared this inventory by the interpretation of aerial photographs taken in 2001. A total of 573 debris flow scarp polygons (with a total area of 4.4 km^2) were mapped. The ILWIS software (ITC 2009) was used for the precise delimitation of the scarp polygons using the aerial photographs and a DEM. The DF2001 inventory has several advantages compared to the GeoIFFI database such as the use of polygons as mapping units instead of points of GeoIFFI database (Fig. 6.2) and the exclusion of the debris flow scarps that were initiated on anthropogenic terraced terrain due to the collapse of man-made dry stone walls supporting the terraces. Because of the scale of this study and a lack of data about the present state of these dry stone walls, only natural landslide-induced debris flow scarps were taken into account.

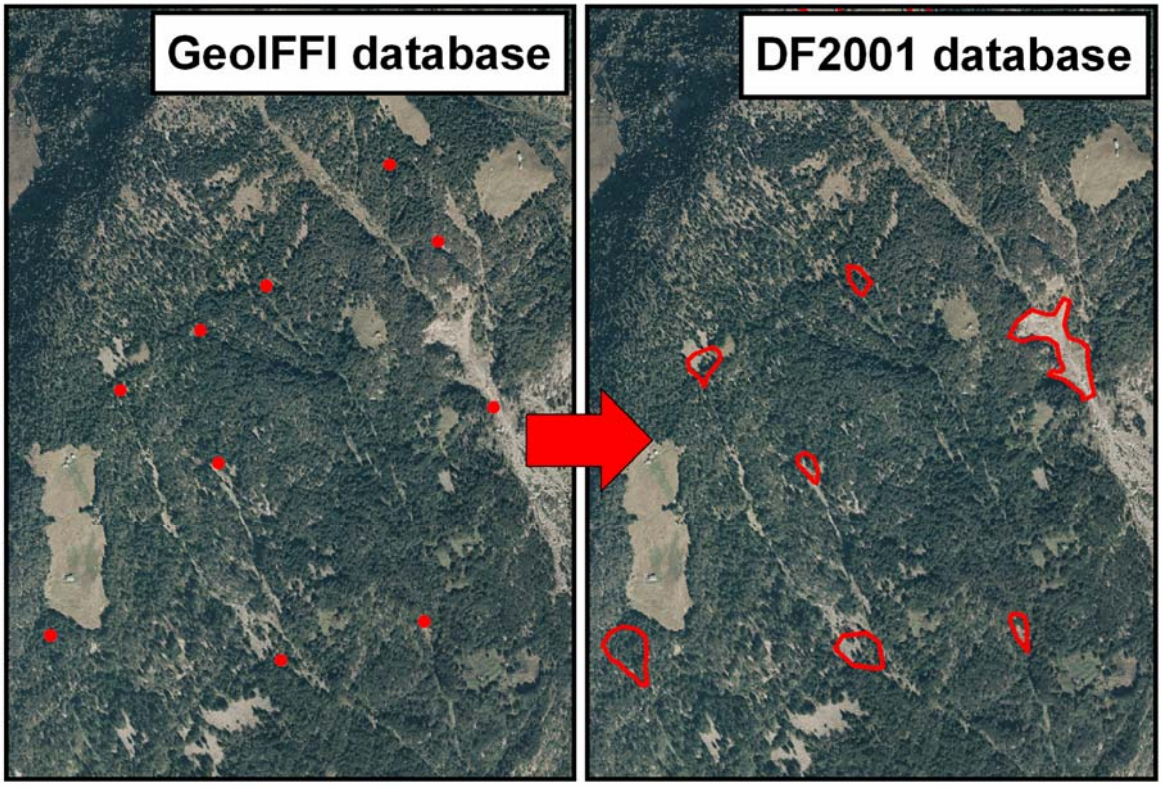

Fig. 6.2 – Scheme showing the generation of the new DF2001 database. Location of the area is shown on Fig. 6.6.

Both the GeoIFFI and the DF2001 inventories were randomly subdivided into two mutually exclusive equally large subsets. As already mentioned, both inventories were also spatially subdivided into three subsets based on their geomorphological position in the study area. The training subsets were used for the construction of the model, and the validation subset was used for independent validation of the predictive power of resulting models.

6.2.2 Factor maps

After evaluating the literature (Carrara et al. 1991; Soeters and van Westen 1996; Guzzetti et al. 1999; Castellanos Abella 2008), a total of 10 causal factor maps were collected (Fig. 6.3). These ten maps could be divided in two groups: DEM derived factors and geo-factors.

For the preparation of these maps, a DEM of the study area with a 10 m resolution was used, which was derived by the Cartographical Office of the Mountain Consortium of Municipalities of Valtellina di Tirano. This DEM was originally made from contour lines (with a contour interval of 1 meter in urbanized areas and 10 m in the rest of the territory) and additional points with spot heights (obtained by photogrammetry from the 2001 air photos). The following maps were derived from the DEM using ArcGIS tools: altitude, internal relief, planar curvature, profile curvature, slope, slope aspects, and flow accumulation. All maps were classified into 10 classes using quantiles, except for the aspect map, which had 9 classes (8 for the main compass directions and 1 for flat areas).

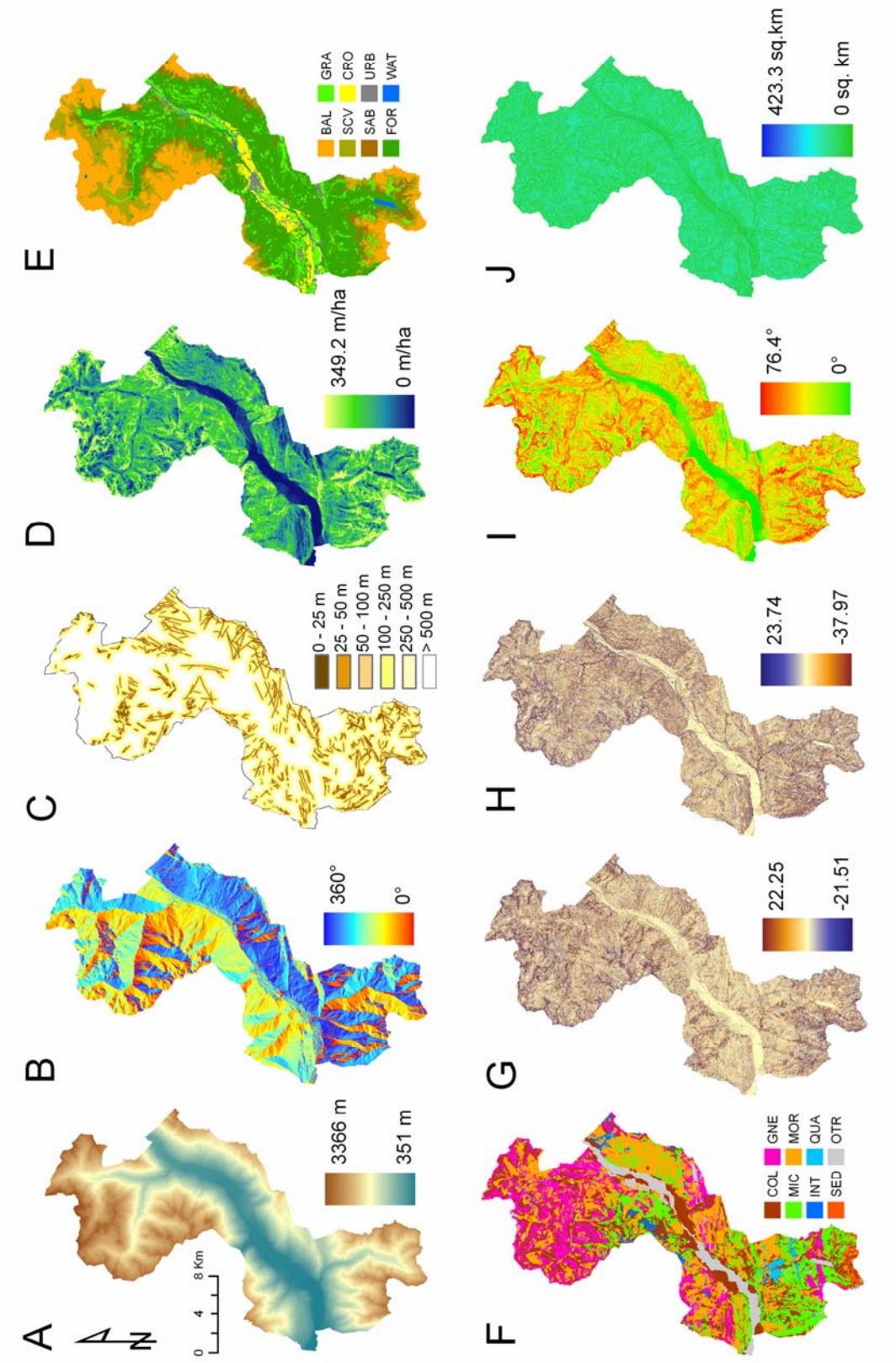

Fig. 6.3 – Ten factor maps used in the WofE analysis. A – altitude, B – aspect, C – distance to faults, D – internal relief, E – land use, F – geology, G – planar curvature, H – profile curvature, I – slope, J – flow accumulation. Land use and geology factor maps are generalised and re-classified. BAL: Bare land, SCV: Scarce vegetation, SAB: Shrubs and bushes, FOR: Forests, GRA: Grassland, CRO: Crops, URB: Urban fabric, WAT: Water courses, COL: Colluvial sediments, MIC: Micaschists, INT: Intrusive rocks, SED: Sedimentary rocks, GNE: Gneiss, MOR: Moraine deposits, QUA: Quartzite OTR: Other rock types.

Usage of quantile classification of factor maps may cause important consequences when extremely skewed data distributions are used as input. By using quantiles, it is possible to better explore the behaviour of the variable with respect to the landslide occurrence because the rank-ordered variables are proportionally distributed.

For the preparation of geo-factor maps several sources were used:

- A land use map, derived from the 1:10,000 scale map of the DUSAF Project (2003), made by Lombardy Region using orthophotos from the year 2001. The map contains 23 classes of which the largest ones are coniferous trees and scarce vegetation.
- A geological surface material map, rasterized from a 1:10,000 scale geological map of Lombardy Region generated by the CARG Project (1992). The map contains 51 classes of lithological as well as soil cover units mapped directly in the field and by photo interpretation. Morainic deposits and gneiss rocks represent the most frequent classes.
- A distance to faults map, derived using tectonic lines extracted from the 1:10,000 tectonic map from the CARG Project (1992). Local experts suggest that the effect of the most important faults mapped in the study site on landslide occurrence may extend up to 500 meters. Thus a six class map was prepared with different buffer limits (25, 50, 100, 250 and 500 meters), in order to consider the possible deterioration of the physical and mechanical characteristics of rock masses along tectonic lines and thus the potential availability of loose material.

6.2.3 Study area characteristics in relation to debris flows source areas

Basic data analysis was firstly applied in order to analyse relations with debris flow inventories and factor maps. Frequency histograms were calculated showing the distribution of GeoIFFI and DF2001 inventories on the factor maps (Fig. 6.4). It can be seen that no particular difference between the inventories distribution could be noted except some minor variation in case of the aspect and geology.

In order to capture different characteristics of debris flow source areas in the different places (Fig. 6.5) of the studied area, the landslide inventories were divided in three subsets: a Northern part, a Central part and a Southern part (Fig. 6.6). The Northern subset lies in the Val Grosina Valleys, which are two tributary valleys of the main valley belonging to the Rhaetic Alps. They represent the highest altitudes in the area with typical alpine relief. Glaciers played a major role in the development of the morphology and they are still present in a limited area in the highest altitudes. The majority of this area is underlain by gneiss bedrock. Rock glaciers and landslide deposits are typical in this part of the territory. Slopes of the Central subset are covered mainly by moraine deposits. On both flanks, Pleistocene glacial terraces are present. The Southern subset covers five parallel valleys from which Val Belviso is the largest one. The southern territory is mainly composed of micaschists but sedimentary rocks are also present in the southernmost part. Geomorphologically, it is part of the Orobic Alps.

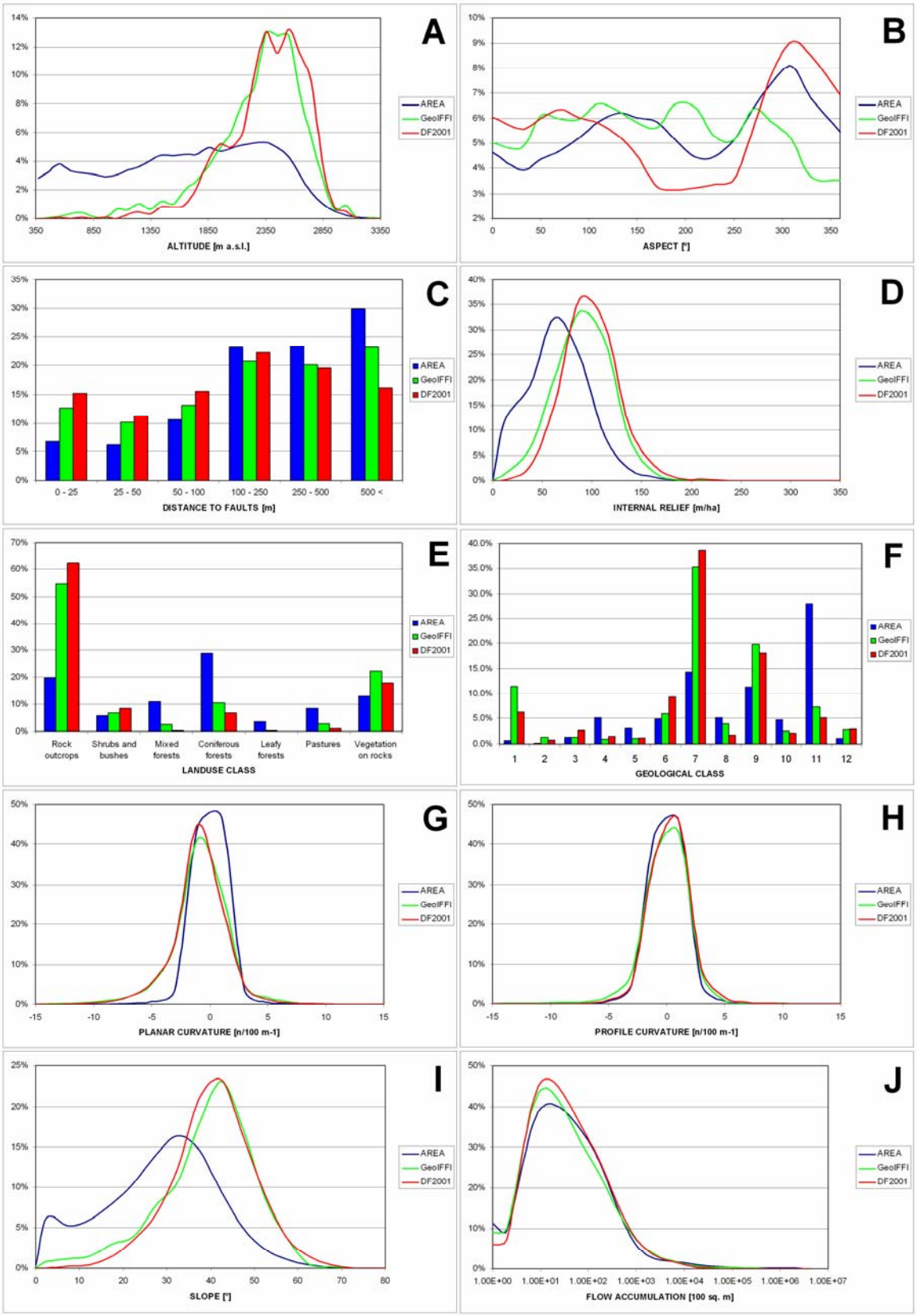

Fig. 6.4 – Frequency histograms of GeoIFFI and DF2001 debris flow inventories and the study area for each factor map. A – altitude, B – aspect, C – distance to faults, D – internal relief, E – land use, F – geology (1: Sandstones, 2: Clays, 3: Non colonized debris cones, 4: Elluvio-colluvium, 5: Colonized debris, 6: Non colonized debris, 7: Gneiss outcrops, 8: Gneiss, 9: Micaschists outcrops, 10: Micaschists, 11: Morainic sediments, 12: Intrusive rocks outcrops), G – planar curvature, H – profile curvature, I – slope, J – flow accumulation. Only classes with higher than 1% frequency are showed.

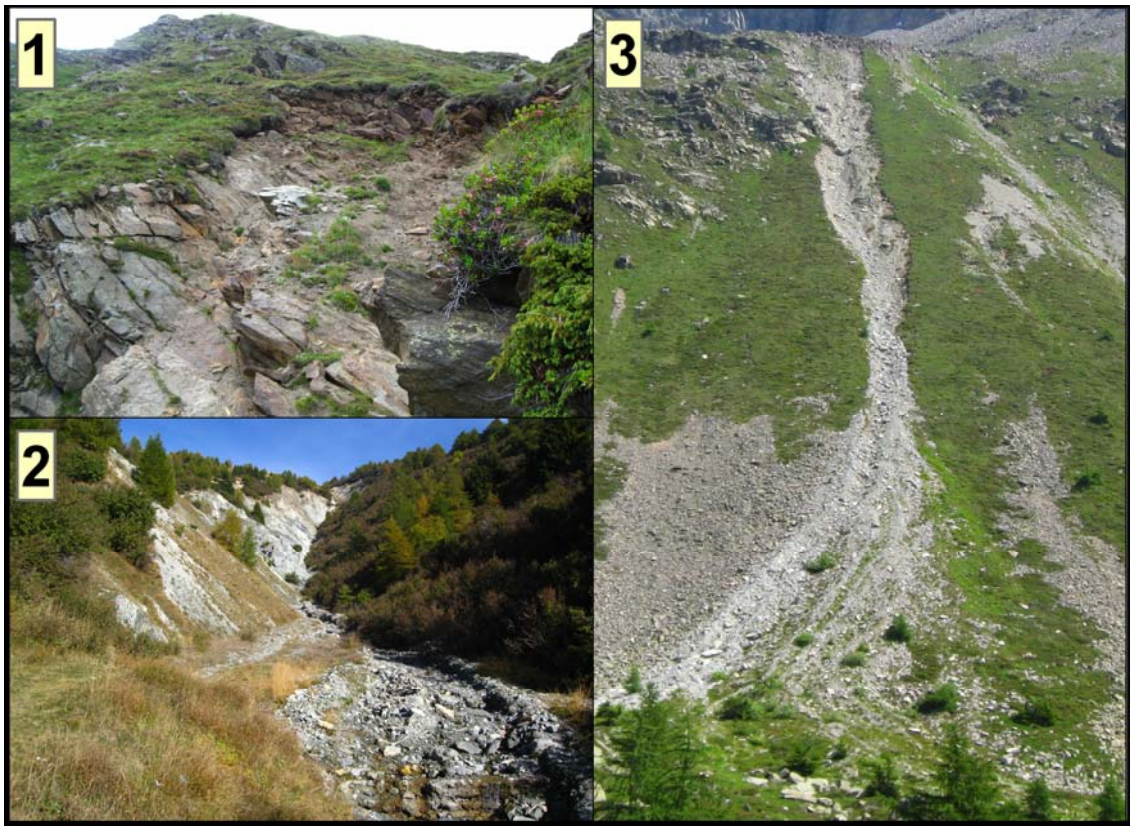

Fig. 6.5 – Photographs of the main types of debris flow scarps in the study area. 1 – debris flow scarp in the Val Grosina Valley in highly fractured gneiss; 2 – Scarp in moraine deposits in the central part of the study area; 3 – debris flow in unconsolidated colluvial sediments in the Val Belviso Valley. Locations of the photos are shown in Fig. 6.6. Photos: J. Blahut.

6.2.4 Methodology

Basic weights estimation, accountability and reliability

As a first step in the susceptibility analysis, the prior probabilities were estimated as overall debris flow scarp densities. For the GeoIFFI database, the prior probability of landslide scarps was relatively small (0.000327) as scarps are represented by 1,478 10×10 m cells in an area of ca. 450 km^2 (4,515,418 cells). Using 573 polygons in the DF2001 database, rasterized as 43,846 10×10 m cells, the prior probability was estimated to be 0.00971. After the subdivision of the inventories in the random and spatial subsets, the prior probabilities obviously declined.

Subsequently, the ten factor maps were overlaid with the two landslide inventories in order to calculate the densities of scarps in all classes of each factor map. These densities were then compared with the prior probabilities discussed above. For the analysis of the different contributing factors to debris flow triggering, two estimators called “accountability” and “reliability” were applied. These were introduced by Greenbaum et al. (1995a, 1995b) and used by Castellanos Abella (2008) as simple indicators of the importance of particular classes of factor maps contributing to landslide occurrence. The accountability is calculated as the sum of landslide pixels in those classes of factor maps with a landslide density greater than the average density in the whole area divided by the sum of landslide pixels over the whole area and

multiplied by 100. The reliability is calculated as the sum of landslide pixels in those classes of factor maps with density values greater than the average density in the whole area divided by the area of these classes and multiplied by 100 (Castellanos Abella 2008).

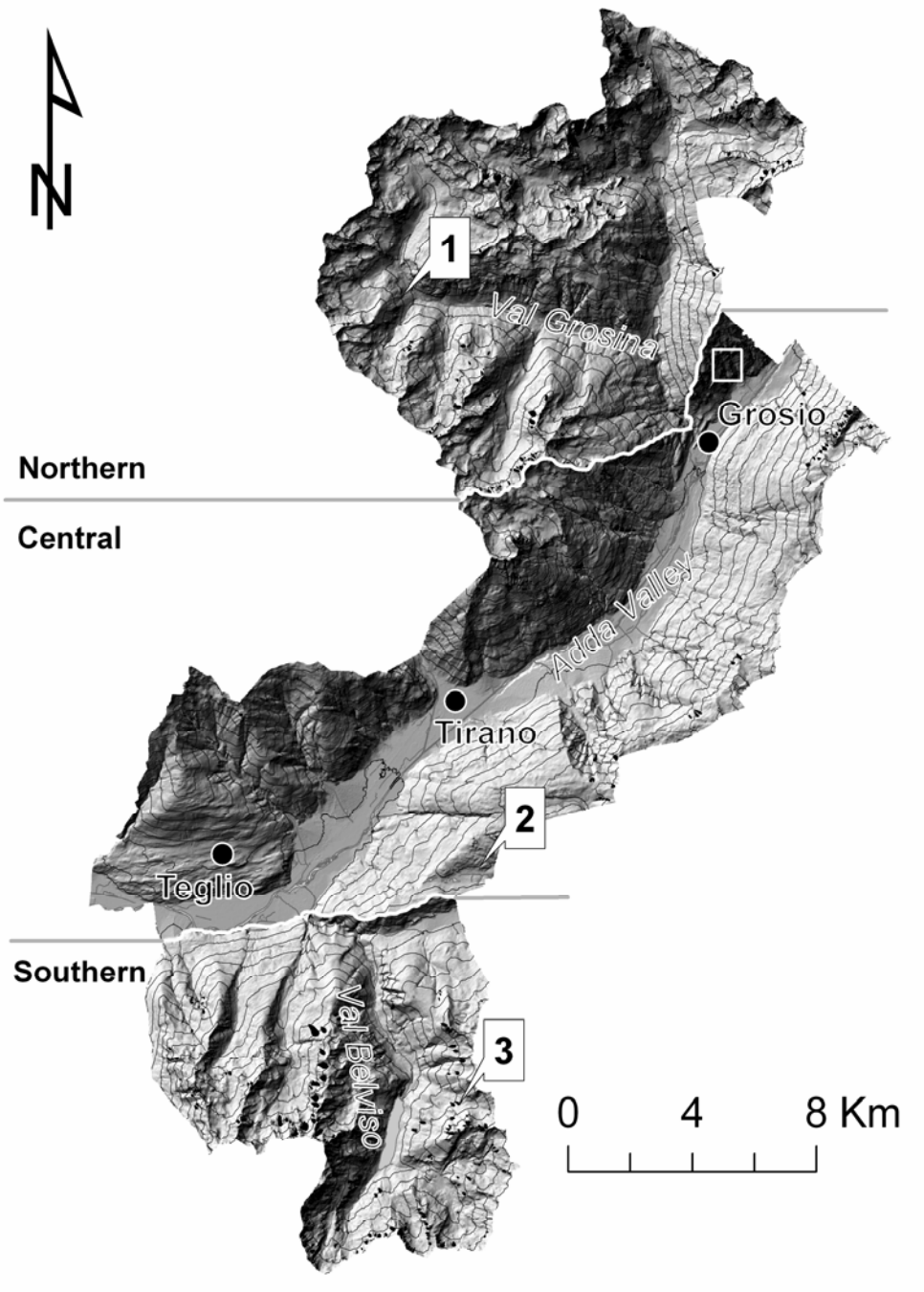

Fig. 6.6 – Three subdivisions of the debris flow inventories. 1 to 3 – Locations of the scarps in Fig. 6.5. Rectangle shows the extent of Fig. 6.2.

Accountability index explains how the classes of factor maps that are relevant for the analysis (with densities higher than regional average) contain all landslide pixels or not. Reliability index gives an idea of the average landslide density in the classes of factor maps that are relevant for landslide occurrence (with values higher than 1). Both indicators provide different but relevant results for landslide prediction, although reliability is more important

(Greenbaum et al. 1995a, 1995b). Using these indicators it is possible to identify the relevance of each factor for landslide occurrence. Moreover, it is possible to better choose the appropriate combination of the most relevant factor classes for the model construction. The main drawback of using accountability and reliability indices is that these are calculated for factor maps where particular classes, which are relevant within the factor maps, cannot be distinguished on the basis of these indices. Accountability and reliability indices were calculated for both the GeoIFFI and DF2001 databases as well as for their spatial subsets.

Weights-of-Evidence

The Weights-of-Evidence modelling technique (WofE) was applied to analyse the debris flow susceptibility. In 90´s this method started to be used in landslide susceptibility evaluation (van Westen 1993; van Westen et al. 2003; Süzen and Doyuran 2004, Thierry et al. 2007). The modelling technique applied is well known; so only a basic introduction is presented here. For further information about the method, the reader is referred to Bonham-Carter et al. (1988) and Agterberg et al. (1989). WofE utilizes a combination of different spatial datasets (evidential themes or factor maps) in order to analyze and describe their interactions and generates predictive models (Bonham-Carter 1994; Raines et al. 2000). WofE is a data-driven process that uses known occurrences (training points or response variables) as model training sites to produce predictive probability maps (response themes) from multiple weighted evidences (Raines 1999). Training points are used in WofE to calculate prior probability, weights of each of the evidential thematic classes, and posterior probabilities of the response theme. The WofE model uses a log-linear form of the Bayesian probability function.

The prior probability {Pprior} that an event {D} occurs per unit area is calculated as the total number of events over the total area (6.1). This initial estimate can be later increased or diminished in different areas by the use of available explanatory variables {B}(6.2, 6.3). The method is based on the calculation of positive (6.4) and negative (6.5) weights by which the degree of spatial association among events and explanatory variables may be modelled.

$$P_{\Pr ior} = \frac{Landslide\_Area}{Total\_Area} \tag{6.1}$$

$$P\{D|B\} = P\{D\}\frac{P\{B|D\}}{P\{B\}} \tag{6.2}$$

$$P\{D|\overline{B}\} = P\{D\}\frac{P\{\overline{B}|D\}}{P\{\overline{B}\}} \tag{6.3}$$

$$W^{+} = \log_e \frac{P\{B|D\}}{P\{B|\overline{D}\}} \tag{6.4}$$

$$W^{-} = \log_e \frac{P\{\overline{B}|D\}}{P\{\overline{B}|\overline{D}\}} \tag{6.5}$$

The over bar sign '¯' represents the absence of an event and/or explanatory variable. The ratios of the probabilities of D presence to that of D absence are called odds (Bonham-Carter 1994). The WofE for all Ds is combined using natural logarithm of the odds (logit), in order to estimate the conditional probability of landslide occurrence. When several Ds are combined, areas with high or low weights correspond to high or low probabilities of presence of the D (Thierry et al. 2007).

An ArcGIS 9.2 extension (SDM – Spatial Data Modeller, Sawatzky et al. 2008) was used for an automatic and iterative calculation of the models. As already mentioned in many studies (Thierry et al. 2007; Castellanos Abella 2008), WofE has an assumption of conditional independence between variables that, if it is not verified, may lead to an overestimation of spatial probabilities. In natural conditions, many factor variables have some dependence (altitude and land use; faults and geology; or slope and internal relief). To overcome this problem, the resulting susceptibility map weight values were treated as relative and not absolute values. Thus, the probability values were ordered from the highest to the lowest ones and, consequently, reclassified into classes. Moreover, as mentioned by Bonham-Carter (1996), WofE provides a simplification that, when used carefully, is used for relative contributions of the separate factors. Therefore, it is often used as a selection procedure for multivariate statistical analysis.

Success rate curves

Success rate curves – SRC (Chung and Fabbri 1999) are used to assess the performances of the models. SRCs are made by plotting the cumulative percentage of susceptible areas (starting from the highest probability values to the lowest ones) on the X axis and the cumulative percentage of corresponding training points on the Y axis. The steeper the curve the better is the capability of the model to describe the distribution of landslides. The steepness of the curve also depends on the landslide distribution in the area. In a situation when a large portion of the area is covered by landslides, it is impossible to get steep curves.

Prediction rate curves

The last step of the analysis was aimed at evaluating the predictive power of the maps using the prediction rate curve method – PRC (Chung and Fabbri 2003). The PRCs are made in the same way as SRCs; but instead of the training subset, a prediction subset (of the scarps that were not used as training subset) is used. For the randomly divided inventories, the second subset which did not enter into the model calculation was used to calculate prediction rate curves. The analysis of the predictive power of the three spatially divided inventory subsets was made by cross-validation (e.g. using central and southern subsets for quantifying the predictive power of the northern subset). The intention of this cross-validation technique was to examine different causal factors of debris flows in different parts of the study area. Moreover, the prediction power of the models, developed using subsets from other parts of the study region, was also analysed. Nevertheless, to evaluate the real predictive capabilities of the model, a multi-

temporal landslide inventory should be used, taking into account that some of the factors, like land use, might have changed in the period between the two landslide inventories of different periods. The model should be made using an older landslide inventory and more recent landslides should be used for the evaluation of the prediction, as applied by Guzzetti et al. (2006b) or Chung and Fabbri (2008).

To summarize SRCs and PRCs for models made using different inventories, the area under the curve (AUC) was calculated. This area is expressed as a percentage of the graph that lies under the curve and allows easy comparison of different SRCs and PRCs of different models. As already stated by Carrara et al. (2008), evaluation of the prediction power of the models is always a difficult task and all known approaches suffer from conceptual or operational pitfalls. The PRC method has been chosen mainly for supporting the model results and assessing the robustness of the model.

6.3. Results and discussion

6.3.1 Landslide densities

The three highest and three lowest density values in the classes of the five most relevant factor maps are summarized in Table 6.1. It can be seen that there are no large differences among the highest and lowest density classes for the two inventories, however the density values differ a lot because the DF2001 inventory has a much higher area extent than the GeoIFFI inventory. The highest densities are present in the largest classes of slope angle, internal relief and planar curvature and in land use classes of bare land and vegetation on rocks. Geology classes with highest scarp densities are sandstones and claystones; however, these classes occupy only a very small portion in the southern part of the study area. The lowest scarp densities are observed in low slope, planar curvature and internal relief classes, and in pastures, mixed and broadleaf forests. Differences exist between GeoIFFI and DF2001 inventory in the low density classes of the geological map. GeoIFFI inventory has low densities in paleolandslide and alluvial-colluvial deposits, while DF2001 has low densities in conglomerate and morainic sediments. However, the lowest density class is in both cases represented by colonized scree slopes.

6.3.2 Accountability and reliability

The accountability and reliability indices calculated for the factor maps are shown in Table 6.2. When assessing the whole area using the GeoIFFI database, the factor maps with the highest accountability and reliability values are altitude, land use, geology and slope. No association was found with profile curvature, aspect and fault distance. The accountability scores for the DF2001 database are consistently higher than those for the GeoIFFI database. This means that the DF2001 database has a better discriminating power of separating relevant classes for landslide occurrence. This can be probably caused by considering the whole scarp polygon in the DF2001 database, instead of the GeoIFFI database where scarps are mapped as single

points. Thus, more information is kept in the new DF2001 database. The DF2001 database shows factors with high indices similar to those for the GeoIFFI database, and internal relief and planar curvature play a more important role. The reliability indices, which are indicators of the average landslide density in the classes that are important for the landslide triggering, are much higher for the DF2001 database. However, it is not methodologically correct to compare the indices between the GeoIFFI and DF2001 databases as the former is based on points (represented by 1,478 10×10 m cells, with a total area of 0.15 km^2) and the latter on polygons with much larger total area (4.4 km^2). The reliability indices in both databases show the highest values in altitude, internal relief, land use, geology, planar curvature, and slope factor maps.

	GeoIFFI factor map class	GeoIFFI density	DF2001 factor map class	DF2001 density
Slope (°)	44.9 - 76.4	0.001100	44.9 - 76.4	0.033668
highest classes	39.8 - 44.9	0.000792	39.8 - 44.9	0.023910
	36.2 - 39.8	0.000434	36.2 - 39.8	0.014894
	22.2 - 26.4	0.000130	16.5 - 22.2	0.002387
lowest classes	8.1 - 16.5	0.000073	8.1 - 16.5	0.000764
	0 - 8.1	0.000055	0 - 8.1	0.000095
Landuse	Bare land	0.000891	Bare land	0.031782
highest classes	Vegetation on rocks	0.000568	Shrubs and bushes	0.014225
	Reforested areas	0.000533	Vegetation on rocks	0.013478
	Pastures	0.000109	Pastures	0.001037
lowest classes	Mixed forests	0.000078	Mixed forests	0.000325
	Broadleaf forests	0.000031	Broadleaf forests	0.000107
Geology	Sandstones	0.005285	Sandstones	0.086039
highest classes	Claystones	0.004514	Claystones	0.072444
	Conglomerate outcrops	0.002161	Intrusive rocks outcrops	0.026998
	Paleolandslides	0.000064	Conglomerates	0.002448
lowest classes	Elluvio-colluvial deposits	0.000056	Morainic sediments	0.001800
	Colonized scree slope	0.000010	Colonized scree slope	0.000086
Internal relief (m/ha)	105.4 - 349.2	0.001095	105.4 - 349.2	0.039923
highest classes	91.7 - 105.4	0.000684	91.7 - 105.4	0.024036
	82.2 - 91.7	0.000473	82.2 - 91.7	0.014005
	37.0 - 49.3	0.000116	37.0 - 49.3	0.002160
lowest classes	19.2 - 37.0	0.000090	19.2 - 37.0	0.000549
	0 - 19.2	0.000029	0 - 19.2	0.000080
Planar curvature (n/100 m-1)	-21.51 - -1.26	0.001257	-21.51 - -1.26	0.038161
highest classes	1.66 - 22.25	0.000453	1.66 - 22.25	0.013184
	-1.26 - -0.57	0.000408	-1.26 - -0.57	0.012720
	0.29 - 0.63	0.000172	0.29 - 0.63	0.004851
lowest classes	-0.23 - -0.06	0.000151	0.11 - 0.29	0.004564
	-0.06 - 0.11	0.000108	-0.06 - 0.11	0.003392

Table 6.1 – Highest and lowest classes of debris flow scarp densities for the five most relevant factors.

According to field surveys, substantial differences in the debris flow predisposing factors are expected in different portions of the study area. Therefore, also separate analysis was done for three selected sub-areas (Fig. 6.7). The differences in debris flow sources are mostly caused by particular geological characteristics in different parts of the area. In the northern part, gneiss outcrops have a much higher influence on debris flow initiation, than in the rest of the study area. On the other side, in the southern part of the area, debris flow initiating areas are occurring mostly on slopes underlain by sandstones and other sedimentary rocks. In the central part of the area the most common rock type in debris flow source areas is micaschists. Also many debris flow source areas indicated in the DF2001 database are found in colluvial deposits.

Factor map	GeoIFFI		GeoIFFI - North		GeoIFFI - Center		GeoIFFI - South	
	A	**R**	**A**	**R**	**A**	**R**	**A**	**R**
Altitude	**83.68**	0.07	**92.16**	0.0304	79.73	0.0079	82.78	0.0311
Aspect	39.95	0.04	60.48	0.0172	73.42	0.0079	75.15	0.0196
Fault distance	35.95	0.05	53.49	0.0189	65.32	0.0068	75.75	0.0239
Internal relief	63.1	0.07	72.74	0.0249	84.68	0.0084	67.22	0.0358
Land use	76.85	**0.08**	88.59	0.0353	65.77	0.0083	82.78	0.0318
Geology	77.12	**0.08**	80.41	**0.0386**	81.08	0.0102	**83.68**	0.0447
Slope	67.3	**0.08**	66.61	0.0299	65.77	0.0112	59.28	**0.0470**
Planar curvature	58.84	0.07	64.05	0.0301	56.31	**0.0128**	62.28	0.0260
Profile curvature	35.68	0.05	65.59	0.0157	55.86	0.0067	41.02	0.0263
Flow accumulation	83.06	0.03	81.95	0.0133	**86.14**	0.0052	83.02	0.0153
Factor map	**DF2001**		**DF2001 - North**		**DF2001 - Center**		**DF2001 - South**	
	A	**R**	**A**	**R**	**A**	**R**	**A**	**R**
Altitude	88.07	2.17	82.17	**1.36**	**94.01**	0.43	**95.48**	0.83
Aspect	61.13	1.21	64.59	0.43	55.20	0.33	83.79	0.57
Fault distance	42.06	1.73	47.68	0.41	70.31	0.34	81.05	0.74
Internal relief	73.41	**2.57**	78.54	0.90	87.83	0.52	68.50	**1.06**
Land use	**91.91**	2.31	**95.98**	0.93	78.63	**0.69**	89.43	0.99
Geology	84.72	2.31	91.72	1.35	80.82	0.52	86.10	1.03
Slope	70.77	2.38	86.13	0.70	85.58	0.49	64.91	0.96
Planar curvature	60.26	2.11	62.86	0.72	65.09	0.53	55.82	0.87
Profile curvature	43.21	1.3	54.43	0.39	48.56	0.29	44.28	0.59
Flow accumulation	88.87	1.03	87.09	0.33	90.48	0.24	89.34	0.46

Table 6.2 – Accountability (A) and reliability (R) for the different factor maps and different subsets used in the analysis. Most important factors and highest accountability and reliability indices for each subset map are highlighted in bold.

Analysis of the northern subset shows that land use and geology together with slope, internal relief and altitude are the main controlling factors of debris flow triggering. More to the south, there is higher influence of altitude, aspect, and distance to faults. In all subsets, there is stronger influence of land use, geology, internal relief, and altitude as factors of debris flow triggering. Slope and planar curvature also play certain roles in the distribution of landslides. The lowest relations are observed in the case of profile curvature and aspect for the northern and central subsets.

The different influence of land use classes between the different subsets is probably caused by a much higher occurrence of bare land in the northern part than in the rest of the study area. In the central part the land use class of coniferous forests has a strong influence on landslide distribution. However, this might be caused mainly by the lower altitudes of scarps in the central part. In the southern part, about half of the debris flow source areas are located in the bare land class and the influence of land use classes of shrubs, bushes and scarce vegetation land use classes is proportionally distributed. In the DF2001 database the bare land class has much higher occurrence than in the GeoIFFI database.

Distributions of scarps in the slope classes do not show any particular differences between the databases or between the subsets. Only in the southern subset, scarps are located on higher slope angles than in the northern and central subsets.

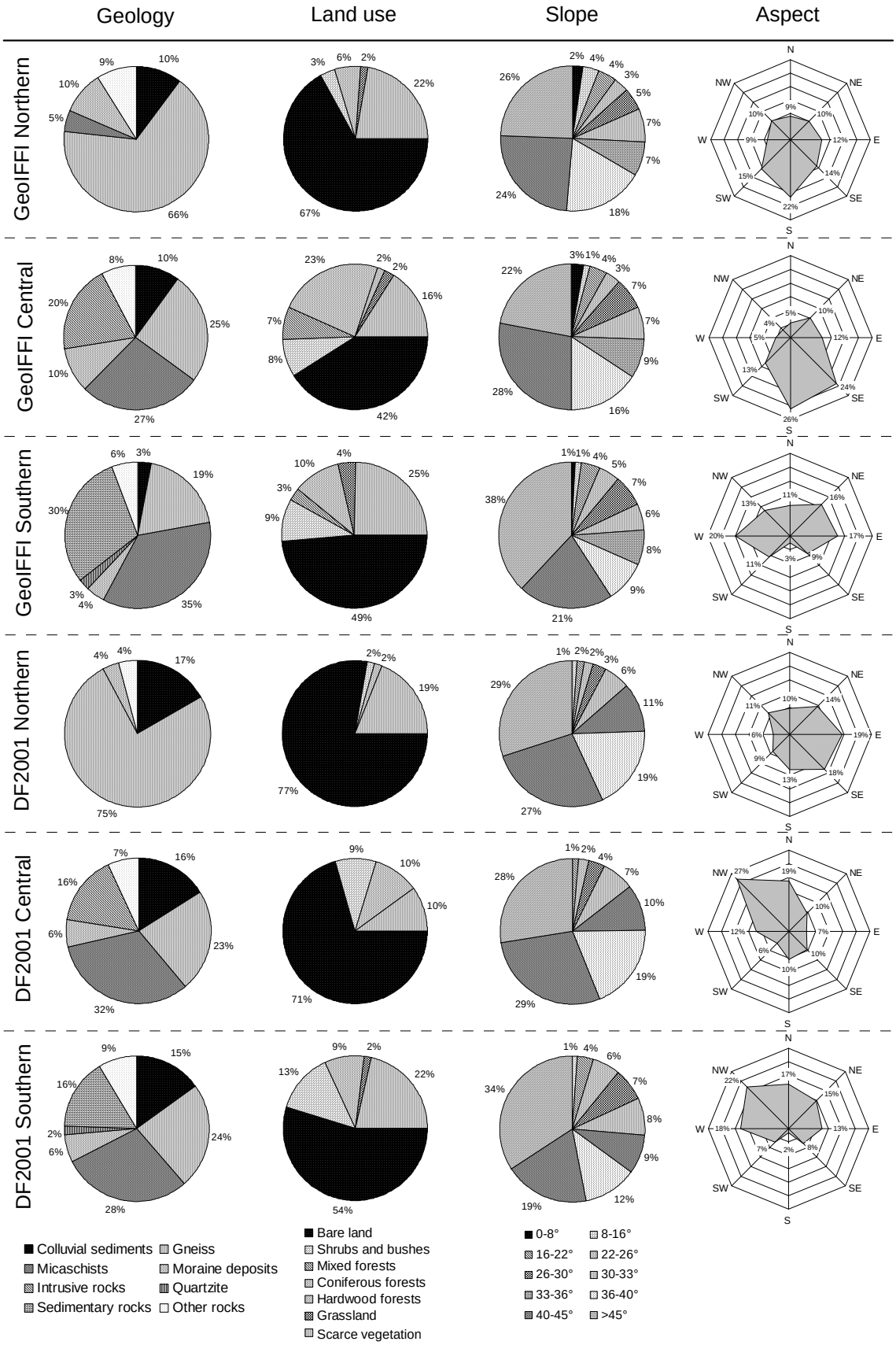

Fig. 6.7 – Main debris flow characteristics for each database and subset. Geological classes are generalised.

There is also a clear difference between the three parts in terms of aspect classes. In the northern part the scarps are located mainly on south and east facing slopes. The southern part has debris flow scarps distributed mostly in east and west directions. This is caused mostly by their presence near ridges with a north to south orientation. A strong difference was found between the GeoIFFI and DF2001 databases in the central subset. In the GeoIFFI database most of the scarps have a south facing orientation, while in the DF2001 database they are prevalently NW facing. This particular difference is caused by different spatial extent of the scarp. The scarps on the north facing slopes are larger than in the south facing slopes.

In the northern part of Valtellina di Tirano, the debris flow scarps are located mainly in higher altitudes (more than 2,338 m a.s.l.), while in the southern part this correlation is not so obvious. Scarps in the central part are distributed on lower altitudes (from 1,723 m a.s.l.) because the slopes adjacent to the main valley of the Adda River do not reach high altitudes.

Faults in the northern part of the study area do not show any significant correlation with debris flow triggering, but more to the south there is a higher influence of fault proximity on scarp occurrence. This could be partially explained by the proximity of the Insubric Line and successive faults and thrusts. However, the main fault crossing the Adda Valley in the central part of the study area is mostly located in the floodplain. The differences in the distribution of debris flow scarps in the classes of internal relief, planar and profile curvatures and flow accumulation do not show any particular differences among the three regions. Scarps are located in classes of high internal relief as well as convex planar and profile curvatures, and low flow accumulation.

6.3.3 Comparison of random partition of the GeoIFFI and DF2001 inventories

The WofE modelling technique was applied several times with different combination of factor maps. In the first model, all factor maps were used; the other models were built by removing less relevant factor maps based on accountability and reliability indices (Tab. 6.2). SRCs were calculated using training subsets and PRCs were calculated using the validation subset. These subsets were generated by random, equal size (50%) subdivision of the inventories. Results of the best performing models are shown in Fig. 6.8. It is visible there that the SRCs and PRCs using the DF2001 databases show slightly better results also in terms of areas under curves, as compared to the GeoIFFI database.

The best performing model of GeoIFFI database was able to classify 80% of debris flow source areas in 30% of the territory with AUC (area under curve) of 84.04%. The model was made by combining altitude, land use, geology, slope, profile and planar curvature factor maps. The best model with the DF2001 database shows slightly better results, which is able to classify more than 85% of the scarps in less than 30% of the area, with an AUC of 86.54%. The best model generated from the DF2001 inventory was made by combination of altitude, land use, geology, slope and planar curvature factor maps.

The AUCs for PRCs using the GeoIFFI database are slightly lower than for SRCs, while for the DF2001 database this is reverse (Fig. 6.8). This result is very particular, because in

general, success rate curves should be higher than prediction rate curves, as SRCs are calculated using training subsets. In this case, the validation subset fits the model better than the training subset.

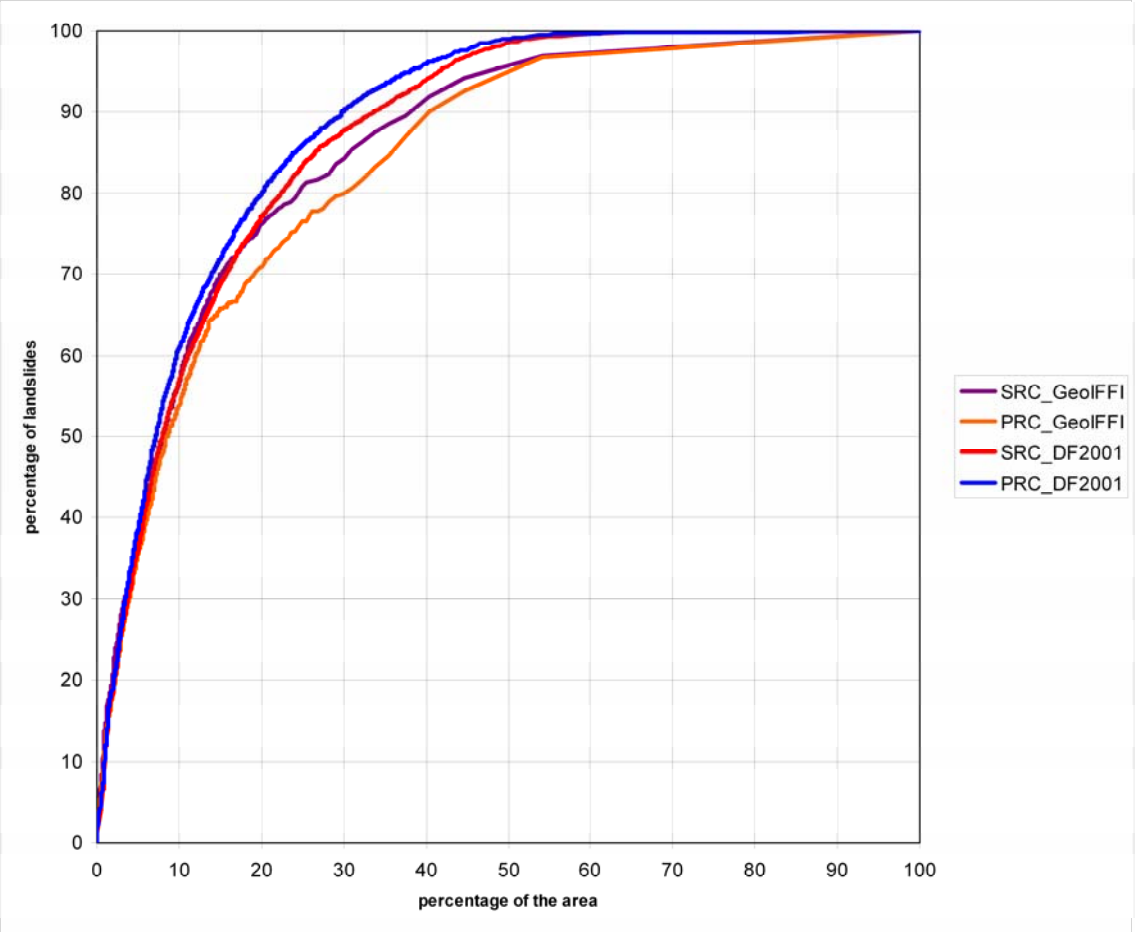

Inventory	SRC	PRC	Factor maps
GeoIFFI	85.74	84.15	altitude, land use, geology, slope, profile curvature, planar curvature, flow accumulation
DF2001	87.16	88.37	altitude, land use, geology, slope, planar curvature, flow accumulation

Fig. 6.8 – Comparison of success and prediction rate curves (SRC and PRC) generated for models with best results for the GeoIFFI and DF2001 databases and random partition of the inventories. AUC values of SRCs and PRCs are shown in the table.

Results show that the use of DF2001 database gives better results in success as well as prediction rate curves than GeoIFFI database. This is most probably caused by the different purposes and ways of producing these databases. Debris flow scarps in the GeoIFFI database were mapped as points and are not often located in the correct place of the debris flow source. This inaccuracy is probably caused by the utilization of different sources of information for the fast generation of the GeoIFFI database for the whole Lombardy Region. On the other hand, scarps of the DF2001 database were mapped very carefully as polygons using stereoscopic photo interpretation, followed by field surveys, with higher precision in scarp location. The DF2001 database seems to better depict the debris flow source areas. However, this difference is not very spectacular, as the DF2001 inventory was mapped only for the purposes of analysing debris flow susceptibility in the CM Valtellina di Tirano area while the GeoIFFI database was made for whole Lombardy Region and for many landslide types.

6.3.4 Comparison of spatial partition of the GeoIFFI and DF2001 inventories

As can be seen from the accountability and reliability indices for both inventories, particular differences in debris flow sources exist within the study area. Results of the analysis of the best performing models for each subset are summarized in Figure 6.9.

The spatially divided GeoIFFI inventory in terms of SRC shows better results than the randomly divided one; however, the PRC results for the randomly divided GeoIFFI inventory are higher than PRCs of the spatially divided subsets. The susceptibility models of all three subsets were always able to classify more than 70% of debris flow source areas in less than 20% of the total territory. The best performing model was made using the southern subset with an AUC of 89.51%. The best models for the northern and central subsets have AUCs of 87.88% and 84.48% respectively. Also results of PRCs for all three subsets are very similar, showing that the differences of the debris flow triggering conditions, among the subsets of GeoIFFI database, are not clearly captured by the database.

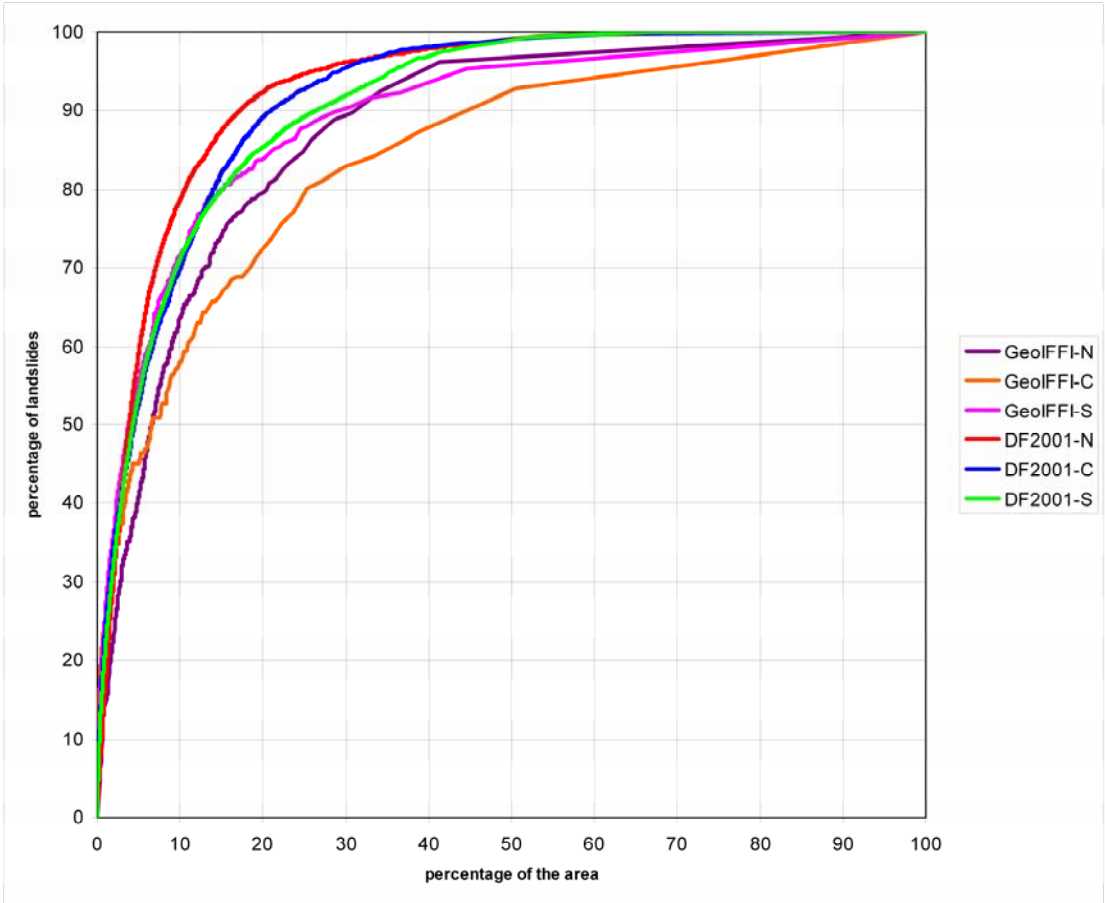

Inventory	SRC	Factor maps
GeoIFFI - N	87.88	altitude, landuse, geology, slope, internal relief, planar curvature
GeoIFFI - C	84.48	altitude, aspect, faults, landuse, geology, slope, internal relief, planar curvature
GeoIFFI - S	89.51	altitude, aspect, faults, landuse, geology, slope, internal relief, planar curvature, flow accumulation
DF2001 - N	92.88	altitude, aspect, landuse, geology, slope, internal relief, planar curvature
DF2001 - C	91.75	altitude, aspect, faults, landuse, geology, slope, internal relief, planar curvature
DF2001 - S	90.96	altitude, aspect, faults, landuse, geology, slope, internal relief, planar curvature

Fig. 6.9 – Comparison of success rate curves (SRCs) generated for models with best results for the GeoIFFI and DF2001 databases and spatial partition of the inventories. AUC values of SRCs are shown in the table.

Much greater differences can be observed when comparing the results produced from the DF2001 inventory. The northern part of the study area clearly shows very particular conditions of debris flow triggering. The model, generated from the northern subset, was able to classify more than 90% of the scarps in less than 20% of the area with AUC of 92.88%. The results from the central and southern subsets were lower; nevertheless, the AUC values always pass over 90% (91.75% and 90.96% for central and southern subset respectively).

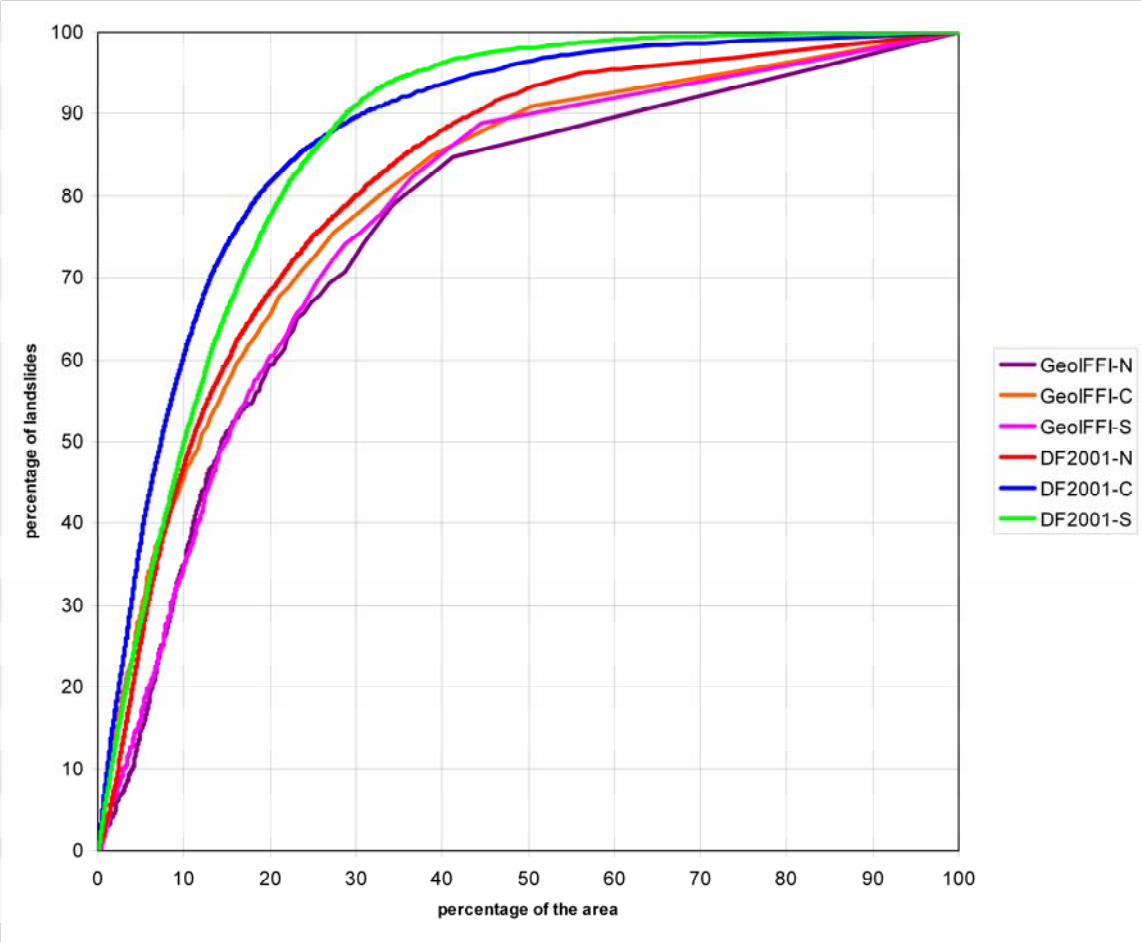

Inventory	PRC	Factor maps
GeoIFFI - N	76.42	altitude, landuse, geology, slope, internal relief, planar curvature
GeoIFFI - C	80.28	altitude, aspect, faults, landuse, geology, slope, internal relief, planar curvature
GeoIFFI - S	77.78	altitude, aspect, faults, landuse, geology, slope, internal relief, planar curvature, flow accumulation
DF2001 - N	82.33	altitude, aspect, landuse, geology, slope, internal relief, planar curvature
DF2001 - C	87.39	altitude, aspect, faults, landuse, geology, slope, internal relief, planar curvature
DF2001 - S	88.35	altitude, aspect, faults, landuse, geology, slope, internal relief, planar curvature

Fig. 6.10 – Comparison of prediction rate curves (PRCs) generated for models with best results for the GeoIFFI and DF2001 databases and spatial partition of the inventories. AUC values of PRCs are shown in the table.

The differences in debris flow predisposing conditions between the northern, central and southern area subsets could be also appreciated after calculation of prediction rate curves for each subset (Fig. 6.10). Each map prediction capability was tested by using inventory dataset from the other parts of the study area, e.g. when a PRC is calculated for the northern subset using the rest of the DF2001 database (central and southern subsets), the differences in areas classified as susceptible could be seen. The results obtained from this cross-validation technique

show the difference between causal factors affecting the debris flow triggering in each part of the study area. The differences in PRCs for central and southern subsets are not very spectacular. This means, that factors contributing to debris flow triggering are very similar in the southern and central part of the study area, and debris flows in the north have different causal factor than rest of the region.

Final maps from the spatially divided inventories of GeoIFFI and DF2001 databases were generated using best performing combinations of the factor maps (in terms of SRC) for the three subsets of spatially divided GeoIFFI and DF2001 databases (see Fig. 6.9). Overlying these maps, the highest posterior probability values were used and afterwards the SRCs were calculated, using the entire GeoIFFI and DF2001 database respectively. The results show that the spatially divided DF2001 model has a SRC of 89.01% and the model from spatially divided GeoIFFI inventory has SRC of 85.06%. As a consequence, it can be concluded that the DF2001 inventory produced the best susceptibility map in terms of standard model performance.

6.3.5 Spatial pattern and main properties of the best performing susceptibility maps

All the best performing models show good and very similar results in terms of AUCs. It was however noticed that the spatial pattern of the final maps differs. To quantify the differences between the maps, a classification was applied putting breakpoints at 10%, 30%, and 50% of the susceptible area (Fig. 6. 11). Four maps, each with a four-class classification, were obtained and simply overlaid using the Rank Difference tool of the Spatial Data Modeller (Sawatzky et al. 2008). Percentages of correspondence between the classes of the susceptibility maps are shown in Table 6.3. The lowest difference in spatial distribution was found between the maps produced by the randomly divided GeoIFFI and DF2001 inventories (81.11% correspondence), while the highest difference was found between maps from spatially divided DF2001 inventory and randomly divided GeoIFFI inventory (70.80% correspondence). These results might have important consequence in choosing the correct model which represents properly the debris flow source areas occurrence. To analyse this problem, the percentage of landslide sources in particular classes were calculated together with the landslide density (Table 6.4). It can be seen from the table that the landslide percentages and densities decrease gradually from the very high to low susceptible classes in all maps. The model which allowed to classify most debris flow sources in the very high class was made by the combination of best northern, central, and southern subset of the DF2001 database. More than 63% of debris flow sources from the DF2001 database fall into less then 10% of the most susceptible area. The DF2001 database shows in both cases better results than the GeoIFFI database. In the GeoIFFI database much more debris flow sources fall into less susceptible half of the study area (4.13% and 5.82% respectively), compared to DF2001 where only 1.17% and 1.56% of debris flow sources, belong to the 50% of less susceptible area.

To evaluate if the DF2001 inventory is a better input for a susceptibility map generation than the GeoIFFI inventory, a cross-validation was performed. The DF2001 inventory was used to calculate PRCs of the best map produced by the GeoIFFI inventory. The PRC for the map

generated from the randomly divided GeoIFFI inventory reached value of 86.28%, which is higher then the SRC of this map (85.74%). This situation leads to a simple conclusion, that GeoIFFI inventory might be enough for production of a reliable susceptibility map. However, the mismatch of almost 30% in the spatial pattern of the maps produced by these inventories does not enable to finish with such a simple conclusion (Tab. 6.3). The situation of good performance of the map produced from GeoIFFI inventory, evaluated by DF2001, could be caused by the high influence of important factor map classes (slope, land use, geology, internal relief, and planar curvature – Table 6.1). It has to be noted that the use of standard evaluation techniques (SRCs, PRCs) has an important drawback that is the loss of spatial information. As a consequence, compared maps can show very similar results in AUCs but their spatial pattern can be highly different.

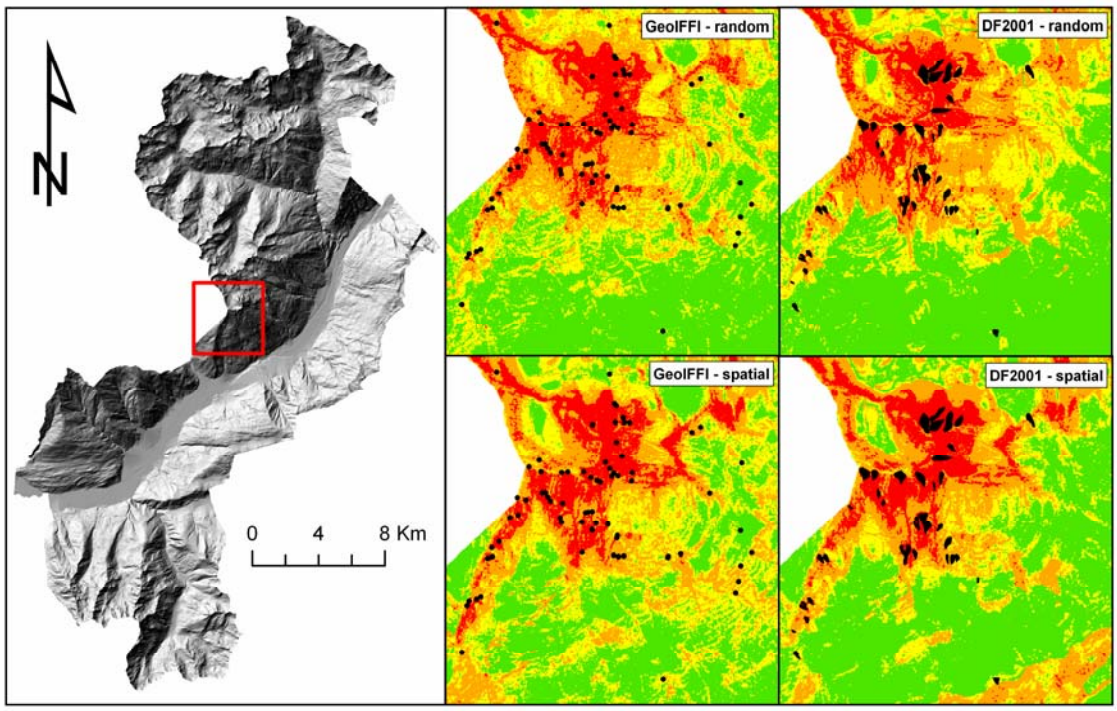

Fig. 6.11 – Example of spatial difference between four best models generated using different inventory subsets. Rectangle shows the location of the enlarged area. Corresponding inventories are superimposed over the enlarged area. VH – very high susceptibility; H – high susceptibility, M – medium susceptibility, L – low susceptibility.

GeoIFFI_S	75.09		
DF2001_R	81.11	73.53	
DF2001_S	70.80	75.55	71.95
	GeoIFFI_R	GeoIFFI_S	DF2001_R

Table 6.3 – Percentage of correspondence in classification between the best susceptibility maps generated from randomly (R) and spatially (S) divided GeoIFFI and DF2001 inventories. Maps were classified into four classes according to the percentage of susceptible area using breakpoints at 10%, 30% and 50%.

GeoIFFI Random	**VH**	**H**	**M**	**L**	**Total**
% of landslides	55.38	26.88	13.61	4.13	100.00
Landslide density	0.00181	0.00044	0.00022	0.00003	0.00033
GeoIFFI Spatial					
% of landslides	56.13	27.49	10.56	5.82	100.00
Landslide density	0.00184	0.00045	0.00017	0.00004	0.00033
DF2001 Random					
% of landslides	61.18	28.50	9.15	1.17	100.00
Landslide density	0.05941	0.01384	0.00444	0.00023	0.00971
DF2001 Spatial					
% of landslides	63.71	28.28	6.46	1.56	100.00
Landslide density	0.06186	0.01373	0.00314	0.00030	0.00971

Table 6.4 – Densities and percentage of debris flow source areas in best maps for the GeoIFFI and DF2001 inventories made by random or spatial subdivision. Maps were classified into four classes according to the percentage of susceptible area using breakpoints at 10%, 30% and 50%.

6.3.6 Final susceptibility map

The resulting susceptibility map with the best potential to predict future landslide-induced debris flow source areas was made from the combination of maps from the spatially divided DF2001 database, which reaches highest SRCs. The final map has AUC for SRC of 89.01% which is a good result, especially when compared to the first application of the randomly divided DF2001 database (AUC for SRC 87.16%). Moreover, this map better captures the differences in debris flow sources in different parts of the study area. The final susceptibility map was reclassified into 5 classes, according to the percentage of debris flow scarps that falls into particular susceptibility classes. Breakpoints were put at 75%, 85%, 95%, and 99% of the landslide scarps (Fig. 6.12). The extent of the very high susceptibility class is 14.52% of the study area and more than a half of the study area (52.99%) belongs to the very low or non susceptible class. Also the density of debris flow scarps decreases from very high to very low susceptibility values (Fig. 6.13).

Moreover, when applying the same classification to the best maps, using the randomly divided GeoIFFI and DF2001 databases, there is significant improvement in restriction of the area classified as very high susceptible. In case of the GeoIFFI database, 75% of debris flow scarps lies within 19.10% of the area; and only 45.80% of the area is classified as very low susceptible. The randomly divided DF2001 database has better results, when 75% of debris flow scarps lies within 18.70% of the area and 48.20% of the area is classified as very low susceptible. Comparison with the best map from spatially divided GeoIFFI inventory shows even higher differences, when the GeoIFFI map has only 39.41% of the area classified as very low susceptible and the highest class covers 19.37% of the area.

After the calculation of the final susceptibility map a confidence map was made. Confidence represents a useful measure of uncertainty of weights and presence of areas with missing data (Raines 1999). The confidence map was made in similar way as the final susceptibility map (Fig. 6.14), for the classification of the confidence map a table with confidence values was used (Table 6.5). The table expresses the levels of confidence as levels of significance (Poli 2006).

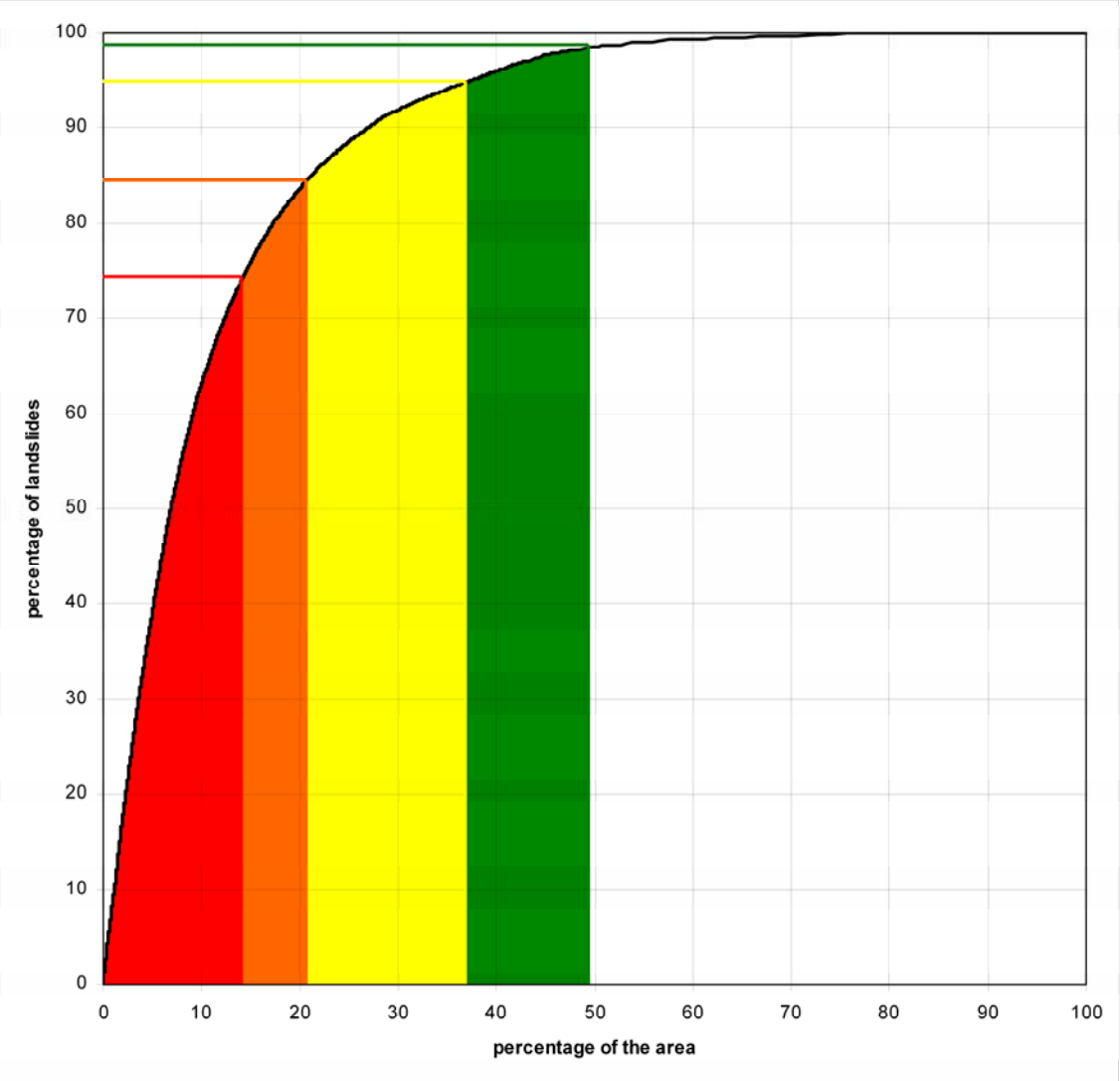

Final map	VH	H	M	L	VL
% of area	14.52	6.63	16.20	9.66	52.99
Landslide density	0.0507	0.0146	0.0058	0.0029	0.0004

Fig. 6.12 – Success rate curve (SRC) of the final susceptibility map. The susceptibility classes from left to right are: very high, high, medium, low, very low or non susceptible. Debris flow source areas densities and percentage according to the DF2001 inventory database for the classes of the final susceptibility map are shown in the table.

As can be seen from the map, areas with low confidence (less than 0.842) cover the floodplain and alluvial fans together with the terraced areas. The areas of high confidence cover the slopes and areas of debris flow sources.

6.3.7 Limitations of susceptibility modelling

First limitation of the statistically based landslide susceptibility modelling is connected with the fact that the landslide inventory is based on information from specific time and the produced susceptibility map shows only the landslide susceptibility for this particular moment. Another limitation arises from different spatial and temporal resolution of input factor maps. In this case,

maps of same resolution should be used as in the case of this study. Data mining procedures (as accountability and reliability indices) might be useful for supporting expert knowledge about the causal factors of landslide triggering. However, the use of such simple indices has a lot of limitations when important information on the particular classes of the causative factor maps is not taken into account.

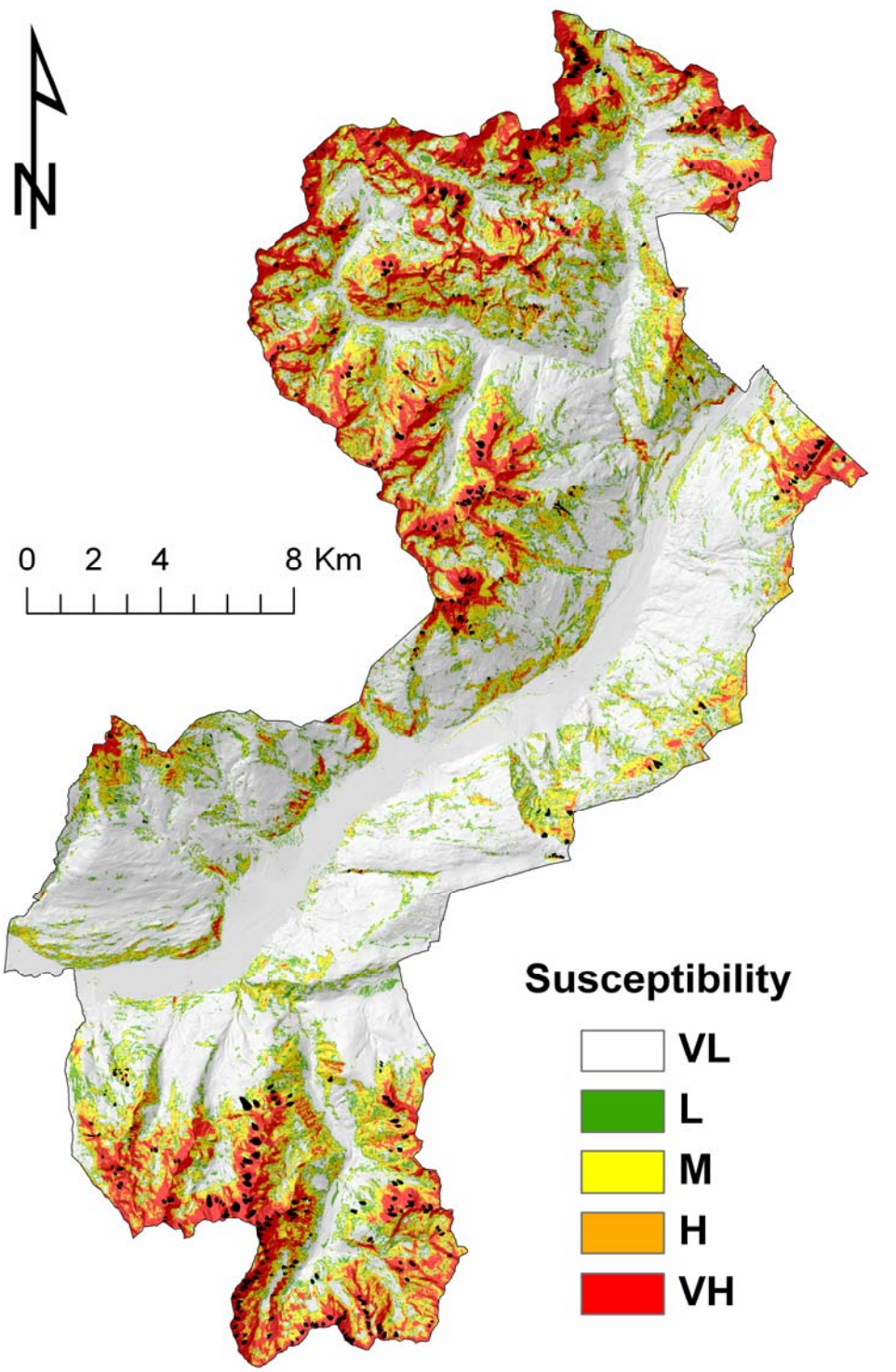

Fig. 6.13 – Final susceptibility map with debris flow scarps of the DF2001 inventory superimposed. VH – very high susceptibility; H – high susceptibility, M – medium susceptibility, L – low susceptibility, VL – very low or non susceptible.

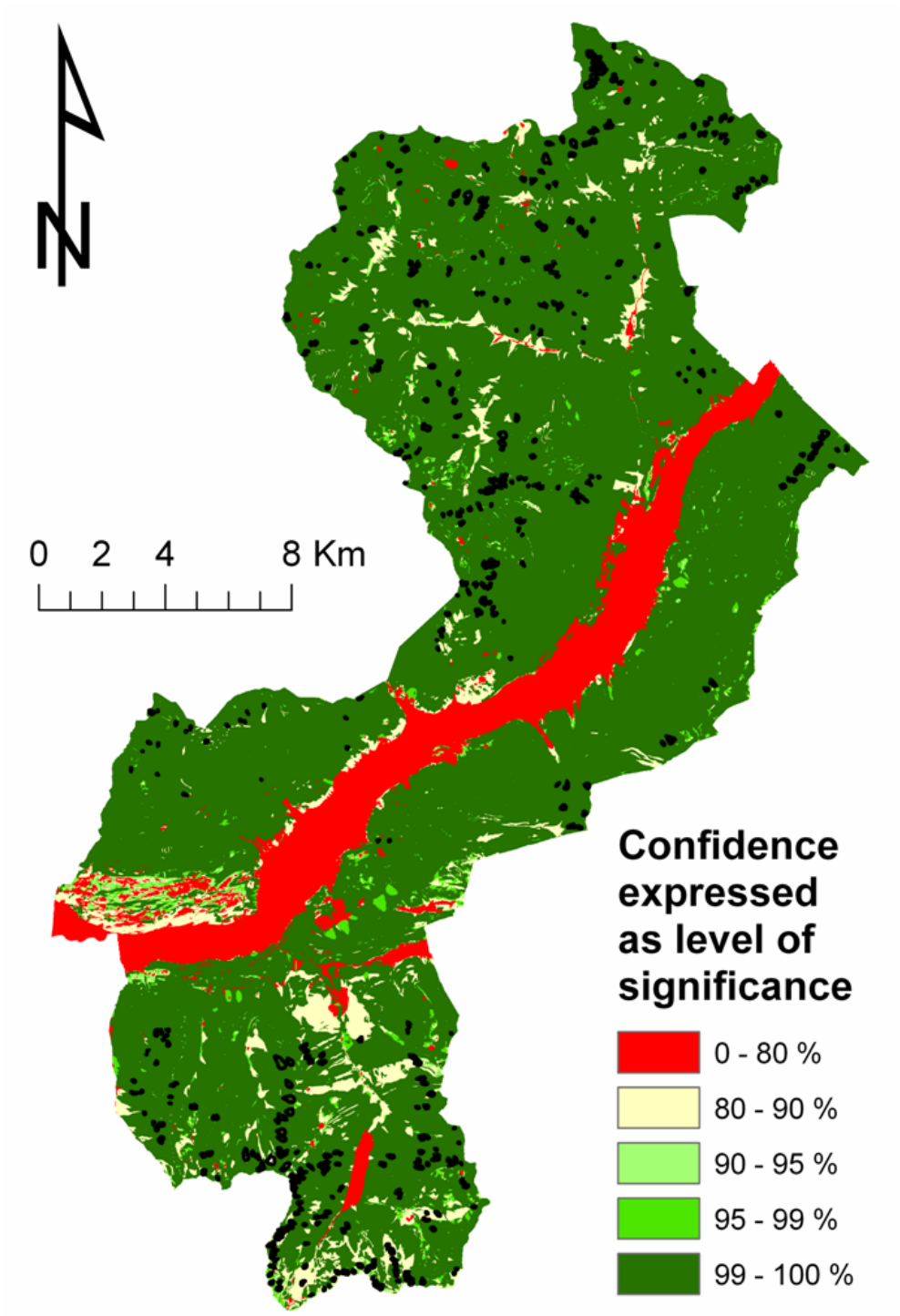

Fig. 6.14 – Confidence map of the final susceptibility map.

Level of significance	Confidence
99%	2.326
95%	1.645
90%	1.282
80%	0.842

Table 6.5 – Levels of confidence.

If the susceptibility maps are well made and evaluated, they could significantly contribute to the public safety in endangered areas. Nevertheless, in the case of automatically calculated maps, their meaning highly depends on the combination of factor maps used as inputs of the analysis. Moreover, it is certain that high knowledge of the territory is essential for the calculation of landslide susceptibility maps. Skills in model calibration alone are not enough to obtain good and reliable results. Thus, an expert knowledge of the territory as well as the landslides is crucial for assessing the credibility of automatically calculated models. It was demonstrated that even within not a large area, the triggering conditions of debris flows could be highly variable. As a consequence, it is advisable to not perform statistical analysis over large areas because particular differences in susceptibility conditions are not shown. To capture specific conditions of landslide sources throughout the entire study area is possible by subdivision of the inventories to sub-inventories of different subtypes of particular landslide type. This approach is advisable in order to avoid mistakes in maps produced from inaccurate inventories which show different spatial patterns.

In the case of debris flow susceptibility mapping, the correct delimitation of susceptible areas is still the beginning of debris flow hazard analysis as subsequent runout analysis has to be performed. When the delimitation of the susceptible areas is not clear and quantification of possible volumes of debris flows is not possible the subsequent runout analysis is difficult to perform.

6.4 Conclusions

A lot of developments have been made in indirect statistically based landslide hazard mapping at medium scale (1:25,000 to 1:50,000) in recent years. Nevertheless, still many limitations exist. One of them is the availability and completeness of landslide inventory databases, which are used for computation of susceptibility and hazard models. Even if landslide inventories are available, they still can have a lot of problems such as inaccuracy and the lack of sufficient temporal information. Available temporal data, if any, would allow to analyse the frequency/magnitude relationships of landslides for a quantitative risk assessment.

The comparison between the official database (GeoIFFI) and the recently mapped inventory (DF2001) did not show marked differences in the importance of particular factor classes, when those inventories were randomly subdivided. The differences between the inventories arise when they were spatially subdivided into three parts in order to capture peculiar triggering factors for each part. In that case, no particular differences in the model performance were observed in the GeoIFFI database. On the contrary, the DF2001 database was able to capture these differences. It is advisable to divide a region into environmentally different subsets to better capture the specific characteristics of landslide controlling factors. The final susceptibility map was made by combining the models from the spatially divided DF2001 inventory. This final map has five classes according to the percentage of debris flow scarps. The improvement of model performance using the DF2001 inventory could be caused by more complete representation of the landslides in the DF2001 inventory.

The improvement in model performance is different from findings of Poli and Sterlacchini (2007). In their work, representation strategies of landslide scarps in susceptibility studies were analysed. They found out that different density of cells used to represent landslide scarp polygons did not greatly influence the posterior probability maps. The dissimilarity with the work of Poli and Sterlacchini (2007) is probably caused by different types of landslides analysed (translational and rotational landslides) and different spatial extents of scarp areas. Moreover, they analysed only one inventory with different point representation, while this study compared two different inventories, one mapped as points, while the other mapped as polygons.

This study shows that the produced susceptibility maps depend on the landslide inventories used as input, and the spatial pattern of the maps produced using different inventories varies a lot, although this difference is not so large when standard evaluation techniques are applied. The spatial distribution of susceptible areas in the best performing maps disagrees by 20% to 30%. The results of this study have significant implications for landslide assessment in which susceptibility maps at medium scale are often used.

6.5 References

Agterberg, F.P., Bonham-Carter, G.F., Wright, D.F. (1989): Weights of Evidence modelling: a new approach to mapping mineral potential. In: Agterberg, F.P., Bonham-Carter, G.F. (Eds.): Statistical Applications in the Earth Sciences. Geological Survey of Canada, Paper 89-9, pp. 171-183.

Beguería, S. (2006): Validation and Evaluation of Predictive Models in Hazard Assessment and Risk Management. Natural Hazards, 37: 315-329.

Bonham-Carter, G.F. (1994): Tools for map pairs. In: Merriam, D.F. (Ed.): Geographic Information Systems for Geoscientists, Pergamon Press, Oxford, pp. 221-265.

Bonham-Carter, G.F. (1996): Geographic Information Systems for Geoscientists: Modeling with GIS. Pergamon, Elsevier Science Ltd., 398 p.

Bonham-Carter, G.F., Agterberg, F.P., Wright, D.F. (1988): Integration of geological datasets for gold exploration in Nova Scotia. Photogrammetric Engineering, 54: 1585-1592.

CARG Project (1992): The New Italian 1:50 000 Geological Map. National Geological Survey, Rome, Italy.

Carrara, A., Cardinali, M., Detti, R., Guzzetti, F., Pasqui, V., Reichenbach, P. (1991): GIS Techniques and statistical models in evaluating landslide hazard. Earth Surface Processes and Landforms, 16: 427-445.

Carrara, A., Cardinali, M., Guzzetti, F., Reichenbach, P. (1995): GIS technology in mapping landslide hazard. In: Carrara, A., Guzzetti, F. (Eds.): Geographical Information Systems in Assessing Natural Hazards, pp. 135-176.

Carrara, A., Crosta, G., Frattini, P. (2008): Comparing models of debris flow susceptibility in the alpine environment. Geomorphology, 94: 353-378.

Castellanos Abella, E.A. (2008): Provincial landslide risk assessment. In: Castellanos Abella, E.A.: Multi-scale landslide risk assessment in Cuba, Utrecht University, Utrecht, ITC Dissertation 154, pp. 101–152.

Chung, C.-J., Fabbri, A.G. (1999): Probabilistic prediction models for landslide hazard mapping. Photogrammetric Engineering and Remote Sensing, 65: 1389–1399.

Chung, C.-J., Fabbri, A.G. (2003): Validation of spatial prediction models for landslide hazard mapping. Natural Hazards, 30: 451-472.

Chung, C.-J., Fabbri, A.G. (2008.): Predicting landslides for risk analysis – Spatial models tested by a cross-validation technique. Geomorphology, 94: 438-452.

Crosta, G. (1990): A study of slope movements caused by heavy rainfall in Valtellina (July 1987). Proceedings of 6th IVCFL, Milan, pp. 247-258.

DUSAF Project (2003.): Destinazione d'Uso dei Suoli Agricoli e Forestali, Lombardy Region, Milano, Italy.

Fell, R., Corminas, J., Bonnard, C., Cascini, L., Leroi, E., Savage, W.Z. (2008.): Guidelines for landslide susceptibility, hazard and risk zoning for land-use planning. Engineering Geology, 102: 99-111.

GeoIFFI (2006.): The Regional Inventory (1:10 000) of Landslides and Hydrogeological Events, Lombardy Region, Italy. Within IFFI Project (1997) – Italian Landslides Inventory, National Geological Survey, Rome, Italy. Available at: http://www.cartografia.regione.lombardia.it/GeoIFFI

Greenbaum, D., Bowker, M.R., Dau, I., Bropsy, H., Greally, K.B., McDonald, A.J.W., Marsh, S.H., Northmore, K.J., O`Connor, E.A., Prasad, S., Tragheim, D.G. (1995a): Rapid methods of landslide hazard mapping: Fiji case study. Technical report WC/95/28, British Geological Survey (BGS), Natural Environmental Research Council, Keyworth, Nottingham.

Greenbaum, D., Tutton, M., Bowker, M.R., Browne, T.J., Buleka, J., Greally, K.B., Kuna, G., McDonald, A.J.W., Marsh, S.H., O`Connor, E.A., Tragheim, D.G. (1995b): Rapid methods for landslide hazard mapping: Papua New Guinea case study. Technical report WC/95/27, British Geological Survey (BGS), Natural Environmental Research Council, Keyworth, Nottingham.

Guzzetti, F., Cardinali, M., Reichenbach, P. (1994): The AVI Project: A bibliographical and archive inventory of landslides and floods in Italy. Environmental Management, 18: 623-633.

Guzzetti, F., Carrara, A., Cardinali, M., Reichenbach, P. (1999.): Landslide hazard evaluation: a review of current techniques and their application in a multi-scale study, Central Italy. Geomorphology, 31: 181-216.

Guzzetti, F., Galli, M., Reichenbach, P., Ardizzone, F., Cardinali, M. (2006a): Landslide hazard assessment in the Collazone area, Umbria, Central Italy. Natural Hazards and Earth System Sciences, 6: 115-131.

Guzzetti, F., Reichenbach, P., Ardizzone, F., Cardinali, M., Galli, M. (2006b): Estimating the quality of landslide susceptibility models. Geomorphology, 81: 166-184.

ITC (2009): ILWIS - Remote Sensing and GIS software: Integrated Land and Water Information System.
Available at: http://www.itc.nl/Pub/Home/Research/Research_output/ILWIS_-_Remote_Sensing_and_GIS_software.html

Lombardy Region (2002.): Inventario delle frane e dei dissesti idrogeologici della Regione Lombardia. Direzione generale territorio e urbanistica. Struttura rischi idrogeologici, Milano, 2 CD-ROM.

Poli, S. (2006): La modellazione spaziale a supporto dell'analisi di rischio idrogeologico. Ph.D. Thesis, University of Milano-Bicocca, Milano, Italy, 180 p. (unpublished)

Poli, S., Sterlacchini, S. (2007): Landslide representation strategies in susceptibility studies using Weights-of-Evidence modeling technique. Natural Resources Research, 16: 121-134.

Raines, G. (1999.): Evaluation of weights of evidence to predict epithermal-gold deposits in the great basin of western United States. Natural Resources Research, 8: 257-276.

Raines, G. L., Bonham-Carter, G. F., Kamp, L. (2000.): Predictive Probabilistic Modeling Using ArcView GIS. ArcUser, 3: 45-48.

Remondo, J., Bonachea, J., Cendrero, A. (2005.): A statistical approach to landslide risk modelling at basin scale: from landslide susceptibility to quantitative risk assessment. Landslides, 2: 321-328.

Sawatzky, D.L., Raines, G.L. , Bonham-Carter, G.F., Looney, C.G. (2008): Spatial Data Modeller (SDM): ArcMAP 9.2 geoprocessing tools for spatial data modelling using weights of evidence, logistic regression, fuzzy logic and neural networks. Available at: http://arcscripts.esri.com/details.asp?dbid=15341

Soeters, R., van Westen, C.J. (1996): Slope Instability. Recognition, analysis and zonation. In: Turner, A.K., Schuster, R.L. (Eds.): Landslides Investigation and Mitigation: Transportation Research Board, Specific Report, 247, National Academy Press, Washington, pp. 129-177.

Süzen, M.L., Doyuran, V. (2004.): Data driven bivariate landslide susceptibility assessment using geographical information systems: method and application to Asarsuyu catchment, Turkey. Engineering Geology, 71: 303–321.

Thiery, Y., Malet, J.-P., Sterlacchini, S., Puissant, A., Maquaire, O. (2007): Landslide susceptibility assessment by bivariate methods at large scales: Application to a complex mountainous environment. Geomorphology, 92: 38-59.

van Westen, C.J. (1993): Application of Geographic Information Systems to landslide hazard zonation. ITC publication, 15. International Institute for Aerospace and Earth Resources Survey (ITC), Enschede.

van Westen, C.J., Rengers, N., Soeters, R. (2003): Use of geomorphological information in indirect landslide susceptibility assessment. Natural Hazards, 30: 399–419.

Chapter 7

Spatial variability of susceptibility maps

All models are wrong,
but some are useful.

(G.E.P. Box)

Based on:

Blahut, J., Sterlacchini, S., Ballabio, C. (2009): Effect of the input parameters on the spatial variability of landslide susceptibility maps derived by statistical methods. Case study of the Valtellina Valley (Italian Central Alps). Geografický časopis / Geographical Journal, 61(1): 3-18.

Sterlacchini, S., Ballabio, C., Blahut, J., Masetti, M., Sorichetta, A. (2010): Spatial agreement of predicted values in landslide susceptibility maps. Geomorphology (submitted, under review).

7.1 Introduction

Landslide susceptibility assessment has shown significant improvements in recent years by using indirect statistically-based methods implemented within GIS (Aleotti and Chowdhury 1999, Chapter 6). Statistical methods are being widely used to analyse landslide prone areas. Although spatial data analysis techniques are now widely adopted as an effective tools for independent validation of predicted results in post-processing operations (Beguería 2006), poor attention is often paid to the evaluation of the spatial variability of the predicted results.

The relationships between past events and predisposing factors may give us information on the likely spatial distribution of future occurrences. However, it seems that the quality of predicted results does not automatically increase with the number of predisposing factors used in the modelling procedures, and the significance of such conditioning factors is frequently not thoroughly evaluated. This chapter focuses on the different spatial patterns of susceptibility maps derived by same statistical method but with different combination of predisposing factor maps (geology, land use, slope, aspect, etc.). To achieve this goal, the same methodology for generation of landslide susceptibility maps was applied, using different combination of factor maps classified in a same way. After that, a comparison of the obtained maps using Kappa Statistic and Principal Component Analysis was performed.

7.2 Materials and methods

7.2.1 Susceptibility maps

As inputs for the spatial variability analysis were used the susceptibility maps derived from the GeoIFFI inventory (GeoIFFI 2006) and DF2001 inventory (for further information on the inventories, please see section 6.2.1). These maps were produced by random subdivision of the inventories into training and prediction subsets. The goodness-of-fit of susceptibility maps was assessed using success rate curves – SRC (Chung and Fabbri 1999). The next step was the evaluation the predictive power of the maps using predictive subset: prediction rate curve method - PRC (Chung and Fabbri 2003) to strength the model prediction power. The PRCs were built in a same way as SRCs, but instead of using training subset, we used prediction subset of debris-flow scarps that did not enter into the model calculation. A count of landslides in the predictive subset that fall into the susceptibility classes of the prediction map yields prediction rates, which are used to estimate the reliability and prediction power of the map generated for predicting locations of future landslides.

After application of the standard evaluation techniques, it has been observed that the results do not show significant differences in terms of success or prediction rate curves, however the spatial pattern was very different (see also section 6.3.5). In order to compare all the models produced in the analysis, statistical techniques were applied. Maps produced by the

GeoIFFI inventory were compared to each other using Kappa Statistic and Principal Component Analysis. More attention was paid to the DF2001 inventory which shows better results in SRCs and PRCs and which was used for the production of the final susceptibility map (section 6.3.6). Maps produced by the DF2001 inventory were compared to each other using 0.95 confidence interval, Kappa Statistic, Principal Component Analysis, and Distance Weighted Entropy (DWE). The methodological approach is described more in detail in the following sections.

7.2.2 Background for the spatial comparison of debris flow susceptibility maps

This study is based on the concept of "statistical sample", which is a subset of the real population (which is usually unobservable) whose properties are "close" to those of the whole population. In the framework of landslide susceptibility, this means that the events observed during a fixed period of time do not represent the whole population of landslides but rather a sample of this population. Moreover, the explanatory variables related to morphological and environmental features influencing the spatial distribution of landslides (commonly referred to as "susceptibility") are often latent (unobservable or not measurable in a precise way). Finally, the distribution of landslides, while related to the susceptibility, is partially dependent on random factors. Thus, the probability distribution of landslides can be formalised as:

$$P[y=1] = \beta(z) + \varepsilon_k + \varepsilon = \sum_{k=1}^{n} \lambda_k(x_k) + \varepsilon \qquad (7.1)$$

Where: $P[y=1]$ expresses the probability of occurrence of an event (landslide), which is a function of $\beta(z)$, where z is the latent variable (susceptibility) and β is the related parameter. Neither z nor β are observable, so we relay on k observable variables x_k (geology, topography, etc.) to approximate z. The terms ε express the random error of the general model, while ε_k expresses the random error between the latent variable and the observable predictors.

The most important thing to consider in this model is that we can have n different future outcomes of landslides distribution. This may seem an odd assumption, but we can consider that in a defined area we may have some subareas in which the value of z is the equivalent, so the fact that a landslide occurs in one subarea and not in all of them is largely due to the stochastic term ε. Of course, ε may be physically determined, but it is still stochastic since we cannot model its behaviour in a deterministic way. This formulation introduces the concept of uncertainty in the landslides susceptibility models, which means that we can associate prediction errors and Confidence Intervals (CI) to our models' outcome.

Given these assumptions, the first step in our approach concerned the production of 11 susceptibility maps using the GeoIFFI inventory and 13 susceptibility maps using DF2001 inventory, respectively. These maps were prepared by different combination of morphometric and geo-environmental variables. The second step involved cross-validation operations on independent samples to identify the best possible success/prediction rates from the set of

descriptors. Finally, statistical comparison was made on a set of susceptibility maps, characterised by similar prediction rates, to assess the degree of spatial agreement among predicted results. The following sub-sections describe our approach in detail.

7.2.3 Classification of the predictive maps and assessment of the model performance

Results from the Weights-of Evidence modelling (section 6.3.3) are expressed as floating point post-probability rasters. In order to compare these post-probability maps, continuous probability values have been reclassified into 10 discrete classes each, by an equal-area criterion. This is a common procedure in hazard zoning, since continuous probability maps are poorly interpretable by end-users. Usually the number of classes into the original maps are reclassified is rather low, normally between 3 and 6 classes. In this case the choice of 10 classes is rather conservative in relation to the preservation of the information stored in the original maps.

After the reclassification, each map has the following characteristics: 1) all 10 classes will include the same number of pixels and therefore each class will cover the same area over the ground ($1/10^{th}$ of the entire study area, about 45 km^2); 2) the 1st class will be the most susceptible; and 3) it will be relatively simple to compare the spatial distribution of the susceptibility classes. In effect, by preparing the maps in such a way, the following steps (concerning the application of Kappa Statistic and Principal Component Analysis) comes out more straightforward.

Usually a success or prediction curve can be seen as the outcome of a specific classifier, whose performance is dependent on the particular set of events chosen for the validation. The common practice is to use all the available events in the cross-validation set to produce a single curve. However, it is clear that the curve obtained is only one of the n possible outcomes of the model, for the n possible combinations of observed events. In this case models' performance could be slightly different due to the random errors in the cross-validation set. For instance, a particular set of observed events could be predicted better by the same model than another one, thus generating a curve which seems to indicate a better performing model. On the other hand, the same model could predict far worse another subset of events. Thus, a success or predictive curve can be seen as the average result of a series of n theoretical realizations of the same underlying model (the "real" susceptibility). By adding a small amount of random events and by computing k ($k<n$) possible realizations of the prediction, it is possible to obtain a sample of the probability distribution of the model performance for each susceptibility ranking class. Then, by adopting a Monte Carlo (MC) sampling, the probability distribution frequencies (PDF) can be reconstructed, even for non-normal distributions.

These confidence intervals are especially useful to compare different models outcome, since these intervals tells us how much different are two or more models in terms of success and prediction curves. So if two models have a different average prediction, but they all lay in the same 0.95 CI interval these models are unlikely to be different and should be considered as statistically equivalent. To further improve the significance of the success and prediction curves 0.95 confidence intervals were calculated for the DF2001 database.

7.2.4 Application of Kappa Statistic and Principal Component Analysis

The original use of the Kappa Statistic (Cohen 1960) was to compare two independent responses in psychological tests. Since then, Kappa Statistic has been applied in a broad range of fields, including mapping (Sim and Wright 2005). In this study we used it to compare two maps with the same thematic classification, referring to the agreement among different classified maps and not the agreement between a map and the measured or observed data.

The procedure for calculation of the Kappa Statistic is rather simple and is based on the creation of a confusion matrix of the class frequencies of two maps. The Kappa Statistic could then be calculated from equation 7.2. The advantage is that it is generally a more robust measure than simple percent agreement calculation, because it takes into account the agreement occurring by chance. Cohen's Kappa measures the agreement between two raters, each one classifying *N* items into *C* mutually exclusive classes:

$$K = \frac{P(a) - P(e)}{1 - P(e)} \tag{7.2}$$

Where *P(a)* is the relative observed agreement among raters, and *P(e)* is the probability that agreement is due to chance. If the raters are in complete agreement then $K = 1$. If there is no agreement among the raters; other than what would be expected by chance; then $K \leq 0$.

A Kappa value of 0 implies that the two maps are unrelated, i.e. the class in a given cell of one map gives no information about the class of the same cell on the other map. A Kappa value of 1 implies complete agreement; a value less than 0 implies more disagreement than a random assignment of classes to one of the maps. Thus, the Kappa Statistic is an effective statistical measure of inter-class reliability. Landis and Koch (1977) gave the following table for interpreting *K* values (Table 7.1); however, it is not universally accepted given that the authors supplied no evidence to support it besides their personal opinions.

Kappa	Interpretation
0	No agreement
0 – 0.2	Very low Agreement
0.2 – 0.4	Low agreement
0.4 – 0.6	Moderate agreement
0.6 – 0.8	Good agreement
0.8 – 1	Almost perfect agreement

Table 7.1 – Relative agreement between rates used by Kappa Statistic. After Rossiter (2004).

A Principal Component Analysis (PCA, Pearson 1901) was also performed to improve the interpretability of the Kappa Statistic outcomes. PCA is an orthogonal linear transformation that transforms the data to a new coordinate system such that the greatest variance by any projection of the data comes to lie on the first coordinate (called the first principal component), the second greatest variance on the second coordinate, and so on. PCA is theoretically the

optimum transform for a given data in least square terms. The first principal component accounts for as much of the variability in the data as possible, and each succeeding component accounts for as much of the remaining variability as possible. Therefore, PCA is a useful technique for finding patterns in data of high dimensions. It reduces data dimensionality by performing a covariance analysis among factors. Dimensionality reduction is performed by retaining those characteristics of the dataset that contribute most to its variance by keeping lower-order principal components and ignoring higher-order ones. It is also useful because it can provide a simple way to plot complex multivariate data structures. When applied on conditions, PCA will explore correlations among samples or conditions. Note that because the goal of PCA is to 'summarise' the data, it is not considered a clustering tool. PCA does not attempt to group data by user-specified criteria as the clustering methods do. PCA is recommended here as an explanatory tool to uncover unknown trends in the data (Shaw 2003).

7.2.5 Application of a Distance Weighted Entropy (DWE) procedure

The Kappa Statistic summarises the agreement among different maps; however, no information is made available about the location where the prediction of two or more maps agreed and where they did not. For instance, two maps could consistently identify similar high susceptibility classes in the same sub-areas but fail to locate the lower ones in other positions; moreover, a third map could fail to locate both low and high susceptibility classes in relation to the other maps. Thus, the necessity to map the consistency of the predictions of different models (with very similar success/prediction rates) arose, making it possible to identify sub-areas in which the predictions could be in agreement or discordant. For this reason, we developed a distance weighted entropy (DWE) procedure to quantify the spatial distribution of different modelling outcomes. Empirical information entropy (EIE) (or Shannon entropy, Shannon 1948) represents an excellent method to estimate the informative contents of a discrete random variable; it can be expressed as:

$$H^{ML} = -\sum_{k=1}^{p} \theta_k^{ML} \log \theta_k^{ML} \tag{7.3}$$

The formulation of 7.3 expresses the Maximum Likelihood (ML) Entropy (H) as a function of θ. Here θ is the empirical frequency of class k, defined as:

$$\theta_k^{ML} = \frac{y_k}{n} \tag{7.4}$$

Where y_k is the number of occurrences of class k in the vector whose entropy we want to estimate and n is the overall number of elements of the vector.

In this study, entropy value has to be calculated for each cell of the reclassified maps, so a stack of the reclassified maps derived from the different models is build; each cell of the stack can now be seen as a vector whose dimension (n) is equal to the number of the maps in the stack

and whose elements are the ranking values of the reclassified maps (k). The computation of the EIE for each pixel is then straightforward.

However, in this specific case, the random vector outcome has a rank attribute (the susceptibility rank) which should be considered in the procedure. So, if two or more models produce classes with a rank close one to each other (i.e., 1, 2, 2, 1), this outcome is clearly preferable to the models producing an outcome with very different classes rank (i.e., 1, 5, 7, 10). The EIE does not take into account this kind of information, so we re-weighted the EIE utilising the sum of Euclidean distances among ranks.

$$H^W = H_k^{ML}\left(\frac{\sum_{i,j=1}^{k}\sqrt{(y_{kj}-y_{ki})^2}+1}{\max\left[\sum_{i,j=1}^{k}\sqrt{(y_{kj}-y_{ki})^2}\right]+1}\right) \tag{7.5}$$

Where H^W is the weighted version of the EIE. In this formulation the entropy score for a cell is maximised when all the map classes within the stack are evenly distributed (each one is different) and when the intra-classes distance is maximised. Thus, the index of equation 7.5 is maximised when each model produces a different ranking class for each pixel and when these classes have scores as different as possible. On the other side, the index reaches its minimum when all classes belonging to different maps but sharing the same geographical position (cell) have the same rank; this represent the situation in which all the reclassified maps produce the same ranking score for a given cell.

7.3 Results and discussion

7.3.1 Comparison of the maps produced by the GeoIFFI inventory

Performance of eleven susceptibility maps, obtained by different combinations of factor maps (Tab. 7.2), was assessed with standard evaluation and validation techniques by the computation of AUC for SRCs and PRCs (Beguería 2006).

According to AUC under SRC, the best working model was represented by map R_08 (84.04%). This map was calculated using combination of geology, land use, slope, planar and profile curvature factor maps. Second best working model was model R_09 (83.98%) composed of these factor maps: geology, land use, slope and planar curvature. Third best working model was model n. 6 (83.34%) built with combination of geology, land use, slope, internal relief, profile curvature and planar curvature factor maps. Practically, the difference of AUC among these maps is almost negligible.

In relation to AUC for PRC, again the best performing map was R_09 (83.65%). Map was, as mentioned before, composed of geology, land use, slope and planar curvature factor maps. Second and third best performing maps were: R_08 (83.57%) and R_11 (82.89%). Map

R_08 was made by combination of geology, land use, slope, planar and profile curvature; while map R_11 was made of geology, land use, slope, internal relief and planar curvature.

The other maps have very similar results in SRC and PRC, except map R_05 that was made by combining only geology and slope factor maps (Fig. 7.1, 7.2). This result has lower SRC and PRC and shows that land use factor map has great added information value to the model. The difference between AUC of all the produced maps is 6.32% in SRC and 5.96% in PRC.

Model	SRC [%]	PRC [%]	Altitude	Slope	Aspect	Internal Relief	Landuse	Geology	Fault dist.	Planar curv.	Profile curv.
R_01	83.30	82.78	X	X	X	X	X	X	X	X	X
R_02	82.07	81.44	X	X	X	X	X	X			
R_03	82.70	82.01	X	X	X		X	X	X		
R_04	82.68	81.99	X	X			X	X	X		
R_05	77.72	77.70		X				X			
R_06	83.34	82.81	X	X		X	X	X	X	X	X
R_07	82.09	81.43	X	X		X	X	X			
R_08	84.04	83.57	X	X			X	X	X	X	X
R_09	83.98	83.65	X	X			X	X		X	
R_10	82.76	81.99	X	X		X	X	X			X
R_11	83.32	82.89	X	X		X	X	X	X	X	

Table 7.2 – Areas under curve for SRCs and PRCs of 11 models produced by randomly divided GeoIFFI inventory. Combination of factor maps used for model calculation is shown by crosses.

For assessment of spatial variability among susceptibility maps, the Kappa values were calculated. The results are shown in Figures 7.3 and 7.4 where the Kappa values of whole susceptibility maps and the highest susceptibility classes are compared. To easily interpret the results from Kappa Statistic a Cluster Analysis was performed (see dendrogram in Fig. 7.3, 7.4). It. shows the proximity between different maps. The analysis shows that only 6 maps have a reliable class consistency (with Kappa values above 0.6). This feature is most striking when compared with the results from SRC and PRC. Excluding map R_05, the other maps (all with almost similar success and prediction rate values) show levels of proximity really variable (many situations are characterized by low level of inter-class correlation). This means that maps with similar prediction rates could have a different spatial class distribution. Inter-class accuracy increases when only the most susceptible areas are taken into account, as shown in figure 7.4. This could be seen as a positive result given that a high accuracy for the higher susceptible classes avoids the problem of false negatives. Anyway, the inter-maps accuracy is still low for many combinations.

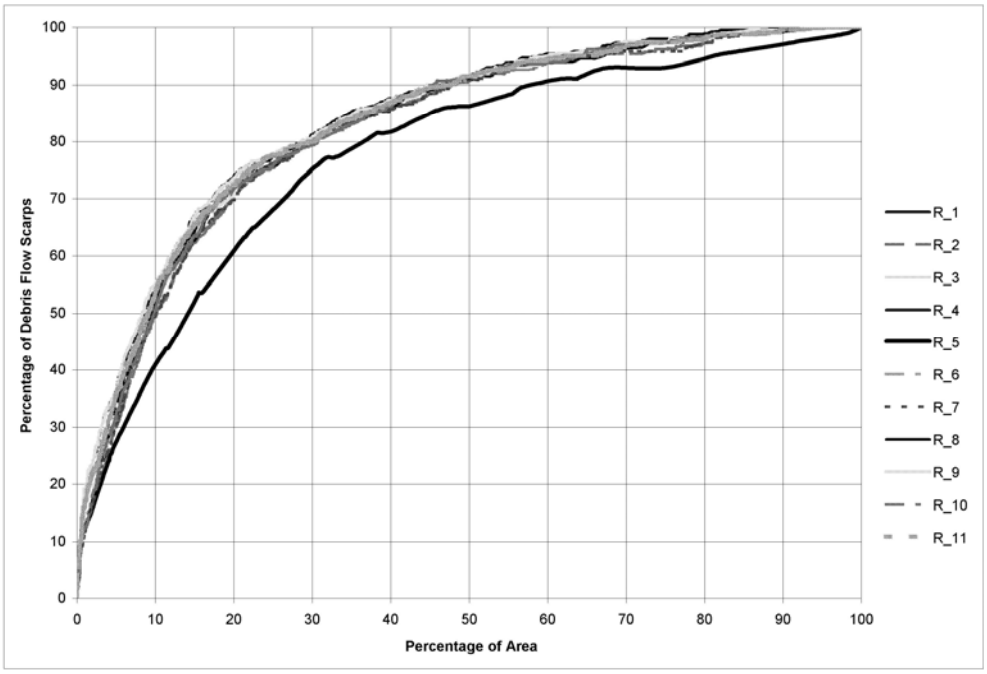

Fig. 7.1 – Success rate curves for eleven models produced by randomly divided GeoIFFI inventory.

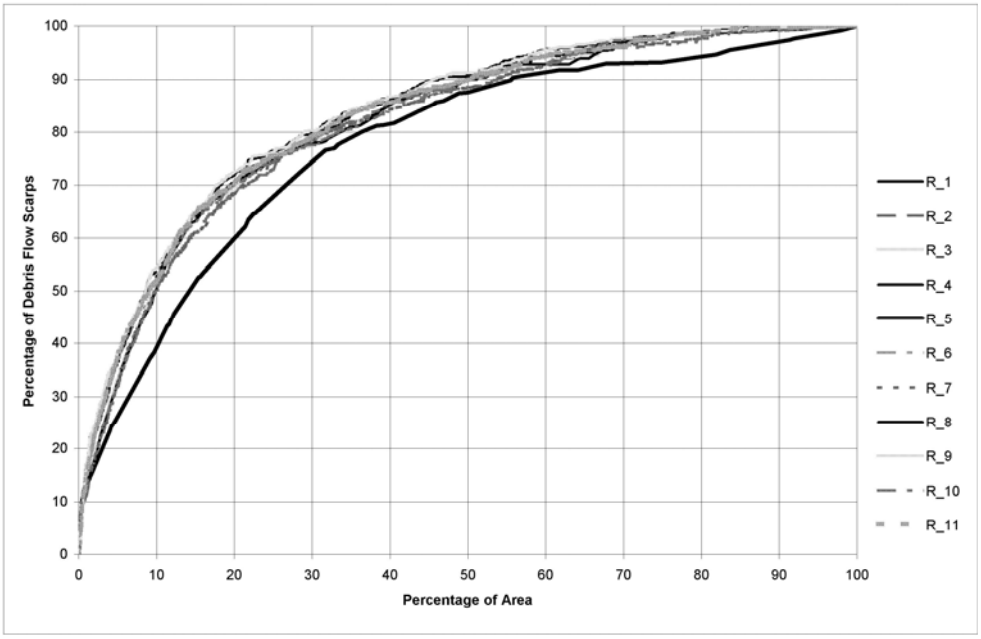

Fig. 7.2 – Prediction rate curves for eleven models produced by randomly divided GeoIFFI inventory.

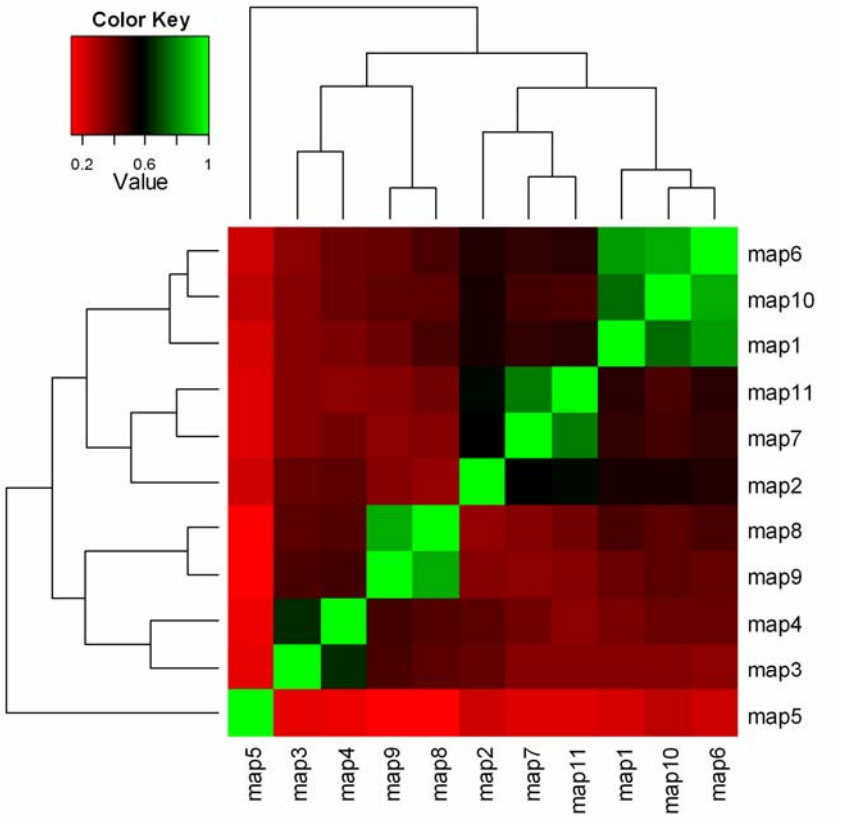

Fig. 7.3 – Results from the Kappa statistic for the 11 susceptibility maps of GeoIFFI inventory (all classes).

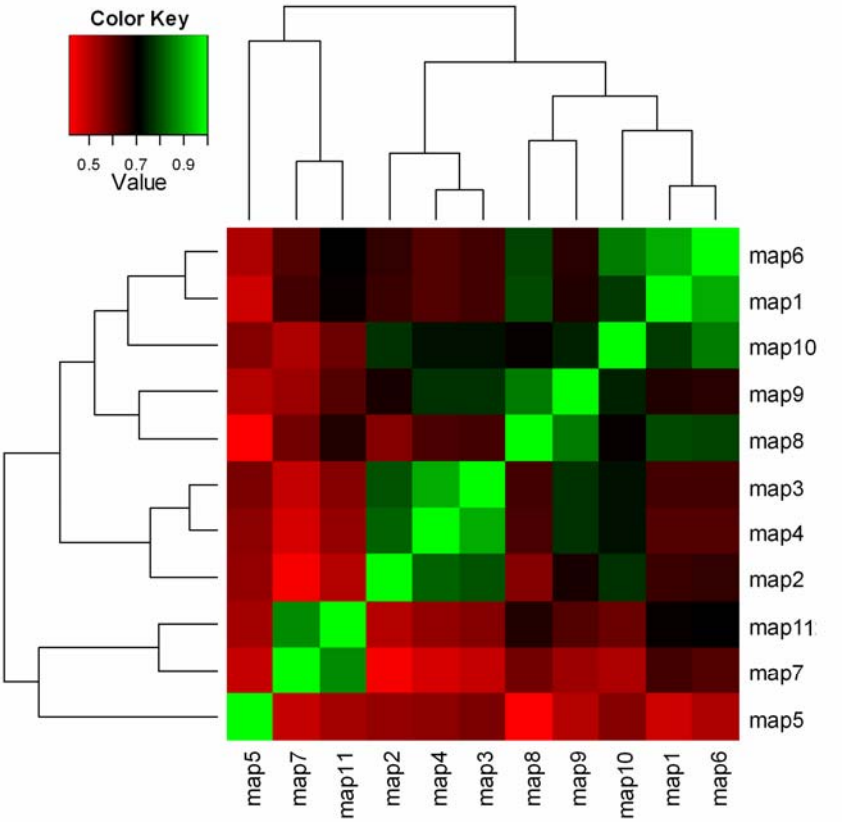

Fig. 7.4 – Results from the Kappa statistic for the 11 susceptibility maps of GeoIFFI inventory (highest class only).

A Principal Component Analysis (PCA) was also applied to strengthen the results abovementioned. The result from PCA shows two main clusters in comparing whole map variability. Their difference is due to presence and absence of internal relief factor map. This result is very important because the effect of presence and absence of one single factor map could have very strong influence on the results. Moreover, the map R_05 seems to be completely different from the two main clusters. When assessing only the highest susceptibility class the results from PCA seem to be much more diffused (Fig 7.5).

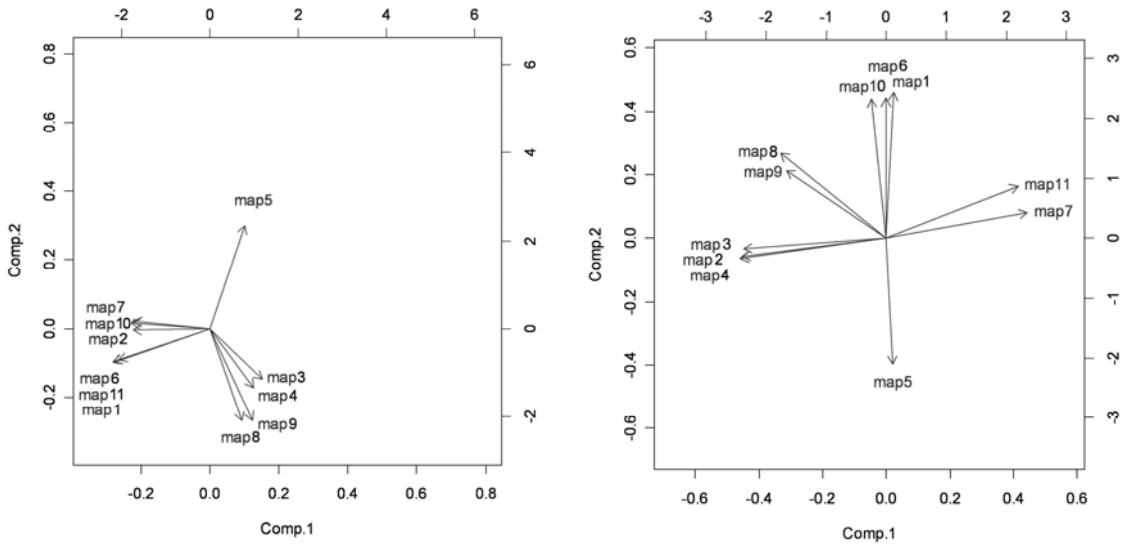

Fig. 7.5 – Results of the PCA of class variability among the susceptibility maps made from GeoIFFI inventory. On the left are the results from all classes' analysis, on the right there are results from the analysis of the highest class only.

7.3.2 Comparison of the maps produced by the DF2001 inventory

Figure 7.6 shows the SRCs and PRCs of the thirteen susceptibility maps produced by using the DF2001 inventory. It can be seen that out of 13 models (Table 7.3), 12 of them seem to be largely overlapping in their performance. Especially in the initial part of the curves, it is impossible to distinguish one model from another, as the curves are very close to each other and the CI are substantially overlapping. However, as human perception can be biased, a statistical test (t-test) was applied to verify against the null hypothesis if the PDF curves are coming from the same distribution or not.

From Figure 7.6, it can be seen that susceptibility maps (apart from map n. 5) are producing a substantially identical outcome; so an agreement between these maps also from the Kappa Statistic should be seen. Figure 7.7 depicts the rate of agreement of the predicted susceptibility maps calculated by using the Cohen's Kappa on the maps classified into 10 equal area classes. These 10 classes correspond to the every 10% of susceptible area of Fig. 7.6. Each of the 13 maps has been tested against each other, thus producing a square matrix of 169 values. To make the matrix interpretable, the values have been translated into a colour scale, with the values close to 1 represented by red and the values close to 0 represented by blue. Along with

the heatmap matrix, the agreement among the maps is also shown by the dendrograms on the top and on the left from the heatmap matrix; two maps with similar success/prediction outcomes are shown as close branches in the dendrogram (as maps 1 and 6 or 7 and 12). The Kappa Statistic only partially confirm the outcomes of the success and prediction rate curves. Even if the Cohen's Kappa does not have relevance as an absolute value, it provides a mean to compare different rates of agreement.

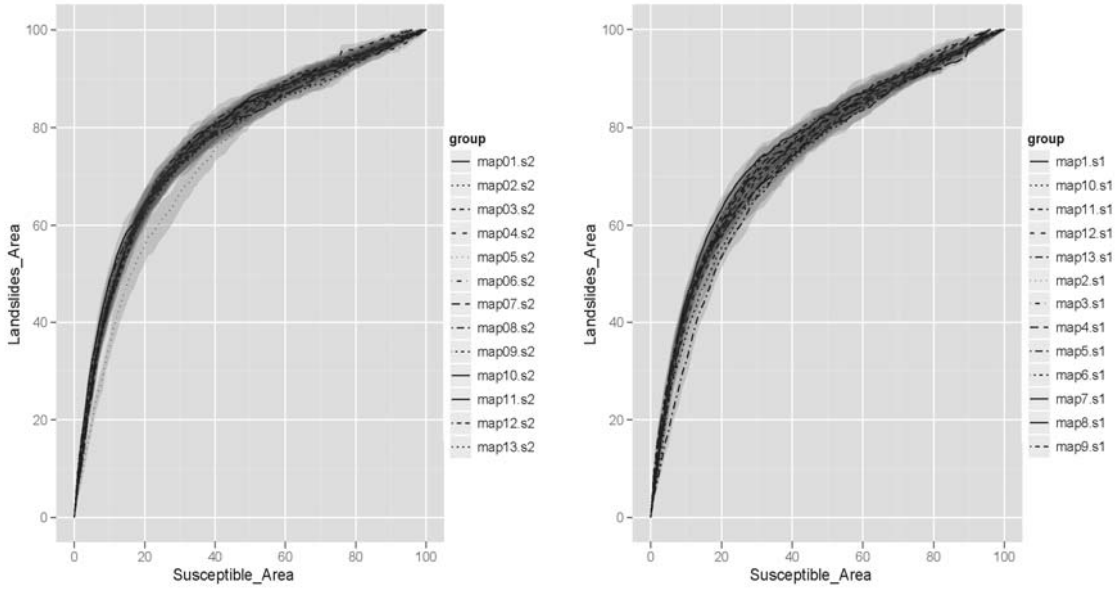

Fig. 7.6 – Success (on the left) and prediction (on the right) rate curves for 12 susceptibility maps of the DF2001 inventory. The dark grey band indicates the 0.95 confidence interval obtained by randomly selecting sets of events by a bootstrap procedure. The curves are mostly coincident and it is substantially impossible to distinguish one curve from another. Map 5 is the only with a statistically different success rate curve.

Model	SRC [%]	PRC [%]	Altitude	Slope	Aspect	Internal Relief	Landuse	Geology	Fault dist.	Planar curv.	Profile curv.
R_01	86.19	88.20	X	X	X	X	X	X	X	X	X
R_02	85.64	87.49	X	X	X	X	X	X			
R_03	86.05	87.80	X	X	X		X	X	X		
R_04	85.66	87.47	X	X			X	X	X		
R_05	80.32	82.52		X				X			
R_06	85.98	88.01	X	X		X	X	X	X	X	X
R_07	85.36	87.28	X	X		X	X	X			
R_08	86.38	88.30	X	X			X	X	X	X	X
R_09	86.54	88.50	X	X			X	X		X	
R_10	85.59	87.39	X	X		X	X	X			X
R_11	86.18	88.24	X	X		X	X	X	X	X	
R_12	85.30	87.22	X	X		X	X	X			X
R_13	85.54	87.14		X			X				

Table 7.3 – Areas under curve for SRCs and PRCs of 12 models produced by randomly divided DF2001 inventory. Combination of factor maps used for model calculation is shown by crosses.

Figure 7.8 analyses this similarity referring to the highest susceptibility classes only. In effect, Figure 7.6 suggests that all maps (apart from n. 5) show similar success and prediction rates for the most susceptible 10 % of the study area. So, we could expect that this agreement will be strengthened by Kappa Statistic too. Figure 7.8 does not confirm this hypothesis at all.

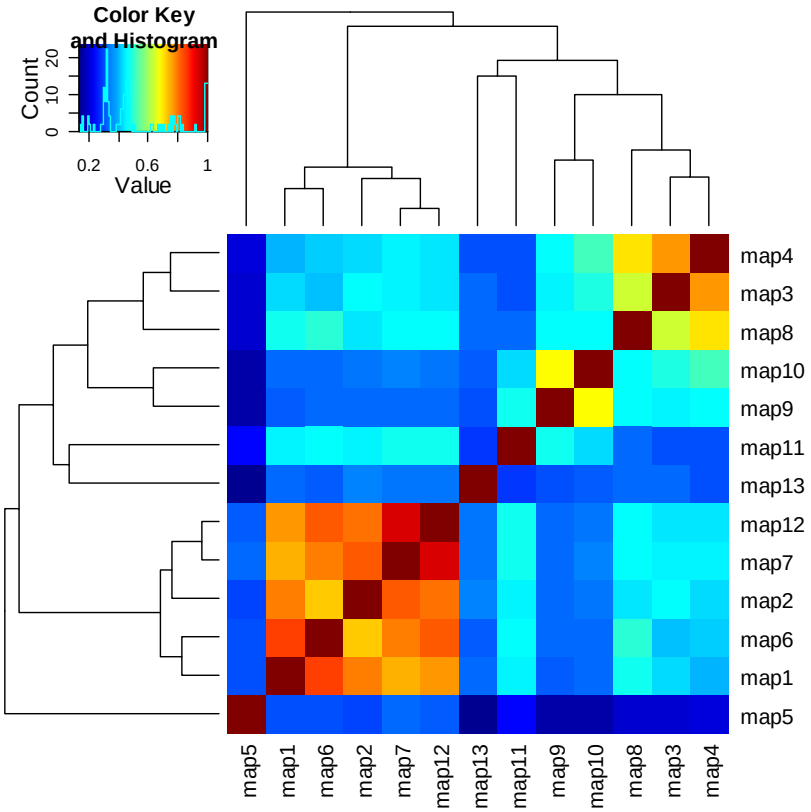

Fig. 7.7 – Results from the Kappa statistic for the 13 susceptibility maps of DF2001 inventory (all classes).

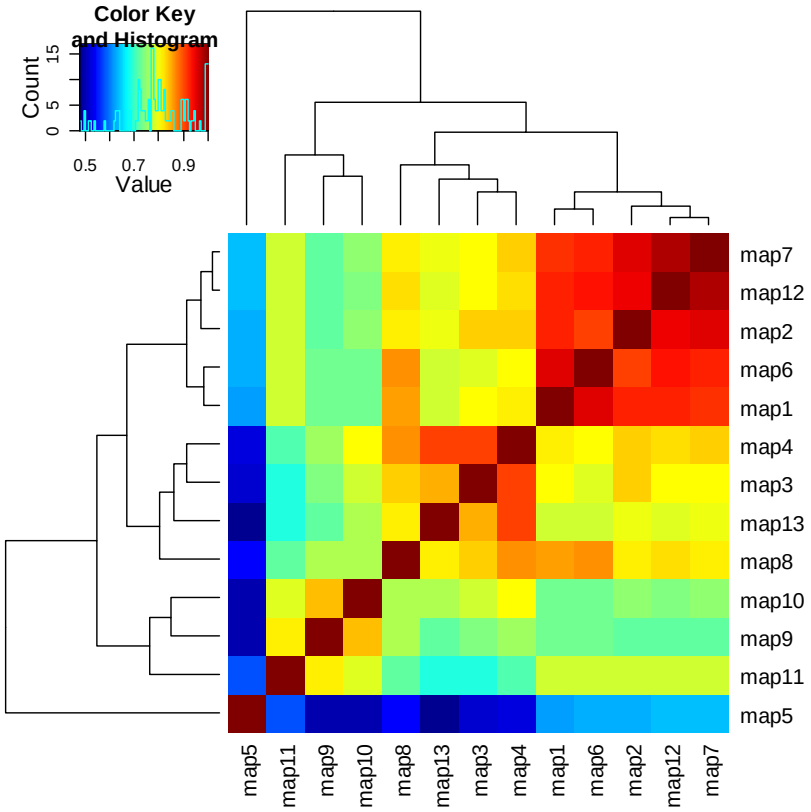

Fig. 7.8 – Results from the Kappa statistic for the 13 susceptibility maps of DF2001 inventory (highest class only).

By treating the Kappa matrix as a covariance matrix, the maps can be projected into a bi-dimensional space, by using the rotation provided by PCA, where the two axis express most of the variance. The outcomes of this procedure are shown in Figure 7.9 and 7.10 (for all classes and for the most susceptible class, respectively): it seems that the maps are clustered into some distinct groups. This is also visible in Figures 7.7 and 7.8, where these clusters are represented by yellow-to-red cells in the heatmap matrix. Maps 1, 2, 6, 7, and 12 show a good agreement even if these maps share only some of the input geo-environmental variables listed in Table 7.2.

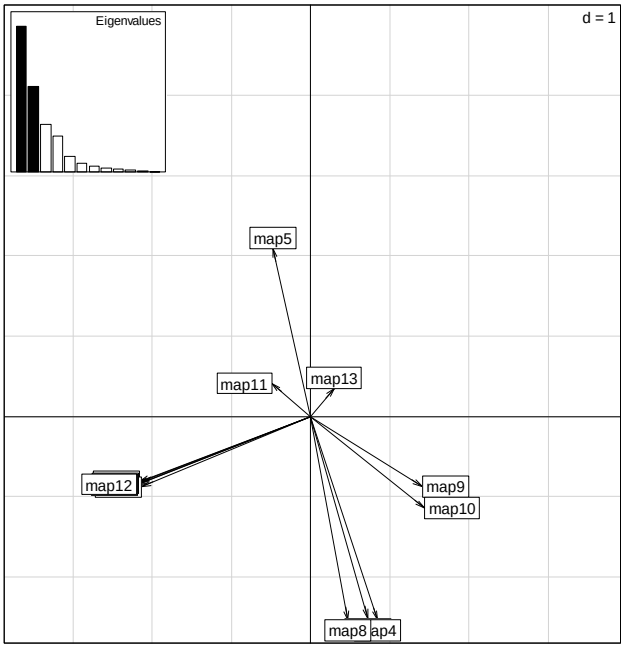

Fig. 7.9 – PCA projection of the Kappa matrix of Figure 7.7. Apart from map n.5, it is possible to distinguish five clusters.

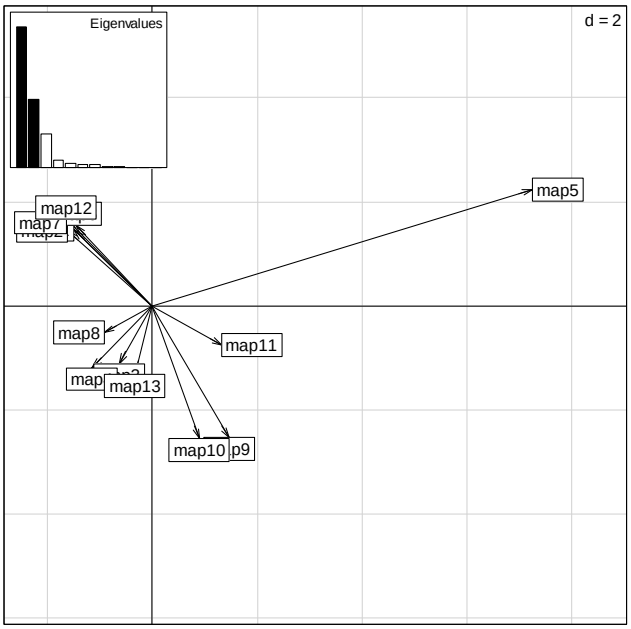

Fig. 7.10 – PCA projection of the Kappa matrix of Figure 7.8. Apart of map n.5, it is possible to distinguish three to four clusters.

Considering only the highest ranking susceptibility classes (Figure 7.10), the structure of the map agreement is clustered into 2/3 groups, while map 5 stands by itself.

This opened a discussion about which model, among the 13 tested, was the best one in terms of prediction. It seemed that the success/prediction rate curves were somewhat unfitted for model selection: only when a modelling outcome was really far worse than that of another model could the success/prediction rate curves be used as a model selection rule; otherwise, they were not sufficiently descriptive for the task for which they were designed. In our study, despite the different modelling outcomes, most of the curves were not statistically different from each other and did not provide any useful information about which was the "right" model. This was especially true for high ranking susceptibility classes, which seemed to be predicted with the same efficiency by all models.

At this stage of the research, it became necessary to evaluate in which pixels of the study area the reclassified susceptibility maps from different models were likely to produce spatial similarities or discrepancies with other maps and estimate how much these predictions differed one from another. Figure 7.11 depicts the distribution of the estimated DWE (standardised in the interval [0,1]); in this case, the valley bottom showed a very low overall entropy as all models predicted this area equally as low susceptible. In contrast, areas characterised by the highest values of DWE were more concentrated in the northern and southern slopes of the study site, lying in zones where landslide density was higher (as shown in Figure 7.12, where an average value of landslide susceptibility is performed by averaging the rank of each susceptibility class belonging to different maps but sharing the same geographical position).

This result could be intrinsically linked to the original post-probability values distribution: these values were not equally scaled, and their distribution was not necessarily the same; so a rank-based reclassification was not likely to identify classes which limits shared identical values of post-probability on different maps (cut-off values). This issue was much more critical for the tails of the post-probability distributions: sampling an equal number of pixels from the tails, we could obtain a class in which very different post-probability values were mixed all together. Figure 7.13 shows this problem with a log-normal distribution: if we segmented the probability interval using theoretical quantiles (dashed vertical lines), so that we had equal-area classes in the case of maps, we observed, for the higher ranking classes, that each class contained a wide range of post-probability values. In Figure 7.14 this example was applied to some of the thirteen empirical distributions obtained from the models: the dashed lines represented the same quantiles as the solid lines, but those quantiles were calculated empirically. It could be easily noticed that the "cut-off values" of the segmentation varied more for the higher post-probability values because we had fewer pixels in this range. If we generalised this behaviour to our post-probability maps, we could remark that the reclassification procedure itself could introduce a certain amount of uncertainty in the relative ranking of the susceptibility maps.

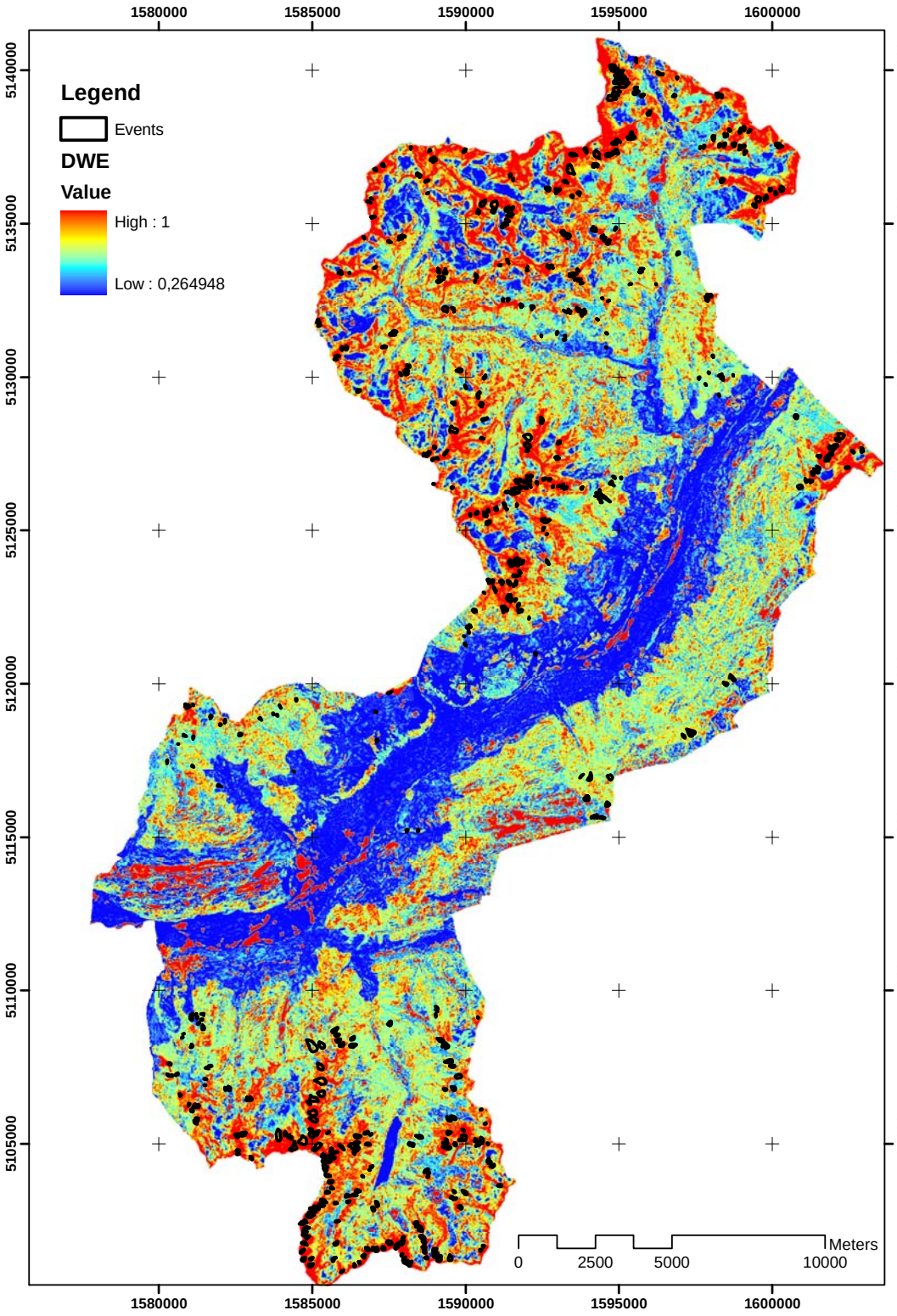

Fig. 7.11 – Distance weighted entropy (DWE) map of the study area. This map was used to assess the spatial agreement among the rank of susceptibility classes belonging to different maps but sharing the same geographical position. Debris flow scarps of the DF2001 inventory are shown on the map.

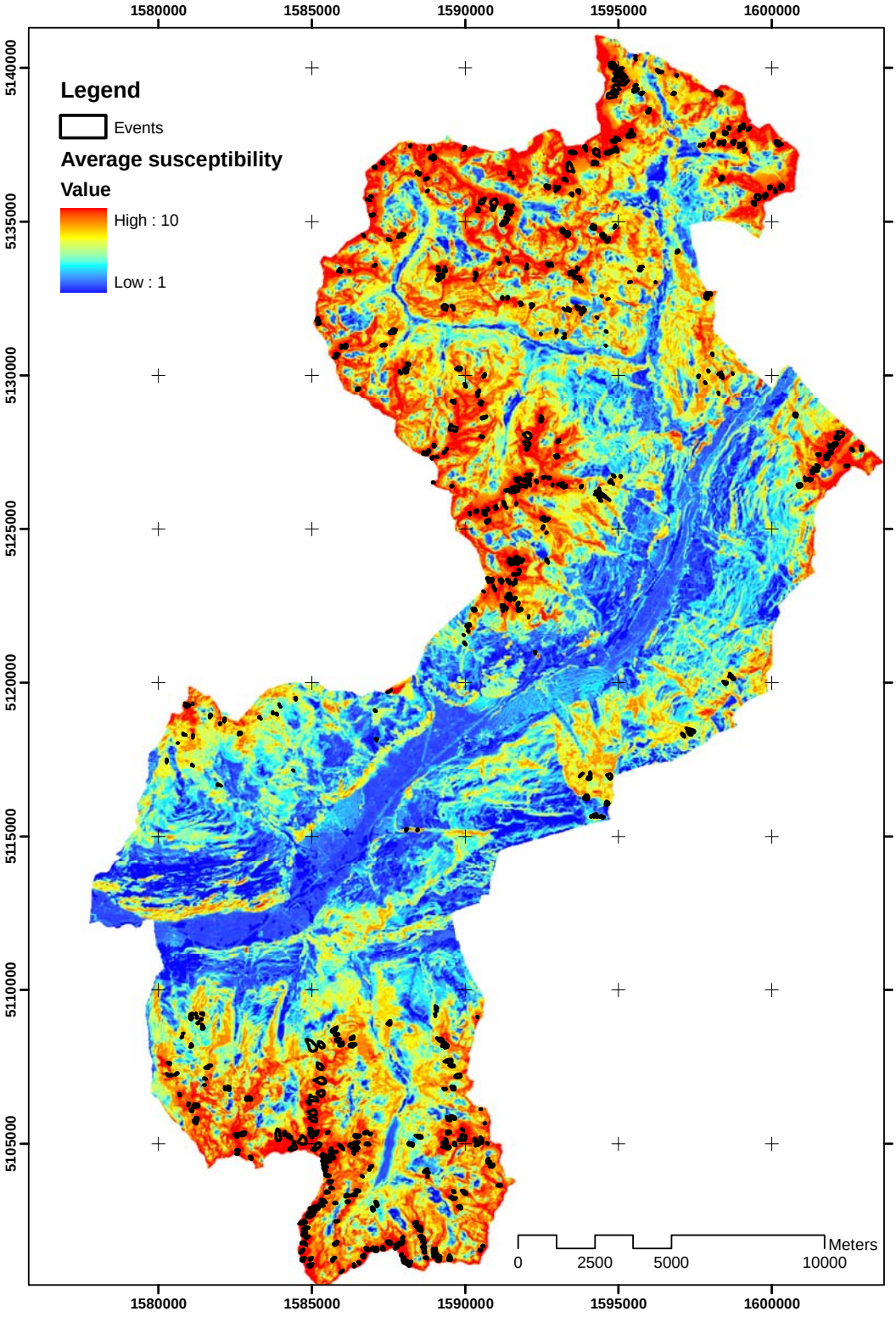

Fig. 7.12 – Map of average value of susceptibility classes. The map was calculated by averaging the rank of each susceptibility class belonging to different maps and sharing the same geographical position. Debris flow scarps of the DF2001 inventory are shown on the map.

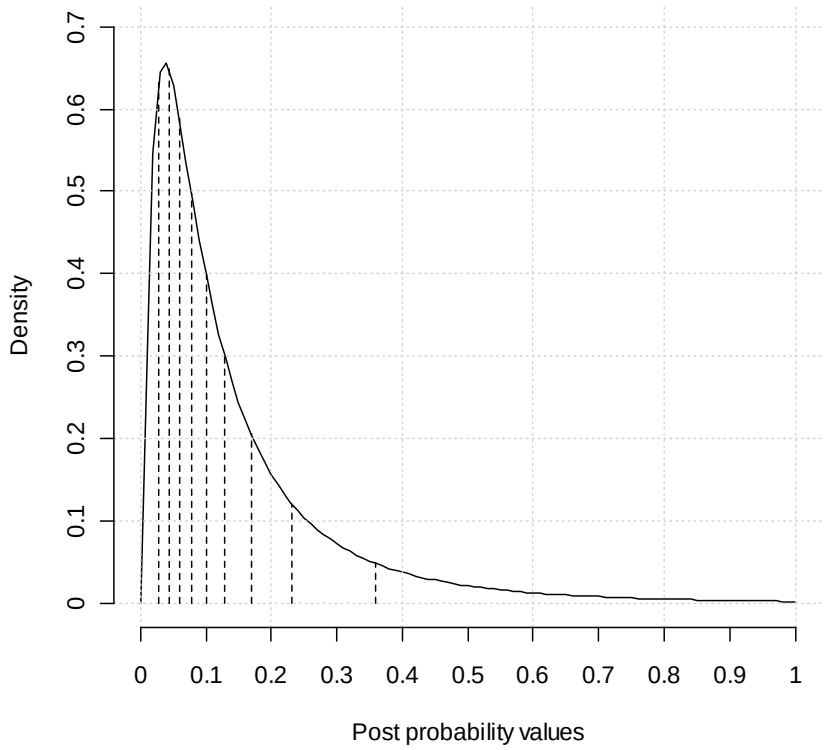

Fig. 7.13 – Theoretical quantiles of the log-normal distribution.

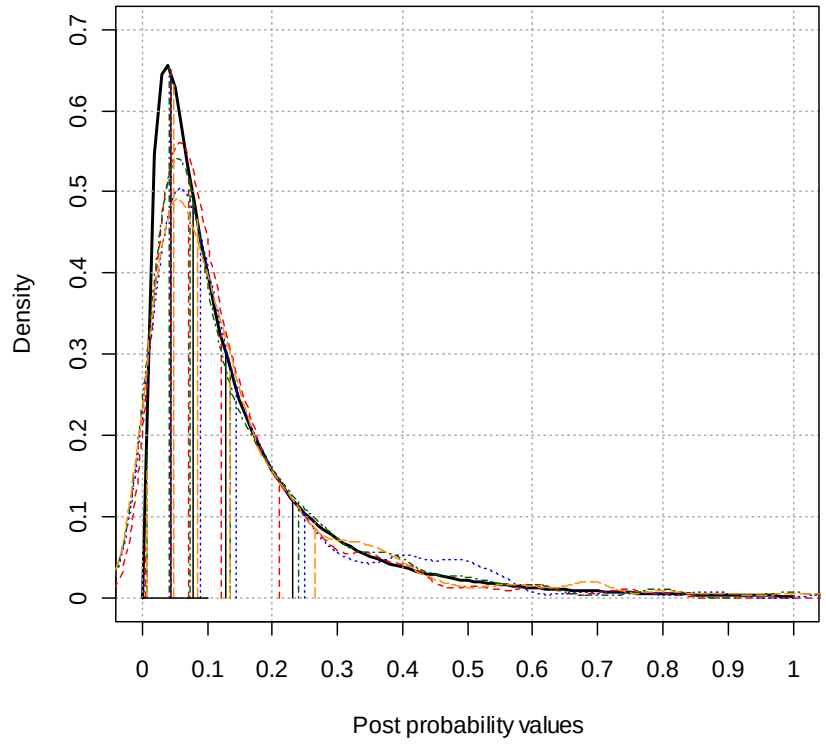

Fig 7.14 – Empirical log-normal distribution and different cut-off values derived from empirical quantiles.

7.4 Concluding remarks

Classified thematic maps are produced for a wide variety of purposes; however, these maps are not very useful without quantitative statements about their accuracy. Map producers must evaluate the outcomes of their mapping efforts, and map users must know the accuracy of the maps for their intended uses. Both producers and users may want to compare several maps to decide which the best is or to evaluate how well the maps agree.

In the field of landslide susceptibility mapping, predicted maps are essential tools for spatial planning and contributing to public safety worldwide (Guzzetti et al. 1999; Glade et al. 2005). Nowadays, two of the main problems in landslide susceptibility assessment are (i) how to measure the accuracy of a susceptibility assessment (Guzzetti et al. 2006) and (ii) how to define strategies for an "optimal" combination of multiple landslide susceptibility assessments and their associated terrain zonation (Rossi et al. 2010). For this reason, the predicted susceptibility maps must be carefully analysed and critically reviewed before disseminating the results to support the end-users with the correct selection criteria.

Predictive methods can be based on sophisticated mathematical models operating on complex databases with advanced software and hardware technologies. However, potential users may face some problems of interpretation of the predicted information. Some effective approaches to testing the accuracy of the spatial predictions by cross-validation techniques are now available. However, it is our opinion that when we transpose predicted values from maps to graphs (for the evaluation of the success and predictive rates of each map); we lose the spatial location of those values. Indeed, two susceptibility maps with similar predictive power may not have the same meaning in terms of spatial pattern of predicted results.

To analyse this hypothesis, we fixed the modelling technique, the number of classes within each explanatory variable, the landslide dataset, the classification technique, changing the number and types of explanatory variables in each experiment. As a result, we appreciated that most of the models we implemented produced equally (or, at least, not statistically different) predictions in terms of success/prediction rate curves (excluding the experiment nr. 5), which validated similarities in the predictive maps. However, the spatial distributions of the post-probability values of each map were not as similar. In effect, the application of appropriate statistical techniques (Kappa Statistic, Principal Component Analysis, and Distance Weighted Entropy) called for an important spatial variability of the predicted patterns within the study area. It is for this reason that landslide susceptibility maps should be distributed together with map documents aimed at defining the level of accuracy of the predicted results to provide the end-users with some selection criteria.

The results from this analysis have serious implications of which combination of factor maps to choose, if the results from standard evaluation procedures are very similar but the spatial pattern of these maps is very different. Also the process of the correct reclassification of the factor maps play important role in the susceptibility assessment. The maps calculated using inappropriate selection of factor maps could show results quite far from reality. On the other hand with a good selection of factor maps reliable susceptibility maps could be obtained.

A careful evaluation of automatically obtained susceptibility maps with the real conditions in the study area and other available information is essential. Moreover, cautious selection of relevant factor maps seems to be the most crucial step in the susceptibility assessment on regional scale using statistically based methods.

7.5 References

Aleotti, P., Chowdhury, R. (1999). Landslide hazard assessment: summary review and new perspectives. Bulletin of Engineering Geology and the Environment, 58(1): 21-44.

Beguería, S. (2006).Validation and Evaluation of Predictive Models in Hazard Assessment and Risk Management. Natural Hazards, 37: 315-329.

Chung, C.-J., Fabbri, A.G. (1999): Probabilistic prediction models for landslide hazard mapping. Photogrammetric Engineering and Remote Sensing, 65: 1389-1399.

Chung, C. F., Fabbri, A. G. (2003). Validation of spatial prediction models for landslide hazard mapping. Natural Hazards, 30, 451-472.

Cohen, J. (1960): A coefficient of agreement for nominal scales. Educational and Psychological Measurement, 20(1): 37-46.

GeoIFFI (2006.): The Regional Inventory (1:10 000) of Landslides and Hydrogeological Events, Lombardy Region, Italy. Within IFFI Project (1997) – Italian Landslides Inventory, National Geological Survey, Rome, Italy. Available at: http://www.cartografia.regione.lombardia.it/GeoIFFI

Glade, T., Anderson, M., Crozier, M. J. (Eds.) (2005): Landslide hazard and risk. John Wiley and Sons, 803 pp.

Guzzetti, F., Carrara, A., Cardinali, M., Reichenbach, P. (1999). Landslide hazard evaluation: a review of current techniques and their application in a multi-scale study, Central Italy, Geomorphology, 31, 181-216.

Guzzetti, F., Reichenbach, P., Ardizzone, F., Cardinali, M., Galli, M. (2006): Estimating the quality of landslide susceptibility models. Geomorphology, 81: 166-184.

Landis, J.R., Koch, G.G. (1977): The measurement of observer agreement for categorical data. Biometrics, 33: 159-174.

Pearson, K. (1901): On lines and planes of closest fit to systems of points in space. Philosophical Magazine, 2(6): 559-572.

Rossi, M., Guzzetti, F., Reichenbach, P., Mondini, A.C., Peruccacci, S. (2010): Optimal landslide susceptibility zonation based on multiple forecasts. Geomorphology, 114: 129-142.

Rossiter, D.G. (2004): Statistical methods for accuracy assesment of classified thematic maps. Technical Note, International Institute for Geo-information Science & Earth Observation (ITC), Enschede, 46 p.

Shaw, P.J.A. (2003): Multivariate statistics for the Environmental Sciences. Hodder Arnold, London, 233 p.

Sim, J., Wright, C.C. (2005): The Kappa statistic in reliability studies: Use, interpretation, and sample size requirements. Physical Therapy, 85(3): 257-268.

Chapter 8

Hazard analysis

There are many good reasons
not to avoid hazards.

Based on:

Blahut, J., Horton, P., Sterlacchini, S., Jaboyedoff, M. (2010): Debris flow hazard modelling on medium scale: Valtellina di Tirano, Italy. Natural Hazards and Earth System Sciences (submitted, under review).

8.1 Introduction

In landslide studies, hazard is usually defined as a likelihood of occurrence of potential damaging phenomena (Crozier and Glade 2005). From its definition, hazard analysis deals with identification of the probability of occurrence of a damaging phenomenon within given period of time (Varnes 1984). The combination of landslide initiation zones with temporal and spatial probability, and runout zones results in a landslide hazard map (van Westen et al. 2005).

Spatial probability of landslides is the likelihood of the occurrence of a landslide in a given location or terrain unit (Chung and Fabbri 1999). An medium scale (1:25,000 – 1:50,000), within GIS environment, the spatial probability estimation is usually performed within the landslide susceptibility analysis. This requires the comparison of landslides that happened in the past with a set of environmental factors, in order to predict areas of landslide initiation that have similar conditions, using heuristic or statistical methods (van Westen et al. 2005).

Temporal probability analysis (landslide frequency) can be divided into absolute, relative or indirect frequency estimation (Corominas and Moya 2008). Absolute frequency is directly measured and expressed as number of events per time on individual slope. On the other hand, relative frequency is the sum of multiple occurrences and might be expressed as number of events per area, per time. Indirect frequency estimation can be obtained e.g. from estimation of accumulated material per time (deposition rate) or by dendrochronological records on trees situated on fans. As already stated by Corominas and Moya (2008), for an analysis on medium scale (1:25,000 – 1:50,000), relative frequency is a good descriptor as it assesses multiple occurrences of regionally distributed landslide events.

In this study, a map of hazard initiation probability of debris flows was firstly made in order to calculate probabilities of debris flow initiation. To make a hazard map, the calculation of runout zones had to be incorporated. For this medium scale study, a model developed at the University of Lausanne (DFGridProb) was used. Unlike other models simulating flow on the DEM (e.g. TauDEM, Guinau et al. 2007), DFGrid Prob takes the advantage of multiple flow direction calculation for debris flow spreading.

For landslide hazard analysis, large amount of data and information is usually needed. However, at medium scale hazard mapping, acquisition of geological factors such as rock composition, structure, texture, degree of weathering, or bedding/foliation, which affects the debris flow occurrence, is very costly (Cararra et al. 1994). The model used in this analysis allowed fast customization and calculation of results with limited input information. Basically, only DEM was needed to perform basic runout calculation. However, this basic calculation was improved by including information about geology, landuse, and hazard initiation probability. As this study is focused on medium scale analysis, the volume of debris flow was neglected taking into account the maximum probable runout of debris flows (see section 8.2.4) from particular hazard initiation class. Result of this study is a debris flow hazard map prepared at medium scale with GIS techniques.

8.2 Materials and methods

8.2.1 Data

For the construction of the hazard map following data was used:

- Digital elevation model (DEM) of a 10 meter resolution, obtained from a 5 meter DEM derived for the study area in 2001 using photogrammetry techniques. The model resolution was decreased in order to reduce the computation time and keep the same resolution of the inputs.
- Landuse map, derived from the 1:10,000 scale map of the DUSAF Project (2003), made by Lombardy Region using orthophotos from the year 2001. The map contains 23 classes of which the largest ones are coniferous trees and scarce vegetation.
- Geological map, rasterized from 1:10,000 scale geological map of Lombardy Region from the CARG Project (1992). The map contains 51 classes of lithological units mapped directly in the field and by photo interpretation. Morainic deposits and gneiss rocks represent the most frequent classes.
- Debris flow susceptibility map calculated by statistical-probabilistic technique Weight-of Evidence (Chapter 6) with five susceptibility classes and at 10 meter resolution.
- Two sets of aerial photographs from 2001 (IT2000) and 1981 (TEM1). These sets were used to create two debris flow inventories, which were consequently compared in order to calculate differences in temporal occurrence of debris flow initiation.

8.2.2 Spatial probability of initiation

The delimitation of spatial probability of occurrence of debris flows is based on debris flow susceptibility map calculated by bi-variate statistical technique (Weights-of-Evidence, Chapter 6). In this map, five susceptibility classes were calculated (very high, high, medium, low, and very low) using success rate curves (Chung and Fabbri 1999). According to the percentage of debris flow scarps that falls into particular susceptibility class, breakpoints were put at 75%, 85%, 95%; and 99% of landslide scarps. The extent of the very high susceptibility class is 14.52% of the study area, high class occupies 6.63%, medium susceptibility class covers 16.20%, and the low susceptibility class represents 9.66%. The remaining 52.99% of the study area belongs to the very low or non susceptible class.

Afterwards, a calculation of spatial probability of debris flow scarp occurrence was made using the following equation:

$$P_S = \frac{N_{DFpixScls}}{N_{pixScls}} \tag{8.1}$$

Where: P_S = spatial probability of debris flow occurrence; $N_{DFpixScls}$ = number of debris flow scarp pixels in particular susceptibility class; $N_{pixScls}$ = number of pixels of the particular susceptibility class.

8.2.3 Temporal probability estimation

In relative temporal probability analysis, the frequency is assessed at each land unit (pixel, polygon, or basin) and expressed in relative terms as the number of landslides per unit area (km^2, pixel, etc.) per year (Corominas and Moya 2008). In this study, this definition was slightly modified due to the data availability, as this work is related to susceptibility class based hazard analysis in a raster format. The temporal probability is thus defined as the area of new debris flow scarps in each susceptibility class per year.

To perform this analysis, two sets of aerial photographs and related debris flow inventories were compared. A debris flow inventory DF1981 from the aerial photographs taken in 1981 (flight TEM1) was compared to the inventory DF2001 made from ortho-photographs taken in 2001 (flight IT2000). Photographs from 1981 (flight TEM1) were scanned and ortorectified within ILWIS software (ITC 2009). Only those scarp areas where new debris flow activity was observed between these two periods were taken into calculation (Fig. 8.1).

Consequently, debris flow scarps where new activity was observed, during the 20-year-period between the photographs, were compared with the five classes of the susceptibility map, obtaining the temporal probability. The equation to obtain the temporal probability of initiation is:

$$P_T = \frac{\frac{N_{NEWDFpixScls}}{N_{pixScls}}}{T} \tag{8.2}$$

Where: P_T = temporal probability of debris flow occurrence; $N_{NEWDFpixScls}$ = area of new debris flow scarp (in pixels) in particular susceptibility class which appeared within a time period; $N_{PixScls}$ = area (in pixels) of the corresponding susceptibility class; T = time period.

For obtaining a map of hazard initiation probability of debris flows, the information from the susceptibility map and temporal probability were combined using the following equation:

$$P_{HI} = P_S \times P_T \tag{8.3}$$

Where: P_{HI} = hazard initiation probability of debris flow; P_S = spatial probability of occurrence; P_T = temporal probability of occurrence.

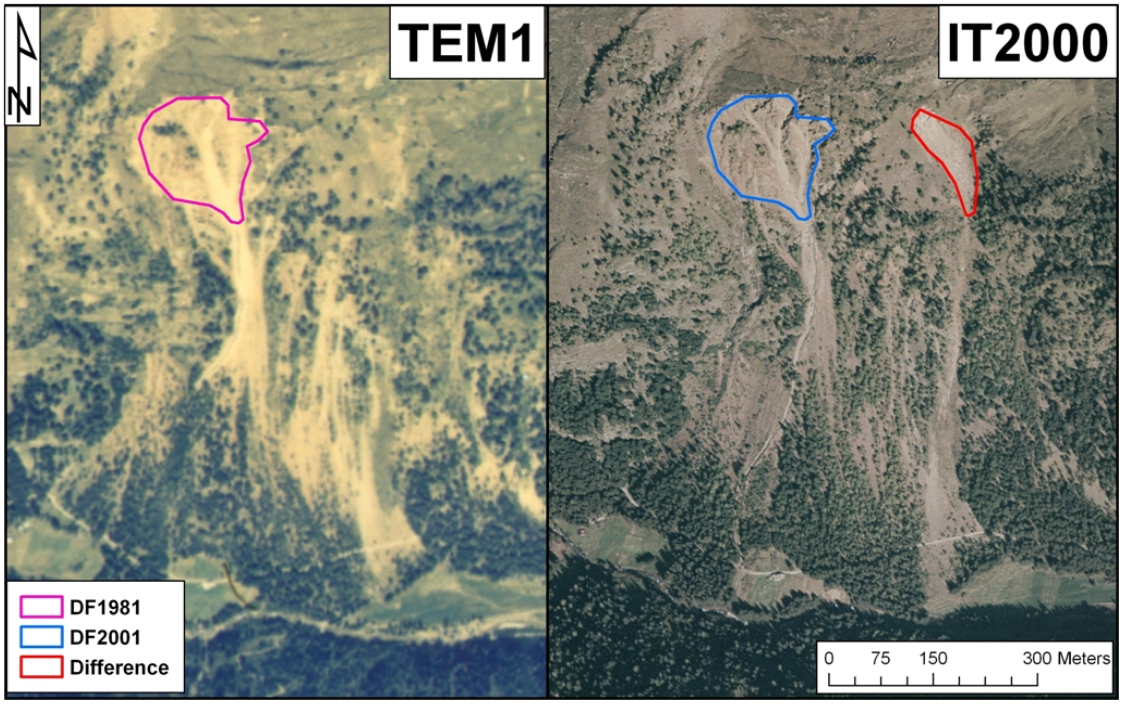

Fig. 8.1 – Example showing differences between DF1981 and DF2001 inventories, allowing to calculate the temporal probability (frequency) of debris flow initiation. On the left is the orthorectified aerial photograph from 1981 (flight TEM1), on the right is the orthophoto from 2001 (flight IT2000).

8.2.4 Runout modelling

In most debris flow hazard studies on medium scale, the runout modelling still remains the biggest problem. In this study, a regional debris flow runout model (DFGridProb), developed at the University of Lausanne was used. Because the model itself was already described in detail by Horton et al. (2008), only brief explanation is done here.

Model is composed of two main parts: 1) identification of debris flow sources, and 2) modelling of debris flow runout. Both, the sources identification and the runout area modelling, are based on a regular DEM with a resolution of 10 meters.

Identification of sources

The sources are identified through different morphological, hydrological, and geological, criteria. Also landuse information or predefined sources can be incorporated into the model in order to identify the potential source areas. According to Rickenmann and Zimmermann (1993) and Takahashi (1981), three criteria in a critical combination are relevant for a debris flow initiation: sediment availability, slope gradient, and water input. Moreover, other criteria such as landuse map, planar curvature map, and hazard initiation map were incorporated to the detection of potential sources of debris flows.

For each described criterion, a grid was generated containing three possible values for each cell: possible source – excluded pixel – ignored pixel. In combining the grids established for the different criteria, a pixel is selected as a source area if it was at least once identified as a possible source but never classified as excluded. Ignored pixels were not taken into account in

the analysis as all possible sources were considered, excluding pixels of those thematic layer classes (geology and landuse), where no debris flow activity was observed in the past.

The sediment availability was linked to the geology, as some geological units produce more or less debris according to their weathering characteristics. The geological units prone to debris flow initiation were selected on expert evaluation, with consideration of debris flow prone areas only those classes where debris flows occurred in the past according to the available inventories.

The slope angle is a major criterion as it is determining factor in triggering a debris flow (Takahashi 1981). Most debris flows occur in areas with a slope higher than 15° (Rickenmann and Zimmermann 1993, Takahashi 1981). As a consequence, all areas with slope higher than 15° were considered as potential sources.

The upslope contributing area was taken into account as a characteristic of water input; a minimum contributing area of 1 hectare was defined. The initiation threshold of slope angle and contributing area was expressed by an empirical equation based on observations from 1987 of Rickenmann and Zimmermann (1993) and Heinimann (1998, Fig. 8.2). For our study an "extreme fitting" curve was selected, as it is covering more possibilities for debris flow initiation.

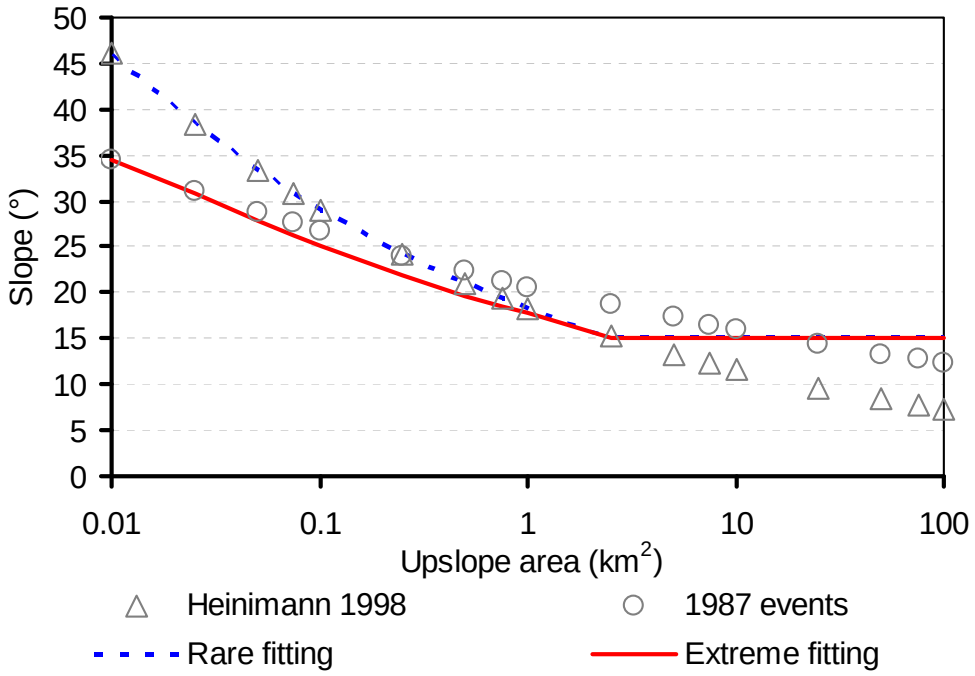

Fig. 8.2 – Curves showing the initiation threshold of debris flows considering the slope angle and the upslope contributing area. In the analysis the extreme fitting curve was used. After Horton et al. (2008).

Planar curvature map (detection of gullies) and the landuse map were added to increase the detection quality of debris flow source areas. In the planar curvature map only areas with curvature lower than -2/100 m^{-1} on a 10 m DEM were considered as possible sources. This observation fits best the occurrence of debris flow initiation areas in Alpine regions, such as Swiss Alps (Horton et al. 2008) or Valtellina. The landuse map classes were selected in the same way as geological classes, considering only pixels of those classes which correspond to

observed debris flow sources. The land use and geological classes with observed debris flow activity are summarized in table 8.1.

Land use class		Geological class	
Bare land	65.5%	Gneiss	40.3%
Vegetation on rocks	17.9%	Micaschists	20.1%
Shrubs and bushes	8.5%	Colluvial sediments	17.9%
Forests	7.2%	Moraine deposits	8.0%
Pastures	0.9%	Sedimentary rocks	7.2%
		Intrusive rocks	3.6%
		Other rock units	2.8%

Table 8.1 – Land use and geological classes with percentage of observed debris flow occurrence in the DF2001 inventory.

To incorporate the results of precedent susceptibility and temporal probability analysis, a map of hazard initiation probability was included for the detection of sources. Each hazard initiation class was used to obtain different debris flow source maps, with corresponding probabilities of initiation. This approach lead to calculation of five different debris flow source maps which were subsequently used as an input in the runout calculation.

Runout and spreading assessment

The debris flow runout and spreading can be mathematically estimated by two types of algorithms: the former are called flow direction algorithms and rule the path that the debris flow will follow; the latter determine the runout distance (Horton et al. 2008). The spreading area assessment selects each source area, and spreads it on the DEM which is the only data needed to perform the calculation of the runout.

Flow direction algorithms rule the direction of the flow from one cell to its eight neighbours. For our purposes, a multiple flow direction algorithm, firstly introduced by Quinn et al. (1991), was used as it best fits to the real situation observed in the study area. For controlling the angle of spreading, Holmgren (1994) introduced an exponent in the algorithm which controls the convergence of the flow (the higher is the exponent, the more convergent the flow becomes). According to Claessens et al. (2005) and Horton et al. (2008), the optimal values of Holmgren exponent for debris flow spreading are between 4 and 6 (8.4).

$$f_{si} = \frac{(\tan \beta_i)^x}{\sum_{j=1}^{8} (\tan \beta_i)^x} \tag{8.4}$$

Where i, j = flow directions (1...8), f_{si} = flow proportion (0...1) in direction i, $tan\beta_i$ = slope gradient between the central cell and the cell in direction i, and x = variable exponent.

A weighting of the directions is included to take into account the persistence of the debris flow, representing its inertia. Based on Gamma (2000), the weight is a function of the change in angle from the last flow direction:

$$\begin{cases} f_{pi} = w_0 \Leftrightarrow a_i = 0° \\ f_{pi} = w_{45} \Leftrightarrow a_i = 45° \\ f_{pi} = w_{90} \Leftrightarrow a_i = 90° \\ f_{pi} = w_{135} \Leftrightarrow a_i = 135° \\ f_{pi} = 0 \Leftrightarrow a_i = 180° \end{cases} \quad (8.5)$$

Where i = flow directions (1...8), f_{pi} = flow proportion (0...1) in direction i, α_i = angle between the previous direction and the direction from the central cell to cell i, $w_{0, 45, 90, 135}$ = weights for the corresponding change in direction.

Resulting probabilities are combination of the multiple flow direction algorithm and persistence:

$$f_i = \frac{f_{si} \times f_{pi}}{\sum_{j=1}^{8} f_{sj} \times f_{pj}} \times f_0 \quad (8.6)$$

Where i, j = flow directions (1...8), f_i = total flow proportion (0...1) in direction i, f_{si} = flow proportion from the slope-related algorithm, f_{pi} = flow proportion from the persistence, f_0 = previously determined flow proportion of the central cell.

This calculation allows including each cell having a minimal probability of being in debris flow path. For the spreading assessment of a source cell, the calculation thus integrates different paths or divergences in one run. There is no need of random multiple runs as the field of all probabilities is covered (Horton et al. 2008).

The outputs from the modelling are expressed in terms of probabilities calculated as functions of slope and persistence, which represents a weighting of the directions according to the previous direction. This allows an integration of the notion of inertia (Horton et al. 2008). On alluvial and debris fans, debris flows tend to easily change direction, after leaving the principal erosion gully, which rules the flow on steeper parts of the terrain. On lower slope gradients, the change of the flow direction is represented by probability function. However, this function is not a mathematical probability in a strict sense and resulting probabilities have to be interpreted in qualitative way (Huggel et al. 2003).

Runout distance algorithms are basic energy-based calculations that define if a part of the debris flow can potentially reach another cell. Thus, they control the distance reached by the debris flow and, in addition, reduce the divergence. In that way, the energy-based algorithms also influence the flow direction, as each cell that cannot be reached has a probability set to zero. In a regional runout model, the source mass is unknown. Thus, runout distance calculation is based on a unit energy balance (8.7), a constant loss function and a maximum threshold. This approach does not aim to represent exactly the physical processes, but to remain realistic.

$$E_{kin}^{i} = E_{kin}^{i-1} + \Delta E_{pot}^{i} - E_{loss}^{i} \quad (8.7)$$

Where i = time step, E_{kin} = kinetic energy, ΔE_{pot} = change in potential energy and E_{loss} = constant loss.

The probable maximum runout is characterized by an average slope angle (Huggel et al. 2002) or shadow angle (Michael-Leiba et al. 2003) which is the average slope between the starting and end point, following the debris flow path. A constant friction loss has been considered, corresponding to that angle, which would result in a runout distance equal to the probable maximum runout. The maximum threshold aims to limit the debris flow energy to reasonable values and corresponds to maximum velocities of debris flow observed in the study area.

8.3 Results and discussion

8.3.1 Debris flow hazard initiation map

For the debris flow hazard initiation map, a susceptibility map of five classes (from very high to very low susceptibility) was used. For each susceptibility class, a spatial and temporal probability was calculated resulting in hazard initiation probabilities (Table 8.2), whose spatial distribution is shown in figure 8.3.

Hazard initiation class	Area in cells	Area in %	New debris flow pixels	Spatial probability	Temporal probability x 10^{-2}	Initiation probability x 10^{-4}
VH	655676	14.52	5814	0.0507	0.0443	0.224783
H	299317	6.63	1384	0.0146	0.0231	0.033754
M	731296	16.20	1628	0.0058	0.0111	0.006456
L	436310	9.66	699	0.0029	0.0080	0.002323
VL	2392818	52.99	505	0.0004	0.0011	0.000042
TOTAL	4515417	100.00	10030	0.0097	0.0111	0.010773

Table 8.2 – Calculated values of the debris flow hazard initiation map. VH – very high, H – high, M – medium, L – low, VL – very low.

There are many difficulties and uncertainties connected with preparation of a debris flow hazard initiation map. Probably the most important uncertainty arises from the temporal probability analysis. As only two temporal slices are compared, many debris flows source areas could be missed or not recognized. A debris flow pattern which could occur immediately after taking an aerial photograph in 1981 could be overlaid by another more recent debris flow or its patterns may not be clearly visible after 20 years. This problem can be over passed by comparing photosets taken with higher frequency and by longer temporal coverage (e.g. 5 photosets in 50 years). As a consequence, less debris flows would be missed and lower error will be connected to the temporal probability. However, no other temporal aerial photosets were available at the time of this analysis, so these errors had to be assumed.

The resulting debris flow hazard initiation map was consequently used as an input for the DFGridProb model together with the parameters described in section 8.2.4.

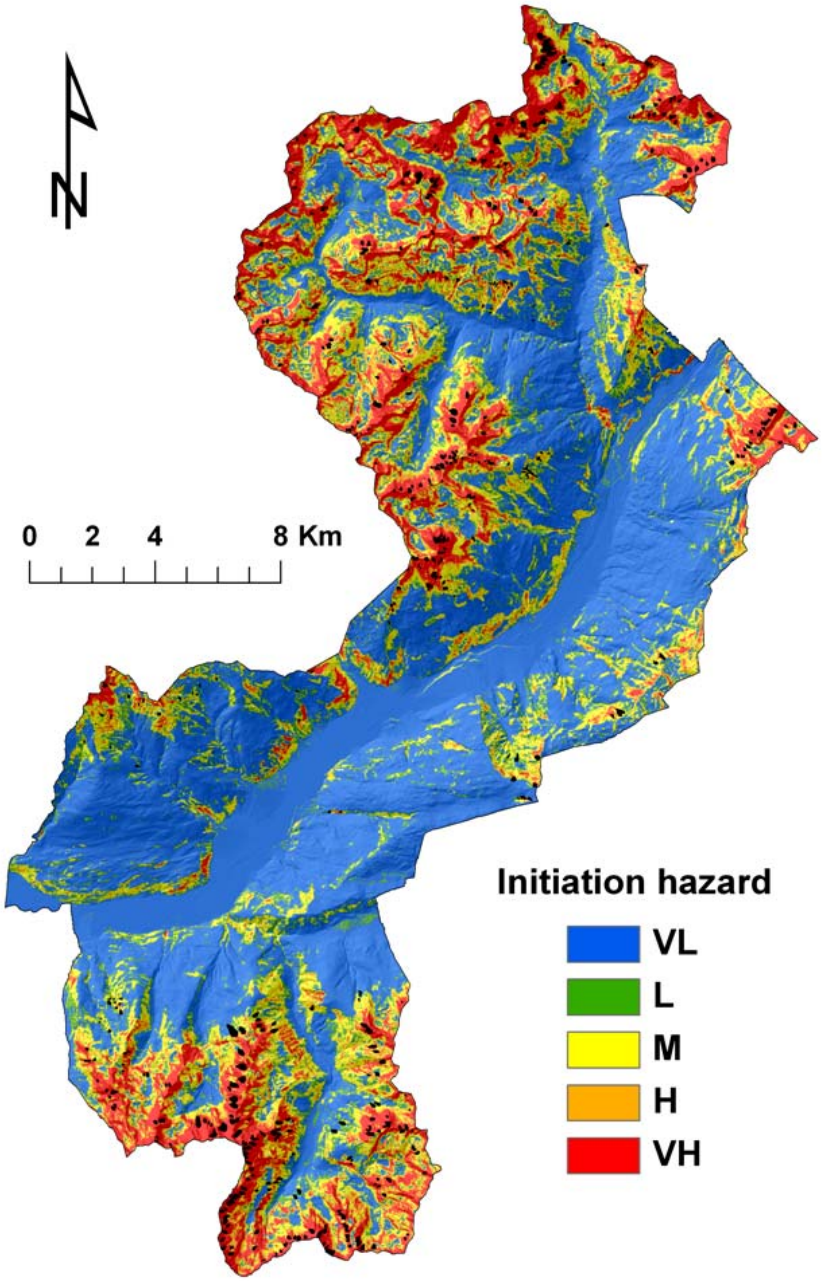

Fig. 8.3 – Debris flow hazard initiation map. VL – very low hazard of initiation; L – low hazard of initiation; M – medium hazard of initiation; H – high hazard of initiation; VH – very high hazard of initiation. Debris flow scarps from the DF2001 inventory are superimposed as black dots.

8.3.2 Runout calibration and calculation

To calibrate the maximum probable runout of debris flows, a well delimited large event from 19th July 1987 from Tiolo (Grosio municipality) was used. Unfortunately, no other well delimited debris flows were available for the entire study area; as a consequence, aerial photographs from 2001 were used to calibrate the possible maximum runout using the edge of alluvial fans where former debris flow activity has been observed (Fig. 8.4, 8.5).

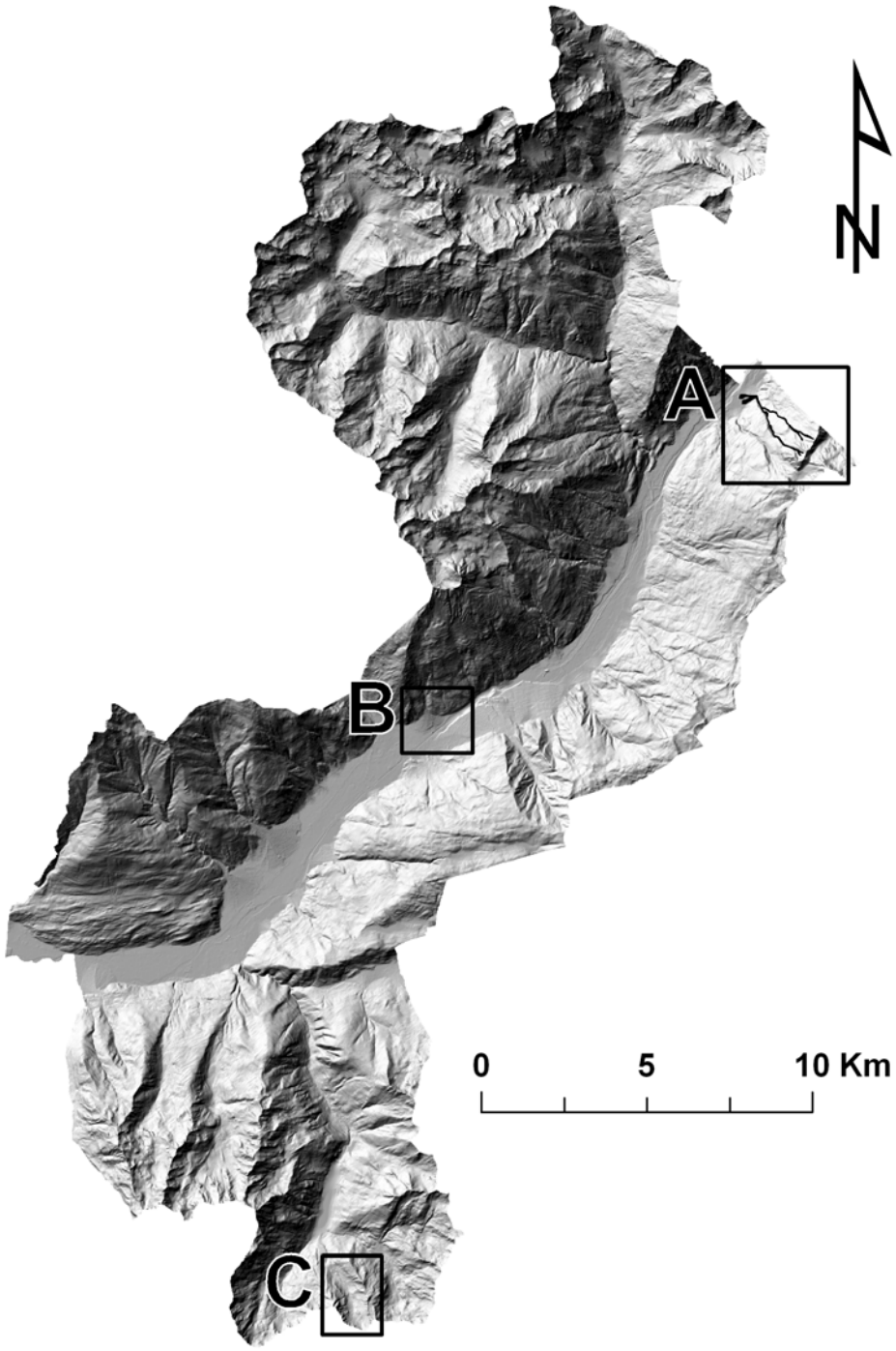

Fig. 8.4 – Hillshade map of the study area, showing the location of the debris flows presented on Figure 8.5 (A, B, C).

From the calibration phase, the following runout characteristics were selected: maximum runout (shadow) angle of 10°; maximum limit velocity of debris flow of 15 m/s; and Holmgren exponent of 5.

Afterwards, a runout map was calculated for the four highest debris flow hazard initiation classes resulting in hazard map A (Fig. 8.6). The final extent of calculated debris flow paths represents the maximum probable extent not taking into account the volume of the debris mobilised.

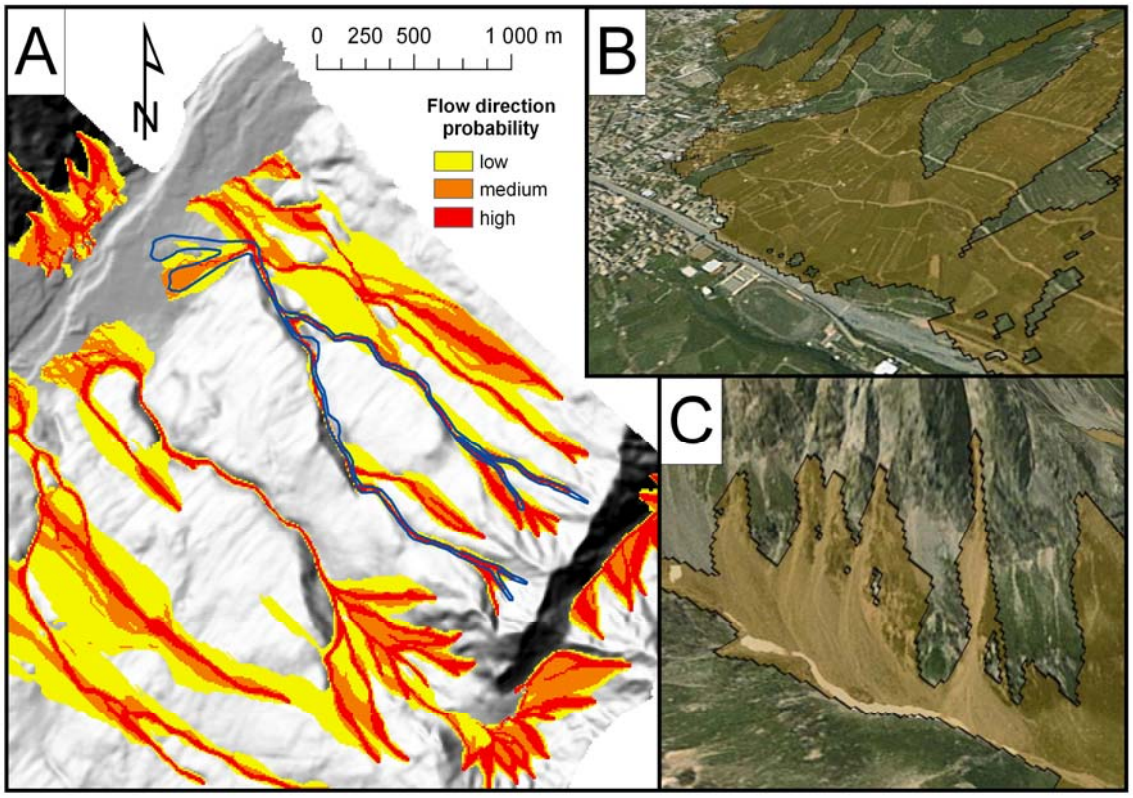

Fig. 8.5 – Examples showing the runout model calibration. A – debris flow from 1987 in Tiolo (Grosio municipality, delimitation after official database GeoIFFI 2006); B – 3D view of alluvial fan near Tirano (visualised in Google Earth); C – 3D view of debris flows in the southern part of the study area (visualised in Google Earth). The location of the examples is shown on figure 8.4.

Main drawback of an analysis on medium scale is that magnitude of particular debris flow remains impossible to calculate. To overpass this problem and to better discriminate the possible different magnitudes (volumes) of debris flows, a qualitative component was added to the hazard map. A reclassification of calculated spreading probabilities was made for four hazard classes (very high, high, medium, low), using geometric interval classification (Fig. 8.7). Three subclasses of spreading direction probabilities were made in order to have better idea about different runout of debris flows of different magnitudes. As it was already stated, these spreading direction probabilities are not probabilities in a strict mathematic sense and they should be interpreted only in a qualitative way. This approach resulted in creation of hazard map B. In this map 13 classes of hazard are present (3 for very high, high, medium, and low hazard classes and 1 for very low hazard class). Higher probabilities of spreading/flow of debris flows are represented by more vivid colours of each class.

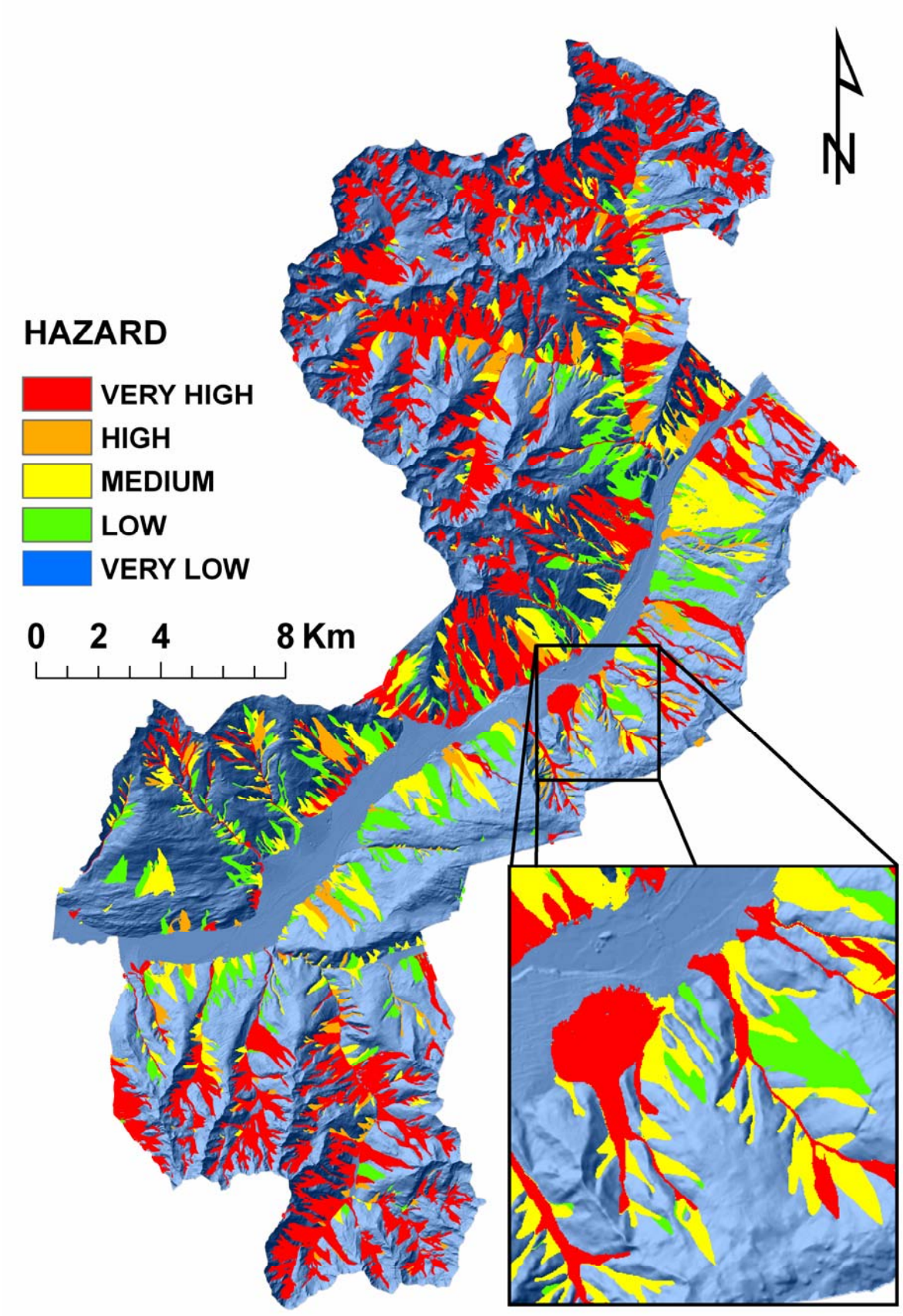

Fig. 8.6 – Final debris flow hazard map A with five hazard classes.

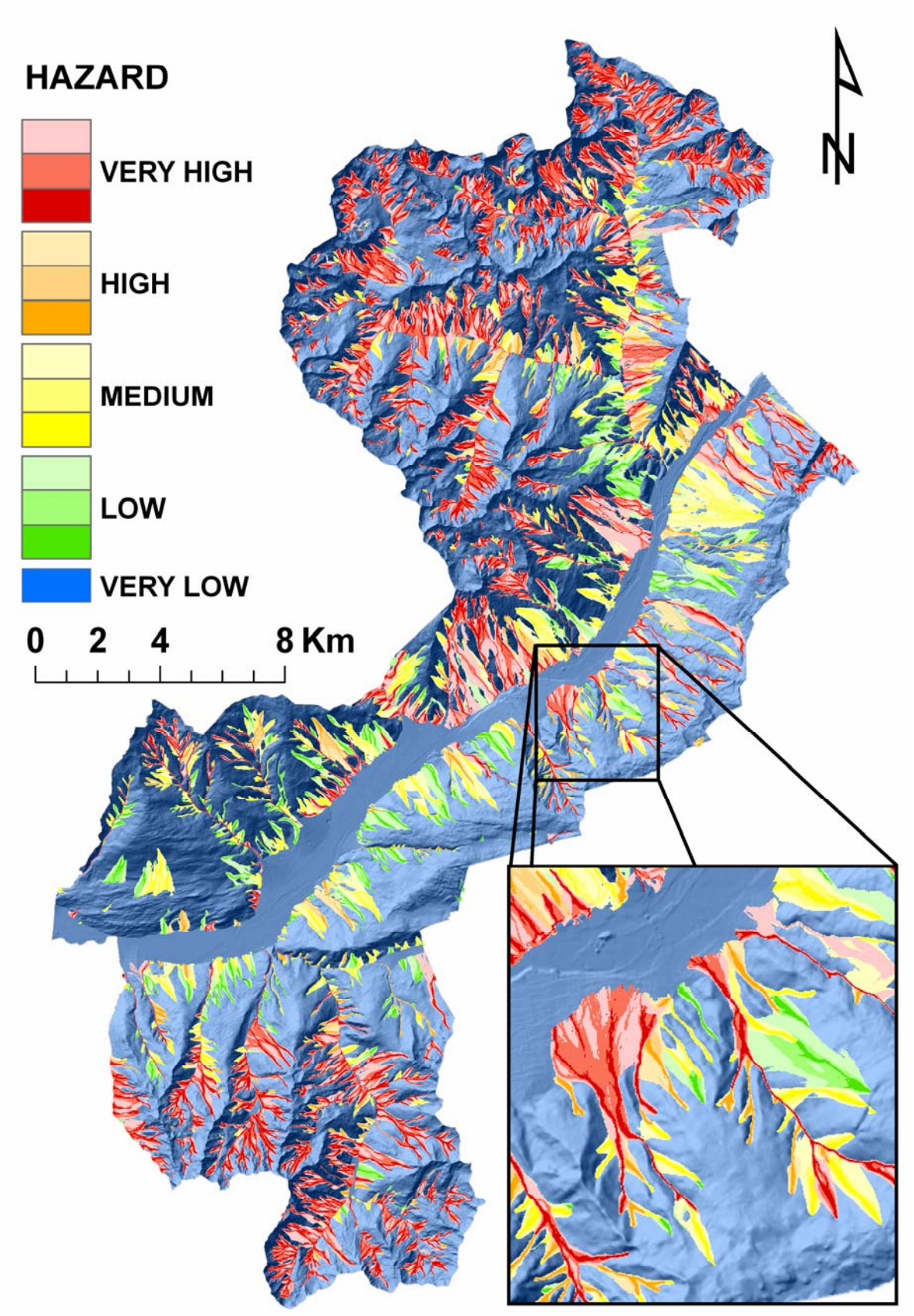

Fig. 8.7 – Debris flow hazard map B incorporating qualitative information about runout spreading probabilities. Map is classified into 5 hazard classes, each one having three subclasses showing the spreading direction probabilities.

8.4 Conclusions

The study shows that the model DFGridProb, coupled with a debris flow hazard initiation map, allows transparent and fast calculation of a debris flow hazard map. Easy customization and choice of parameters for fast production of debris flow runout maps is the main advantage of applied methodology. The energy-based algorithm in run out calculation has a physical basis and only a minimum of data is required, as the DEM and debris flow hazard initiation map is the basis of all calculations (source area identification and runout assessment).

Although the presented approach allows preparation of a hazard map on medium scale, the problem of local controlling factors has to be mentioned. Unlikely, for a study on local/site specific scale, where deterministic modelling and precise calculation of return periods can be performed, on medium scale not enough geotechnical information is available and more assumptions have to be made. Major limitations in the model happen in case of misinterpretation of the reality in the DEM; as a consequence, the spreading areas will contain errors. The multiple flow direction has no physical basis and, as it is regional model, it does not take into account the debris flow volume. However, as it was shown, the magnitude representation can be approximated by reclassification of the spreading direction probabilities.

Automatic delimitation of sources of natural debris flows only from DEM probably overestimates their total number, but fortunately it is possible to improve the results by incorporating the hazard initiation map for source areas identification. The parameters could be extrapolated afterwards for the whole region after calibration, but the problem of local controlling factors still remains. It can be concluded, that using the presented approach, a medium scale hazard map can be calculated for natural debris flows and critical areas can be pinpointed for site-specific numerical analysis, where enough data can be obtained with less resources than for a medium scale analysis. However, for the validation and transferability of the parameters and results to other study areas, more testing is needed.

8.5 References

Cararra, A., Cardinali, M., Guzzeti, F., Reichenbach, P. (1994): GIS technology in mapping landslide hazard. In: Carrara, A., Guzzetti, F. (Eds.): Geographical Information Systems in Assessing Natural Hazards, Kluwer, Amsterdam, pp. 135-175.

CARG Project (1992): The New Italian 1:50 000 Geological Map. National Geological Survey, Rome, Italy.

Chung, Ch.-J., Fabbri, A. (1999): Probabilistic prediction models for landslide hazard mapping, Photogrammetric Engïneerign and Remote Sensing, 65: 1389-1399.

Claessens, L., Heuvelink, G.B.M., Schoorl, J.M., Veldkamp, A. (2005): DEM resolution effects on shallow landslide hazard and soil redistribution modelling. Earth Surface Processes and Landforms, 30: 461-477.

Corominas, J., Moya, J. (2008): A review of assessing landslide frequency for hazard zoning purposes. Engineering Geology, 102: 193-213.

Crozier, M.J., Glade, T. (2005): Landslide Hazard and Risk: Issues, Concepts and Approach. In: Glade, T., Anderson, M., Crozier, M.J. (Eds.): Landslide Hazard and Risk, Wiley & Sons, Chichester, pp. 1-40.

DUSAF Project (2003): Destinazione d'Uso dei Suoli Agricoli e Forestali. Lombardy Region, Milano, Italy.

Gamma, P. (2000): dfwalk-Ein Murgang-Simulationsprogramm zur Gefahrenzonierung. Geographisches Institut der Universität Bern. (unpublished)

GeoIFFI (2006.): The Regional Inventory (1:10 000) of Landslides and Hydrogeological Events, Lombardy Region, Italy. Within IFFI Project (1997) – Italian Landslides Inventory, National Geological Survey, Rome, Italy. Available at: http://www.cartografia.regione.lombardia.it/GeoIFFI

Guinau, M., Vilajosana, I., Vilaplana, J.M. (2007): GIS-based debris flow source and runout susceptibility assessment from DEM data – a case study in NW Nicaragua. Natural Hazards and Earth Sysstem Sciences, 7: 703-716.

Heinimann, H.R. (1998): Methoden zur Analyse und Bewertung von Naturgefahren. Bundesamt für Umwelt, Wald und Landschaft (BUWAL).

Holmgren, P. (1994): Multiple flow direction algorithms for runoff modelling in grid based elevation models: An empirical evaluation. Hydrological Processes, 8: 327-334.

Horton, P., Jaboyedoff, M., Bardou E. (2008): Debris flow susceptibility mapping at a regional scale. Géorisques IV Geohazards: 4e Conférence canadienne sur les géorisques - 4th Canadian Conference on Geohazards, 20-24 May 2008 Québec, Canada.

Huggel, C., Kaab, A., Haeberli, W., Teysseire, P., Paul, F. (2002): Remote sensing based assessment of hazards from glacier lake outbursts: a case study in the Swiss Alps. Canadian Geotechnical Journal, 39: 316-330.

Huggel, C., Kääb, A., Haeberli, W., Krummenacher, B. (2003): Regional-scale GIS-models for assessment of hazards from glacier lake outbursts: evaluation and application in the Swiss Alps. Natural Hazards and Earth System Sciences, 3: 647-662.

ITC (2009): ILWIS - Remote Sensing and GIS software: Integrated Land and Water Information System.
Available at: http://www.itc.nl/Pub/Home/Research/Research_output/ILWIS_-_Remote_Sensing_and_GIS_software.html

Michael-Leiba, M., Baynes, F., Scott, G., Granger, K. (2003): Regional Landslide Risk to the Cairns Community. Natural Hazards, 30: 233-249.

Quinn, P., Beven, K., Chevallier, P., Planchon, O. (1991): The prediction of hillslope flow paths for distributed hydrological modelling using digital terrain models. Hydrological Processes, 5: 59-79.

Rickenmann, D., Zimmermann, M. (1993): The 1987 debris flows in Switzerland: documentation and analysis. Geomorphology, 8: 175-189.

Takahashi, T. (1981): Estimation of potential debris flows and their hazardous zones: Soft countermeasures for a disaster. Natural Disaster Science, 3: 57-89.

van Westen, C.J., van Asch, T.W.J., Soeters, R. (2005): Landslide hazard and risk zonation : why is it still so difficult? Bulletin of Engineering Geology and the Environment, 65: 176-184.

Varnes, D.J. (1984): Landslide hazard zonation: A review of principles and practice. Paris, UNESCO.

Chapter 9

Risk analysis

If you don't risk anything,
you risk even more.

(E. Jong)

Based on:

Blahut, J., Sterlacchini, S. (2010): Risk analysis on medium scale: case of Valtellina di Tirano. Natural Hazards and Earth System Sciences. (under preparation).

9.1 Introduction

Within the integrated risk management, an analysis of risk is the crucial point when information about hazard is overlaid with information about elements at risk. Risk is identified as expected loss in a unit of time or, more generally, as the likelihood of consequences from particular hazard (Crozier and Glade 2005). In landslide risk studies, two approaches are usually applied – quantitative risk assessment (QRA) at large/local scale and qualitative risk assessment at smaller scale. Quantitative risk analysis and consequent assessment uses information about hazard probability, values of elements at risk and their vulnerability. Qualitative risk analysis and assessment use expert based classifications of hazard as well as the elements at risk in order to obtain risk classes. According to Varnes (1984), landslide risk evaluation aims to determine the expected degree of loss due to a landslide (specific risk) and the expected number of lives lost, people injured, damage to property and disruption of economic activity (total risk). In this medium scale study, specific risk is evaluated in a quantitative way and total risk is analysed on a qualitative basis.

Estimation of prospective losses and information about landslide risk can serve as an essential tool for spatial and urban planners, as well for the authorities responsible for civil protection. Quantification of potential losses can serve as a basis for cost-benefit analysis or for allocation of resources needed to deal with disaster consequences. However, according to findings of van Westen (personal communication), a proper landslide QRA at medium scale (1:25,000 to 1:50,000) still seems to be a step to far. Presented analysis tries to bridge this gap by quantifying economic risk from debris flows at a medium scale. In this study, two quantitative economic risk maps were calculated together with corresponding risk curves. Afterwards, a qualitative risk map based on official classification (Lombardy Region 2005) was prepared and the maps were compared to each other.

9.2 Data and methodological approach

In this analysis, economic risk maps were prepared using the basic risk equation:

$$R = H \times V \times E \qquad (9.1)$$

Where R: risk, H: hazard, V: vulnerability, E: value of the elements at risk.

On the other hand, qualitative risk map was prepared by using an official risk matrix (see section 9.2.3). Risk map A and B can be considered as quantitative economic risk maps with different values of vulnerability, while risk map C is a qualitative risk map based on official elements at risk classification. The flowchart of the methodology applied in the risk analysis is shown in Fig. 9.1.

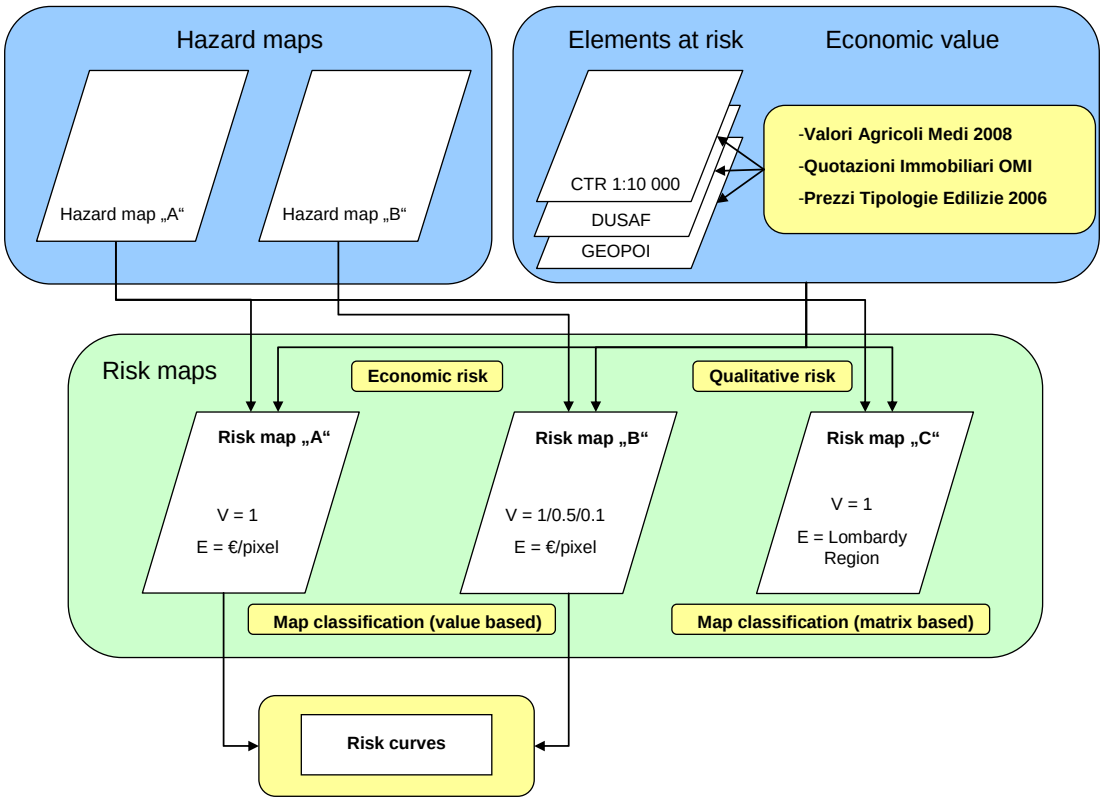

Fig. 9.1 – Flowchart of the risk mapping and analysis methodology.

9.2.1 Data preparation

Information needed for creation of a medium scale risk map consists of two main parts: 1) hazard information and 2) elements at risk information. For the first part of the risk estimation, hazard maps calculated by statistical and empirical models were used (Chapter 8). Hazard map A delimits five debris flow hazard areas with corresponding probabilities. Hazard map B has the same area delimitation of potential debris flows as hazard map A and, moreover, four hazard classes (very high, high, medium, low) have three sub-classes, qualitatively delimiting potential spreading areas according to magnitude and volume of potential debris flows.

Information about elements at risk was acquired according to available data, taking into account the same resolution of inputs. To have most precise information, several datasets were used:

- Land use map from the DUSAF Project (2003) was used to delimit urban and rural areas as well as forests and areas without vegetation.
- Regional database at 1:10,000 scale (CT10 2006) in vector format was used to obtain transport ways (roads and railways) in the study area.
- GEOPOI® polygons (GEOPOI 2009) from Territorial Agency of Lombardy Region were used to obtain more precise delimitation of urban areas with different market values of houses.

Firstly, GEOPOI® polygons (GEOPOI 2009) were imported from the KML format into SHP format and several corrections had to be made to obtain precise delimitation of areas with homogenous prices of real properties matching the areas of municipalities of CM Valtellina di Tirano (Fig. 9.2). Consequently, those polygons were used to subdivide urban areas in the land use map of the DUSAF Project (2003). Afterwards, roads and railways from the database CT10 (mapped at 1:10,000 scale) were divided into two groups: primary and secondary. State roads (Strada Statale – S.S.) number 38 connecting Sondrio with Bormio and number 39 connecting Tirano with Edolo via Aprica Pass were considered as primary roads and all the other roads were considered as secondary. The main two-track railway from Sondrio to Tirano was considered as primary railway and the narrow-track railway from Tirano to St. Moritz via Bernina Pass was considered as secondary railway. Finally, a raster map layer of elements at risk was prepared by joining formerly described layers (Fig. 9.3).

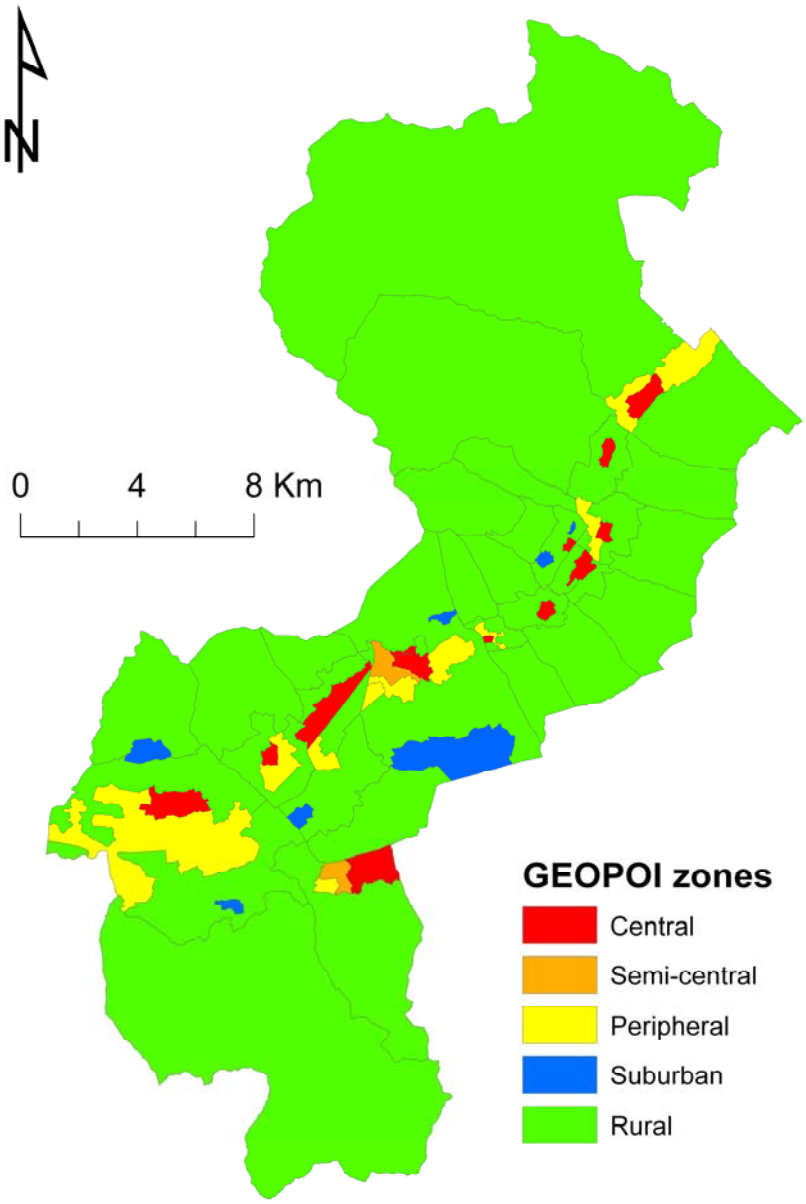

Fig. 9.2 – GEOPOI® polygons of the study site used to delimit areas of different real estate values.

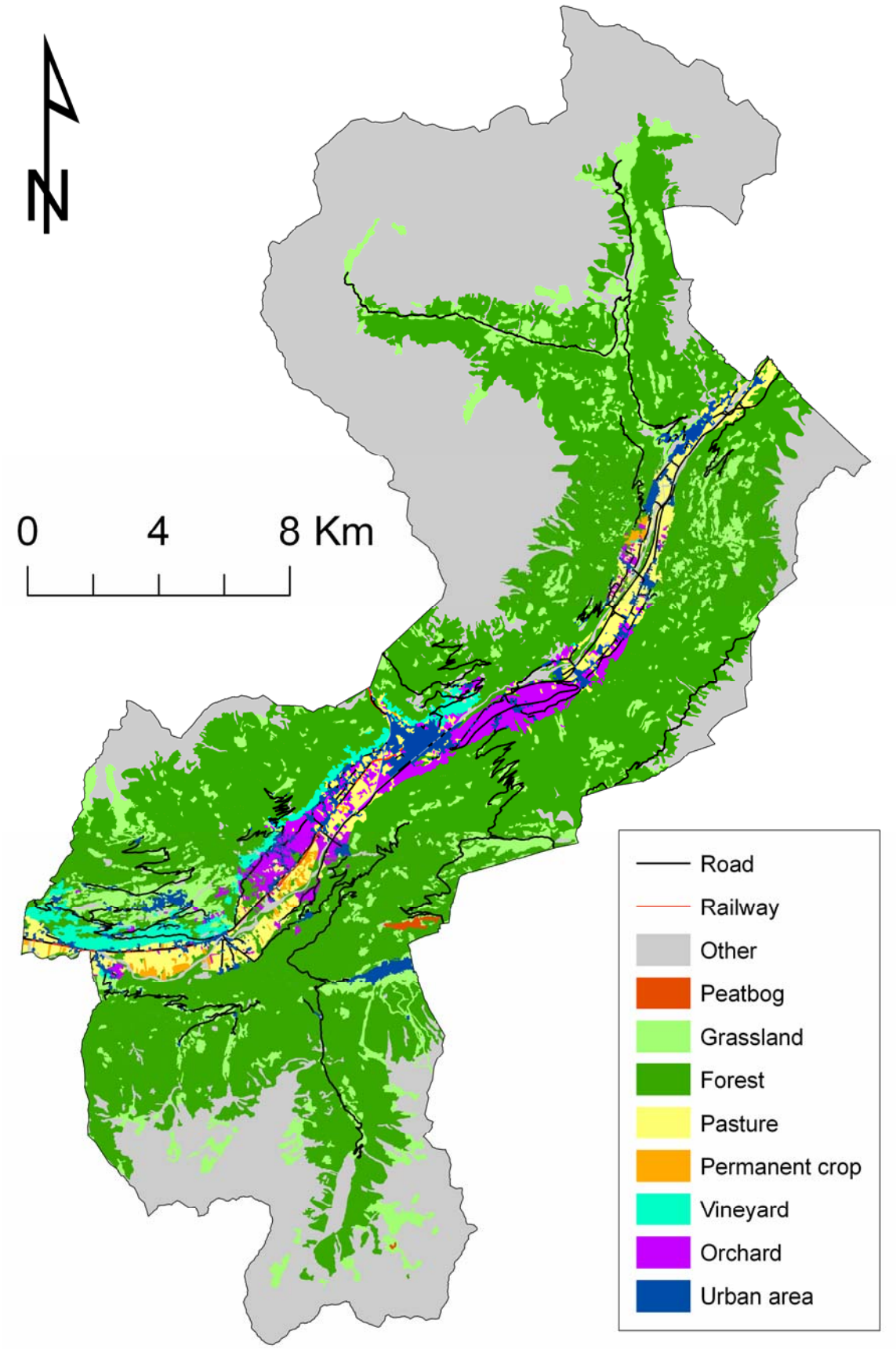

Fig. 9.3 – Elements at risk map derived for the study area. The classes are generalized in order to keep visual readability.

9.2.2 Economic value of elements at risk

To obtain a quantification of economic risk, economic value to the elements at risk had to be assigned. Economic value of assets can be estimated using two main approaches. Reconstruction costs approach or market costs approach can be used to estimate the value of areas and assets in the territory. Both approaches have advantages and disadvantages. Main disadvantage of using reconstruction values is that they are uniformly distributed over the area and particular disparities between economically different zones can not be distinguished. Main advantage of the use of reconstruction values for prospective damage estimation is that these values do not represent subject of speculative changes during time and in the case of an incident (natural disaster). Reconstruction values are also usually used for insurance purposes.

Main disadvantage in the use of market values is that these values are subject of larger changes during time, mostly due to speculative reasons. As a consequence, all risk and loss estimations have to be considered "static" in the sense that they are relevant only for the date of preparation of a map or for the time of an analysis. However, the use of market values to estimate risk and prospective losses has also important advantage. By using market values, areas of higher and medium economic importance can be distinguished from economically marginal areas. For example, a tourist resort will have higher costs of buildings than rural areas, or high quality vineyards producing D.O.C or D.O.C.G. wines will have higher value than low quality vineyards. In both described cases, the reconstruction values will be very similar, while market values will be highly different. In this analysis, market values were preferred as they describe better the actual distribution of economic activities and prices. To each raster class, a monetary value was assigned using available information from several sources:

- Real estate values for the second half of 2008 available from the webpage of the Territorial Agency (Agenzia del Territorio – OMI 2009)
- Values of the agricultural land in Sondrio Province in 2008 (Valori Agricoli Medi 2009).
- Construction costs of roads issued by the Society of Engineers and Architects of Milano (DEI 2006).

Urbanized areas in the land use map (1:10,000) do not delimit well each house or building. As a consequence, it was assumed that houses cover 25% of each urban area polygon of the land use map. This is also in accordance to calculations and comparisons made between the land use map and database DB2000 (2003). DB2000 is a database of assets in the study area, mapped at 1:2,000 scale, and it is originally used by local planners and civil protection authorities. Values of real properties in urbanized areas were estimated from house market values of the second half of 2008, available from the webpage of the Territorial Agency (Agenzia del Territorio – OMI 2009). On this webpage a minimum and maximum prices per m^2 of different types of houses in different GEOPOI® polygons are available. As the working scale (1:25,000 – 1:50,000) and data availability do not permit to fully distinguish between different types and usage of houses (private, public, commercial, etc.), an average value for GEOPOI® polygon for

normal state of private building was calculated. Private buildings form more than 90% of building types in the study area and, according to observations and fieldwork, an average building in the study area consists of two storeys. Consequently, to obtain an average value of urban areas per cell (10×10 m), the average price per m^2 of house was divided by 4 (1/4 of the urban area is covered by houses) and multiplied by 2 (number of storeys in an average house).

Prices per pixel of the non-urban areas were estimated using information about average market values of agricultural land in the Sondrio Province in 2008 (Valori Agricoli Medi 2009). Highest values per hectare are located on apple orchards (90,500 €/ha) and vineyards (59,200 €/ha), while the lowest values represent the forested areas (4,000 €/ha) and grassland/pastures (2,400 €/ha). It has to be noted that low values of forested areas are caused by the system of calculation. In this cost estimation only value of land is considered without taking into account the value of the timber. The estimation of the price of timber is very difficult. However, majority of the forests have protective function and are not considered as market goods, only the value of the land is considered in this analysis.

Public roads do not represent a private property, so only construction costs (and not market values) were estimated per m^2 of primary and secondary roads using information available from the construction costs of roads (DEI 2006). Unfortunately, it was not possible to acquire any information about values or construction costs of railways in the study area, not even for Italy, so no values were assigned to primary and secondary railways in the study area. All the values calculated for the elements at risk are summarized in Table 9.1

There are many elements at risk classes that do not have any specified economic value set by the official resources. However, it has to be noted that many of them have intangible value associated with its environmental importance as natural resource (glaciers, rivers, lakes), or linked with its public importance (junkyards, quarries). These values are hardly definable even to environmental economists (M. Turvani, personal communication). As a consequence, it was decided to use only available official values, which are easily accessible and updateable in further studies.

Element at risk class	2008 value	€/pixel
urban area	640-2375 €/sq.m	32000-118750
primary road	20 €/sq.m	2000
secondary road	15 €/sq.m	1500
railway	N.A.	N.A.
orchard	90500 €/ha	905
vineyard	59200 €/ha	592
permanent crop	50400 €/ha	504
pasture (intensive)	49200 €/ha	492
swamp/peat-bog	7700 €/ha	77
forest (without timber)	4000 €/ha	40
pasture/grassland (high altitudes)	2400 €/ha	24
junkyard	N.A.	N.A.
quarry	N.A.	N.A.
degraded land	N.A.	N.A.
shrubs and bushes	N.A.	N.A.
vegetation on rocks	N.A.	N.A.
scarce vegetation	N.A.	N.A.
glacier	N.A.	N.A.
water	N.A.	N.A.
river	N.A.	N.A.
bare land (sandy)	N.A.	N.A.
bare land	N.A.	N.A.

Table 9.1 – Values of the elements at risk used in the analysis of prospective direct economic damage.

9.2.3 Qualitative classification of elements at risk

Qualitative risk maps are usually prepared using risk matrices, which classify risk areas according to the possible consequences to the elements at risk caused by a natural hazard and by the probability of such hazard. In this analysis, an official qualitative risk matrix used by the Lombardy Region (2005) was applied. In this matrix (Fig. 9.1) five classes of hazard are plotted against four classes of elements at risk. The elements at risk are divided into four groups, considering their strategic importance and severity of possible outcomes in case of being affected by a hazard. Classification of the elements at risk is shown in Table 9.2.

In the highest class, urban areas and public infrastructure are considered. In the E3 class, all primary roads and two-track railways are classified together with junkyards and quarries present in the study area. E2 class comprises all other roads and narrow-track railway. Moreover, valuable agricultural area such as vineyards and orchards are also considered. In the E1 class, all the remaining areas are present.

The qualitative approach adopted from Lombardy Region shows some differences compared to the situation when only economic values are considered. The most important thing is that railways, quarries and junkyards are considered in the second highest class but they do not have a precise economic value in the former part. However, this situation is mostly caused by the impossibility to estimate or evaluate the direct value of these assets from official sources.

	H1	H2	H3	H4	H5
E1	R1	R1	R1	R1	R2
E2	R1	R1	R2	R2	R3
E3	R1	R2	R2	R3	R4
E4	R1	R2	R3	R4	R4

Fig. 9.4 – Official risk matrix used by Lombardy Region (2005). H – hazard level, E – elements at risk level, R – risk level.

Class	Element at risk
E4	urban areas public infrastructure
E3	primary roads and railways quarries and junkyards
E2	secondary roads and railways valuable agricultural areas
E1	other agricultural areas forests and other areas

Table 9.2 – Classification of the elements at risk applied in this study according to the official classification of Lombardy Region (2005).

9.2.4 Preparation of risk maps

Risk map A

As already stated in the beginning of section 9.2, the basic equation was used to prepare risk maps A and B. In case of risk map A, hazard values from hazard map A (Chapter 8) were overlaid by elements at risk with corresponding values (section 9.2.2). Vulnerability was assumed to be 1.0, meaning that an impact of a debris flow will lead to a total loss of the exposed asset. This assumption does not express the realistic situation but it is often applied as definition of vulnerability at medium scale analysis is difficult to perform and no volume/intensity information is available from the hazard map A. Risk map A was calculated by multiplying overlaid maps and reclassification of the resulting map.

Risk map B

In calculation of risk map B an innovative approach was tested by using different vulnerability values which were derived from the hazard map B. In this map three sub-classes of each hazard class served as a proxy to estimate hazard intensity. Afterwards, a simple vulnerability relationship was applied in order to obtain more reliable risk map.

Physical vulnerability displays possible degree of loss using the information of process intensity and characteristics of the elements at risk. The process intensity is usually quantified as height of accumulation (Borter 1999; Fuchs et al. 2007) or in a qualitative way (Fell and Hartford 1997; Bell and Glade 2004). In this medium scale analysis, an assumption was made by delimiting the debris flow runout areas into three classes depending on the probability of debris flow spreading (hazard map B). For each class, a different vulnerability value was assigned considering the fact that vulnerability should be higher in those areas where the debris flow spreads with higher probability, having also at the same time higher intensity in terms of velocity and height of accumulation. As a consequence, vulnerability was directly linked with the debris flow spreading probability.

After literature review (Table 9.3), three vulnerability values (0.1, 0.5, and 1.0) were assigned to the respective debris flow spreading sub-classes. The low spreading probability class has a vulnerability value of 0.1, which causes only aesthetic or light functional damage to the assets. Medium spreading probability class has vulnerability value of 0.5 and it represents medium to high functional or light structural damage to the assets. The highest spreading probability has assigned a vulnerability value of 1.0, which corresponds to a total destruction of the asset (building, road, vineyard, etc.).

		Hazard intensity		
Author	**Low**	**Medium**	**High**	**Very High**
Cardinali et al. (2002)	aesthetic	functional	structural	structural
Fell and Hartford (1997)	0.1	0.4	0.7	1.0
Michael-Leiba et al. (2003)	0.1		1.0	
Bell and Glade (2004)	0.1	0.2	0.5	not specified
Romang (2004)	not specified	0.1 - 0.2	0.5	not specified
Borter (1999)	not specified	0.1	0.5	not specified
Applied approach	**0.1**	**0.5**	**1.0**	

Table 9.3 – Different suggested values related to vulnerability assessment with respect to debris flows. Approach adopted in this study uses only three-class classification. Modified after Fuchs et al. (2007).

The author is aware of strong assumptions used in this part of the analysis, however, the results should represent more realistically the risk situation, than simply estimating the vulnerability to 1.0 for the whole debris flow spreading area (risk map A), or considering vulnerability and hazard as independent variables (Alexander 2000; Galli and Guzzetti 2007 in Ardizzone et al. 2008). Risk map B was (as risk map A) calculated by multiplying the overlaying maps. The resulting map was also reclassified in the same way as risk map A in order to compare these two maps.

Risk curves

After the calculations of risk maps A and B, corresponding risk curves were calculated. Risk curves can be considered as a special type of F-N curves, which are traditionally used in societal landslide risk assessment (Lee and Jones 2004; Cascini et al. 2008; Ho and Ko 2009). In F-N curves, probability of hazard causing N or more fatalities (F) per year is plotted against the number of fatalities. Such curves are used to express societal risk criteria (Düzgün and Lacasse 2005) and they describe the safety levels of particular facilities. In this analysis, risk curves show the relationship of the hazard probability and the total value of exposed elements at risk (possible losses). Hazard probabilities were extracted from the hazard map and total value of the elements at risk was calculated by summarizing all the assets laying in the corresponding hazard areas.

Risk map C

Risk map C was calculated by purely qualitative way, considering the hazard classes of the hazard map A and classification of the elements at risk according to the Regional Directive of Lombardy Region (2005). From the methodological point of view risk map C can not be compared with risk maps A and B, however these maps could be qualitatively compared.

9.3 Results and discussion

9.3.1 Economic risk maps and risk curves

Calculated economic risk maps A and B are shown in Fig. 9.5 and 9.6. Maps were classified into four classes showing the probability of economic loss per pixel per year. In the very low/no risk class (dark green), the areas without expected future economic losses are delimited. These areas cover 39.66% of the study area on both maps. Low risk class (light green) is attributed to zones with low prospective economic loss (0-10 € × 10^{-4}/cell/year). These areas cover 58.95% and 59.12% of the area on risk maps A and B respectively. Areas in the low risk class are usually zones of low economic value (forests, pastures, and agriculture areas) and low to medium hazard. Medium risk class (yellow, 10-1000 € × 10^{-4}/cell/year) covers an area of 1.20% and 1.08% respectively. In this class usually roads and valuable agricultural areas with medium to high hazard are present. High economic risk class (red, >1000 € × 10^{-4}/cell/year) covers area of 0.19% and 0.14% respectively. Only urban areas are present in this class within high to very high hazard zones. All the results are also summarized in Table 9.4.

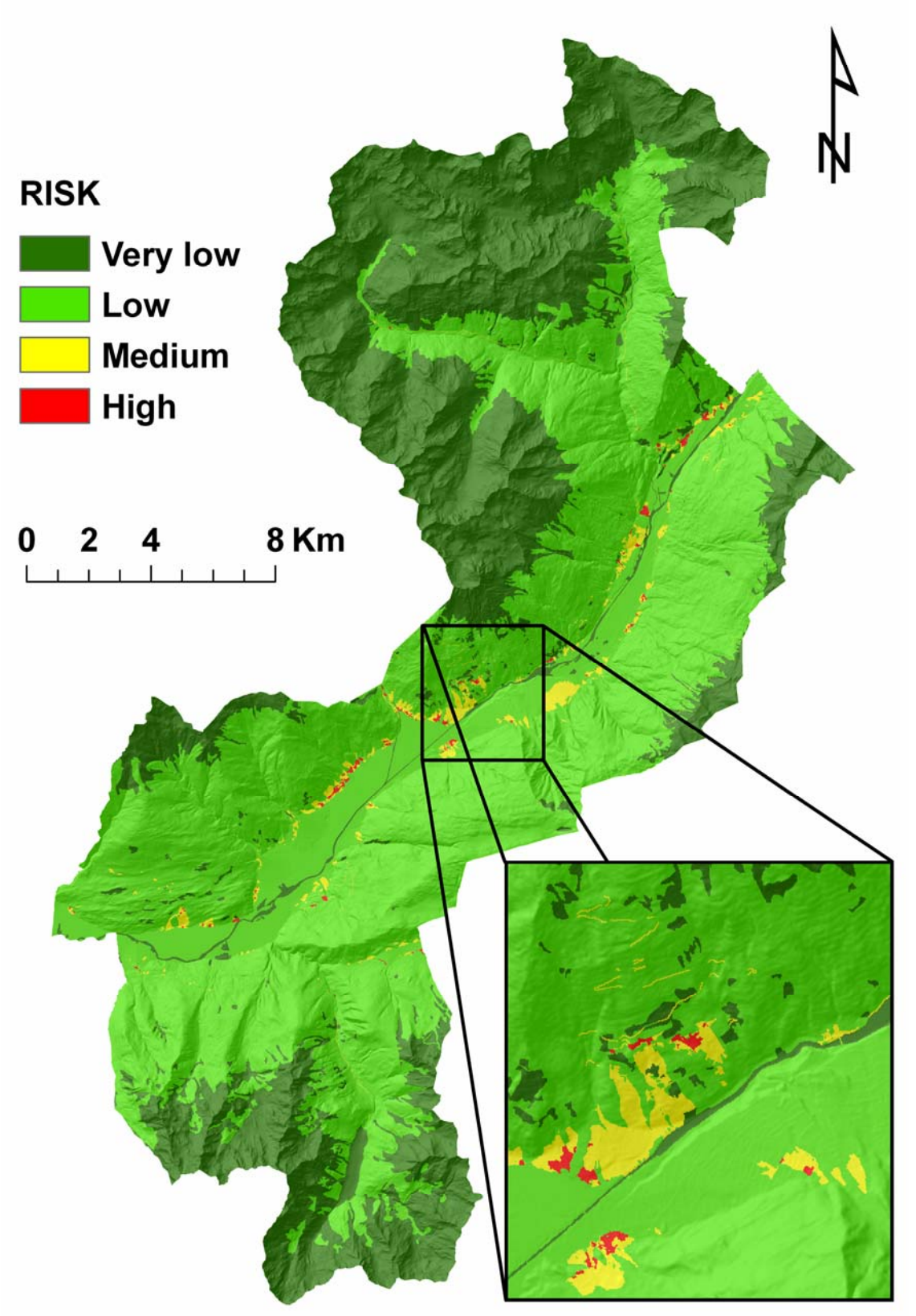

Fig. 9.5 – Economic risk map A.

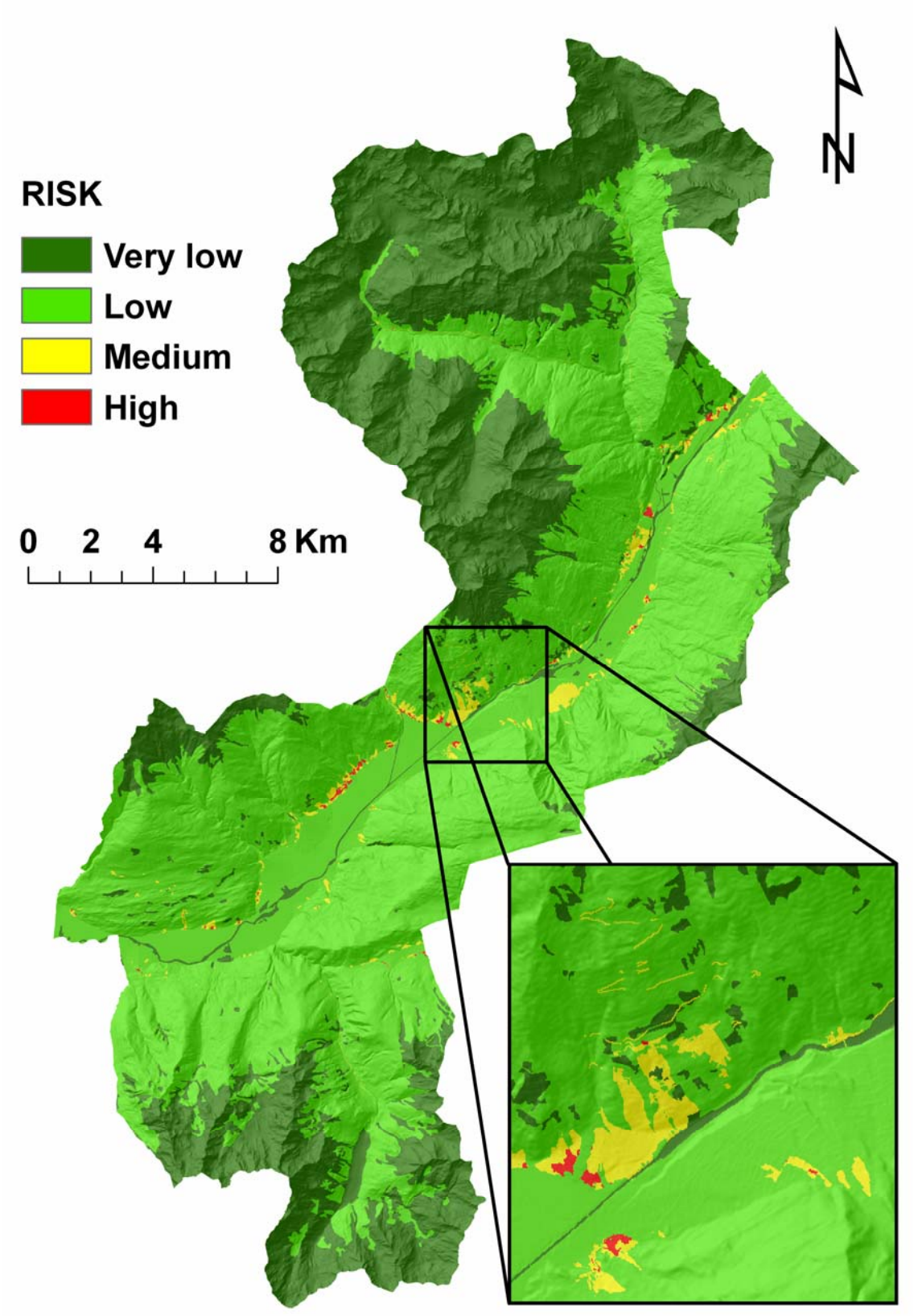

Fig. 9.6 – Economic risk map B.

Risk class	Class value map A	Area (km2) map A	% of area map A	Class value map B	Area (km2) map B	% of area map B
Very low	0	179.08	39.66	0	179.08	39.66
Low	0 - 10	266.20	58.95	0 - 10	266.97	59.12
Medium	10 - 1 000	5.43	1.20	10 - 1 000	4.88	1.08
High	1 000 - 26 704	0.85	0.19	1 000 - 16 859	0.62	0.14

Table 9.4 – Summary of area and percentage of risk classes of risk maps A and B.

From the results it can be seen that no particular restriction in the high and medium risk class was made after application of the different vulnerability criteria in the preparation phases of the economic risk maps. However, some restriction can be noted when only the highest class is analysed. In this case, the high risk area was restricted by 27.12% (0.23 km^2) in the risk map B compared to the high risk area in the risk map A. As a result, risk map B should be used to better delimit potential areas affected by debris flow hazard which can cause significant damage. Some other difference between the maps can be seen also after calculation of the risk curves (Fig. 9.7, Table 9.5)

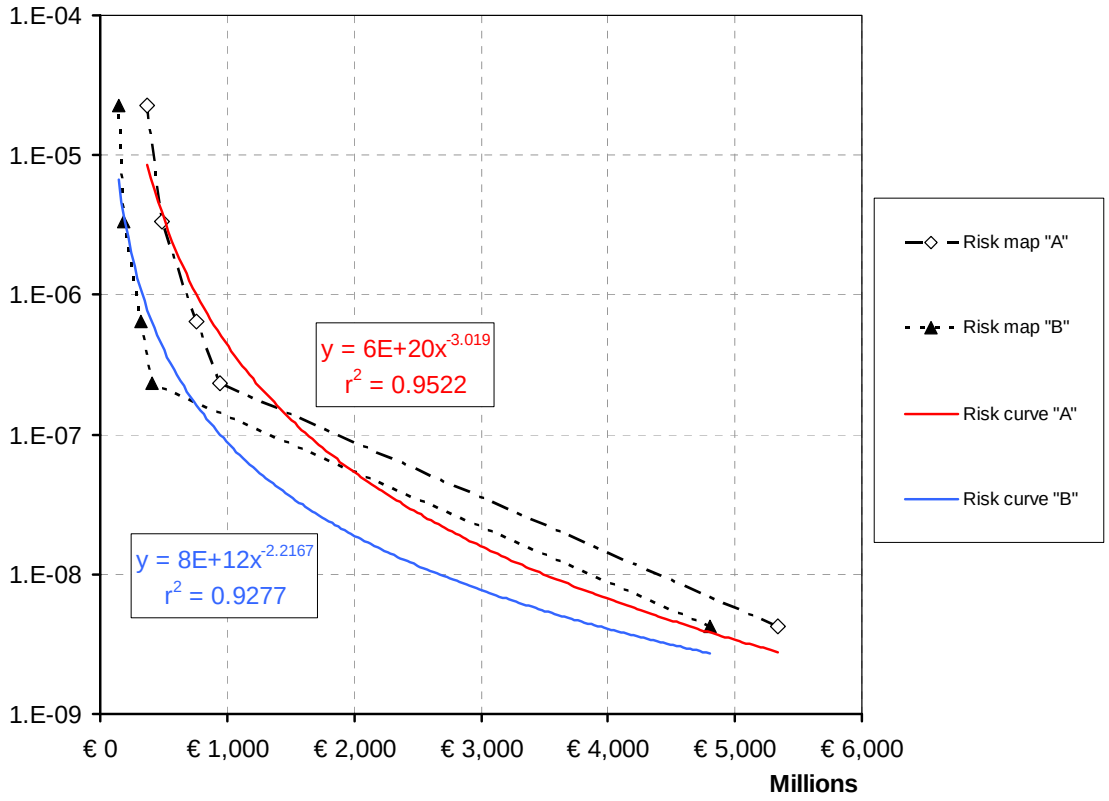

Fig. 9.7 – Risk curves calculated for the risk map A and B.

In the graph, the hazard probability is plotted against the cumulated amount of prospective losses in each hazard class on a log-normal scale. Calculated curves for risk maps A and B have almost similar shape. However, risk curve for map B is shifted down and left, showing lower prospective losses. This is caused by application of different vulnerability criteria in the preparation of these two maps. Calculated risk curves could be easily used by local authorities to calculate the cost-benefit ratio for potential countermeasures. For example, if the

total cost of countermeasures in the high risk zones of map A exceeds the value of assets in these zones (374 millions €), these measures are not economically convenient because the total cost preventive measures is higher than the cost of assets which might be protected. It has to be noted, however, that it is not sufficient to perform the cost-benefit analysis without considering intangible prospective consequences (potentially injured and dead people, environmental damage). These consequences have to be evaluated in a qualitative way as assigning a monetary value to human lives opens ethical issues.

	Hazard map A		Hazard map B	
Hazard	Value of assets per class	Cumulative value of assets	Value of assets per class	Cumulative value of assets
VL	€ 4 394 263 573	€ 5 336 624 903	€ 4 394 263 573	€ 4 799 551 183
L	€ 185 026 781	€ 942 361 330	€ 86 796 010	€ 405 287 610
M	€ 268 797 286	€ 757 334 549	€ 131 225 336	€ 318 491 600
H	€ 114 671 746	€ 488 537 263	€ 46 096 905	€ 187 266 264
VH	€ 373 865 517	€ 373 865 517	€ 141 169 359	€ 141 169 359

Table 9.5 – Total economic value of assets in hazard areas of maps A and B.

9.3.2 Qualitative risk map

Hazard map A was overlaid with the elements at risk map classified according to the methodology of Lombardy Region (2005). After reclassification by using the official risk matrix, a qualitative risk map for the study area was obtained (Fig. 9.8)

From the comparison of the qualitative map with the economic risk maps, some similarities and differences arise. The highest differences can be found in the two lowest risk classes. This situation is due to the presence of low, but quantifiable, areas of potential economic losses on the economic risk maps which are considered as no risk areas in the qualitative classification. In the two highest risk classes, fewer differences appear comparing the economic risk maps A and B, to the qualitative map C. This situation is caused by urban areas, which have highest values in economic as well as in expert based estimates.

There is no simple solution how to choose an appropriate risk map from the three possibilities. Economic risk maps have the advantage of more objective and quantified values; however, they do not respect some non-economic properties of the area and the elements at risk as the qualitative map. As a result, economic risk maps should be used to help allocate future investments and focus on areas with high potential economic losses. On the other hand, qualitative risk map should be used to inform better the inhabitants about potential debris flow risk.

9.3.3 Limitations of risk mapping and possible sources of uncertainties

In risk mapping on medium scale (1:25,000 – 1:50,000) several limitations exist and many uncertainties are present within the results (Table 9.6). As already stated by Bell and Glade (2004), due to the uncertainties inherent in each input factor of risk analysis, the resulting risk values also indicate a considerable uncertainty. Main limitation such as in the case of

susceptibility and hazard mapping at medium scale is connected with the spatial resolution and reliability of the inputs. The approach proposed in this study used only inputs with similar resolution (1:10,000) which were consequently rasterized as 10 m cells to avoid errors and misunderstandings due to the working scale. However, other uncertainty arises from the computed probabilities of hazard and risk, when there is no guarantee that all the information about past events was used in the analysis. Another limitation is connected with the "static" expression of hazard and risk, showing only the situation according to the date of acquisition of the inputs of the analysis. IUGS Working Group on Landslides – Committee on Risk Assessment (1997) and Heinimann (1999) recommended that final results should be treated as relative results and not as absolute ones. This is probably the only way of using the very many valuable tools of hazard and risk analysis in natural disaster mitigation on one hand, but not to lose the trust in the results on the other (Bell and Glade 2004).

From the methodological point of view, many limitations still exist for a proper QRA at medium scale. Specific risk maps (economic, social, environmental, etc.) should be used for calculation of a total quantitative risk map. However, this still seems to be a long journey because of the high-resolution data needs on large areas and the usage of static type of data. Some future developments in remote (near) real-time data acquisition of inputs and automated (but supervised) processing of the results might result in dynamic quantitative risk maps at medium scale, which represents the ultimate goal in QRA at this scale of study.

FACTOR	UNCERTAINTY	REASON	SIGNIFICANCE	IMPROVEMENT
Susceptiblity analysis				
Inventories	low-medium	inprecision	high	increase of data collection
DEM	low	resolution	medium	increase of resolution
Geo-factors	low	resolution	low-medium	up-to-date information
Susceptibility model	low-medium	model limitations	medium-high	non-linear models
Map classification	medium	subjectivity	medium-high	---
Hazard analysis				
Temporal probability	medium-high	average values	high	higher frequency of photos
DEM	medium	inprecision	very high	increase of resolution
Model calibration	medium-high	average values	high	analysis of past events
Map classification	low-medium	subjectivity	high	---
Risk analysis				
Value of elements at risk	low	data availability	low-medium	up-to-date information
Vulnerability aproximation	high	subjectivity	very high	analysis of past events
Elements at risk class.	low	subjectivity	low-medium	analysis of past damages
Map classification	high	subjectivity	high	risk perception studies

Table 9.6 – Qualitative estimation of uncertainties in diverse steps of the risk analysis on medium scale approach used in this thesis. For more information about the data, please refer to the corresponding chapters in the thesis. Table structure adopted from Bell and Glade (2004).

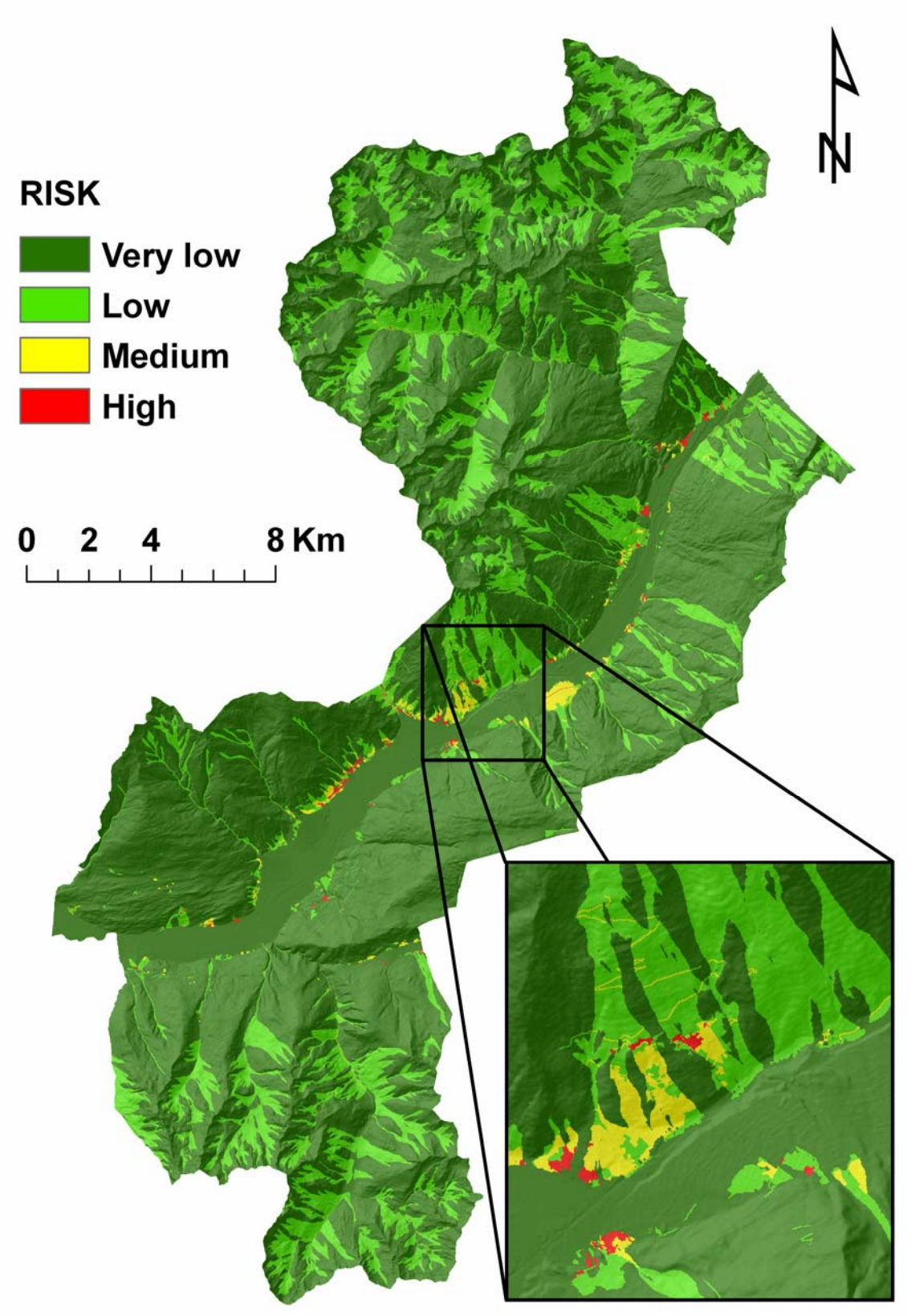

Fig. 9.8 – Qualitative debris flow risk map prepared according to the methodology of Lombardy Region (2005).

9.4 Conclusions

In the presented study three debris flow risk maps were prepared. Firstly, two economic risk maps were calculated showing the prospective economic losses due to debris flows in the study area of CM Valtellina di Tirano. Risk curves were also calculated to summarize expected monetary damage against the respective probability. These curves can be used by the local stakeholders for preliminary cost-benefit analyses. Afterwards, a qualitative risk map, using the official risk matrix, was prepared. The results show areas of high economic as well as general importance which might be affected by debris flows in the future and where important consequences may arise. Aside from its limitations (temporal validity and spatial resolution), delimitation of high risk areas allows local authorities to focus their attention on the “hot-spots”, where local (large) scale analysis can be performed with more convenient cost-benefit ratio.

9.5 References

Agenzia del Territorio – OMI (2009): Quotazioni immobiliari: Osservatorio mercato immobiliare. Agenzia del Territorio.
Available at: http://www.agenziaterritorio.it/site.php?id=2158.

Alexander, D.E. (2000): Confronting catastrophe. Terra Publishing, Harpenden, 282 p.

Ardizzone, F., Cardinali, M., Guzzetti, F., Reichenbach, P. (2008): Landslide Hazard Assessment, Vulnerability Estimation, and Risk Evaluation at the Basin Scale. In: Casagli, N., Fanti, R., Tofani, V. (Eds.): Web Proceedings of The First World Landslide Forum, 18-21 November 2008 United Nations University, Tokyo, Japan, pp. 449-452. Available at: http://150.217.73.85/wlfpdf/12_Reichenbach.pdf.

Bell, R. and Glade, T. (2004): Quantitative Risk Analysis for Landslides– Examples from Bíldudalur, NW Iceland, Natural Hazards and Earth System Sciences, 4: 117-131,

Borter, P. (1999): Risikoanalyse bei gravitativen Naturgefahren. Bundesamt für Umwelt, Wald und Landschaft, Bern.

Cascini L., Ferlisi, S., Vitolo, E. (2008): Individual and societal risk owing to landslides in the Campania region (southern Italy). Georisk: Assessment and Management of Risk for Engineered Systems and Geohazards, 2(3): 125-140.

Cardinali, M., Reichenbach, P., Guzzetti, F., Ardizzone, F., Antonini, G., Galli, M., Cacciano, M., Castellani, M. and Salvati, P. (2002): A geomorphological approach to the estimation of landslide hazards and risk in Umbria, Central Italy. Natural Hazards and Earth System Sciences, 2: 57-72.

CT10 (2006): CT10 - Base Dati Geografica alla Scala 1:10,000. Lombardy Region, Milano, Italy. CD-ROM.

Crozier, M.J., Glade, T. (2005): Landslide Hazard and Risk: Issues, Concepts and Approach. In: Glade, T., Anderson, M., Crozier, M.J. (Eds.): Landslide Hazard and Risk. John Wiley & Sons Ltd, Chichester, pp. 1-40.

DB2000 (2003): Database of the CM Valtellina di Tirano mapped at 1:2,000 scale. CM Valtellina di Tirano. CD-ROM.
Available at: http://www.cmtirano.so.it/sistemainformativo.php

DEI (2006): Prezzi Tipologie Edilizie 2006. DEI Tipografia del Genio Civilie. CD-ROM.

DUSAF Project (2003): Destinazione d'Uso dei Suoli Agricoli e Forestali. Lombardy Region, Milano, Italy.

Düzgün, H.S.B., Lacasse, S. (2005): Vulnerability and acceptable risk in integrated risk assessment framework. In: Hungr, O., Fell, R., Couture, R., Eberhardt, E. (Eds.): Landslide risk management. Taylor & Francis, London, pp. 505-516.

Fell, R., Hartford, D. (1997): Landslide risk management. In: Cruden, D., Fell, R. (Eds.): Landslide risk assessment. Balkema, Rotterdam, pp. 51-109

Fuchs, S., Heiss, K. and Hübl, J. (2007): Towards an empirical vulnerability function for use in debris flow risk assessment. Natural Hazards and earth System Sciences, 7: 495-506.

Galli, M., Guzzetti, F. (2007): Landslide vulnerability criteria: a case study from Umbria, Central Italy. Environmental Management, 40: 649-664.

GEOPOI (2009): GEOcoding POints of Interest. Agenzia del Territorio.
Available at: http://www.agenziaterritorio.it/?id=3081.

Heinimann, H. R. (1999): Risikoanalyse bei gravitativen Naturgefahren – Methode, Umwelt-Materialien, 107/I, Bern, 115 p.

Ho, K.K.S., Ko, F.W.Y. (2009): Application of quantified risk analysis in landslide risk management practice: Hong Kong experience. Georisk: Assessment and Management of Risk for Engineered Systems and Geohazards, 3(3): 134-146.

IUGS Working Group on Landslides – Committee on Risk Assessment (1997): Quantitative assessment for slopes and landslides – The state of the art. In: Cruden, D. M., Fell, R.

(Eds.): Landslide risk assessment. Proceedings of the Workshop on Landslide Risk Assessment, Honolulu, Hawaii, USA, 19–21 February 1997, A. A. Balkema, Rotterdam, pp. 3-12.

Lee, E.M., Jones, D.K.C. (2004): Landslide risk assessment. Thomas Telford Publishing, London, 454 p.

Lombardy Region (2005): Direttiva Regionale N. VIII/1566, 2005. Criteri e indirizzi per la definizione della componente geologica, idrogeologica e sismica del Piano di Governo del Territorio. Bolletino Ufficiale della Regione Lombardia, Milano, Italy.

Michael-Leiba, M., Baynes, F., Scott, G., and Granger, K. (2003): Regional landslide risk to the Cairns community, Natural Hazards, 30: 233–249.

Romang, H. (2004): Wirksamkeit und Kosten von Wildbach-Schutzmassnahmen, Verlag des Geographischen Instituts der Universität Bern, Bern.

Valori Agricoli Medi (2009): Valori Agricoli Medi della Provincia di Sondrio. Agenzia del Territorio, Ufficio del territorio di Sondrio, 6 p. Available at: http://www.agenziaterritorio.it/sites/territorio/files/servizi/Osservatorio%20immobiliare/valori_agricoli_medi/lombardia/SO_2008_E.pdf

Varnes, D.J. (1984): Landslide hazard zonation: a review of principles and practice. IAEG Commission on Landslides and other Mass–Movements, UNESCO, Paris, 63 p.

Chapter 10

Selvetta case study

I always tried to turn every disaster
into an opportunity.

(J. D. Rockefeller)

Based on:

Quan Luna, B., Blahut, J., van Westen, C.J., Sterlacchini, S., van Asch, T.W.J., Akbas, S.O. (2010): Vulnerability functions from a debris flow event reconstruction for a quantitative risk assessment. Natural Hazards and Earth System Sciences. (under preparation).

10.1 Introduction

At local scale, a quantifiable integrated approach of both hazard and risk is becoming a required practice in landslide risk reduction management (Bell and Glade 2004; van Westen et al. 2006). This quantitative assessment should include the expected losses as the product of the hazard, the costs of the elements at risk and their vulnerability (Uzielli et al. 2008).

In order to improve the results of a debris flow risk assessment, it is necessary to analyze the hazard event, determining quantitative information in every step of the process (van Asch et al. 2007) and the vulnerability of the elements exposed. Dynamic runout models can reproduce the distribution of the material along the course of a landslide, model its intensity and delimit the zone where the elements will experience an impact. For this reason, dynamic runout models have been used in recent years as tools that link the outputs of a debris flow hazard initiation/susceptibility modelling (released volumes) and physical vulnerability curves.

Different approaches and methods have been developed in the past for a quantitative risk analysis using dynamic runout models and the exposed vulnerability described in a quantitative or qualitative manner. Calvo and Savi (2008) proposed a method for a formal risk analysis in a debris flow-prone area in Ardenno, Italian Alps; utilizing a Monte Carlo procedure to obtain synthetic samples of debris flows. They obtained probability density functions of the outputs of a dynamic runout model (forces) and adopted three different vulnerability functions to examine their effect on risk maps. Muir et al. (2006) presented a case study of quantitative risk assessment to a site-specific natural terrain in Hong Kong, where various scenarios were generated with different source volumes classes and sets of rheological parameters. They derived probability distributions from past events runouts and calculated the probability distribution of debris mobility for each volume class. Regarding the vulnerability, they used an "Overall Vulnerability Factor" (OVF) and the average number of vulnerable population in a given facility directly hit by a landslide. The OVF was derived from the landslide volume, location of the elements at risk and the protection that a facility can offer. Individual risk was calculated as the summation of the product of the frequency of a flow affecting the facility and the vulnerability of the most vulnerable individual for each of the scenarios. Societal risk was also calculated. Castellanos Abella (2008) performed a local risk assessment based on the back-analysis of one historical landslide in Cuba. Based on the parameters obtained from the modelling, runout simulations were carried out for twelve potential zones. Vulnerability curves based on the depth of the flow and the conditions of the buildings were calculated using detailed building typology characteristics and runout results. Economic risk values were computed for three scenarios. Zimmerman (2005) described Switzerland's new approach of natural hazards and risk management using the Sörenberg debris flow as an example. For the Sörenberg event, hazard maps were prepared according to three probability classes scenarios. The scenarios were based on past events and field verification. Debris flow runout was modelled and displayed on intensity maps. Swiss Federal recommendations provide definite criteria for the intensity classes which are based on the height and the velocity of the flow. Adjustment of the land use plans and

building codes were established regarding the intensity classes. Jakob and Weatherly (2005) quantified debris flow hazard and risk on Jonas Creek fan in Washington, USA. They constructed frequency-magnitude graphs to build different return period scenarios as an input to a debris flow runout model. Hazard intensity maps were developed based on the maximum flow depth, inundated area and flow velocity of each modelled scenario. Potential deaths were calculated assuming that in the high intensity areas the vulnerability was equal to 1, while the vulnerability was equal to 0 in the medium and low intensity zones.

This chapter presents an integrated approach coupling detailed rainfall data and the FLO-2D runout dynamic model to calculate the intensity and runout zone of the 2008 Selvetta debris flow that caused damage to thirteen buildings. The debris flow event was reconstructed and back-analyzed using geomorphologic and numerical approach. Field work geomorphologic investigations directed towards evidences related to the behaviour of the flow and intensity aspects such as run-out distances, velocities and depths. Four main section of the path were identified regarding the activity and deposits of the flow during its course. It was observed that entrainment played an important role in the development of the debris flow. The entrained material was modelled during the course of the flow accounting for the increase of pore pressures induced by the undrained loading exerted by the flow. The outputs from the model were consequently used for the calculation of vulnerability curves for buildings present in the study area. These curves relate the physical outputs of the modelling and the economic values of the elements at risk.

10.2 Selvetta study site and description of the event

10.2.1 Location of the study site

Selvetta study site is situated in Valtellina Valley (Fig. 10.1), on the border between CM Valtellina di Morbegno and CM Valtellina di Sondrio. Selvetta village administratively belongs to two municipalities – Forcola and Colorina. The area affected by the debris flow lies, however, inside the Colorina municipality. Geomorphologically, it belongs to Orobic Alps which are forming north-facing slopes of the Valtellina Valley. These slopes are composed of metamorphic rocks (mainly tabular gneiss, micaschists and quarzites). On less steep parts there could be distinguished two terraces with glacial sediments from quaternary glaciations at the height of about 560-760 m a.s.l. and 1,120-1,240 m a.s.l.

10.2.2 Description of the event

On Sunday morning of 13th July 2008 majority of Valtellina Valley has been isolated from the rest of Lombardy because of intense precipitations that caused blockage of the state road S.S.38 connecting capital of the province Sondrio with the lower part of the valley. There were several roadblocks put near Ardenno because the road S.S.38 was blocked by water that inundated the

road near Berbenno. On the railway line there were about 60 cm of water. The only accesses to the upper part of the valley were via Aprica Pass and from Switzerland.

The civil protection corps and another fast response teams were evacuating people from the affected area. Total number of evacuees in Valtellina was around 220 people and reached around 300 in Lombardy Region. The most severely affected municipalities were Berbenno, Valmasino, Talamona, Forcola and Colorina where several debris flows and mud flows occurred.

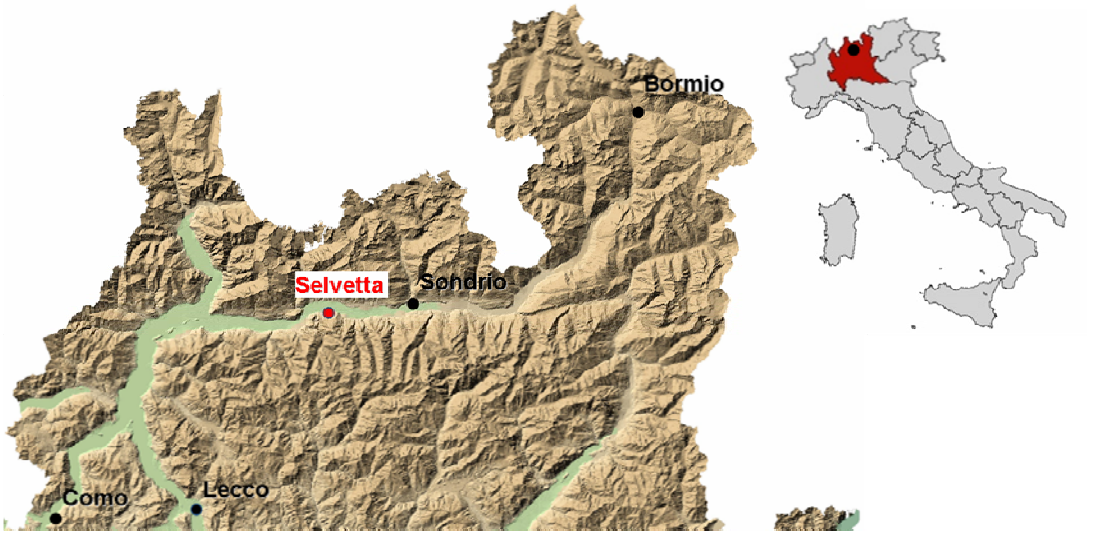

Fig. 10.1 – Location of the Selvetta case study area.

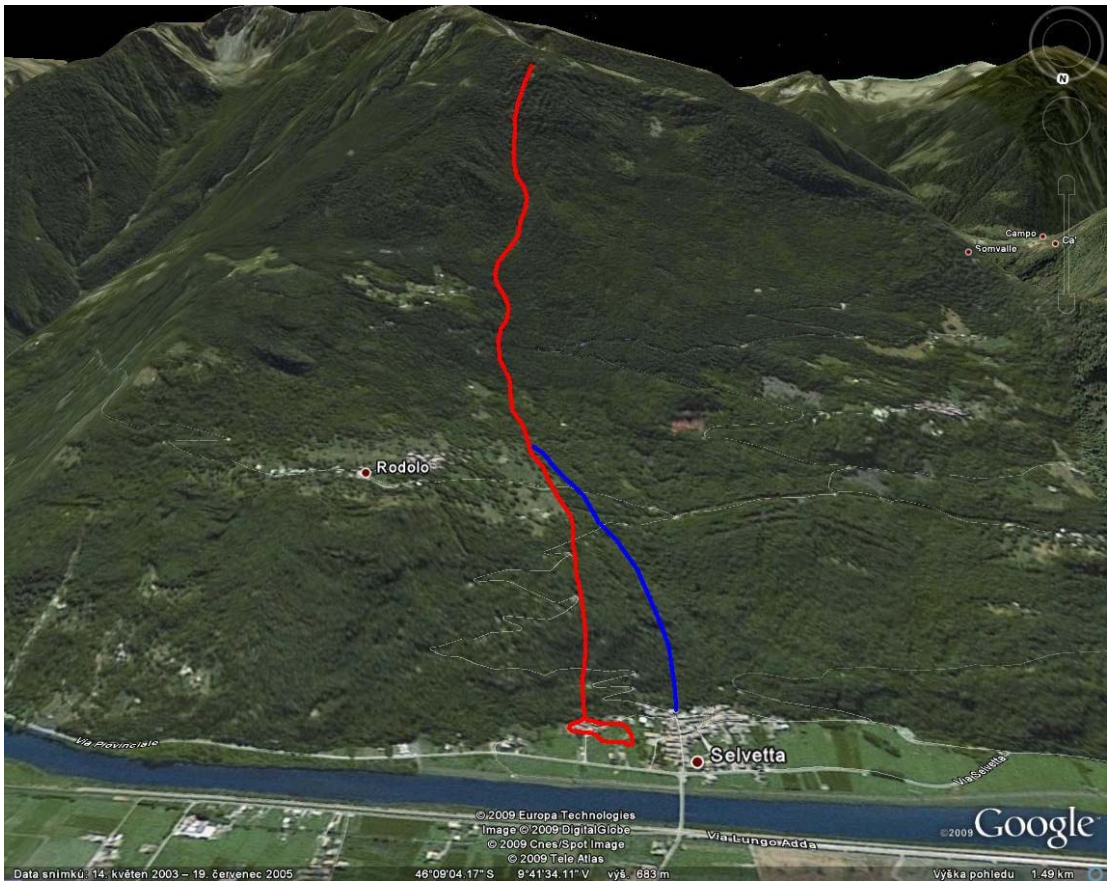

Fig. 10.2 – Google Earth view of the Selvetta debris flow (red line). The blue line shows the original drainage channel of the torrent (from the CTR 1:10,000 map).

One of the largest mud-debris flows occurred in the village of Selvetta (Fig. 10.2, 10.3 and 10.4). According to the information given by the Civil Protection of Lombardy Region, the debris flow occurred between 10:06 and 10:15 a.m. The debris flow event was reconstructed after extensive field work and interviews with local inhabitants and civil protection teams. At first, several rock blocks of a size of almost 2 m^3 fell down from the direction of a small torrent above the village. The blocks were followed by a first surge of debris and mud that damaged the houses. This surge caused the most damage in the deposition area. There could be distinguished also a second hyperconcentrated wave with fine mud content that partially washed away the accumulation from the second wave (Fig.10.5).

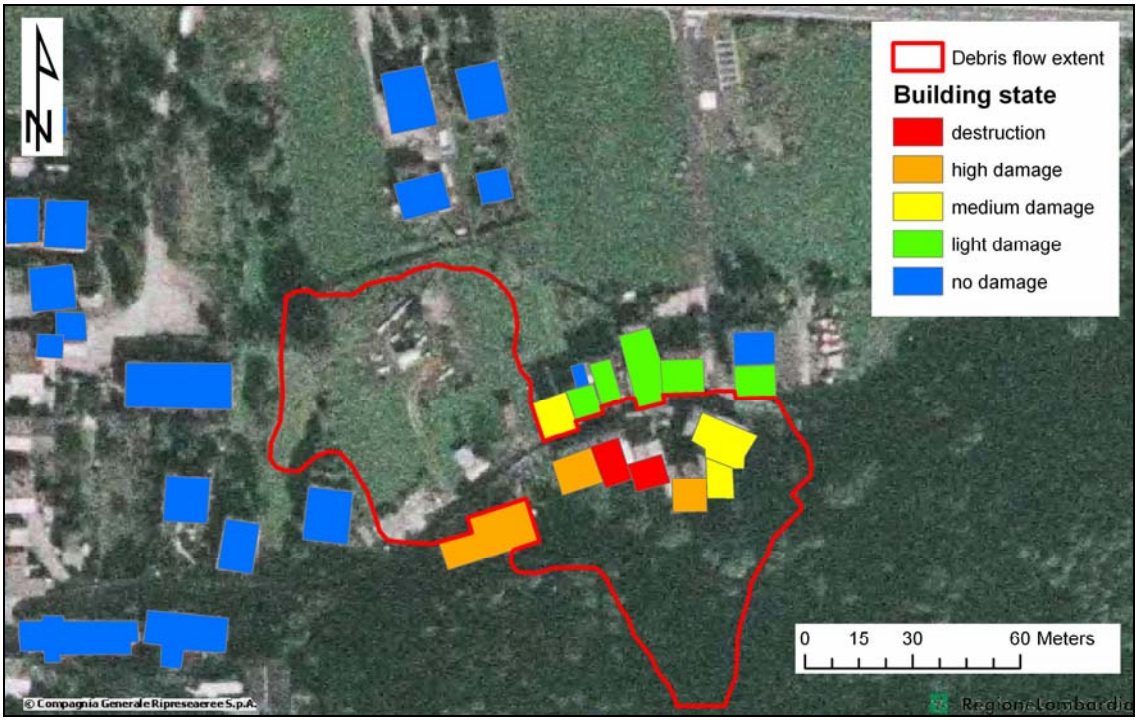

Fig. 10.3 – Extent of the Selvetta debris flow overlaid over an aerial photograph from 2003. Occurred damage to buildings is shown. Destruction: V=1; heavy damage: V=0.5-1; medium damage: V=0.1-0.5; light damage: V=0-0.1.

Principal part of the fieldwork was aimed at collecting information to describe the behaviour of the flow during its course. Flow depths were measured along the travelled path and sedimentation features that hinted out when the flow evolved were carried out. Entrainment and deposition features according to their pattern were recognized and quantified. The deposits in and out of the channel were considered and channel profiles were made in locations where the velocities and discharge of the flow could be deduced.

The evolution of the flow in terms of velocity was reconstructed by the use of empirical formulas. Estimation of the velocity is important when evaluating the flow behavior and assessing its rheology. To derive the mean flow velocity in each channel cross-section, the superelevation formula (10.1) proposed by McClung (2001) and Prochaska et al. (2008) was applied:

Fig. 10.4 – Aerial photograph showing lower part of the Selvetta debris flow. Photo F. Luino.

Fig. 10.5 – Deposit traces left by the flow on one of the houses situated in the alluvial fan of Selvetta. The two surges of the flow can be distinguished. Photo J. Blahut.

$$v = \sqrt{\frac{R_c g}{k}\frac{\Delta h}{b}} \tag{10.1}$$

Where, v is the mean velocity of the flow (m/s), R_c is the channel's radius curvature (m), g is the gravity (m/seg2), Δh is the superelevation height (m), k is a correction factor for the viscosity and b is the flow width (m). Hungr (2007) in Prochaska et al. (2008) believes that the value of the correction factor can be "1" with the exception of cases with sharp bends where some shock waves develop.

Geomorphologic investigations allowed to distinguish five main sections of the flow: 1) the proper scarp; 2) path in forested area; 3) path on alpine meadows; 4) accelerating section; and 5) accumulation area (Fig. 10.6).

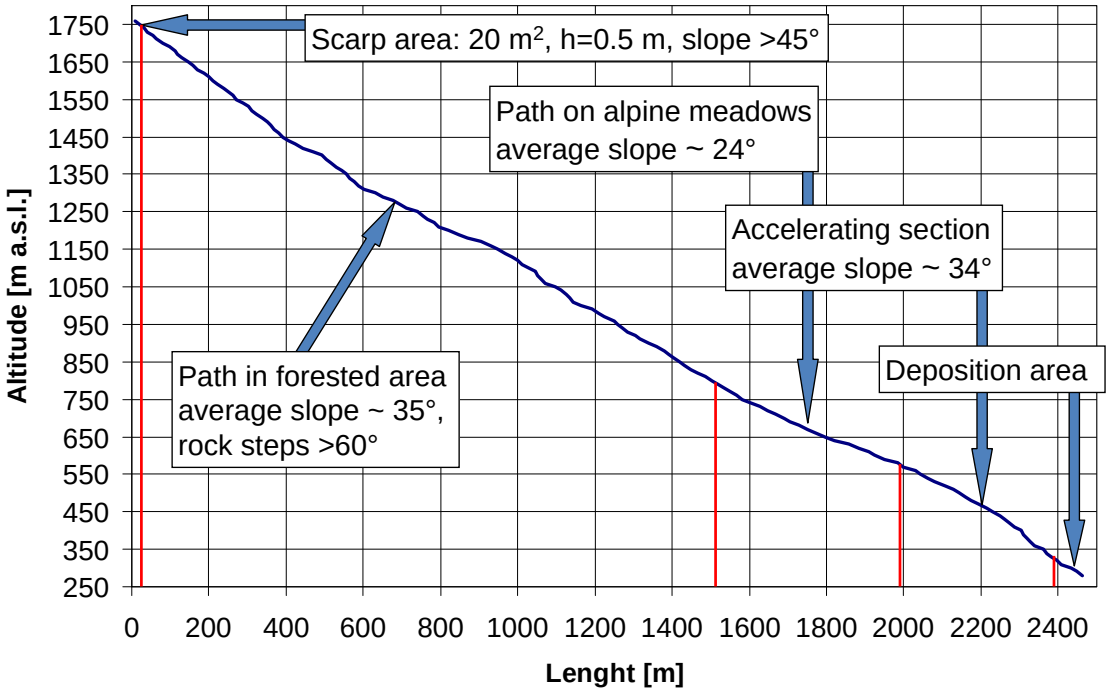

Fig. 10.6 – Profile of the Selvetta debris flow with five main morphological sections.

Initiation area of the flow was situated approximately at 1760 m a.s.l. in a coniferous forest. The proper scarp was very small with an area of about 20 m^2 and height about 0.5 m. The debris flow originated as a soil-slip in thin colluvial cover on very steep (>45°) forested slope. This suggests that the flow started as a small failure and gained momentum with additional entrained material from the channel (bed and walls). Another important source for the increase of volume and the mobility of the flow was the inclusion to the flow of the rainfall run-off and the reactivation of water springs formed by the increase of the ground water table.

After some tens of meters the flow became larger and started to denudate the channel to the bedrock (Fig. 10.7). The denudation of this channel to the bedrock was tightly associated with acceleration of the flow on steeper parts of the slope and on rock steps. The average

inclination of the path in forested area is 35° but there are several steps with inclination higher than 60°. There could be distinguished a subsection of this part of the flow from 1,240 and 1,120 m a.s.l. in morainic sediments, with lower inclination and consequent lower erosion. In these subsections there was significant decrease of velocity of the flow and decrease of the erosion as well. The average calculated mean velocity was 3.83 m/s. The measured maximum flow depth was 2.85 m and the average measured flow depth was 1.75 m.

Fig. 10.7 – Selvetta debris flow path in the forested area. Typical profile of the flow is shown by the black line. Photo J. Blahut.

At 760 m a.s.l. the flow has decreased its velocity again when reached another less steep part of alpine meadows on morainic sediments near Rodolo village (Fig. 10.8). The flow channel in this section of the flow was rarely denuded to the bedrock and flow itself accumulated a lot of material from the upper section. The average inclination of the third section is 24°. The average calculated mean velocity was 2.72 m/s. The measured maximum flow depth was 2.6 m and the average measured flow depth 1.68 m.

At the height of around 640 m a.s.l., on a flat glacial terrace, the flow did not follow its original channel of Rodolo torrent and diverged more to the right side where joined a small ravine. The fourth part of the flow has an inclination about 34° and could be characterized by a significant increase of velocity and denudation of the channel (Fig. 10.9). The average calculated mean velocity was 5.28 m/s. The measured maximum flow depth was 4.8 m and the average measured flow depth 2.38 m.

Fig. 10.8 – Selvetta debris flow path on the alpine meadows near Rodolo village. Sedimentation can be noticed on the typical profile (black line). Photo J. Blahut.

Fig. 10.9 – Selvetta debris flow path in the acceleration section. Increased erosion can be noticed on the profile of the flow (black line). Photo J. Blahut.

At 310 m a.s.l. starts the apex of the accumulation zone. It has an area of about 9,500 m^2 and the volume of the debris was estimated by field mapping to be around 15,000 m^3. Activity of the debris flow in the deposition area was reconstructed based on the recognition of characteristic patterns such as: sediment sorting, sediment grading and the angle of rest in the borders of the final deposit. Deposits consisted of a fine-grained fluid mixture with suspended coarse debris on the top and fine material on the bottom. A typical "Brazilian Nut" (inverse grading) sorting of a debris flow behaviour was recognized. The average calculated mean velocity was 1.28 m/s. The measured maximum flow depth was 4.1 m and the average measured flow depth 1.62 m.

According to the morphological classification of debris flows for South-Central Alps proposed by Crosta (1990), this debris flow can be classified as debris avalanche evolving into channelled debris flow.

Precipitation records showed that the flow did not occur immediately after the peak precipitation which was recorded at 7 A.M., but with more than three-hour delay. Unfortunately, there is not any rain gauge in the proximity of the initiation zone. The closest one is in Morbegno (about 8 km far from the scarp) and shows hourly peak rainfall of 22 mm/hour between 6 and 7 A.M (Fig. 10.10). The cumulated rainfall during 48 hours before the event reached 92 mm. Although this record did not precisely describe the situation in the initiation area, it could be used for a rough estimation of precipitation and for measuring the delay of initiation after peak precipitation because records from other gauges in the vicinity show also the rainfall peak between 6 and 7 A.M.

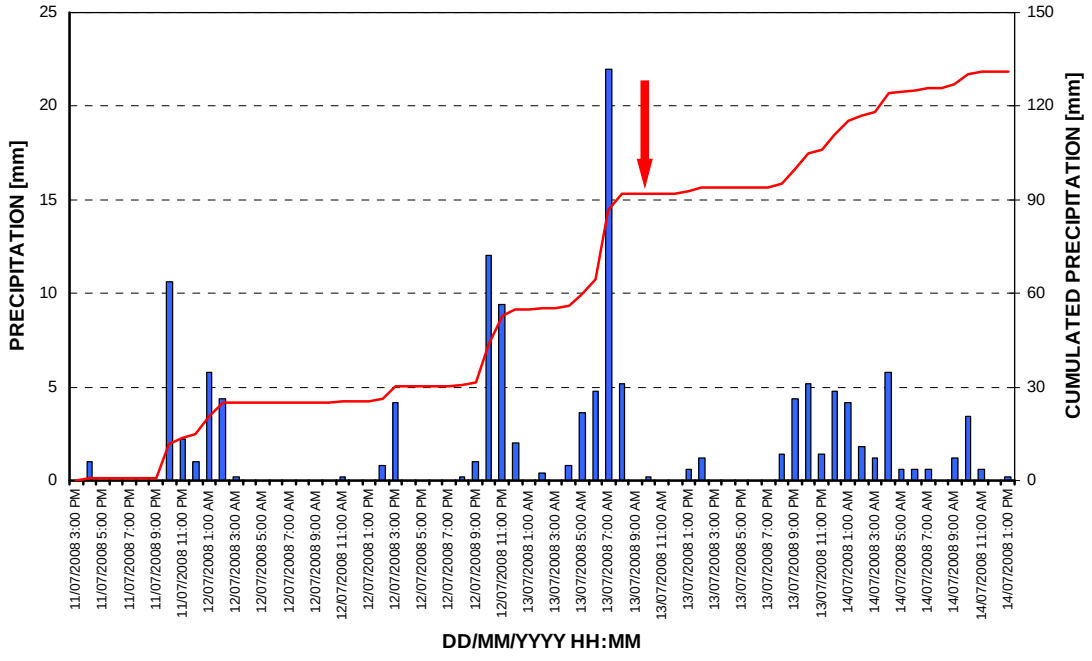

Fig. 10.10 – Hourly precipitation records from the Morbegno rain gauge. The red arrow signs the time of occurrence of the Selvetta debris flow.

One of the main characteristic of the event is the influence of the entrainment process on the flow. The channel experienced considerably deepening and bank erosion. Evidence of the

debris flow was found where the stream flows mainly in bedrock. In several parts of the channel, it was found that obstruction by large boulders and trees may have temporarily influenced the flow behaviour causing a dam-break effect that resulted in the two different surges in the deposition area and lower velocities.

There are 95 buildings situated in Selvetta. The debris flow affected thirteen buildings, destroying two of them, and causing damage of varying levels of severity to the remaining eleven (Fig. 10.11). Structural damage was reported to the facilities located on the alluvial fan (roads). Moreover, lot of damage was reported on car and agricultural machinery. Fortunately, no victims or injuries were reported, mainly because of the awareness of local inhabitants who were evacuated from their houses. More information about the damage to the houses is described in section 10.4.2.

Fig. 10.11 – Remnants of the destroyed building with completely denudated channel of the debris flow behind. Photo J. Blahut.

10.3 Modelling of the event

The field observations concerning the debris-flow event in Selvetta were taken into account and used for the back analysis. These were the basis to calibrate the models and simulate the debris flow process during its course. The most influential processes that control the behaviour of the flow were modelled: entrainment of the flow during its course and the rainfall-runoff that introduced superficial discharge to the flow.

The modelling of the Selvetta debris flow was divided in three parts (Fig. 10.12). The first part was a simulation of the rainfall in the area to calculate a discharge hydrograph and the effect of the rainfall intensity in the flow. The second part was the modelling of the entrainment of the channel bed caused by the flow. The third part was a simulation of the debris flow that included the results of modelling of the rainfall and the entrained material.

The DEM available and used for the Selvetta area was a 2 m grid model obtained form a LIDAR survey. The FLO-2D software was used to simulate the rainfall and the debris flow event.

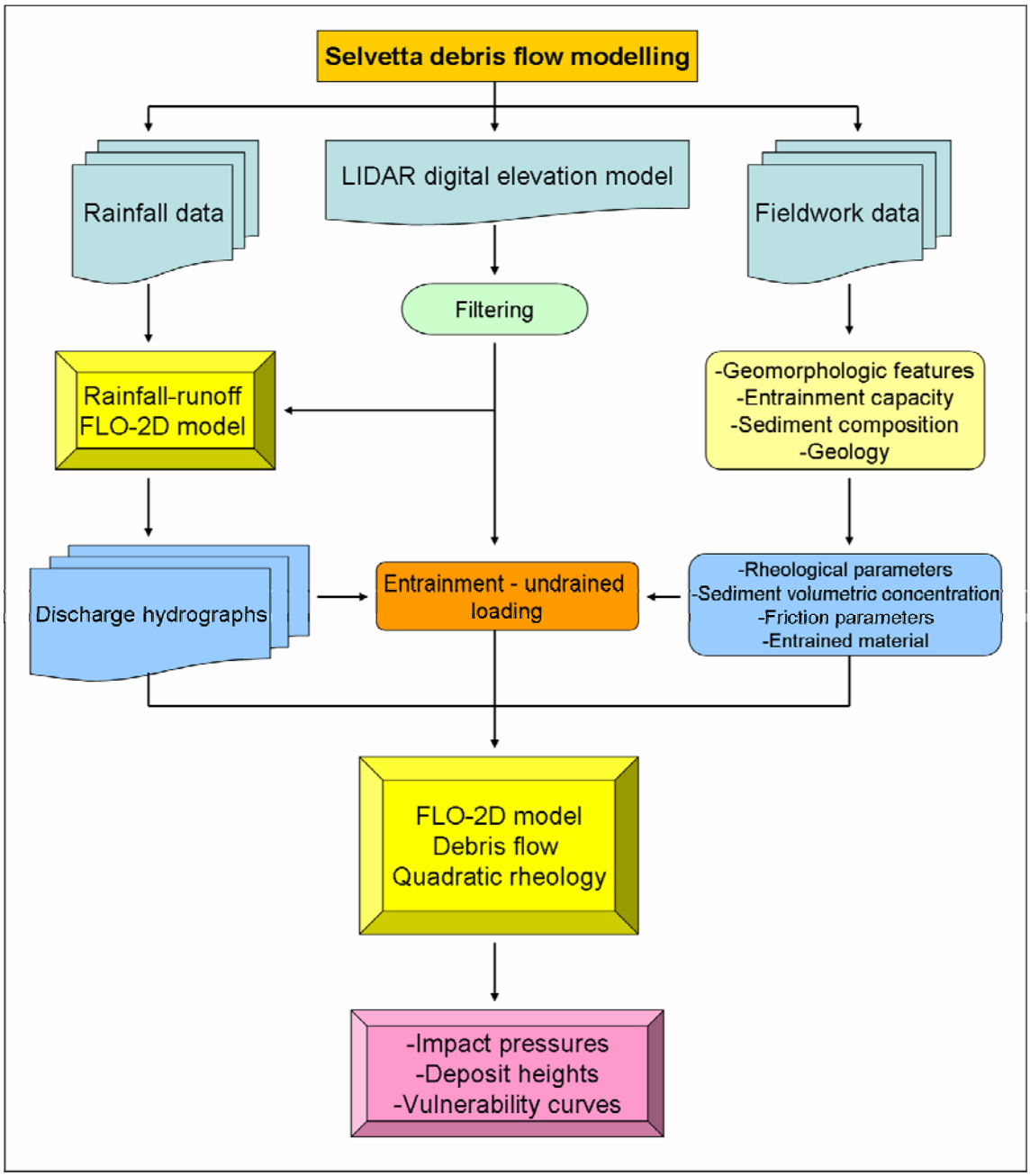

Fig. 10.12 – Flowchart of the methodology applied in the Selvetta case study area.

10.3.1 FLO-2D model description

FLO-2D is an Eulerian two-dimensional finite difference model that is able to route non-Newtonian flows in a complex topography based on a volume-conservation model. The flow volume is routed through a series of tiles that simulates overland flow (2D flow), or through line segments for channel routing (1D flow). Flow in two dimensions is accomplished through a numerical integration of the equations of motion and the conservation of fluid volume. The governing equations, originally presented by O'Brien et al. (1993), are the continuity equation:

$$\frac{\partial h}{\partial t} + \frac{\partial h V_x}{\partial x} + \frac{\partial h V_y}{\partial y} = i \tag{10.2}$$

and the two-dimensional equations of motion:

$$S_{fx} = S_{ox} - \frac{\partial h}{\partial x} - \frac{V_x}{g}\frac{\partial V_x}{\partial x} - \frac{V_y}{g}\frac{\partial V_x}{\partial y} - \frac{1}{g}\frac{\partial V_x}{\partial t} \tag{10.3}$$

$$S_{fy} = S_{oy} - \frac{\partial h}{\partial y} - \frac{V_y}{g}\frac{\partial V_y}{\partial y} - \frac{V_x}{g}\frac{\partial V_y}{\partial x} - \frac{1}{g}\frac{\partial V_y}{\partial t} \tag{10.4}$$

Where h is the flow depth and V_x and V_y are the depth-averaged velocity components along the horizontal x- and y-coordinates. The excess rainfall intensity (i) may be nonzero on the flow surface. The friction slope components S_{fx} and S_{fy} are written as function of bed slope S_{ox} and S_{oy}, pressure gradient and convective and local acceleration terms.

The FLO-2D software models the shear stress as a summation of five shear stress components: the cohesive yield stress, the Mohr-Coulomb shear, the viscous shear stress, the turbulent shear stress and the dispersive shear stress. All these components can be written in terms of shear rates giving a quadratic rheological model function of sediment concentration, adding a turbulent and dispersive term to the Bingham equation (FLO-2D 2009). The depth-integrated rheology is expressed (after dividing the shear stresses by the hydrostatic pressure at the bottom of the flow $\gamma_m h$) as:

$$S_f = \frac{\tau_y}{\gamma_m h} + \frac{K\eta V}{8\gamma_m h^2} + \frac{n_{td}{}^2 V^2}{h^{4/3}} \tag{10.5}$$

Where S_f is the friction slope (equal to the shear stress divided by $\gamma_m h$); V is the depth-averaged velocity; τ_y and η are the yield stress and viscosity of the fluid, respectively, which are both a function of the sediment concentration by volume; γ_m is the specific weight of the fluid matrix; K is a dimensionless resistance parameter that equals 24 for laminar flow in smooth, wide, rectangular channels, but increases with roughness and irregular cross section geometry;

and n_{td} is an empirically modified Manning n value that takes into account the turbulent and dispersive components of flow resistance.

The Bingham parameters τ_y and η are defined as exponential functions of sediment concentration which may vary over time. The resistance coefficient n accounts for both collisional (inertial grain shear) and turbulent frictional losses. The friction slope is determined separately for both orthogonal flow directions. The yield stress, the viscosity, and the empirically modified Manning n value is calculated as follows:

$$\tau_y = \alpha_1 e^{\beta_1 C_v} \tag{10.6}$$

$$\eta = \alpha_2 e^{\beta_2 C_v} \tag{10.7}$$

$$n_{td} = n_t b e^{m C_v} \tag{10.8}$$

Where α_1, β_1, α_2, and β_2 are empirical constants, C_v is the fine sediment concentration (silt- and clay-size particles) by volume of the fluid matrix, n_t is the turbulent n-value, b is a coefficient (0.0538) and m is an exponent (6.0896).

The differential equations of motion are solved using a central difference scheme. The boundary conditions are specified as follows: the inflow condition is defined in one or more upstream grid elements with a hydrograph (water discharge vs. time) and values of C_v for each point in the hydrograph; the outflow condition is specified in one or more downstream grid elements. Time steps vary according to the Courant-Friedrich-Lewy stability condition. The model requires the specification of the terrain surface as a uniformly spaced grid. Within the terrain surface grid, a computational grid, i.e. a domain for the calculations, must be specified. The Manning n value should be assigned to each grid element to account for the hydraulic roughness of the terrain surface. The values can be spatially variable to account for differences in surface coverage (FLO-2D 2009).

10.3.2. Rainfall modelling

The rainfall was simulated in the FLO-2D program. The hourly accumulated rainfall during the period of 11th and 13th July 2008 was used as an input (Fig. 10.10). The accumulated rainfall was distributed all over the area domain in a real time. Outflow sections were selected where the accumulated rain of the whole area domain was discharged. The outflow sections are artificial sections whose purpose is to discharge flow off the area domain system (FLO-2D 2009). For the Selvetta area, two zones were selected with outflow parts: 1) the scarp, where the release area and the slope failure are located. The release hydrograph is calculated adding the release volume of the failed mass and; 2) the debris flow path channel, where the amount of rain influenced the mobility of the flow and where the contribution of the water added to the flow was canalized. Due to the Eulerian nature of the FLO-2D software and finite differences scheme, the parameter

that mainly controls the numerical performance is the grid spacing. In the simulations using FLO-2D, the grid spacing was taken as 2 m, which corresponds to the grid size in the digital elevation model. The result is a discharge hydrograph of the released material (Fig. 10.13).

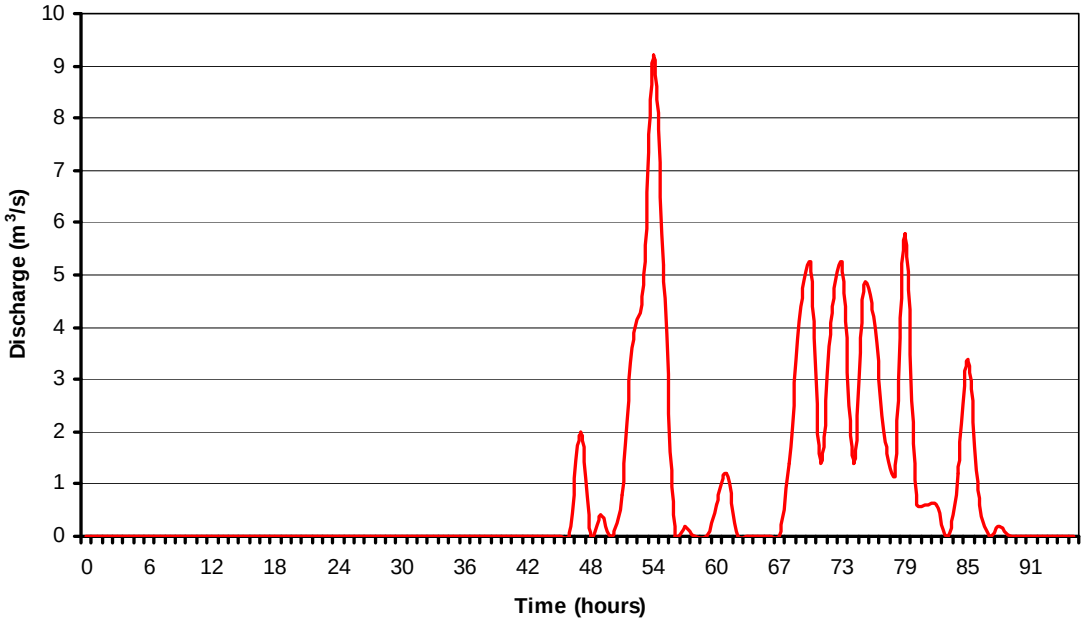

Fig. 10.13 – Simulated hydrograph of the debris flow release area. Simulation started at 3 P.M. on 11th July 2008.

The estimation of the peak discharge is of vital importance as it determines the maximum velocity and flow depth, momentum, impact forces, ability to overrun channel walls, as well as the runout distance.

10.3.3 Entrainment modelling

Based on the calculated release hydrograph and the rainfall that converge into the channel path of the flow, the entrained material was calculated by assuming that the flow travelling on the channel bed deposits causes an undrained loading that generates a high-pore water pressure and this helps incorporate those deposits into the moving mass. This concept has been described in detailed by Sassa (1988), Remaître et al. (2008) and Quan Luna et al. (submitted 2010) explaining the long travelling motion of some debris flow saturated with water. A loading of the bed deposits is generated when the sliding mass flows on top. The applied loading of the channel soil was calculated by the change of vertical normal stress and the shear strength caused by the flow. The increase in pore pressure is calculated based on the proposed equation by Sassa (1988) for an undrained direct shear test.

$$\Delta p = B_D(\Delta \sigma + A_D \Delta \tau) \tag{10.9}$$

Where, A_D and B_D are the pore pressure parameters in the direct shear state. B_D value is affected with the degree of saturation. The pore pressure parameter A_D value changes with

strain. It is assumed that a ground water table is formed in the surface bed layer. When there is ground water flowing perpendicular to the channel bed soil making the bed completely saturated. New stresses on the bottom in-situ soil are then calculated:

$$\sigma_{tot} = \left(\rho_{fl} gh + \rho_{id} gd\right) cos^2 \alpha \tag{10.10}$$

$$\tau_{tot} = \left(\rho_{fl} gh + \rho_{id} gd\right) sin\alpha \, cos\alpha \tag{10.11}$$

Where, ρ_{id} is the density of the bed channel soil, ρ_{fl} is the density of the flow material, g is the gravity force, h the height of the flow, α the angle of the slope and d is the depth of the erodible layer. The factor of safety of the bed channel soil is calculated:

$$FS = \frac{c_{id} + \left(\sigma_{tot} - \Delta p\right) tan\delta_{id}}{\tau_{tot}} \tag{10.12}$$

Where, c_{id} is the cohesion and δ_{id} the friction angle of the channel bed soil. If the mass fails is then incorporated with the complete depth of failure to the flow enlarging its volume.

After the field work and in relation to the slope gradient, the amount of material that could be entrained varied from 1.2 m to 2.3 m. A value of the internal friction angle of $\varphi = 30^{\circ}$ and cohesion = 0.3 kPa were selected. The pore pressure parameters used were $A_D = 0.6$ and $B_D = 0.9$. These values correspond to an in-situ soil that has a high degree of saturation and rich in water discharge. The surface flow occurs in usual time and no air is entrapped under the water table.

An estimated released volume (rain + failed mass) of 2,337 m^3 was computed. The final deposition volume is around 15,324.68 m^3 (554% of increase in mass balance). Figure 10.14, shows the distribution of the entrained volume during the course of the flow and the accumulated entrained material. These values are influenced mostly by the slope gradient and the amount of material to be entrained inside the channel.

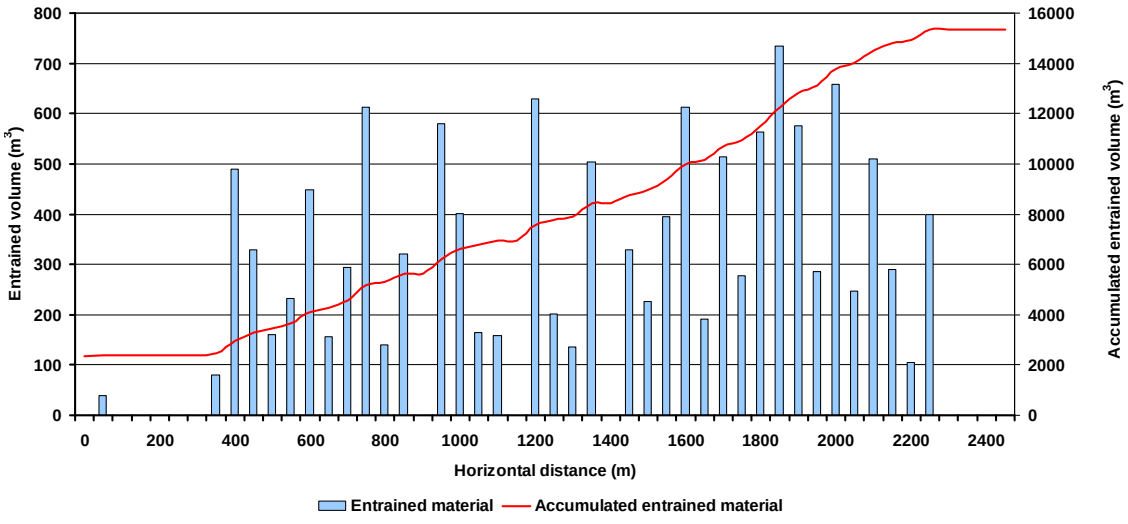

Fig. 10.14 – Chart of the modelled entrained material during the course of the flow.

The volumes of the entrained material were introduced as an additional and variable sediment concentration into the hydrographs of the debris flow used in the FLO-2D model with the empirical formula proposed by Mizuyama et al. (1992), who proposed a relation between the magnitude of the debris flow (volume in m^3) and the peak discharge for muddy-debris flow:

$$Q_p = 0.0188 M_t^{0.790} \tag{10.13}$$

10.3.4 Debris flow modelling

Parameterization of the FLO-2D model has been done by calibration, since no independent estimates of the model friction parameters were available. The calibration of the model was based on a trial-and-error selection of rheological models and parameters, and the adjustment of the input parameters which define the flow resistance. Parameters were adjusted until good agreement between the simulated and observed characteristics were accomplished with the following criteria: (i) velocity and height of the debris flow along the channel; (ii) final runout and; (iii) accumulation pattern in the deposition area. The parameters that filled reasonable the calibration criteria and had the best results were τ_y = 1,950 Pa and η = 5,000 Pa. These rheological parameters were calculated according to the sediment concentration inside the hydrograph and appropriate values of α and β were selected from O'Brien and Julien (1988). The chosen Manning *n*-value that characterizes the roughness of the terrain was 0.04 $sm^{-1/3}$ were the flow was channelled and 0.15 $sm^{-1/3}$ in the deposition zone. A value of "*K*" (laminar flow resistance parameter for overland flow) of 24 was used in the channelled section and of 2,350 for the rough surface on the deposition zone. The Maninng *n*-value and *K*-value were selected as suggested in the FLO-2D manual.

A time-stage of sediment concentration was produced based on the shape of the hydrograph. This was done to agree with observations that the peaks in debris flow hydrographs correspond to high sediment concentrations, while the raising and final parts of the hydrograph have a more diluted composition. The procedure also reproduced the distribution of sediment concentration influenced by a dilution in the raising and falling tails of the hydrograph. The maximum and minimum concentrations were 0.55 and 0.25, respectively.

The FLO-2D software can display for each part of the flow the impact force, velocity, discharge and flow height during all times in the simulation. Figures 10.15 and 10.16 show the maximum runout and deposition modelled by FLO-2D and the field-measured extent of the event which underlines the good agreement of the simulation with what actually happened. The ability of the FLO-2D to model the shadow effect created by the houses can be noted.

The modelled heights of accumulation show good coincidence with the real situation measured in the field. The highest accumulations are reached upslope from the destroyed and heavily damaged houses. Afterwards, they decrease to the edges of the deposition area. It has to be noted that in some cases the flow did not reach some of the lightly damaged houses. This is caused by the fact that FLO-2D does not model the destruction of the house and thus it remains as an obstacle causing the shadow effect. Apparent increase of heights of accumulation in the distal parts of the flow is most probably caused by imprecision in the used DEM. Highest values

of impact pressure are reached immediately near the start of the apex. Afterwards, the pressures continuously decrease. This is caused by the progressive decrease of accumulation heights and velocities on the alluvial fan.

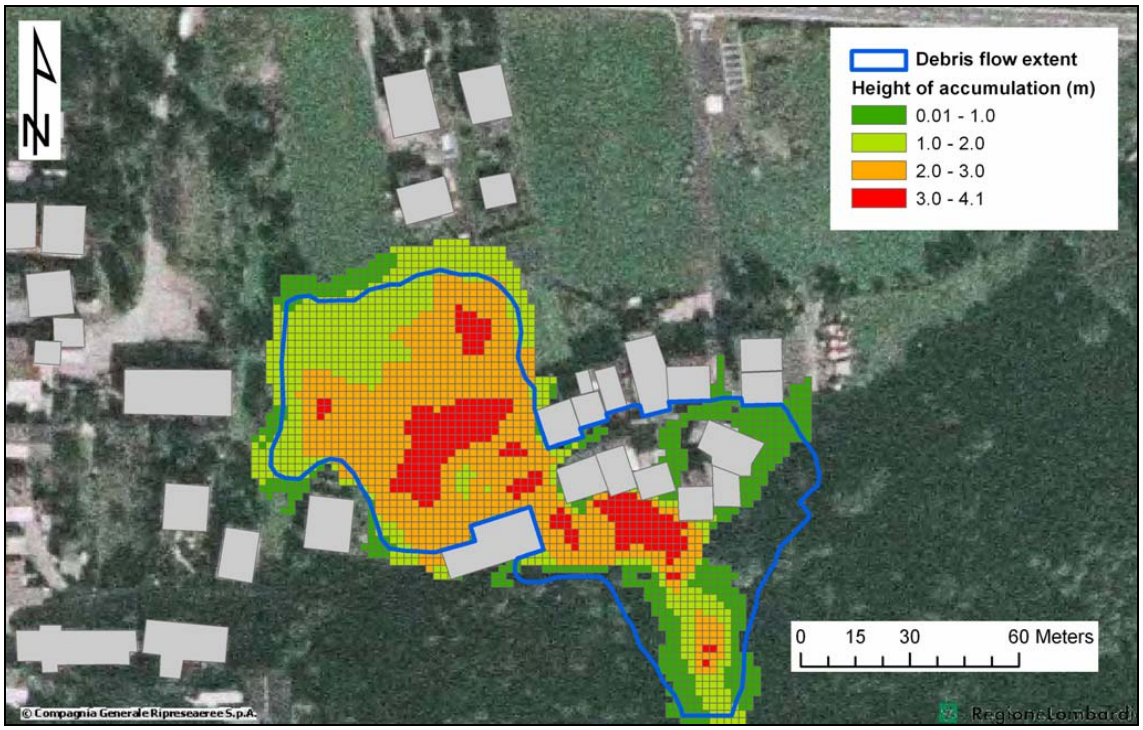

Fig. 10.15 – Comparison of the real and modelled debris flow runout extent. The maximum heights of the accumulation modelled by the FLO-2D model are shown.

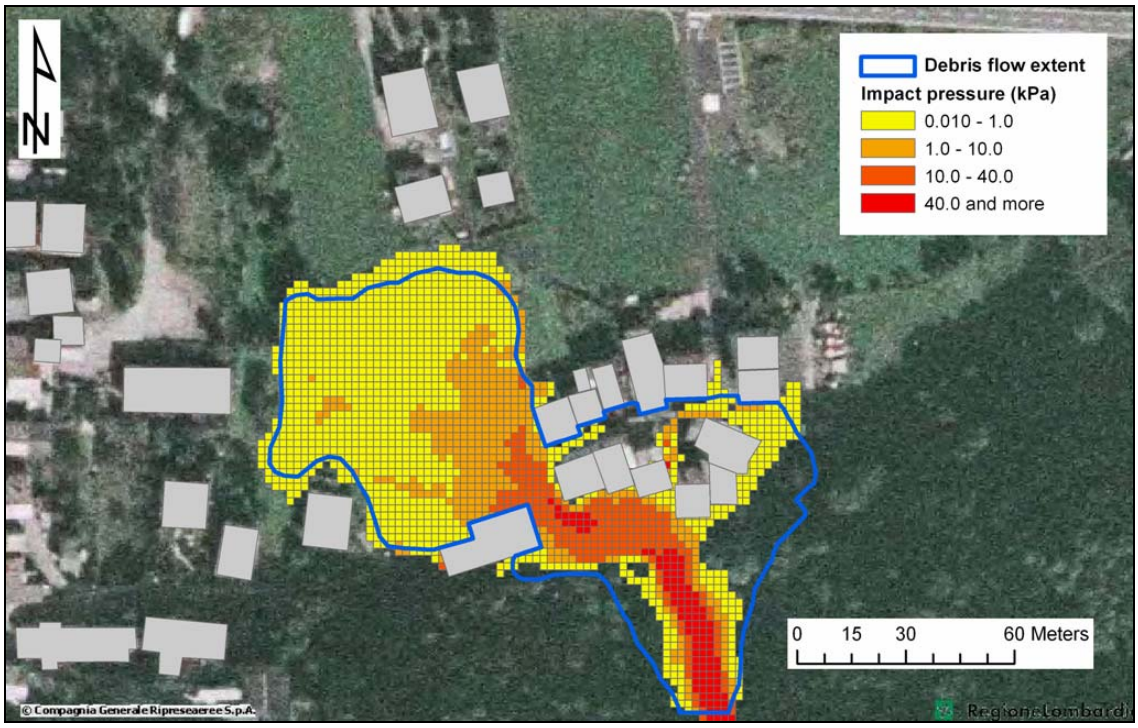

Fig. 10.16 – Comparison of the real and modelled debris flow runout extent. The maximum impact pressures modelled by the FLO-2D model are shown.

10.4 Vulnerability curves

Selvetta represents a very important case study due to the fact that both hazard information and consequence information is present for a deep analysis. This is not the case of most present studies. The different range of damage to the houses makes it easier to assess the vulnerability than from data-limited zones.

10.4.1 Method applied

In landslide hazard and risk studies, physical vulnerability is commonly expressed as the expected degree of loss to a given element at risk, particularly to built structures, resulting from the occurrence of a hazard. Physical vulnerability is commonly expressed on a scale of 0 (no loss) to 1 (total loss), which is a representation of the expected level of damage, e.g. % of buildings destroyed, or relative monetary loss for a single structure (Akbas et al. 2009). It is at least a function of construction materials and techniques, state of maintenance, presence of early warning systems and protection measures, as well as the hazard intensity (Fell 1994; Fell and Hartford 1997). According to our experience, a theoretical vulnerability function for buildings impacted by a landslide hazard shall have more less the shape shown on Figure 10.17.

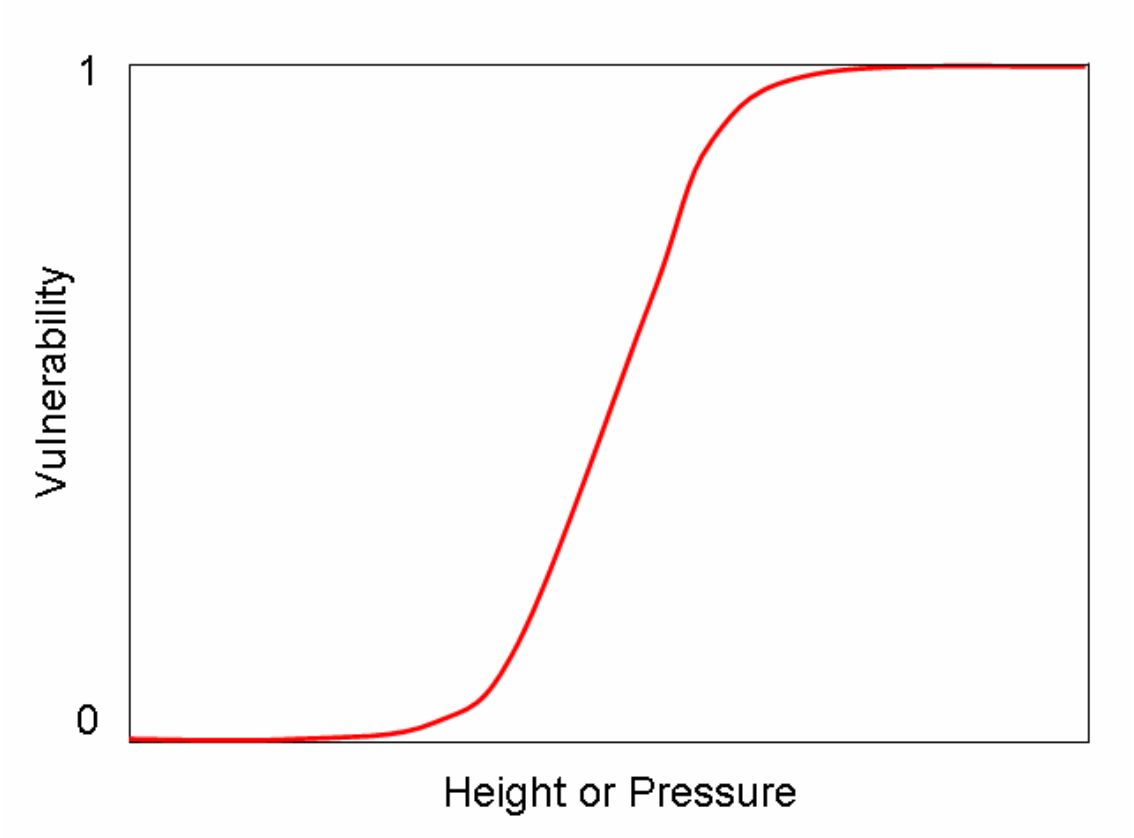

Fig. 10.17 – Theoretical shape of the vulnerability function.

Vulnerability functions that express the expected level of damage with respect to the hazard intensity are almost universally used for earthquake and hurricane risk assessments

(Douglas 2007). For snow avalanches Wilhelm (1998) and Barbolini et al. (2004) proposed vulnerability functions based on the relationship between expected loss of structure and impact pressures. Heinimann (1999) estimated vulnerability against rock falls using building type and rock fall magnitude as input parameters. Mavrouli and Corominas (2008) presented a methodology for the vulnerability assessment of three structural typologies for different intensity levels of rock fall block impact, which is expressed in terms of the boulder kinetic energy. Most of the existing approaches for vulnerability assessment of structures struck by landslides do not distinguish between types of processes, the physical mechanisms, or the structural resistance of the endangered objects (Glade 2003; Fuchs et al. 2007). More importantly, information on process intensity is often missing or described only qualitatively (Cardinali et al. 2002) and semi-quantitatively (Borter 1999). In particular for debris flows, very few quantitative relationships have been proposed between intensities and vulnerability values. To this date, probably one of the most important attempts for the calculation of vulnerability functions for debris flow risk assessment is that of Fuchs et al. (2007). This study used data from a well-documented debris flow event in the community of Nussdorf-Debant in the Austrian Alps to derive a quantitative vulnerability function applicable to brick masonry and concrete buildings. It differs from the previous studies mainly due to its use of official damage data in calculating vulnerability instead of estimations that are based on assumptions. Although the presented intensity-vulnerability relationship is stated to be applicable to the general construction type within European mountains, Fuchs et al. (2007) indicated that a wider application of the method to other test sites is required for further refinement and standardization. Other important contribution is presented by Akbas et al. (2009); they calculated empirical vulnerability function for the Selvetta debris flow using the approach of Fuchs et al. (2007).

In our approach we calculated vulnerability functions using damage data obtained from the official documents coupled with the information from modelling outputs. This approach has an important advantage compared to the approach of Akbas et al. (2009). It allows calculation of vulnerability functions using the height of debris accumulation and also the impact pressure. The impact pressure information is widely used in snow avalanche risk assessment but it is not widely applied for debris flows risk calculations.

The damage data were analysed from the RASDA documents (RAccolta Scheda DAnni – Damage Assessment Form), which are mandatory to be drafted within 48 hours after a disaster for claim purposes. For the Selvetta debris flow, these documents were prepared by the engineers of the General Directorate of Civil Protection of the Lombardy Region, and the local police. For each building, they contain a detailed analysis of damage, which is converted to a monetary value of losses. For each building, the approximate reconstruction value was calculated according to building type and size, using the data given in the Housing Prices Index prepared by the Engineers and Architects of Milan (DEI 2006). The building sizes were obtained from the available blueprints of the buildings. For those buildings which do not have blueprints, the reconstruction values were calculated using geometrical dimensions measured through the field study, and GIS resources (Akbas et al. 2009).

Afterwards, vulnerability was calculated using an economic approach, defined as the ratio between the loss and the individual reconstruction value. This ratio was calculated for each of the thirteen building structures that were affected by the debris flow event. The obtained ratios were consequently coupled with the modelling results (height of accumulation, impact pressures).

10.4.2 Results

Reconstruction value of the buildings ranges from about € 66,000 to € 455,000. Damage records for individual buildings ranges from about € 2,000 to € 290,000 (Fig. 10.18). Individual vulnerabilities are ranging from 0.015 to 1. These values result in a mean vulnerability of 0.35 per exposed building. All of the buildings are single to three storey brick masonry and concrete structures. It should be emphasized that the state of maintenance and the age of the structures somewhat vary among the site; however, the building stock in Selvetta carries the characteristics of those in a typical Italian Alpine village in general.

Fig. 10.18 – Building with highest reported damage reaching more than € 290,000. Photo J. Blahut.

Vulnerability curve using heights of accumulation

Height of accumulation values were extracted for each affected building. For every building the maximum and minimum heights of accumulation vary a lot. As a consequence, an average height near building walls oriented towards the flow direction was considered. Figure 10.19 shows the relationship between the vulnerability and deposition height values.

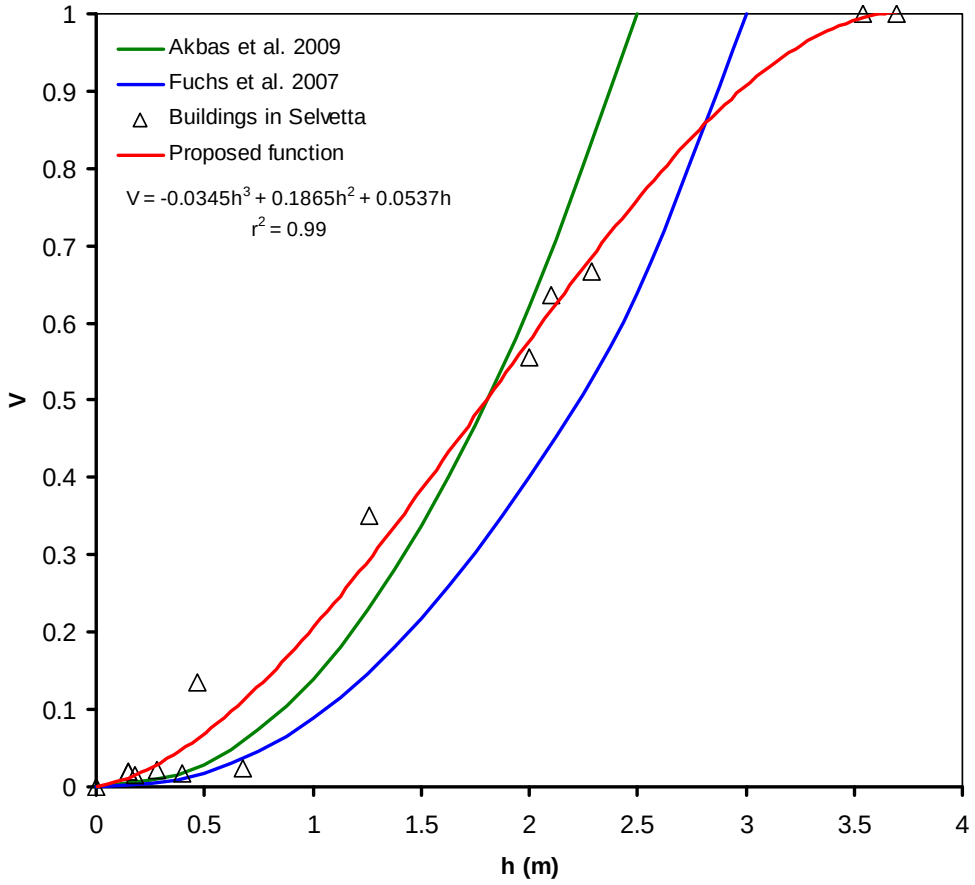

Fig. 10.19 – Proposed vulnerability function for accumulation heights obtained from the modelling.

An examination of Fig. 10.19 indicates that the vulnerability increases with increasing deposition height, i.e., intensity of debris flow, as expected. Fuchs et al. (2007) and Akbas et al. (2009) used a second-order polynomial function to fit the observed points. We propose to use a third-order polynomial function. In our opinion this better corresponds to the theoretical vulnerability function presented in Fig. 10.17 and also fits our data better. The calculated function has coefficient of determination (r^2) is 0.99, for intensities between 0 and 3.55 m:

$$\begin{cases} V = -0.0345h^3 + 0.1865h^2 + 0.0537h & \text{for } h \leq 3.55 \text{ m} \\ V = 1 & \text{for h} > 3.55 \text{ m} \end{cases} \quad (10.14)$$

Where V is vulnerability and h is the modelled height of accumulation. From its definition the vulnerability cannot exceed 1, thus for intensities higher than 3.55 m, the vulnerability is equal to 1.

The vulnerability function obtained in this study suggests different vulnerabilities compared to those obtained using the equations given by Fuchs et al. (2007) and Akbas et al. (2009), which are also shown in Fig. 10.19. Proposed function shows higher vulnerabilities to the height of 1.75 m, than the curve of Akbas et al. (2009) and to 2.75 m compared to the curve

of Fuchs et al. (2009). Vulnerability 1.0 (total destruction) is reached at 3.55 m, which is considerably higher than 2.5 m of Akbas et al. (2009) and 3.0 m of Fuchs et al. (2007).

However, the number of data points in both studies is limited; therefore, it is not possible to reach a robust conclusion about whether the observed discrepancy is the result of the difference in modelling, construction techniques, or a combination of both. The difference may also be partly due to the significant inherent uncertainty involved in the modelling outputs and estimation of the average accumulation height.

Vulnerability curve using impact pressures

Impact pressure values were extracted in the same way as accumulation heights considering the values near building walls oriented towards the flow direction. Average impact pressure values cannot be used because they showed a difference up to three-orders. For that reason only maximum modelled impact pressures were used to calculate the vulnerability function (Fig. 10.20).

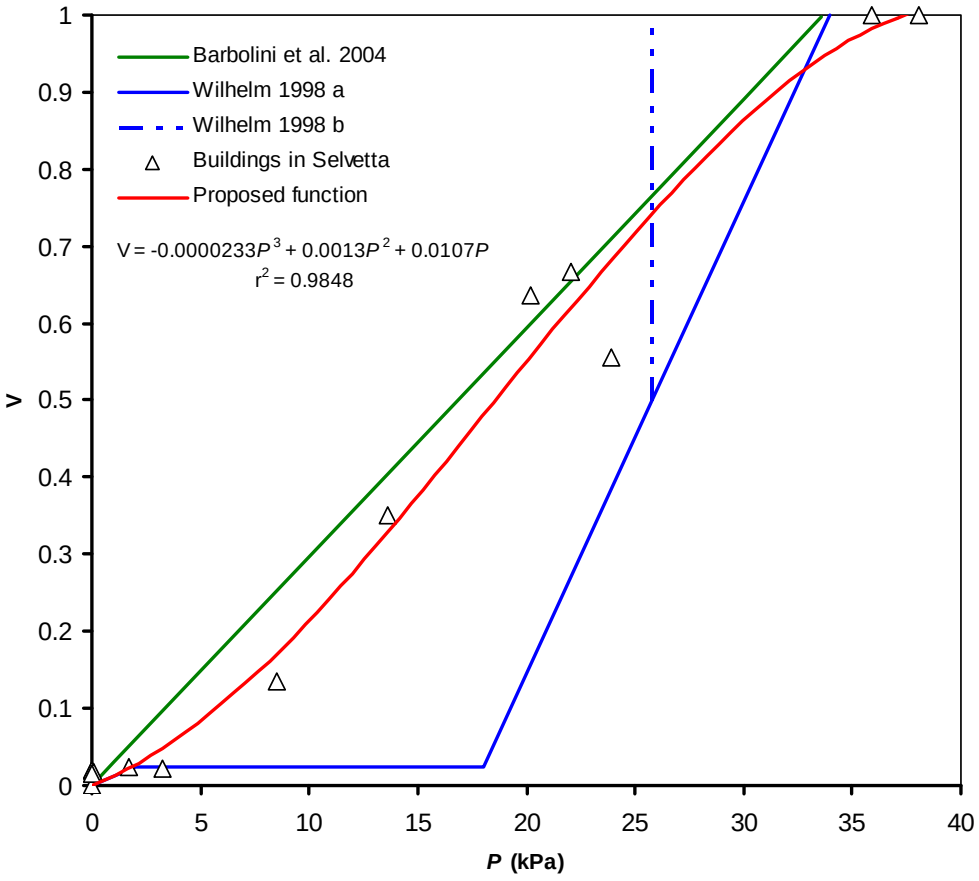

Fig. 10.20 – Proposed vulnerability function for modelled impact pressures.

As in the case of the previous vulnerability function, the vulnerability increases with intensity. A third-order polynomial function which fits the results has a high coefficient of determination (r^2) reaching 0.9848 for impact pressures up to 37 kPa:

$$\begin{cases} V = -0.0000233P^3 + 0.0013P^2 + 0.0107P & \text{for } P \leq 37 \text{ kPa} \\ V = 1 & \text{for } P > 37 \text{ kPa} \end{cases} \quad (10.15)$$

Where V is vulnerability and P is the modelled impact pressure. As vulnerability cannot exceed 1, for intensities higher than 37 kPa, the vulnerability is equal to 1.

Calculated vulnerability equation was compared to two functions used in snow avalanche risk assessment. Similar behaviour of the function can be noticed in comparison with the linear function of Barbolini et al. (2004) which was developed from avalanche data from West Tyrol, Austria. Wilhelm (1998) proposed two different relationships for vulnerabilities higher than 0.5. The former (a) continues its linear trend and reaches vulnerability 1.0 at 34 kPa. The latter (b) indicates that structures are considered beyond repair in case of impact pressures higher than 25 kPa. Functions of Wilhelm (1998) were calculated from data about reinforced structures impacted by avalanches in Switzerland. Compared to our equation, results from Wilhelm (1998) vary a lot in lower vulnerabilities (up to 0.6). At vulnerability of 0.9 (33 kPa) our function crosses the function of Wilhelm (a) and reaches V = 1.0 at 37 kPa. This is also different from Barbolini et al. (2004), who put vulnerability of 1.0 at impact pressure of 34 kPa (similar as Wilhelm 1998). The difference between the functions is probably caused by insufficient data points in case of the Selvetta event. Also the uncertainty connected with the modelling outputs remains an important issue.

10.5 Conclusions

The Selvetta debris flow event was reconstructed in a geomorphologic, empirical and numerical approach (quadratic model). Field geomorphologic investigations were directed towards evidences related to the behaviour of the flow and intensity aspects such as runout distances, velocities and depths in different parts of the debris flow. Four main sections of the flow path were identified regarding the activity and deposits of the flow during its course. It was observed that entrainment played an important role in the development of the debris flow.

The FLO-2D model was applied for the back-calculation and the results coincide in a good manner with the real event. With FLO-2D, an accurate analysis can be performed, accounting for the increase of discharge due to the lateral inflow from basin sides and minor tributaries, the entrained material of the channel based on the undrained loading of the flow, and the deposition process in the alluvial fan.

The most significant results obtained by the model are the maximum height and impact pressures reached by the flow in each cell throughout the entire simulation. These outputs were investigated in terms of the resulting damage to the affected buildings. Synthetic vulnerability curves were prepared based on the average height of accumulation and maximum impact pressures. These curves relate the physical outputs of the modelling and the economic damage

to the affected buildings. More data is needed to increase the robustness of the curves. However, the current results are very promising for an application in quantitative risk assessment.

10.6 References

Akbas, S.O., Blahut, J., Sterlacchnini, S. (2009): Critical assessment of existing physical vulnerability estimation approaches for debris flows. In: Malet, J.-P., Remaitre, A., Bogaard, T. (Eds.): Proceedings of the International Conference "Landslide Processes", Strasbourg, France, pp. 229-233.

Barbolini, M., Cappabianca, F., and Sailer, R. (2004): Empirical estimate of vulnerability relations for use in snow avalanche risk assessment. In: Brebbia, C. (Ed.): Risk analysis IV, WIT Press, Southampton, pp. 533-542.

Bell, R., Glade, T. (2004): Quantitative risk analysis for landslides – Examples from Bíldudalur, NW-Iceland. Natural Hazards and Earth System Sciences, 4: 117-131.

Borter, P. (1999): Risikoanalyse bei gravitativen Naturgefahren. Bundesamt für Umwelt, Wald und Landschaft, Bern, 117 p.

Calvo, B., Savi, F. (2008): A real-world application of Monte Carlo procedure for debris flow risk assessment. Computers & Geosciences, 35(5): 967-977.

Cardinali, M., Reichenbach, P., Guzzetti, F., Ardizzone, F., Antonini, G., Galli, M., Cacciano, M., Castellani, M. and Salvati, P. (2002): A geomorphological approach to the estimation of landslide hazards and risk in Umbria, Central Italy. Natural Hazards and Earth System Sciences, 2: 57-72.

Castellanos Abella, E.A. (2008): Local landslide risk assessment. In: Castellanos Abella, E.A.: Multi-scale landslide risk assessment in Cuba, Utrecht, Utrecht University, ITC Dissertation 154, pp. 193-226.

Crosta, G. (1990): A study of slope movements caused by heavy rainfall in Valtellina (Italy – July 1987). In: Cancelli, A. (Ed.): Proceedings of ALPS90, Alpine Landslide Practical Seminar – 6th ICFL International Conference and Field Workshop on Landslides, University of Milano, Milano, pp. 247-258.

DEI (2006): Prezzi Tipologie Edilizie 2006. DEI Tipografia del Genio Civilie. CD-ROM.

Douglas, J. (2007): Physical vulnerability modelling in natural hazard risk assessment. Natural Hazards and Earth System Sciences, 7: 283-288.

Fell, R. (1994): Landslide risk assessment and acceptable risk. Canadian Geotechnical Journal, 31:261-272.

Fell, R., Hartford, D. (1997): Landslide risk management. In: Cruden, D., Fell, R. (Eds.): Landslide risk assessment. Balkema, Rotterdam, pp. 51-109.

FLO-2D (2009): Reference manual 2009. FLO-2D Software Inc., 73 p. Available at: http://www.flo-2d.com/wp-content/uploads/FLO-2D-Reference-Manual-2009.pdf

Fuchs, S., Heiss, K., Hübl, J. (2007): Towards an empirical vulnerability function for use in debris flow risk assessment. Natural Hazards and Earth System Sciences, 7: 495-506.

Glade, T. (2003): Vulnerability assessment in landslide risk analysis. Die Erde, 134: 123-146.

Heinimann, H.R. (1999) Risikoanalyse bei gravitativen Naturgefahren. Umwelt-Materialien 107/1, 115 p.

Jakob, M., Weatherly, H. (2005): Debris flow hazard and risk assessment, Jones Creek, Washington. In: Hungr, O., Fell, R., Couture, R., Eberhardt, E. (Eds.): Landslide Risk Management. Taylor & Francis, London, pp. 533-541.

Mavrouli, O., Corominas, J. (2008): Structural response and vulnerability assessment of buildings in front of the rockfall impact. Geophysical Research Abstracts, 10.

McClung, D.M. (2001): Superelevation of flowing avalanches around curved channel bends. Journal of Geophysical Research, 106(B8): 16489-16498.

Mizuyama, T., Kobashi, S., Ou, G. (1992): Prediction of debris flow peak discharge. In: International Symposium Interpraevent. Bern, pp. 99-108.

Muir, I., Ho, K.S.S., Sun, H.W., Hui, T.H.H., Koo, Y.C. (2006): Quantitative risk assessment as applied to natural terrain landslide hazard management in a mid-levels catchment, Hong

Kong. In: Nadim, F., Pöttler, R., Einstein, H., Klapperich, H., Kramer, S. (Eds.): "Geohazards", ECI Symposium Series, Volume P07, 8 p.

O'Brien J.S., Julien, P.Y. (1988): Laboratory analysis of mudflow properties. Journal of Hydraulic Engineering, 114(8): 877-887.

O'Brien, J.S., Julien, P.Y., Fullerton, W.T. (1993): Two-dimensional water flood and mudflow simulation. Journal of Hydraulic Engineering, 119(2): 244-261.

Prochaska, A., Santi, P., Higgins, J., Cannon, S. (2008): A study of methods to estimate debris flow velocity. Landslides, 5(4): 431-444.

Quan Luna, B., Remaître, A., van Asch, T., Malet, J.-P., van Westen, C.J. (2010): Analisis of debris flow behaviour with a one dimensional run-out model incorporating entrainment. Engineering Geology. (submitted, under review)

Remaître, A., van Asch, Th.W.J., Malet, J.-P., Maquaire, O. (2008): Influence of check dams on debris flow run-out intensity. Natural Hazards and Earth System Sciences, 8: 1403-1416.

Sassa, K. (1988): Geotechnical model for the motion of landslides. In: Proceedings of 5th International Symposium on Landslides. Balkema, Rotterdam, pp. 37-55.

Uzielli, M., Nadim, F., Lacasse, S., Kaynia, A.M. (2008): A conceptual framework for quantitative estimation of physical vulnerability to landslides. Engineering Geology, 102(3-4): 251-256.

van Asch, T.W.J., Malet, J.-P., van Beek, L.P.H., Amitrano, D. (2007): Techniques, issues and advances in numerical modelling of landslide hazard. Bulletin de la Société géologique de France, 178(2): 65-88.

van Westen, C.J., van Asch, T.W.J., Soeters, R. (2006): Landslide hazard and risk zonation—why is it still so difficult? Bulletin of Engineering Geology and the Environment, 65: 167-184.

Wilhelm, C. (1998): Quantitative risk analysis for evaluation of avalanche protection projects. In: Proceedings of the 25 Years of Snow Avalanche Research, Oslo, Norway, pp. 288–293.

Zimmerman, M.N. (2005): Analysis and management of derbis-flow risks at Sörenberg, Switzerland. In: Jakob, M., Hungr, O. (Eds.): Debris-Flow Hazards and Related Phenomena, Praxis, Springer, Berlin, Heidelberg, pp. 305–324.

Chapter 11

Tresenda case study

The worst case scenario
is not the worst that can happen.

Based on:

Quan Luna, B., Blahut, J., Camera, C., van Westen, C.J., Sterlacchini, S., Apuani, T. (2010): Debris flow quantitative risk assessment and estimation of economic damage. Landslides. (under preparation).

11.1 Introduction

The main purpose of Civil Protection is to better protect people, their environment, property, and cultural heritage in case of major natural events or man-made disasters (Foster 1980; Alexander 1999, 2000, 2002). The requirement to protect people and to correctly manage resources during a crisis phase is strictly linked to the capability to profile the potential damaging events in advance (Sterlacchini et al. 2010).

Critical situations are unique because of their intrinsic uncertain nature, and human behaviour changes in relation to the critical state; therefore, standardization of activities in an emergency situation can be hardly definable in a rigorous way (Daines 1991; Drabek and Hoetmer 1991). As a consequence, different spatial and temporal scenarios have to be outlined, analysed, and integrated in emergency plans (Sterlacchini et al. 2010). Starting from hazard scenarios, identifying the temporal and physical characteristics of the expected hydrogeological events, risk scenarios should be defined, describing the possible effects on the social, economic and environmental systems.

In this site-specific study which is located in the Tresenda village, hazard scenarios are prepared and risk is quantified in economic terms as potential loss to buildings. For the hazards scenario preparation, available meteorological and geological data are used as inputs for dynamic runout modelling of possible debris flows. Afterwards, risk is quantified in economic terms for three return periods, using vulnerability curves for buildings extracted from the fieldwork and modelling in the Selvetta study site. Application of information from one study site to another is usually connected with problems of local conditioning factors. However, in this case vicinity of the areas and similar characteristics of the elements at risk allowed this application.

11.2 Case study area

11.2.1 Tresenda

The village of Tresenda in the municipality of Teglio (Fig. 11.1) was selected as a suitable test-site, because its geological and geomorphological settings are favourable for a debris flow occurrence. Spatial distribution of past damage and disruptions derived from historical records, local chronicles, and interviews with local people (that suffered losses in the past) suggested this site to be one of the most hazardous and subject to significant potential losses (Sterlacchini et al. 2010).

Soil slips-debris flows can be triggered on the steep slopes above Tresenda by the collapse of dry-stone walls retaining vineyards, or by the movement of unconsolidated material from one of the areas identified as unstable by the geological map of Teglio Municipality.

As the soil thickness varies between 70 and 150 cm, and material could involve both earth and stones, it is supposed that a flow could cross minor roads on the vineyards and impact buildings in Tresenda, while running along main drainage lines.

Casualties and serious damages can be expected, the obstruction of a main road could occur, and it will be necessary to remove the accumulated material. The Adda Valley floor between the toe of the slope and the Adda River is very narrow with a width less than 50-60 m and a time-extended obstruction of important transport corridor S.S. 38 joining the Como Lake with the municipality of Bormio can also lead to high indirect losses.

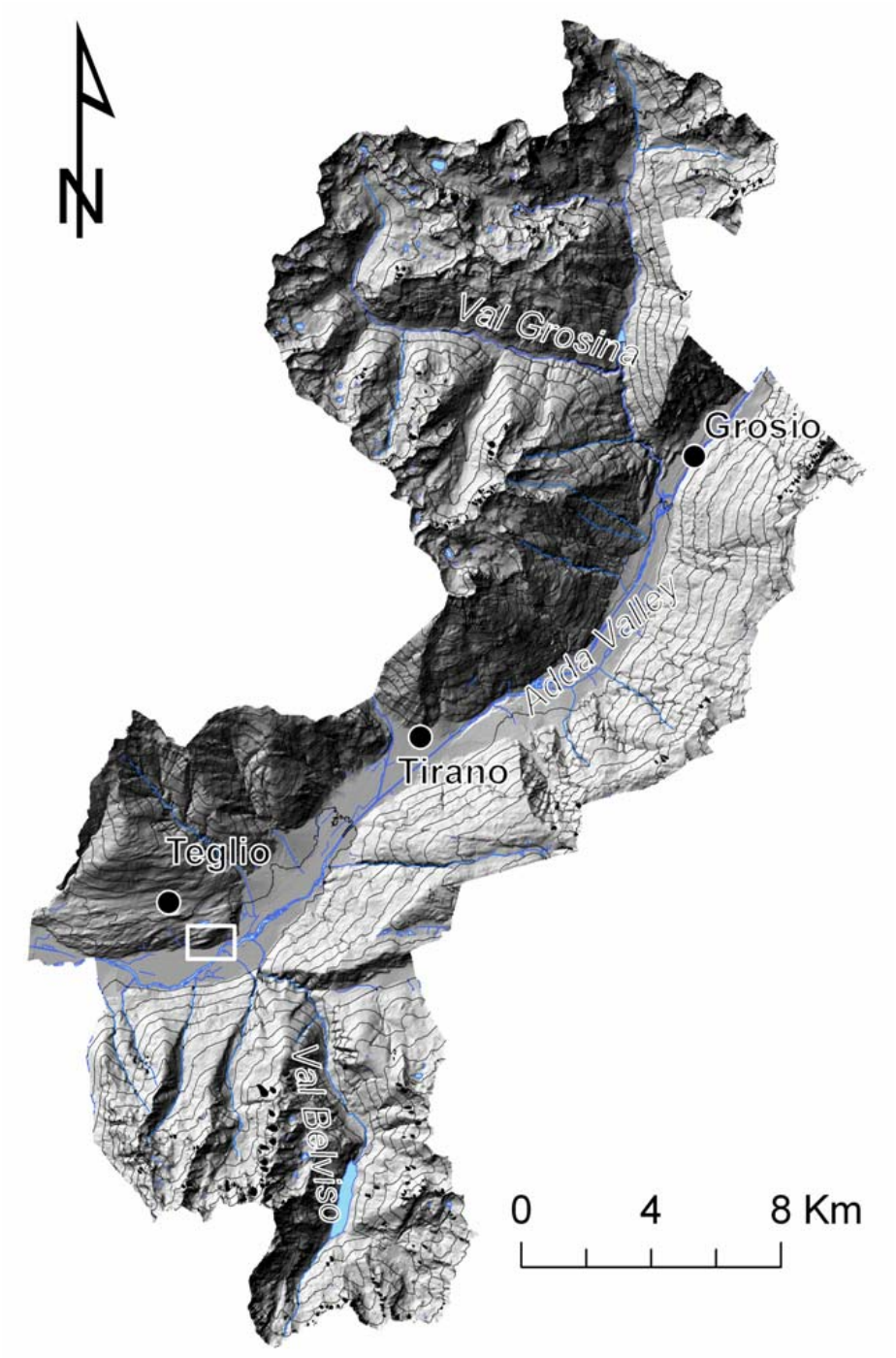

Fig. 11.1 – Location of the Tresenda case study area shown as white rectangle.

11.2.2 Past damaging events

Steep vine-terraced slopes immediately above the village of Tresenda (Fig. 11.2) in Teglio municipality were chosen as they already experienced twice earth-debris flows caused by intense and prolonged rainfalls and dry-stone walls collapse. Both events caused considerable casualties to people and losses to infrastructure and the environment.

In May 1983, severe precipitations triggered more than 200 shallow landslides and debris flows in Valtellina (Cancelli and Nova 1985). In Aprica, a cumulated precipitation of 453 mm was measured during the month, which corresponds to 34% of the total annual precipitation (Guzzetti et al. 1992). Landslides occurred mainly on vine-terraced slopes between Tirano and Sondrio. Most of the landslides started on slopes between 30° and 40°, and were shorter than 50 m (Cancelli and Nova 1985).

In Teglio, on 22nd and 23rd of May 1983, three soil-slips evolved into larger debris flows with lengths from 300 to 460 m and areas reaching 60,000 m^2 (Fig. 11.3) Two of them occurred on 23rd May on the slopes above the village of Tresenda (Fig. 11.4), and the other one on the close slope of Valgella the day before (Fig. 11.5). In Tresenda, a debris flow caused 14 casualties (Cancelli and Nova 1985), buildings were destroyed and properties damaged. The national road S.S. 38 was blocked, and this made impossible to reach the upper part of the valley for few days. In Valgella, 3 victims were reported on 22nd May.

Crosta et al. (2003) described as causes of failure severe precipitation and bad maintenance of dry-stone walls supporting terraces. However, according to interviews with local inhabitants, another important reason is closely connected with the paving of paths and roads on the vineyards, made at the beginning of 80's. As a consequence, the water was unable to infiltrate the soil and was discharged rapidly on the steep roads which acted as channels. The water left the road wherever it was possible (curves, serpentines, etc.) causing a rapid increase of water table which lead to the outburst of dry-stone walls and the consequent development of soil slips-debris flows.

A similar event happened on the same slope on 26th of November 2002 (Fig. 11.3), producing less damage than in year 1983 and, fortunately, no victims. The flow remained confined and caused a minor flooding of the area close to the village due to an obstruction in the drainage channel. In this case the triggering factor was locally emerging groundwater (Di Trapani 2009, personal communication).

Fig. 11.2 – Photograph of Tresenda with vineyards situated on steep slopes above the buildings. Debris flow path from 2002 is recognizable in the central part of the photo. Photo J. Blahut.

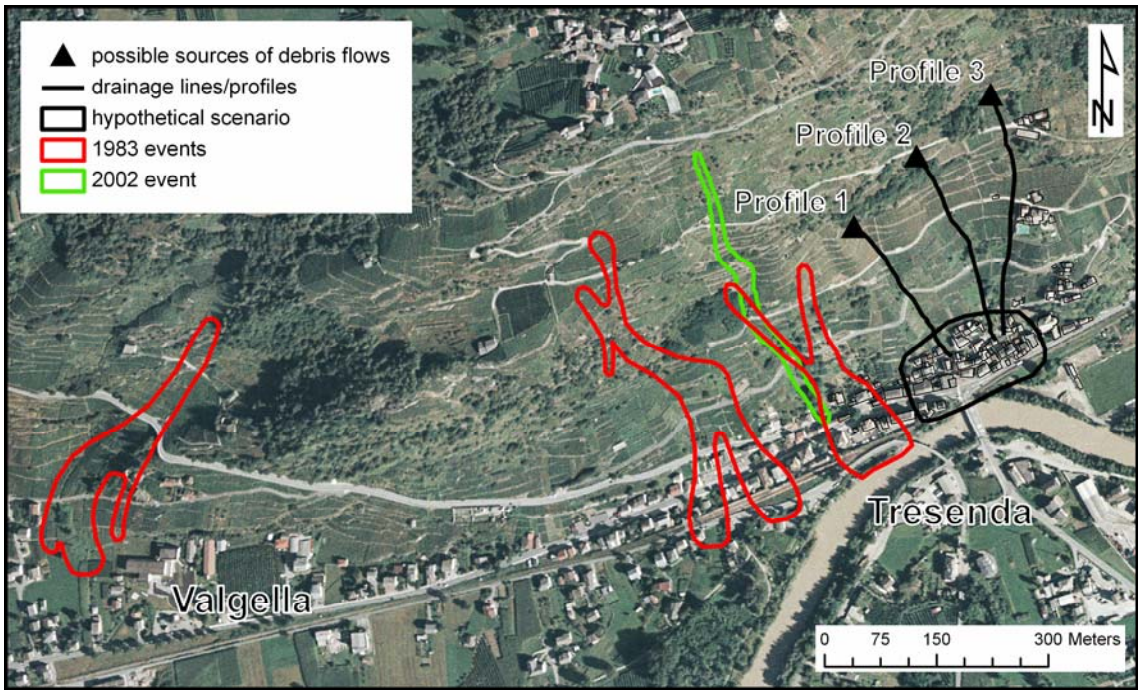

Fig. 11.3 – Delimitation of the 1983 and 2002 debris flow according to GeoIFFI database and CM Valtellina di Tirano. Possible sources and drainage lines/profiles of new debris flows are shown and area of a hypothetical risk scenario is delimited.

Fig. 11.4 – Photographs of two debris flow from 23rd May 1983 in Tresenda. Photo: Archive of CNR-IRPI, Torino.

Fig. 11.5 – Photograph of debris flow from 22nd May 1983 in Valgella. Photo source: Giacomelli (1987).

11.3 Preparation of hazard scenarios

11.3.1 Methodological approach

It was assumed that potential debris flows occurring in the study area will be triggered in areas of high slope and high flow accumulation. After the field surveys and DEM analysis, three potential debris flow sources were selected (Fig. 11.3). These potential sources were modelled in a dynamic numerical approach to assess the runout intensity.

To delimit the hazard of these debris flows, several steps have to be implemented in order to be modelled (Fig. 11.6): (i) detailed analysis and estimation of rainfall return periods for the study area and modelling the rainfall-runoff process based on the different return period scenarios; (ii) filtering of the Airborne Laser Scanning (ALS) digital surface model and analysis of the terrain features; (iii) laboratory tests of soil samples and determination of the debris flow rheology; (iv) estimation of entrainment and sediment concentration of the flow; and (v) modelling of the debris flows.

Firstly, available hourly-rainfall records were used to calculate rainfall return periods of 10, 50, and 100-years. A 48-hour rainfall, which may trigger a debris flow, was simulated in the study area and the time of exceedance of rainfall threshold was investigated for different return periods. The simulated rainfall was used to specify the time when rainfall threshold was exceeded and a debris flow triggered. The rainfall-runoff modelling allowed to specify nine input hydrographs for the three potential debris flow sources and three return periods.

Soil samples were collected during the fieldwork and analysed in geotechnical laboratory. Two representative samples were selected based on the criteria of the proximity location to the initiation and runout zones. Geotechnical parameters and particle size distribution for each sample were obtained and used to compute the failed material caused by the undrained loading of the flow. The calculated failed material was included as sediment concentration in the routed hydrographs to account for the entrained material. Rheological parameters for the dynamic runout model were also inferred based on the laboratory test results.

The debris flows scenarios were modelled with the 2-dimensional depth averaged FLO-2D software. FLO-2D uses a quadratic rheological model that incorporates a Bingham shear stress as a function of sediment concentration, and a combination of turbulent and dispersive stress components based on a modified Manning *n* value.

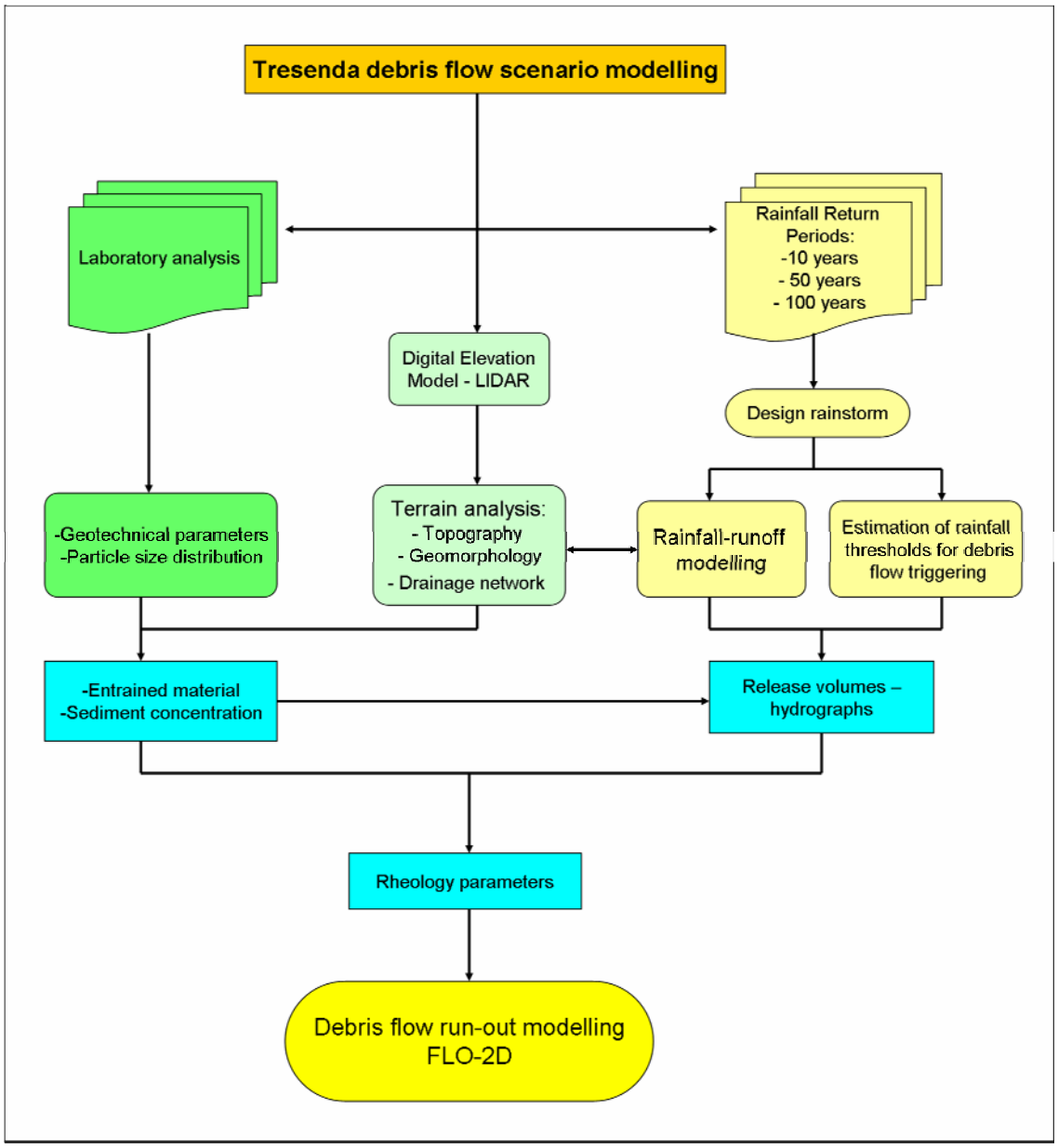

Fig. 11.6 – Flowchart of the debris flow hazard scenario modelling of the Tresenda case study.

11.3.2 Rainfall modelling

Estimation of rainfall return periods

Hourly rainfall data from Castelvetro rain gauge were analysed in order to calculate return periods of rainfalls. Castelvetro rain gauge lies in the vicinity of the study zone, about 3 km west from Tresenda, and is managed by Fojanini Foundation to provide hydro-meteorological information for vine cultivation. The hourly rainfall data available cover a 30-year period from 1980 to 2009.

To calculate the rainfall return period of 10, 50, and 100-years a Gumbel Extreme Value Type I distribution was used (Gumbel 2004). The distribution has following probability density function:

$$f(x) = \frac{1}{\sigma}\exp(-z - \exp(-z)) \tag{11.1}$$

Where: $z = (x-\mu)/\sigma$, μ is the location parameter, and σ is the distribution scale ($\sigma>0$).

The results for the three return periods are summarized in Table 11.1 and Figure 11.7.

Return period	**10**	**50**	**100**
Duration (h)	**Precipitation (mm)**		
1	27.48	36.07	39.70
2	39.57	53.37	59.20
3	45.93	61.31	67.81
6	60.93	80.31	88.50
12	85.40	113.24	125.02
24	111.87	147.30	162.28
48	143.18	191.90	212.49

Table 11.1 – Calculated precipitation for different return periods and rainfall duration.

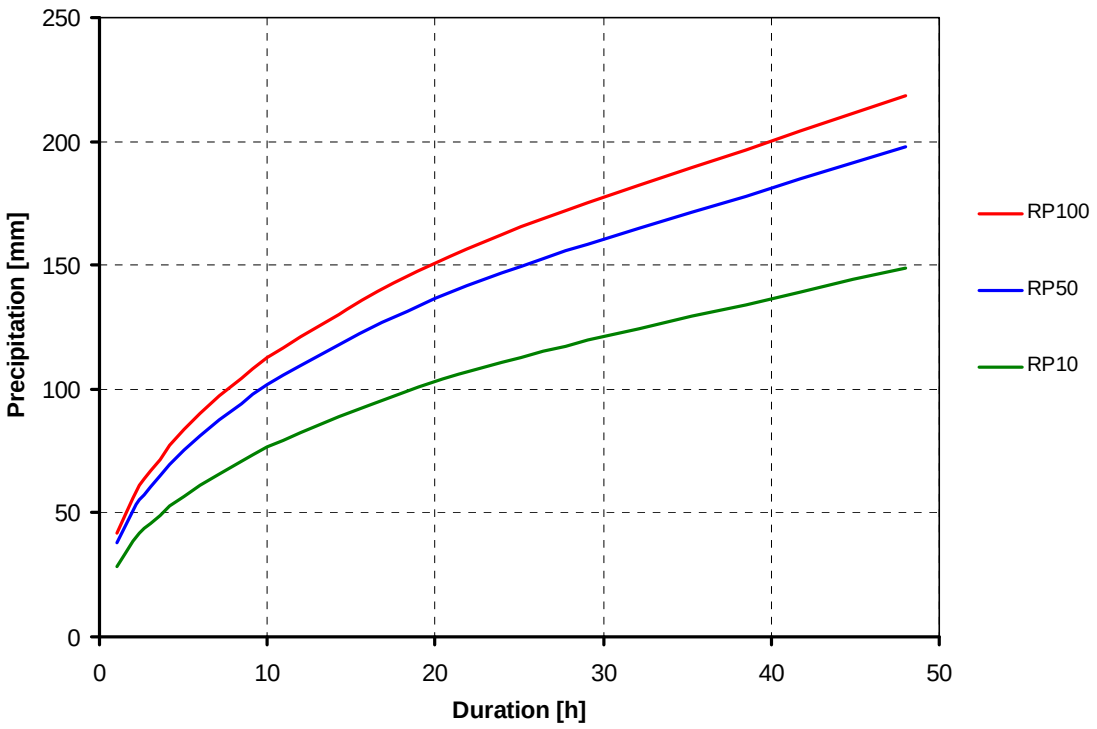

Fig 11.7 – Chart of the calculated precipitation for return periods (RP) of 10, 50 and 100 years for the Castelvetro rain gauge.

Rainfall-runoff simulation

A 48-hour rainfall storm was modelled using the FLO-2D model. 48-hour storm was chosen because historical information (Guzzetti et al. 1992; Crosta et al 2003; Di Trapani, personal communication) showed that past debris flow events, which happened on terraced areas, were usually caused by prolonged rainfalls of duration of more than 1 day.

The storm rainfall is discretized as a cumulative percentage of the total. This discretization of the storm distribution was established through local rainfall data that defines storm duration and intensity. The storm was modelled spatially over the grid system with areas of different intensity of rainfall. The rainfall distribution selected was the SCS non-dimensional distribution. The distribution is expressed as a mass curve indicating what fraction of the total 48-hour precipitation has fallen at any time (Fig. 11.8). This curve was used to calculate the rainfall intensity distribution for all three rainfall return periods.

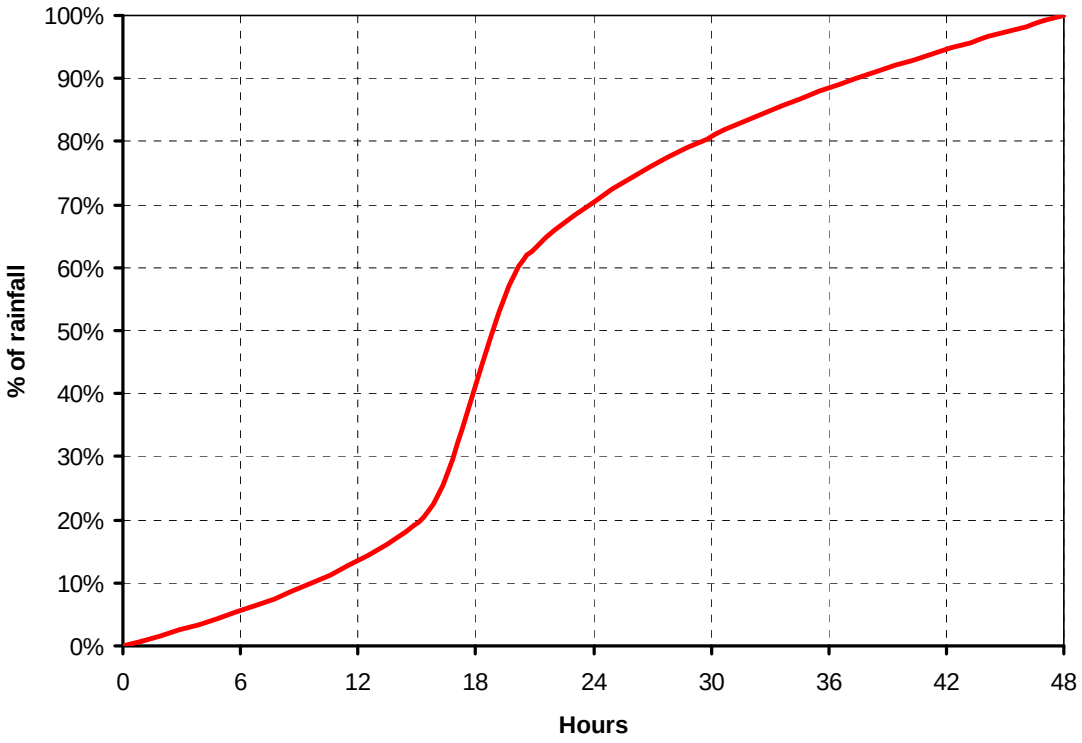

Fig. 11.8 – Chart of the simulated 48-hour rainfall using SCS non-dimensional distribution.

Rainfall threshold exceedance

There are several rainfall thresholds available for the study area (see Chapter 5, Table 5.1). Debris flow initiation thresholds were calculated for all of them, and for the 48-hour rainfall (Table 11.2).

Rainfall thresholds show very similar results, except for the threshold calculated in 2008 by Luino, which shows lower intensities of rainfall to trigger a debris flow. This threshold is sometimes criticized as being too conservative, however it was used to recognize the

initiation time of the debris flows as this represents a recently calculated threshold using all the available data and this study is focused on the worst case scenario preparation. For a 10-year return period this threshold was exceeded after 9.6 hours of rainfall. For a 50-year return period this threshold was reached after 5.76 hours of the modelled rainfall and for the 100-year return period was this threshold reached after 3.84 hours of the modelled rainfall (Fig. 11.9).

Author	Threshold type	Threshold value
Govi et al. (1984)	I-D	2.74 mm/h
Cancelli and Nova (1985)	I-D	2.18 mm/h
Ceriani et al. (1992)	I-D	2.38 mm/h
Agostoni et al. (1997)	IMAP-D	2.51 mm/h
Luino et al. (2008)	IMAP-D	1.74 mm/h

Table 11.2 – Rainfall thresholds for debris flow initiation using a 48-hour rainfall in Castelvetro rain gauge.

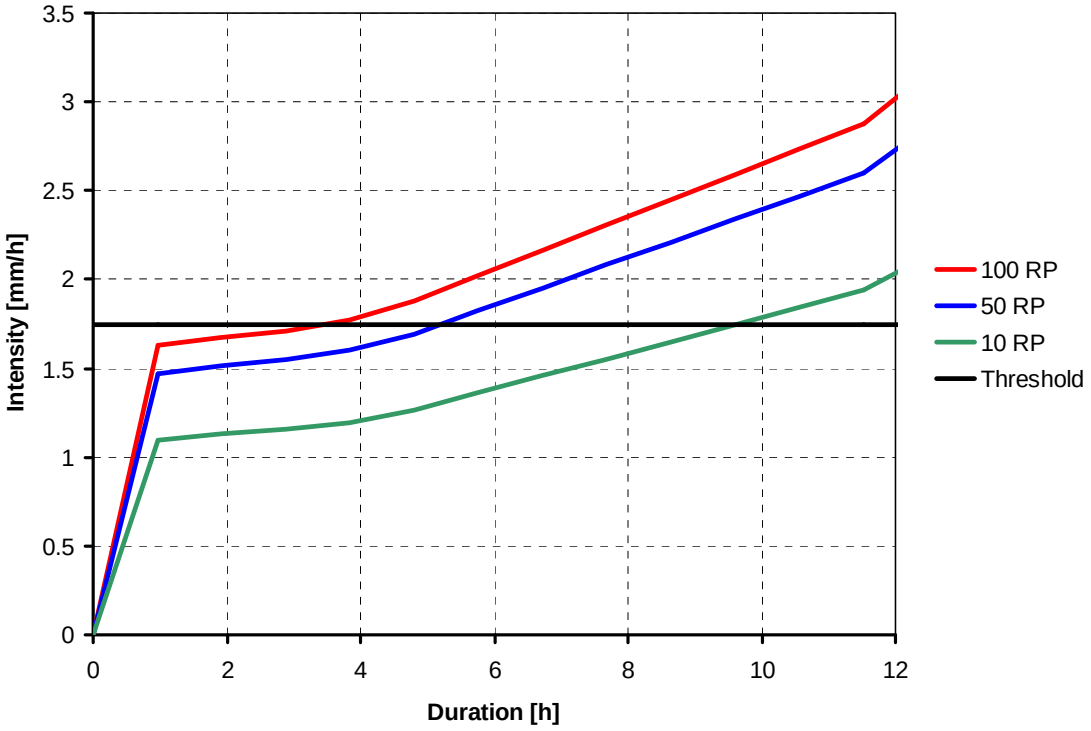

Fig. 11.9 – Threshold exceedance of rainfall intensities of 10, 50, and 100-year return periods for the 48-hour modelled rainfall.

11.3.3 Laboratory analysis

Soil samples were collected between July 2009 and February 2010 along the slope uphill from Tresenda. The materials are mixed loose deposits mostly composed of gravel and sand with a consistent percentage of silt and almost absent clay. According to the Unified Soil Classification System (U.S.C.S.), chosen by the American Society for Testing and Materials (A.S.T.M.) as

standard, they are GM (silty gravel with sand) or SM (silty sand with gravel), with a uniformity coefficient (CU) between 20 and 157. The mean sample has the following composition: gravel 36%, sand 44%, silt 19% and clay 1% (Fig. 11.10). All the samples are very superficial so they are particularly rich of organic matter (3.3-7.3%). The natural water content (W_0) is strictly dependent on the climatic condition during sampling, and its value range from 0.5% to 14.5%. The bulk unit weight (γ_0), measured in place by the sand-cone method, ranges between 13.8-16.1 kN/m^3 while the calculated γ_{dry} ranges between 12.8-15.7 kN/m^3. With an estimated specific gravity of the soil solids (G_s) equal to 27.2 kN/m^3, the calculate porosity (n) is 42-53% and the sediment volumetric concentration varies between 0.47 and 0.58 m^3/m^3. Atterberg limit results are not determinable because of the almost total lack of clay: this means that the studied material pass from the semi-solid to the liquid state in a while. Direct shear tests were performed to obtain the peak and residual values of the shear strength parameters: c_p = 3.4-18.5 kPa; φ_p = 28°-36°;c_r = 0-17 kPa; φ_r = 26°-35°. These values are in good agreement with past laboratory analysis of the area (Cancelli and Nova 1985; Crosta et al. 2003).

11.3.4 Debris flow hazard modelling

The time where the rain storm exceeded the threshold was registered and liquid discharge hydrographs were produced from the rainfall-runoff modelling. Volumes were calculated from the hydrographs peak discharge (Table 11.3). Percentage of sediments based on the entrained material assuming that the flow will have a scouring effect during the course of the flow was added into the hydrographs.

	10 RP		50 RP		100 RP	
	Q	V	Q	V	Q	V
Profile 1	4.89	390.70	11.44	1162.75	13.43	1424.51
Profile 2	4.24	330.91	11.28	1142.79	13.32	1410.27
Profile 3	5.17	425.45	12.13	1251.95	14.12	1518.76

Table 11.3 – Peak discharges (Q) and release volumes (V) in m^3 for the three profiles and different return periods.

Rapid loading by the weight and momentum of a moving mass may cause failure and mobilization of these materials, which can have significantly different properties from the bulk of the initial material (McDougall and Hungr 2005). Sassa (1988) stated the importance of knowing the pore pressure during the motion of the flow. This process assumes the flow travels on the bed deposits causing an undrained loading that generates a high-pore water pressure within the deposits and this helps incorporate the material into the moving mass. Loading of the bed deposits is generated when the sliding mass flows on top. This loading can be estimated by the changes in stresses and strength caused by the moving mass and the increase of pore water pressure. Our analysis is based on the proposed equation (11.2) for change in pore pressures by Sassa (1988) for an undrained direct shear test:

$$\Delta p = B_D(\Delta\sigma + A_D\Delta\tau) \tag{11.2}$$

Where, Δ is the increase of pore pressures, A_D and B_D are the pore pressure parameters in the direct shear state, Δσ is the change in the normal stress, Δτ is the change of shear strength. For further details about the applied entrainment modelling, please refer to Chapter 10, section 10.3.3 .

Based on the laboratory tests of compressibility of the soils and assuming that the soils are not anisotropic, Sassa et al. (1985) proposed that the pore pressure parameter B_D value is affected by the loaded stress level and its value changes with the degree of saturation. In a saturated soil the compressibility of the soil skeleton is almost infinitely greater than that of the pore water and essentially all of a stress increment applied to a saturated soil is carried by the pore fluid. A value of A_D at failure can be assumed for the pore pressure parameter during motion. In general, soft loose soils have high values of A_D and the higher the shear strain the higher the value of A_D. The pore pressure parameters used in our case to compute the increase in pore pressures were A_D = 0.6 and B_D = 0.9, assuming that the soil is in an almost complete saturated state.

Debris flow hydrographs were produced based on the amount of entrained material that the initial release volume could introduce inside the flow (Fig. 11.10, 11.11, 11.12). Based on field observation, a homogeneous erodible in-situ soil depth of 2.5 m was selected as the maximum possible material to be incorporated in the flow during its course.

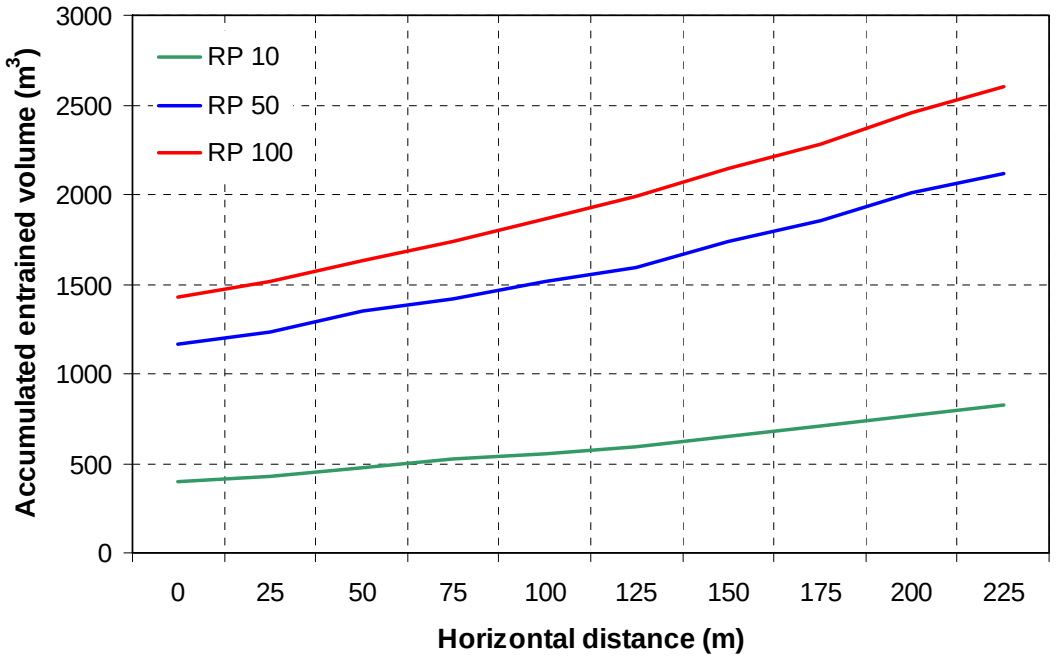

Fig. 11.10 – Accumulated entrained volumes for profile 1.

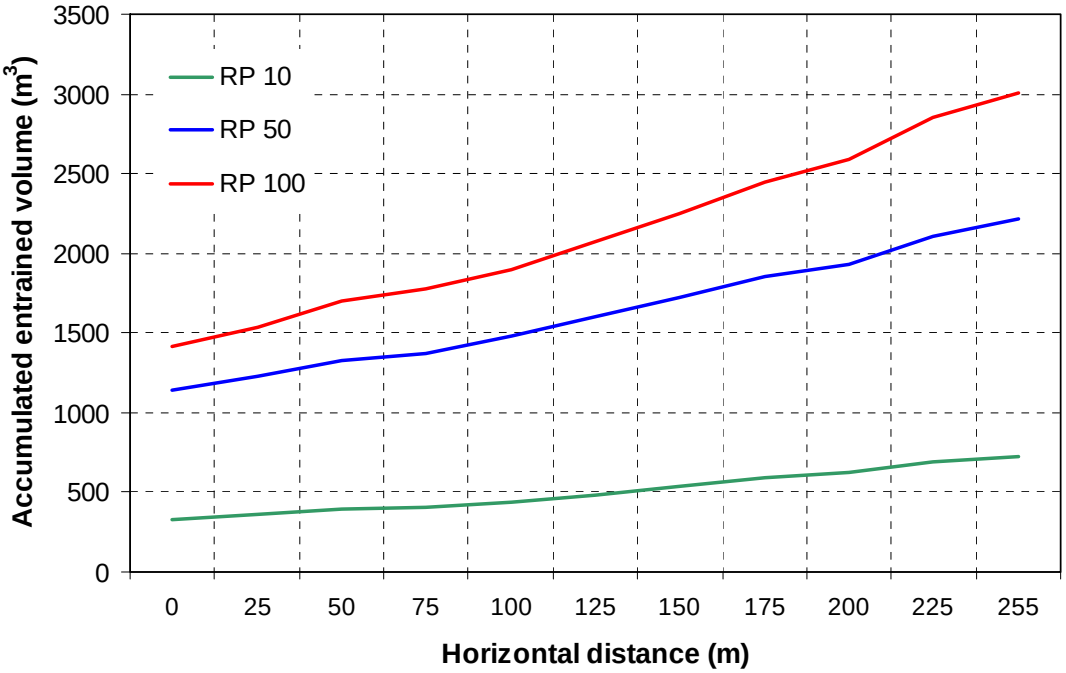

Fig. 11.11 – Accumulated entrained volumes for profile 2.

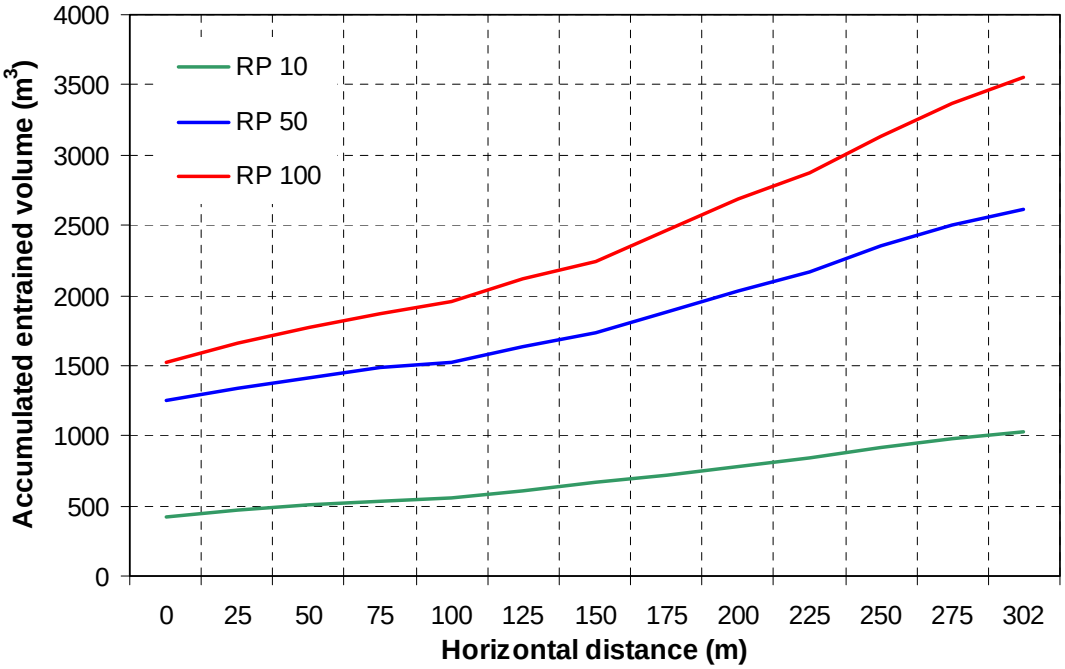

Fig. 11.12 – Accumulated entrained volumes for profile 3.

The debris flows runout was modelled with the FLO-2D software. For further description about the model, please see Chapter 10, section 10.3.1.

Time-stage hydrographs used as inputs inside the model were calculated using variable sediment concentrations based on the results of the entrainment/sedimentation analysis. The rheological properties of the flow were estimated based on the results of the laboratory analysis. The final parameters used in the modelling were τ_y = 1,500 Pa and η = 2,800 Pa. These

parameters agree with the amount of sediment concentration entrained by the flow and the particle size distribution. On this basis, appropriate values of α and β were selected from the set of materials presented by O'Brien and Julien (1988) and suggested in the user manual of FLO-2D (2009). A *K*-value of 2480 was used for a rough surface. The Manning *n*-value that characterises the roughness of the terrain was selected as 0.04 $sm^{1/3}$; this value corresponds to the lower bound for open ground with no debris. The above definitions are established in the FLO-2D user's manual (FLO-2D 2009) and are based on guides and manuals published by the United States Army Corps of Engineers.

11.4 Quantification of risk and prospective economic damage

Quantification of damage to buildings in the case study was done by examination of the results from the hazard modelling to the respective building. As in the Selvetta case study (Chapter 10), average heights of accumulation and highest impact pressures near the walls, oriented towards the expected flow direction, were extracted for each interested building. The results were used to calculate risk maps for the three return periods by using two vulnerability curves (for heights and impact pressures, respectively). Direct losses to the buildings were calculated by multiplying the calculated vulnerability by the building value (Fig. 11.13).

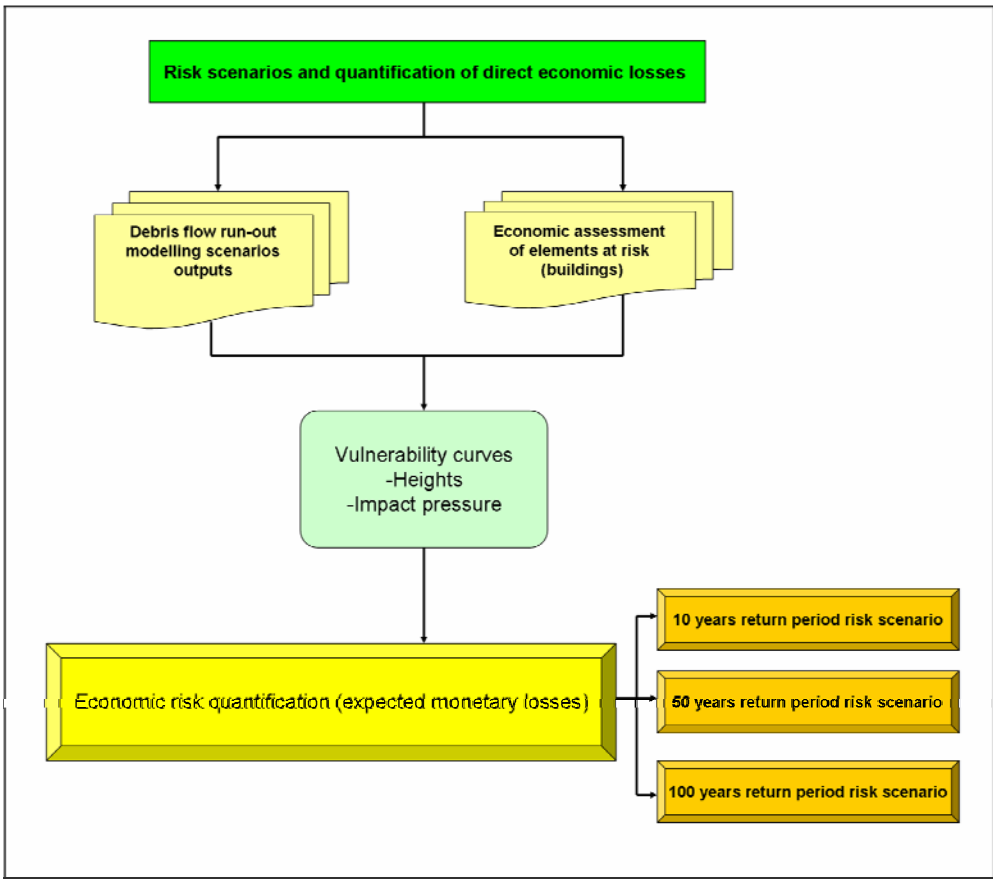

Fig. 11.13 – Flowchart of the methodological framework for the risk scenario quantification.

11.4.1 Elements at risk in the study area

There are 111 buildings in the immediate vicinity of the Tresenda scenario, 57 of them within the delimited hypothetical scenario area (Fig. 11.3). Majority of them are three storey buildings constructed with brick masonry and concrete structures. Value of each building was estimated using the construction prices provided by Engineers and Architects of Milan (DEI 2006). According to them, a construction cost of 801 €/m^2 corresponds to single standing house with 2-3 storeys. The value of the buildings was calculated by multiplying their area from the DB2000 (2003) database by the number of floors and by the reconstruction value per m^2. Total value of the buildings within the scenario area is reaching € 14,895,500 with a range from € 34,360 to € 1,079,000 for a single building, and with an average reconstruction cost of € 261,324 per building.

Beside the buildings, a state road S.S.38 lies between the buildings and the Adda River and minor paved roads are present. A principal railway line is running along the state road, connecting province capital Sondrio with Tirano and Switzerland upstream the Adda River. According to the database of Registry Office, 173 people are living in the houses within the delimited scenario. In this approach, only economic risk to buildings is quantified, neglecting the damage to other infrastructure and to the people living in the area.

11.4.2 Hazard scenarios and damage to buildings

Totally six hazard scenarios were prepared, for each return period and for accumulation heights and impact pressures, respectively. The results are presented in Figures 11.14, 11.15, and 11.16 showing the difference in the magnitude of the hazard. Moreover, information about the possible damage to the houses is shown, resulting from the calculated vulnerability using the respective vulnerability function (see Chapter 10). Light damage means vulnerability between 0 and 0.1, medium damage represents vulnerability 0.1-0.5 and heavy damage relates to vulnerabilities between 0.5 and 1. Destruction means that vulnerability of 1 was reached.

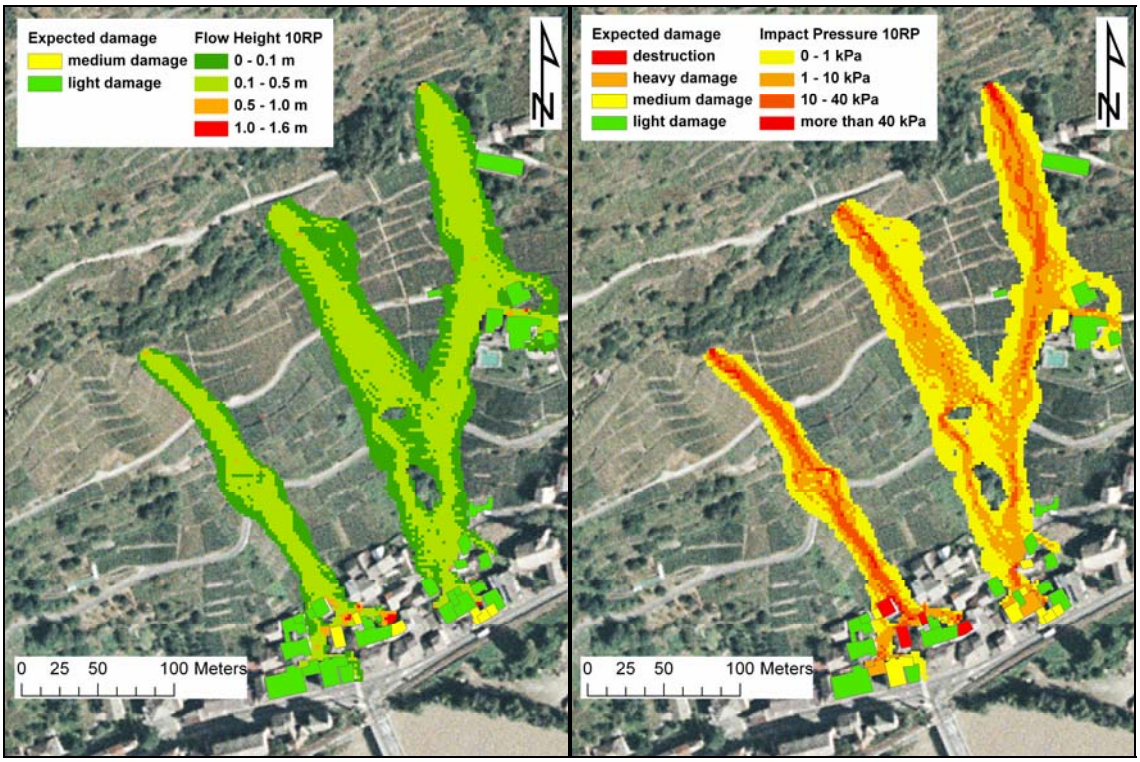

Fig. 11.14 – Results of the hazard modelling for the 10-year return period showing the calculated degree of damage to the buildings. On the left height of accumulation, on the right impact pressures.

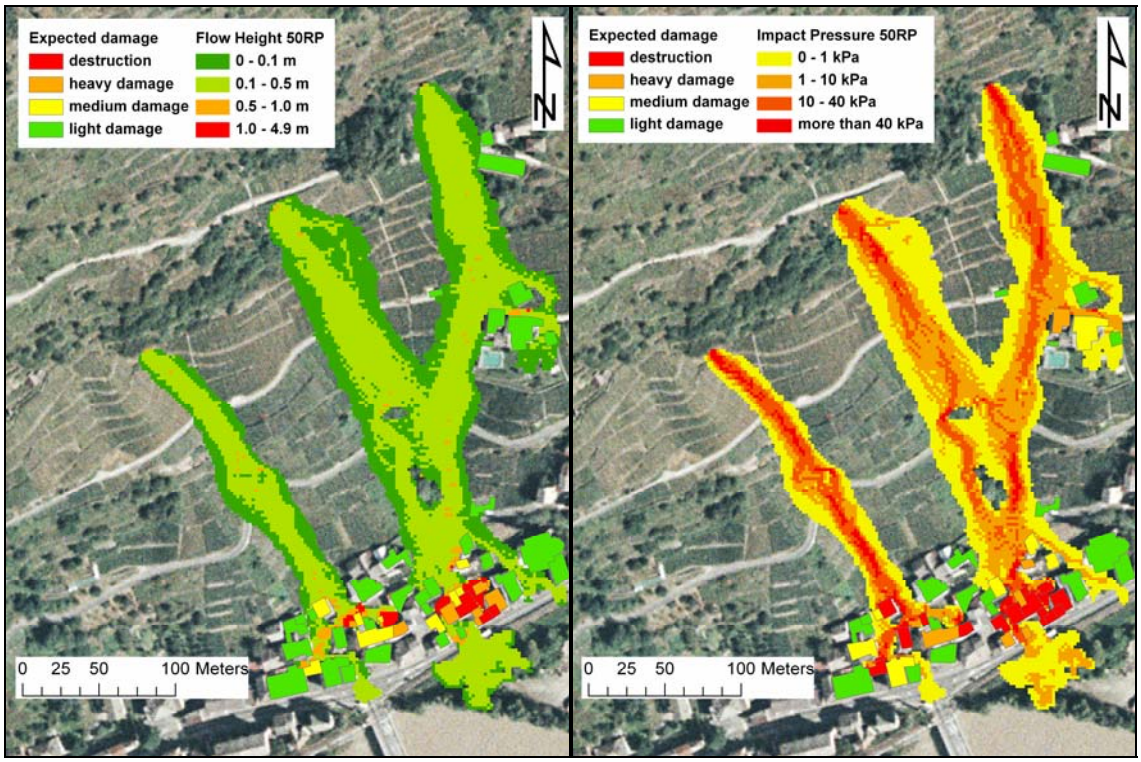

Fig. 11.15 – Results of the hazard modelling for the 50-year return period showing the calculated degree of damage to the buildings. On the left height of accumulation, on the right impact pressures.

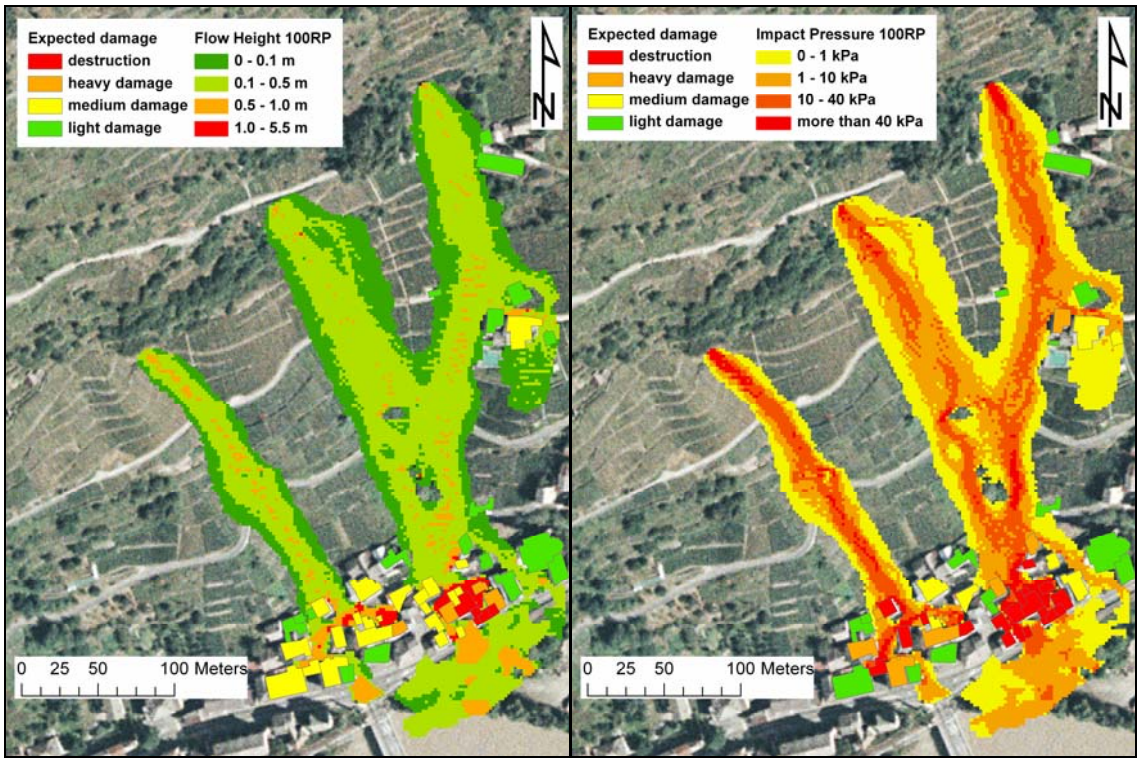

Fig. 11.16 – Results of the hazard modelling for the 100-year return period showing the calculated degree of damage to the buildings. On the left height of accumulation, on the right impact pressures.

11.4.3 Risk scenarios and quantification of direct economic losses

10-year return period

In the hazard scenario considering the 10-year return period (0.1 probability) of the debris flows, 35 buildings are likely to be impacted. After the application of the vulnerability function using as an intensity parameter height of accumulation, 29 buildings will suffer light damage and 6 buildings medium damage. None of the buildings will be destroyed or suffer heavy structural damage. After application of the impact pressure vulnerability function, very different risk pattern appears: 19 buildings will suffer light damage, 10 buildings will have medium damage and 2 buildings will be heavily damaged. Three buildings are likely to be destroyed in this scenario. These results are very different one from another and the question about the appropriate vulnerability function arises. The difference is mostly caused by the fact, that the flow heights in Tresenda are much lower (up to 1.6 m) than those observed in the Selvetta study case (reaching more than 4 m). After an expert evaluation, it turned out that the use of impact pressure vulnerability function is probably more appropriate in this case, as the volume of sediments mobilised is much lower than in the Selvetta case and the water content is higher. According to previous debris flow events in Tresenda in 1983, even small height of debris flow (up to 1 m) is probably able to destroy a house.

The total direct damage to houses is considerably affected by the use of different vulnerability functions. Considering the height vulnerability function, the direct damage reaches € 610,088. In the case of impact pressure vulnerability function, the total direct monetary loss to the buildings is estimated to € 2,059,321 (337.55% of the first damage estimate). Risk levels

span from 0 (no risk) to 8,271 €/year for a single building in case of the height of accumulation vulnerability function and from 0 to 27,780 €/year for a single building in case of the use of impact pressure vulnerability function (Fig 11.17).

50-year return period

In the 50-year return period hazard scenario (0.02 probability), 49 buildings are likely to be impacted. After the application of the vulnerability function using as an intensity parameter height of accumulation, 32 buildings will suffer light damage, 9 buildings medium damage, and 5 buildings high damage. Three buildings will be completely destroyed. After application of the impact pressure vulnerability function, different results were obtained: 21 buildings will suffer light damage, 8 buildings will have medium damage and 6 buildings will have heavy damage. Fourteen buildings will be probably destroyed. These results show the same pattern as in the case of 10-year return period. However, as this scenario considers much higher debris flow volume, higher accumulations of deposits are reached, resulting in higher expected damage.

The total direct damage to houses is considerably affected by the used of the different vulnerability functions as in the case of the previous scenario. Considering the height of accumulation vulnerability function, the direct damage reaches € 2,311,219. In the case of impact pressure vulnerability function, it reaches € 5,059,011. This is 218.89 % of the first damage estimate, which is lower than the previous case. Risk reaches 7,644 €/year for a single building in both cases of risk calculation (Fig. 11.18).

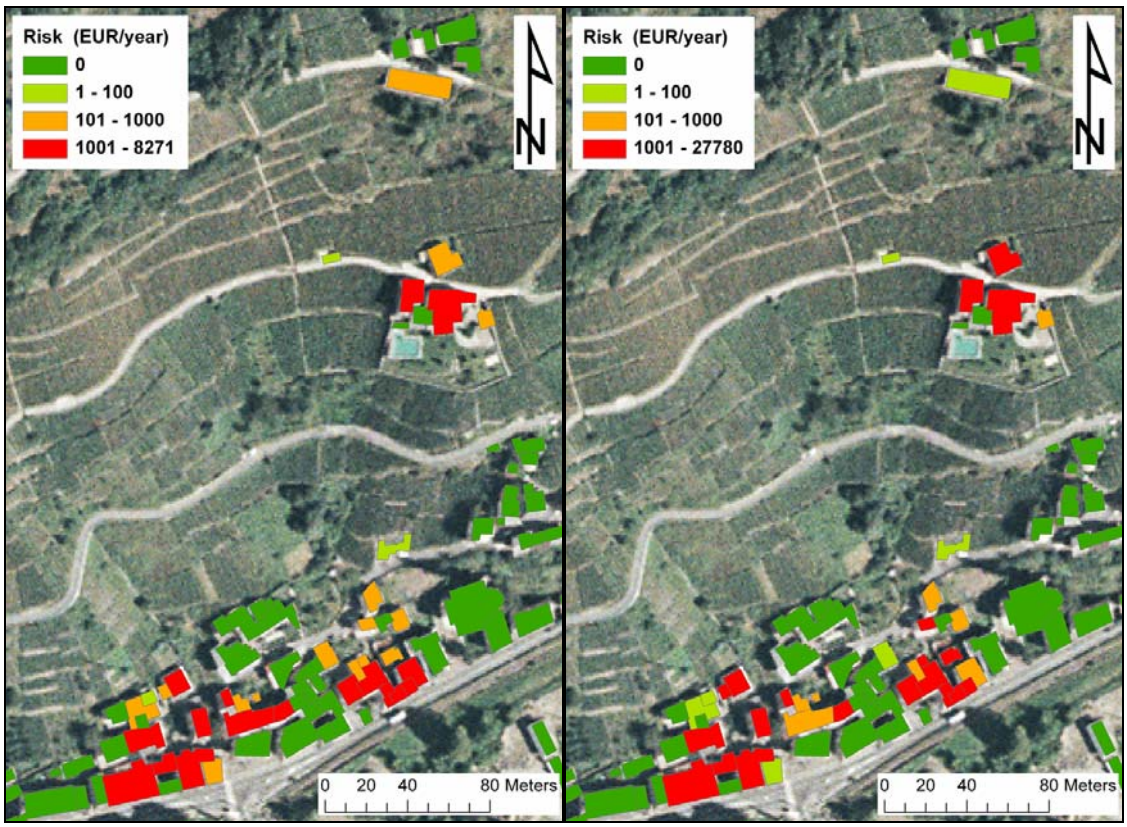

Fig. 11.17 – Risk maps for a 10-year return period debris flows using heights of accumulation vulnerability curve (on the left) and impact pressure vulnerability curve (on the right). The risk is expressed in a monetary terms as expected damage in €/year per exposed building.

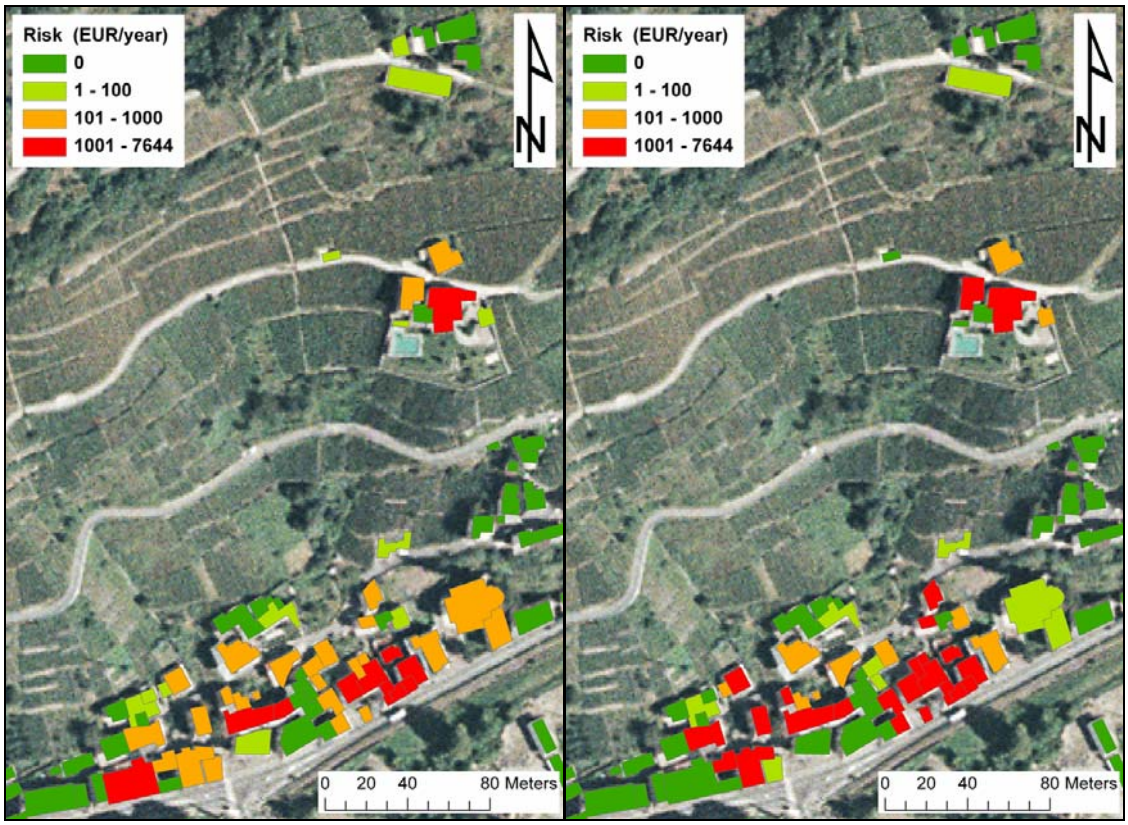

Fig. 11.18 – Risk maps for a 50-year return period debris flows using heights of accumulation vulnerability curve (on the left) and impact pressure vulnerability curve (on the right). The risk is expressed in a monetary terms as expected damage in €/year per exposed building.

100-year return period

In the 100-year return period hazard scenario (0.01 probability), 49 buildings are likely to be impacted as in the case of the 50-year scenario. After the application of the vulnerability function using as an intensity parameter height of accumulation, 19 buildings will suffer light damage, 22 buildings medium damage, and 4 buildings high damage. Four buildings will be completely destroyed. After application of the impact pressure vulnerability function, higher damage pattern was obtained: 16 buildings will suffer light damage, 7 buildings will have medium damage and 8 buildings will have heavy damage. Eighteen buildings will be probably destroyed. These results show the same pattern as in the case of 10 and 50-year return periods. The number of affected houses is similar to the previous scenario. Expected damage is, however, much higher.

The total direct damage to houses is considerably affected by the used of the different vulnerability functions as in the case of the previous scenarios. Considering the height of accumulation vulnerability function, the direct damage reaches € 3,151,675. In the case of impact pressure vulnerability function application, the total direct monetary loss to the buildings is estimated to € 6,453,366 (204.76%). This estimate is only two times higher (much lower than in previous 10 and 50-year return period scenarios). Risk reaches 3,822 €/year for a single building in case of the accumulation heights vulnerability calculation and 6,127 €/year for a single building in case of the impact pressure use (Fig. 11.19).

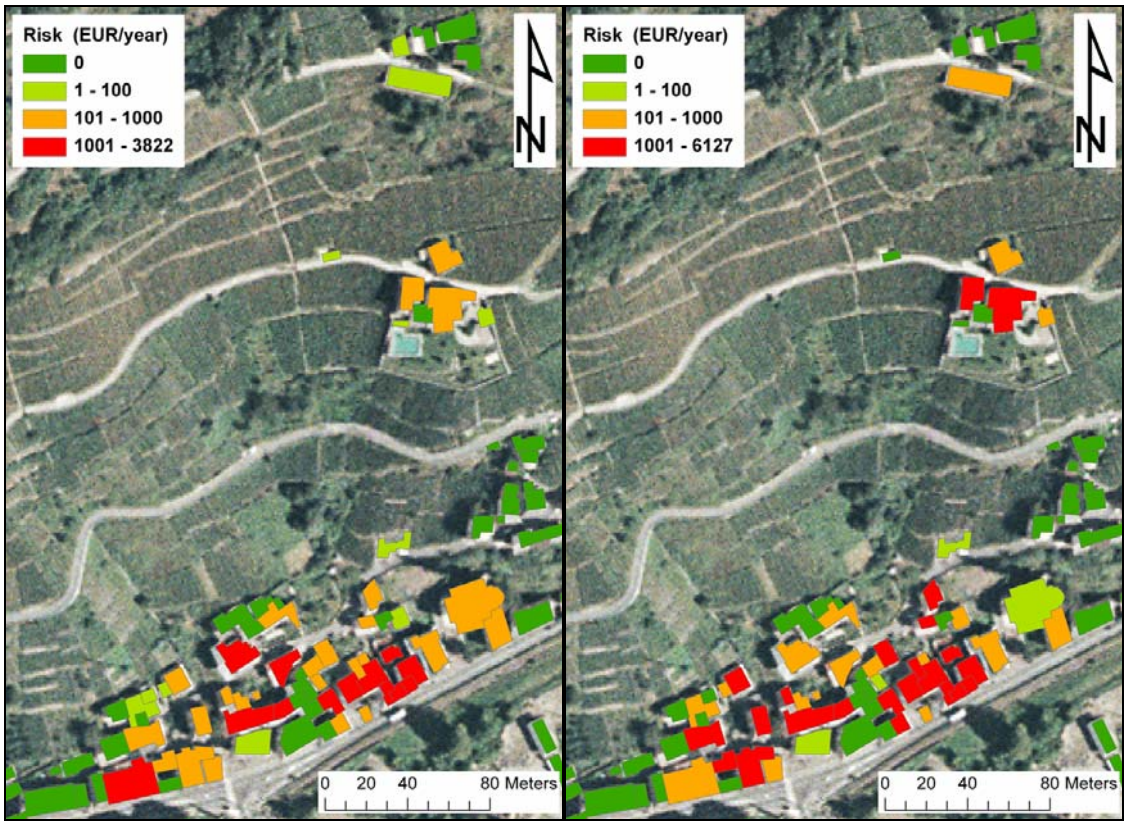

Fig. 11.19 – Risk maps for a 100-year return period debris flows using heights of accumulation vulnerability curve (on the left) and impact pressure vulnerability curve (on the right). The risk is expressed in a monetary terms as expected damage in €/year per exposed building.

Risk and damage estimates comparison

Six risk scenarios were compared (for the three return periods and for the two vulnerability functions each). The results are summarized in Figure 11.20. It can be noted that the total damage estimate is increasing with the debris flows magnitude. There are, however, considerable differences between the estimates for the same return periods. Usage of impact pressure vulnerability curve gives higher estimates than the application of height of accumulation vulnerability function. This difference is, however, decreasing with the magnitude/volume of the debris flows. This situation is most probably caused by different behaviour, magnitude and velocities of the debris flows than in case of the Selvetta case study (Chapter 10), which affects most the calculated impact pressures. Moreover, the distribution of elements over the entire slope is different from the Selvetta situation where the buildings were situated on the fan at minimum of some meters from its apex.

Vulnerability estimates comparison

The results show that high difference between the two vulnerability curves applied arises when they are used for the prospective damage estimation. The comparison of the results is shown in Figure 11.21. In an ideal case, the comparison between the curves would make a straight line going from 0 to 1. However, the scatter cloud shows the differences for each potentially affected building. Height accumulation vulnerability curve is probably underestimating the final results, because it was calculated from a very specific debris flow reaching high accumulation heights

with low velocities in the deposition area. This is different from the modelling results in Tresenda where lower accumulation heights-high velocity debris flows can be expected to arrive in the deposition zone.

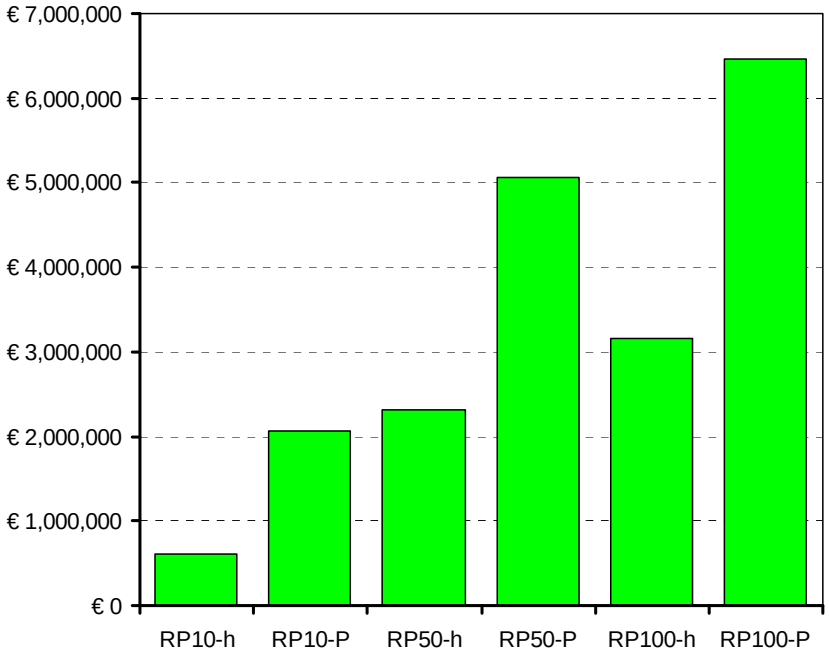

Fig. 11.20 – Comparison of loss estimations for the three return periods using two vulnerability curves. RP – return period; h – height of accumulation vulnerability function; P – impact pressure vulnerability function.

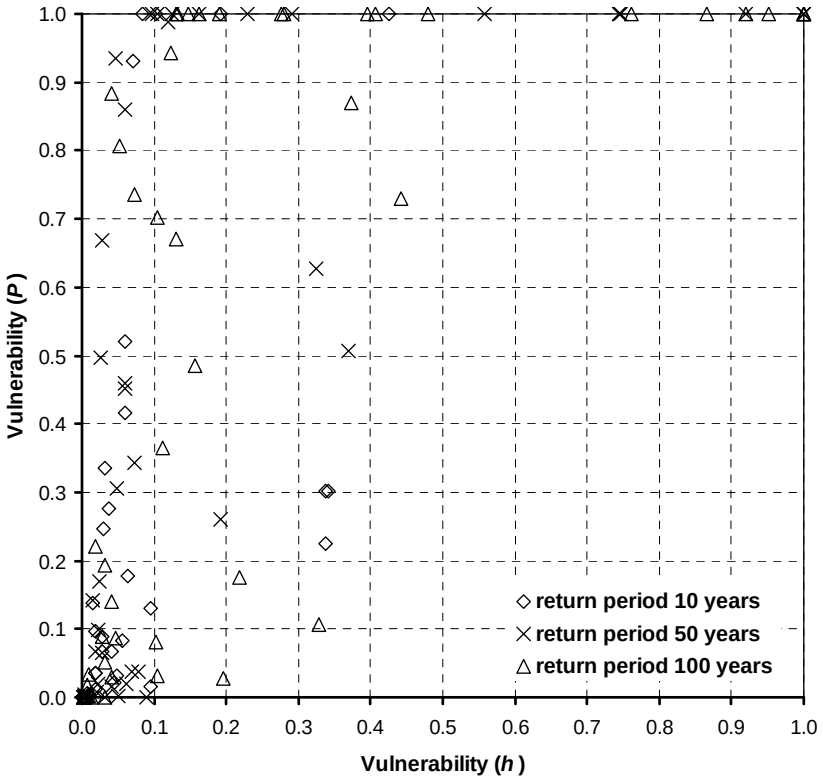

Fig. 11.21 – Comparison of vulnerability estimates for three return periods using two vulnerability curves.

11.4.4 Limitations of the results

The modelling itself as well as the results allow to express the economic risk to exposed buildings in a quantitative way. However, there are still some limitations, which need to be addressed. Firstly, it is assumed that the return period of a rainfall, potentially causing a debris flow, is the same as the return period of the resulting debris flow. Other assumptions arise from the modelling itself: DEM resolution, rheological properties acquired in the laboratory and upscaled to the entire area, entrainment modelling hypotheses, and volume estimates. Other implications arise from the application of vulnerability curves obtained in the Selvetta study case and applied to Tresenda scenario which might seriously affect the resulting damage and risk estimates.

Estimated economic value of the building has also important effect on the results, as it is assumed similar unit value of buildings, neglecting its particular conditions and current state. Finally, estimates about the value of the furniture and expenses needed to remove and re-deposit the debris material, or damage to the roads and lifelines are not taken into account.

It turned out, that the use of impact pressure-based vulnerability curve is giving much higher damage estimates than the accumulation height-based vulnerability curve. In our opinion, the use of impact pressures is more reliable as the direct effects on the stability conditions of the buildings can be assessed on a case-by-case basis considering the particular conditions of each building.

Besides the presented limitations, we believe that the approach applied in this analysis is generally applicable to other areas and may give important information to the local stakeholders.

11.5 Concluding remarks

Presented approach allowed to assess debris flow hazard and risk in a quantitative way and to calculate prospective direct damage to buildings in the case study area. Direct economic losses to the buildings were estimated, reaching € 610,088 to 6,453,366, depending on the hazard scenario and vulnerability curve used. This is more than 10-times difference in the estimate supporting the importance of a deep analysis.

The approach proposed in this study may assist local decision makers in determining the nature and magnitude of the expected losses due to a dangerous event. Besides, a preventive knowledge of the prospective physical effects and economic consequences may help to properly allocate financial resources for disaster prevention and for mitigation measures. Improved information may support decision makers on how to allocate and manage resources to deal with future hazards in the area.

It is obvious that the approach still has some weak points (e.g. delimitation of initiation areas, assessment of people's vulnerability, etc.). However, beside its limitations, it increases the knowledge about prospective outcomes of future hazards and thus contributes to the protection of the people and their assets.

11.6 References

Agostoni, S., Laffi, R., Sciesa, E. (1997): Centri abitati instabili della provincia di Sondrio. CNR-GNDCI, Milano, 59 pp. + Annexes.

Alexander, D. (1999): How are emergency plans written, tested and revised? In: Fontanari, P., Pittino, S., Alexander, D., Boncinelli, S. (Eds.): La protezione civile verso gli anni 2000. CISPRO, CNR, Florence, pp. 151-177.

Alexander, D. (2000): Confronting Catastrophe: New Perspectives on Natural Disasters. Terra Publishing, Harpenden, 282 p.

Alexander, D.E. (2002): Principles of Emergency Planning and Management. Oxford University Press, New York, 374 p.

Cancelli, A., Nova, R. (1985): Landslides in soil debris cover triggered by rainstorms in Valtellina (Central Alps – Italy). In: Proceedings of 4th International Conference and Field Workshop on Landslides. The Japan Geological Society, Tokyo, pp. 267–272.

Ceriani, M., Lauzi, S., Padovan, N. (1992): Rainfall and landslides in the Alpine area of Lombardia Region, Central Alps, Italy. In: Proceedings of the Internationales Symposium Interpraevent. Bern, 2: 9-20.

Crosta, G.B., Dal Negro, P., Frattini, P. (2003): Soil slips and debris flows on terraced slopes. Natural Hazards and Earth System Sciences, 3: 31-42.

Daines, G.E. (1991): Planning, training and exercising. In: Drabek, T.E., Hoetmer, G.J. (Eds.): Emergency Management: Principles and Practice for Local Government. International City Management Association, Washington, D.C..

DB2000 (2003): Database of the CM Valtellina di Tirano mapped at 1:2,000 scale. CM Valtellina di Tirano. CD-ROM.
Available at: http://www.cmtirano.so.it/sistemainformativo.php

DEI (2006): Prezzi Tipologie Edilizie 2006. DEI Tipografia del Genio Civilie. CD-ROM.

Drabek, T.E., Hoetmer, G.J. (1991): Emergency Management: Principles and Practice for Local Government. International City Management Association, Washington, D.C., 416 p.

FLO-2D (2009): Reference manual 2009. FLO-2D Software Inc., 73 p. Available at: http://www.flo-2d.com/wp-content/uploads/FLO-2D-Reference-Manual-2009.pdf

Foster, H.D. (1980): Disaster Planning: The Preservation of Life and Property. Springer-Verlag, New York, 275 p.

Giacomelli, L. (1987): Speciale Valtellina 1987: Cronaca, storia, commenti. Notiziario della Banca Popolare di Sondrio, No. 45, Bergamo, 227 p.

Govi, M., Mortara, G., Sorzana, P. (1984): Eventi idrologici e frane. Geologia Applicata e Idrogeologia, XCVIII, 3 p.

Gumbel, E.J. (2004): Statistics of extremes. reprint of the 1958 edition, Dover Publications, Mineola, 375 p.

Guzzetti, F., Crosta, G., Marchetti, M., Reichenbach, P. (1992): Debris flows triggered by the July, 17–19, 1987 storm in the Valtellina area (Northern Italy). International Symposium Interpraevent 1992, Bern, Switzerland, pp. 193-203.

Luino, F., Nigrelli, G., Biddoccu, M., Cirio, C.G., Di Palma, M., Missaglia, M., Fassi, P. (2008): Definizione delle soglie pluviometriche d´innesco di frane superficiali e colate torrentizie: accorpamento per aree omogenee. IRER, Milano, 125 p.

McDougall, S., Hungr, O. (2005): Dynamic modelling of entrainment in rapid landslides. Canadian Geotechnical Journal, 42(5): 1437-1448.

O'Brien J.S., Julien, P.Y. (1988): Laboratory analysis of mudflow properties. Journal of Hydraulic Engineering, 114(8): 877-887.

Sassa, K. (1988): Geotechnical model for the motion of landslides. In: Proceedings of 5th International Symposium on Landslides. Balkema, Rotterdam, pp. 37-55.

Sassa, K., Kaibori, M., Kitera, N. (1985): Liquefaction and undrained shear of torrent deposits as the cause of debris flows. Proceedings of the International Symposium on Erosion, Debris flows and Disaster Prevention, pp. 231-236.

Sterlacchini, S., Akbas, S.O., Blahut, J., Frigerio, S., Poretti, I., De Amicis, M., Sironi, S. (2010): A Methodological Approach for Landslide Risk Assessment and Loss Estimation – Application to the Village of Tresenda, Valtellina di Tirano, Italy. Natural Hazards and Earth System Sciences. (submitted – under review).

Chapter 12

Conclusions

The difference between stupidity and genius
is that genius has its limits.

(A. Einstein)

12.1 Specific findings

During my Ph.D. research studies tasks presented at the beginning of thesis were accomplished. Firstly, historical information about natural disasters was collected for the study area of CM Valtellina di Tirano. A geo-database was consequently built to visualize these records. The database couples information from available sources (i.e. official databases, newspaper articles, historical records) and it covers period from year 1600 till 2008. It turned out, that this database is a valuable source of information. It provides first overview of the natural hazards acting in the study area and it shows how disastrous these hazards can be. However, this database could not be used for further hazard analyses due to the fact that temporal information about the hazards is mainly limited to the year of occurrence. Nevertheless, this database can be used as a valuable source of information by local planners and civil protection authorities to delimit areas of higher occurrence of past disastrous events and to show approximate magnitudes of these events.

Further steps of the hazard and risk analysis focused on debris flows. Debris flows were chosen because they represent very dangerous phenomena because of their hard prediction and high damage potential. Most effort was made in debris flow risk analysis at medium scale (1:25,000 – 50,000). At the beginning of the work, a new debris flow scarps database was prepared from the existing official database GeoIFFI, DEM, and aerial photographs with photo-interpretation techniques. Consequently, the new and the official databases were compared to thematic layers in order to find causative factors of debris flows. Afterwards, a Weights-of-Evidence modelling technique was applied to randomly and spatially divided inventories and the best resulting model – susceptibility map – was chosen according to the standard model evaluation techniques. It turned out however, that standard techniques have an important feedback of loss of information. For that purpose, an assessment of the spatial agreement of susceptibility map was performed using advanced statistical techniques (Kappa statistic, PCA, DWE). The results show that even standard techniques show very similar results, the map's spatial pattern may be quite different. As a consequence, special attention has to be paid on correct selection of thematic layers which enter into the analysis as explanatory variables. Moreover, the results from the susceptibility analysis have to be confronted to the real situation in the field in order to avoid sever mistakes.

Analysis of temporal probability of debris flows was performed by comparing two temporal debris flow inventories. It turned out, that this approach has several limitations caused mainly by the temporal span between aerial photographs that are used for the construction of the inventories. This temporal span (20 years) caused that some debris flow scarp were very hard to recognize and probably not all of the scarps have been considered in the analysis. This problem can be over passed by using multi-temporal inventories acquired with shorter time span. However, at the time of this study these datasets were not available. The analysed temporal probability was consequently coupled with information from the susceptibility map into debris flow initiation hazard map. This map was used together with the DEM as inputs of the consequent runout assessment. The DFGridProb model for regional debris flow runout and

spreading mapping was used to delimit areas of very high, high, medium and low debris flow hazard. Main advantage of the model is that works even with limited data (DEM) and is able to calculate the spreading areas very fast which allows rapid preparation of first results. The model was calibrated for large debris flows recorded in the study area using aerial photographs. Moreover, a qualitative component of spreading was added to the hazard map which allows to distinguish areas of higher probability of being hit by a future debris flow.

Information about the debris flow hazard was coupled with the information about elements at risk in order to calculate quantitative economic (specific) risk maps and qualitative total risk map. The value of the elements at risk was assigned using official sources about agricultural and forest land values and market values of the real estates. In case roads (public property), only reconstruction values were used. Two economic risk maps were calculated with corresponding risk curves. The risk curves give information to the stakeholder about prospective economic costs and losses which may originate in the area. It has to be noted, however, that these values have high level of uncertainty, which increased during all steps of the analysis. A qualitative risk map was also prepared using official elements at risk classification and a risk matrix. This map depicts the total debris flow risk better than economic risk maps but it has to be taken in mind that classification of the elements at risk, as well as the final map, has important level of subjectivity.

At local scale (1:2,000 – 1:10,000) two case studies were analysed. Recent damaging debris flow event from July 2008 in Selvetta allowed to gather extensive information about the process characteristics as well as the caused damage. This permitted to back-calculate the event and derive physical vulnerability curves which were consequently used in the second case study scenario. It was showed, that vulnerability curves derived from modelling match quite well existing debris flow and snow avalanche vulnerability curves. However, more data is needed to increase the robustness of these curves and to transfer them in other mountain regions.

Second case study was situated in Tresenda, place where debris flows took lives of 14 people in 1983. Available data allowed to prepare three hazard scenarios for rainfall return periods of 10, 50, and 100-years. Afterwards two vulnerability functions obtained in the Selvetta study case were applied to the results of the modelling in order to obtain quantification of risk and direct economic damage. Results show, beside its limitations, that usage of vulnerability functions allow to better estimate the prospective losses and to evaluate the risk in a really quantitative way. This information is of great importance for the local stakeholders (municipality, civil protection, CM Valtellina di Tirano). On the basis of this information, they can allocate resources to manage natural hazards/debris flows in a more effective way.

12.2 General remarks and recommendations

During the Ph.D. research, several general remarks regarding landslide hazard and risk arose. Susceptibility, hazard and risk maps turned to be of great interest by local stakeholders. They used them to have a general overview over the study area. However, as these maps are automatically calculated, they need to be carefully validated in the field and uncertainties have

to be pointed out in each step of the analysis. Otherwise serious mistakes can be involved in the interpretation and usage of the maps.

To improve the overall performance of the susceptibility maps a better inventory and high resolution data is needed. As a consequence, high attention has to be paid to the improvement of automated data acquisition techniques. This information will certainly improve the resulting models and it will be moreover possible to create near real-time preparation of the maps after incorporating the recent changes in the inventories as well as factor maps.

Regarding the spatial variability of the outputs, more attention has to be paid for the assessment of the spatial pattern of the susceptibility maps. As it was observed, in some cases the mismatch between the susceptibility classes of two maps can reach more than 25%. In the future, better validation methods shall be introduced, over-passing the problem of loss of spatial information during the validation.

Important drawback in debris flow hazard analysis at medium scale is the estimation of temporal probability. During analysis of larger areas using aerial photographs a multitemporal debris flow inventory is of great value. However, the time span between the inventories should not be longer than approx. 10 years; otherwise some debris flow events can be missed. Multitemporal debris flow inventory covering the period of e.g. 50 years with 10-year frequency of acquisition will also allow to estimate the magnitude/frequency properties of debris flow in the particular study area. This will continually lead to improvement of calibration of runout/spreading models and consequent upgrading of the hazard map.

It was shown, that quantitative risk estimation at medium scale has still many limitations. Specific risk estimation (economic risk in this case) is feasible at this scale. However, the obtained results have high level of uncertainties. These were assessed in a qualitative way. The total risk estimation using qualitative risk matrix is easily achievable. However, quantification of possible damage is not possible in this case.

More effort in the future has to be paid to the vulnerability estimations. Most hazard models are producing reliable results which can be used for very precise hazard estimation. However, for the risk estimation, vulnerability (and not only physical) is probably more important.

Presented thesis proposed a debris flow hazard and risk analyses approach at medium and local scale. Besides its feedbacks arising from available data, models, changing natural and socio-economic conditions and other intrinsic limitations, the thesis shows a possible approach applicable within integrated debris flow risk management framework.

As it was already stated, most attention has to be paid to the estimation of uncertainties in the models and validation of the modelling outputs. Because: *"don't believe any numbers you don´t make up yourself"*! Thank you for reading.

Acknowledgments

There are many people who took part in preparation of this thesis and helped me to conduct my research far from my home country. I would like to thank to all of them, namely to:

First of all, I would like to thank to my tutor Simone, who introduced me to the research of landslide hazard and risk in Italy and who has made important contribution to the success of this work. Moreover, he also showed me to the world of tasty red wine, pizzocheri and sciat of Valtellina. Thank you for that. My special thanks to Thomas, who raised critical thinking and ever-present doubts on the results. He made important contribution to my professional and personal formation. I would like to thank Cees for catalyzing more and more tests and experiments during the susceptibility analysis and thus making it more reliable and robust. This work could not be possible without Giovanni Di Trapani who provided me with a lot of data and information about the study area. Mattia helped me with the geo-referencing of aerial photographs and has done a lot of administrative work. Thanks to all members of SIT laboratory of DISAT, namely Ilaria, Carolina, Arianna, Sirun, Simone (il Terzo), Ivan and specially to Corrado for the return period estimation and geotechnical tests. It was really nice to work with all of you during last three years. My special thanks are to "Buznito" Byron Quan Luna who made the FLO-2D modelling of Selvetta and Tresenda event with me. I think this cooperation was a beginning of long friendship. Thanks also to Cristiano Ballabio who calculated the Kappa statistic, PCA and the DWE. Michel Jaboyedoff and Pascal Horton helped me a lot with the DFGridProb model and allowed me to spend nice time in Lausanne. Special thanks to Rainer, Kirsten, Yannick and Melanie from Vienna, where I spend really nice and inspiring internship. I want to thank also to Jean-Philippe Malet and Olivier Macquaire for the Mountain Risks project and to all of its participants.

Last but not least, I would to thank my family, Klára and Alžběta, for a full support during my all studies. Without you, the work would never be done.

Author's resume

Contact address: Šimonova 1109, Prague 6, 163 00, Czech Republic

Email: jan.blahut@unimib.it, jan.blahut@gmail.com

Telephone: +420 777 610 592

Summary of professional career:

Jan Blahut studied Physical Geography at the Charles University in Prague, Czech Republic. He finished his studies in 2006 by presenting a M.Sc. thesis focusing on snow avalanches in the Krkonoše Mountains. In 2007 he enrolled to the Department of Environmental and Territorial Sciences at the University of Milano-Bicocca, Italy as a Ph.D. student. He is employed by the department as an Early Stage Researcher within EC 6th Framework Program "Mountain Risks: from prediction to management and governance".

His research interests are:

- Rapid geomorphological hazards
- Hazard, vulnerability and risk analysis an assessment
- GIS
- Civil protection and disaster management

Scientific activities performed during the Ph.D. study

Peer reviewed papers

Quan Luna, B., Blahut, J., van Westen, C.J., Sterlacchini, S., van Asch, T.W.J., Akbas, S.O. (2010): Vulnerability functions from a debris flow event reconstruction for a quantitative risk assessment. Natural Hazards and Earth System Sciences. (manuscript under preparation).

Quan Luna, B., Blahut, J., Camera, C., van Westen, C.J., Sterlacchini, S., Apuani, T. (2010): Debris flow quantitative risk assessment and estimation of economic damage. Landslides. (under preparation).

Blahut, J., Sterlacchini, S. (2010): Risk analysis on medium scale: case of Valtellina di Tirano. Natural Hazards and Earth System Sciences. (under preparation).

Sterlacchini, S., Ballabio, C., Blahut, J., Masetti, M., Sorichetta, A. (2010): Spatial agreement of predicted values in landslide susceptibility maps. Geomorphology (submitted, under review).

Blahut, J., Horton, P., Sterlacchini, S., Jaboyedoff, M. (2010): Debris flow hazard modelling on medium scale: Valtellina di Tirano, Italy. Natural Hazards and Earth System Sciences. (submitted, under review).

Blahut, J., Klimeš, J. (2010): Contribution to the Czech terminology in landslide risk studies. Geografie – Sborník ČGS, 17 p. [in Czech]. (submitted, under review)

Blahut, J., Poretti, I., Sterlacchini, S., De Amicis, M. (2010): Database of Historical Disasters for Civil Protection Purposes. Natural Hazards. (submitted, under review)

Sterlacchini, S., Akbas, S.O., Blahut, J., Frigerio, S., Poretti, I., De Amicis, M., Sironi, S. (2010): A Methodological Approach for Landslide Risk Assessment and Loss Estimation – Application to the Village of Tresenda, Valtellina di Tirano, Italy. Natural Hazards and Earth System Sciences (submitted, under review).

Akbas, S. O., Blahut, J., Sterlacchini, S. (2010): Estimation of a vulnerability function for debris flow risk assessment using a well-documented event in Selvetta, Italy. Environmental Management, (submitted, under review).

Blahut, J., Sterlacchini, S., Horton, P., Jaboyedoff, M. (2010): Modellazione a media scala del runout dei debris flow: il caso studio della Valtellina di Tirano. Rendiconti online Soc. Geol. It. (in press).

Poretti, I., Blahut, J., Sterlacchini, S. (2010): Database di eventi storici a supporto della definizione di scenari di evento nella Valtellina di Tirano. Rendiconti online Soc. Geol. It. (in press).

Blahut, J., van Westen, C.J., Sterlacchini, S. (2010): Analysis of landslide inventories for accurate prediction of debris-flow source areas. Geomorphology (in press).

Blahut, J., Sterlacchini, S., Ballabio, C. (2009): Effect of the input parameters on the spatial variability of landslide susceptibility maps derived by statistical methods. Case study of the Valtellina Valley (Italian Central Alps). Geografický časopis / Geographical Journal, 61(1): 3-18.

Sorichetta, A., Masetti, M., Sterlacchini, S., Blahut, J. (2009): Aquifer vulnerability assessment using positive and negative evidences of contamination. Rendiconti online Soc. Geol. It., 8: 143-146.

Blahut, J. (2008): Snow avalanche susceptibility map of Krkonoše Mountains produced by GIS and statistical-probabilistic techniques. Opera Corcontica, 45: 35-44. [in Czech]

Conference proceedings

Blahut, J., Akbas, S. O., Sterlacchini, S., Quan Luna, B. (2009): Modelling and Estimation of damage from Debris Flow: the Case of Selvetta Debris Flow, Valtellina, Italy. In: Pašek, J., Marschalko, M., Pospíšil, P. (eds.): Sborník 1. Národního inženýrskogeologického kongresu s mezinárodní účastí – Rizika v inženýrské geologii, VŠB – TU, Ostrava, Czech Republic, p. 69-72. ISBN 978-80-248-2026-2

Akbas, S. O., Blahut, J., Sterlacchini, S. (2009): Critical assessment of existing physical vulnerability estimation approaches for debris flows. In: Malet, J.-P., Remaitre, A., Bogaard, T. (eds.): Proceedings of the International Conference "Landslide Processes", Strasbourg, France, p. 229-233.

Sterlacchini, S., Blahut, J., Ballabio, C., Masetti, M., Sorichetta, A. (2008): Proposta di una metodologia per il confronto dei risultati previsionali derivati da modelli statistici per la valutazione della predisposizione dei versanti agli eventi franosi. In: Pellegrini, E. (ed.): Riassunti convegno: Una nuova geologia per la Lombardia – in onore di Maria Bianca Cita, Milano, Italy, p. 78.

Blahut, J., De Amicis, M., Frigerio, S., Poretti, I., Sironi, S., Sterlacchini, S. (2008): Rischio idrogeologico: valutazione della pericolosità e della vulnerabilità per la stima economica dei Danni e per gestione in tempo reale delle emergenze. In: Pellegrini, E. (ed.): Riassunti convegno: Una nuova geologia per la Lombardia – in onore di Maria Bianca Cita, Milano, Italy, p. 68.

Blahut, J. (2008): Risk analysis: quantitative hazard analysis and economic evaluation by GIS techniques. In: Glade, T., Kappes, M., van Westen, C. J., Giacomelli, P., Sterlacchini, S., Keiler, M., Malet, J.-P., Maquaire, O. (eds.): Proceedings of the MOUNTAIN RISK Meeting "Risk Governance and Multi-hazard Assessment", Topical Workshop on "Multi-hazard consequences, vulnerability and risk analysis, Kempten, Germany, p. 30-34.

Blahut, J., Sterlacchini, S., Ballabio, C. (2008): Spatial variability of landslide susceptibility maps. In: Máčka, Z., Kallabová, E. (eds.): Geomorfologický sborník 7 - Stav geomorfologických výzkumů v roce 2008. ÚG AV ČR, Brno, Czech Republic, p. 6-7. ISBN 978-80-86407-39-5

Other papers

Blahut, J. (2010): Dangerous Italy? Geografické rozhledy, Kartografie, Praha, 19(4): 28-29. [in Czech]

Blahut, J. (2008): Civil protection in Italy. GUARD, Oxport, Praha, 4: 4-5. [in Czech]

Blahut, J. (2008): Geographic Information Systems for anybody. Geografické rozhledy, Kartografie, Praha, 18(2): 10-11. [in Czech]

Conference presentations

Blahut, J., Sterlacchini, S., Frigerio, S. (2009): Preparation of risk scenarios for civil protection purposes: case study of Valtellina di Tirano, Central Alps, Lombardy, Italy. Conference on social, economic and ecological aspects of flash floods. DNV, Brno, Czech Republic, 26th November 2009, Oral. [in Czech]

Blahut, J., Akbas, S. O., Sterlacchini, S., Quan Luna, B. (2009): Modelling and Estimation of damage from Debris Flow: the Case of Selvetta Debris Flow, Valtellina, Italy. 1. National Engineering Geological Congress – Risks in Engineering Geology, VŠB – TU, Ostrava, Czech Republic, 31st August – 3rd September 2009, Oral.

Quan Luna, B., Blahut, J., van Westen, C.J., Sterlacchini, S., Akbas, S.O. (2009): Debris flow reconstruction for risk assessment. International Seminar on „Capacity Building in Disaster Geo-information Management in Developing Countries". ITC, Enschede, Nizozemsko, 23th – 25th September 2009, Poster.

Ballabio, C., Blahut, J., Sterlacchini, S. (2009): Modelli non-lineari ed autocorrelazione spaziale per la valutazione della suscettibilità da frana. 4a Riunione Nazionale GIT, Geology and Information Technology Group, Italian Geological Society, Cagli (Pu), Italy, 15th – 17th June 2009, Oral.

Blahut, J., Sterlacchini, S., Horton, P., Jaboyedoff, M. (2009): Modellazione a media scala del runout dei debris flow: il caso studio della Valtellina di Tirano. 4a Riunione Nazionale GIT, Geology and Information Technology Group, Italian Geological Society, Cagli (Pu), Italy, 15th – 17th June 2009, Poster.

Poretti, I., Blahut, J. (2009): Database di eventi storici a supporto della definizione di scenari di evento nella Valtellina di Tirano. 4a Riunione Nazionale GIT, Geology and Information Technology Group, Italian Geological Society, Cagli (Pu), Italy, 15th – 17th June 2009, Poster.

Blahut, J., Horton, P., Jaboyedoff, M., Sterlacchini, S. (2009): Debris flow runout mapping on medium scale: application to Valtellina di Tirano, Central Alps, Italy. „SVAHOVÉ DEFORMACE A PSEUDOKRAS", Vsetín, Czech Republic, 13th – 15th May 2009, Oral.

Frigerio, S., Sterlacchini, S., van Westen, C. J., Akbas, S. O., Blahut, J., De Amicis, M., Sironi, S. (2009): Hazard and potential damage evaluation in a web-gis as support for risk Management. EGU General Assembly, Vienna, Austria, 19th – 24th April 2009, Poster.

Ballabio, C., Blahut, J., Sterlacchini, S. (2009): Assessment of the spatial agreement of landslide susceptibility maps. EGU General Assembly, Vienna, Austria, 19th – 24th April 2009, Poster.

Blahut, J., Quan Luna, B., Akbas, S. O., van Westen, C. J. (2009): Debris flow reconstruction - geomorphologic and numerical approach. A case study from the Selvetta event in Valtellina, Italy, July 2008. EGU General Assembly, Vienna, Austria, 19th – 24th April 2009, Oral.

Blahut, J., Sterlacchini, S., van Westen, C. J. (2009): Debris flow susceptibility assessment on medium scale using official and recently mapped inventories. EGU General Assembly, Vienna, Austria, 19th – 24th April 2009, Oral.

Akbas, S. O., Blahut, J., Quan Luna, B., Sterlacchini, S. (2009): Estimation of Vulnerability Functions for Debris Flows Using Different Intensity Parameters. EGU General Assembly, Vienna, Austria, 19th – 24th April 2009, Oral.

Akbas, S. O., Blahut, J., Sterlacchini, S. (2009): Critical assessment of existing physical vulnerability estimation approaches for debris flows. International Conference "Landslide Processes" – a tribute to Prof. Theo van Asch, 6th – 7th February 2009, Strasbourg, France, Poster.

Sterlacchini, S., Blahut, J., Ballabio, C., Masetti, M., Sorichetta, A.: Approccio metodologico per il confronto di mappe di previsione derivate da modelli statistici. Una nuova geologia per la Lombardia – in honore di Maria Bianca Cita, 6th – 7th November 2008, Milano, Italy, Poster.

Blahut, J., De Amicis, M., Frigerio, S., Poretti, I., Sironi, S., Sterlacchini, S.: Rischio idrogeologico: valutazione della pericolosità e della vulnerabilità per la stima economica dei danni e per la gestione in tempo reale delle emergenze. Una nuova geologia per la Lombardia – in honore di Maria Bianca Cita, 6th – 7th November 2008, Milano, Italy, Poster.

Blahut, J., Sterlacchini, S., Ballabio, C.: Spatial variability of landslide susceptibility maps. State of the geomorphological research in the year 2008, 3rd – 5th June 2008, Šlapanice (Brno), Czech Republic, Poster. [in Czech]

Blahut, J., Akbas, S.O., Brambilla, M., De Amicis, M., Frigerio, S., Poretti, I., Sironi, S., Sterlacchini, S.: "Mountain Risks": Challenges in Risk Analysis. 3a Riunione Nazionale GIT, Geology and Information Technology Group, Italian Geological Society, Offida (Ap), Italy, 3rd – 5th June 2008, Poster.

Sterlacchini, S., Blahut, J., Ballabio, C., Masetti, M., Sorichetta, A.: A methodological approach for comparing predictive maps derived from statistic-probabilistic methods. 3a Riunione Nazionale GIT, Geology and Information Technology Group, Italian Geological Society, Offida (Ap), Italy, 3rd – 5th June 2008, Poster.

Sorichetta, A., Masetti, M., Sterlacchini, S., Blahut, J.: Valutazione della vulnerabilità dell´acquifero superficiale della Provincia di Milano attraverso l´uso di un approccio statistico di tipo spaziale denominato Weights of Evidence. 3a Riunione Nazionale GIT, Geology and Information Technology Group, Italian Geological Society, Offida (Ap), Italy, 3rd – 5th June 2008, Oral.

Blahut, J., Brambilla, M., De Amicis, M., Frigerio, S., Poretti, I., Sironi, S., Sterlacchini, S (2008): Hydrogeological risks: hazard and vulnerability assessment for economic evaluation of consequences and real-time management of emergency situations. EGU General Assembly, Vienna, Austria, 13th – 18th April 2008, Poster.

Sterlacchini, S., Blahut, J., Ballabio, C., Masetti, M., Sorichetta, A. (2008): A methodological approach for comparing predictive maps derived from statistic-probabilistic methods. EGU General Assembly, Vienna, Austria, 13th – 18th April 2008, Poster.

Sorichetta, A.; Sterlacchini, S.; Poli, S.; Masetti, M.; Blahut, J. (2008): Groundwater Vulnerability Assessment: using the Weight of Evidence model with positive and negative evidences of contamination. EGU General Assembly, Vienna, Austria, 13th – 18th April 2008, Poster.

Internships

- Geomorphic Systems and Risk Research Unit, Institute of Geography and Regional Research, University of Vienna, Vienna, Austria, November 2008 – January 2009 (three months), Prof. T. Glade, Landslide Hazard and Risk Analysis.
- Institute of Geomatics and Risk Analysis, University of Lausanne, Switzerland, September 2009 (one week), Prof. M. Jaboyedoff, DFGridProb modelling.
- Department of Earth Systems Analysis, International Institute for Geo-Information Science and Earth Observation ITC, Enschede, the Netherlands, February 2008 – March 2008 (two months), Prof. C. J. van Westen, Spatial Data for Landslide Hazard Assessment.

Workshops, Courses and Seminars attended

- MOUNTAIN RISKS Topic workshop: "Dynamic spatial modelling of landslide hazards"; "Risk governance"; "Risk and emergency management", 11th – 14th November 2009, CNR-IRPI, UNIMIB, Padova (PD), Italy.

- Early warning systems: integrating technical, social and urban planning aspects, 12th October 2009, Politecnico di Milano, Milano (MI), Italy.
- International Summer School on Rockslides and Related Phenomena, 31st July – 14th August 2009, ICL, Kokomeren River Valley, Central Tien Shan, Kyrgyzstan.
- MOUNTAIN RISKS Intensive Course: "Multi-technique landslide investigation for hazard assessment", 21st – 26th June 2009, UNIL, Les Diablerets, Switzerland.
- "Protezione Civile: dalla previsione al superamento dell'emergenza. Confronto e sinergie per affrontare le sfide del futuro", 7th October 2008, Lombardy Region, Varenna (LC), Italy.
- International School on "LAndslide Risk Assessment and Mitigation", 7th – 20th September 2008, UNISA, Ravello (SA), Italy.
- MOUNTAIN RISKS Topic workshop: „Landslide risk management", 5th September 2008, UPC, Barcelona, Spain.
- FORM-OSE and MOUNTAIN RISKS Intensive Course: "Quantitative Landslide Risk Assessment and Risk management", 1st – 4th September 2008, UPC, Barcelona, Spain.
- MOUNTAIN RISKS Topical Workshop: "Multi-hazard consequences, vulnerability and risk analysis, 20th – 22nd June 2008, UNIVIE, Kempten, Germany.
- MOUNTAIN RISKS Intensive Course: "Mountain Risks and Risk Governance", 15th – 19th June 2008, Kempten, Germany.
- MOUNTAIN RISKS Topic Workshop II: "Single Hazard Analysis", 26th – 30th November 2007, UNIL, Lausanne, Switzerland.
- Cyberseminar on Population Dynamics and Natural Hazards, 5th – 19th November 2007, Population-Environment Research Network, Co-ordinated by Center for International Earth Science Information Network (CIESIN), Columbia University, Palisades, New York, USA.
- MOUNTAIN RISKS Topic Workshop I: "Risk governance principles", 26th – 27th September 2007, UNIDO, Dortmund, Germany.
- MOUNTAIN RISKS Stakeholder Workshop 1, 25th – 26th September 2007, UNIDO, Dortmund, Germany.
- LAndslide Risk Assessment and Mitigation (LARAM) Workshop, Teoria, zonazione e mitigazione del rischio da frana, 5th – 6th September 2007, Villa Rufolo, Ravello (SA), Italy.

Co-tutored thesis

- Sangalli, L. (2009): Predisposizione dei versanti ai movimenti di massa attraverso curve di tasso di predizione. Studio statistico dell´area di Tirano sud. Diploma thesis, University of Milano-Bicocca, Department of Environmental and Territorial Sciences, Milano, 140 pp.
- Mauriello, M. (2009): Previsione di pericolo di frana nell´area di Tirano nord: incertezza di valori di favorabilitá. Diploma thesis, University of Milano-Bicocca, Department of Environmental and Territorial Sciences, Milano, 146 pp.

Opposed thesis

- Juras, R. (2009): Danger of slush-flows in the territory of KRNAP and possibilities of their prediction. Diploma thesis, Czech University of Life Sciences Prague, Faculty of Environmental Sciences, Department of Water Resources and Environmental Modelling, Prague, 98 pp. + 24 suppl.

19th April 2010
Milano, Italy
The Thesis is printed on FSC paper

***